

Pharmacology, Toxicology, and Therapeutics of Minerals in Traditional Medicine

Lead Guest Editor: Jie Liu

Guest Editors: Uma Maheswari Krishnan, Swaminathan Sethuraman, and Lixin Wei





Pharmacology, Toxicology, and Therapeutics of Minerals in Traditional Medicine

Evidence-Based Complementary and Alternative Medicine

**Pharmacology, Toxicology, and
Therapeutics of Minerals in Traditional
Medicine**

Lead Guest Editor: Jie Liu

Guest Editors: Uma Maheswari Krishnan,
Swaminathan Sethuraman, and Lixin Wei



Copyright © 2023 Hindawi Limited. All rights reserved.

This is a special issue published in "Evidence-Based Complementary and Alternative Medicine." All articles are open access articles distributed under the Creative Commons Attribution License, which permits unrestricted use, distribution, and reproduction in any medium, provided the original work is properly cited.

Chief Editor

Jian-Li Gao , China

Associate Editors















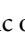


Hyunsu Bae , Republic of Korea
Raffaele Capasso , Italy
Jae Youl Cho , Republic of Korea
Caigan Du , Canada
Yuewen Gong , Canada
Hai-dong Guo , China
Kuzhuvelil B. Harikumar , India
Ching-Liang Hsieh , Taiwan
Cheorl-Ho Kim , Republic of Korea
Victor Kuete , Cameroon
Hajime Nakae , Japan
Yoshiji Ohta , Japan
Olumayokun A. Olajide , United Kingdom
Chang G. Son , Republic of Korea
Shan-Yu Su , Taiwan
Michał Tomczyk , Poland
Jenny M. Wilkinson , Australia

Academic Editors

Eman A. Mahmoud , Egypt
Ammar AL-Farga , Saudi Arabia
Smail Aazza , Morocco
Nahla S. Abdel-Azim, Egypt
Mona Abdel-Tawab, Germany
Ana Lúcia Abreu-Silva , Brazil
Gustavo J. Acevedo-Hernández , Mexico
Mohd Adnan , Saudi Arabia
Jose C Adsuar , Spain
Gabriel A. Agbor , Cameroon
Sayeed Ahmad, India
Touqeer Ahmed , Pakistan
Wan Mohd Aizat , Malaysia
Basiru Ajiboye , Nigeria
Bushra Akhtar , Pakistan
Muhammad Furqan Akhtar , Pakistan
Fahmida Alam , Malaysia
Mohammad Jahoor Alam, Saudi Arabia
Clara Albani, Argentina
Ulysses Paulino Albuquerque , Brazil
Mohammed S. Ali-Shtayeh , Palestinian Authority
Ekram Alias, Malaysia







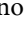




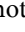














Terje Alraek , Norway
Sergio R. Ambrosio , Brazil
Samson Amos, USA
Vijaya Anand, India
Adolfo Andrade-Cetto , Mexico
Letizia Angiolella , Italy
Makoto Arai , Japan
Daniel Dias Rufino Arcanjo , Brazil
Duygu AĞAGÜNDÜZ , Turkey
Neda Baghban , Iran
Ahmed Bari , Saudi Arabia
Samra Bashir , Pakistan
Rusliza Basir , Malaysia
Jairo Kenupp Bastos , Brazil
Arpita Basu , USA
Daniela Beghelli , Italy
Mateus R. Beguelini , Brazil
Juana Benedí, Spain
Andresa A. Berretta , Brazil
Samira Boulbaroud, Morocco
Mohammed Bourhia , Morocco
Abdelhakim Bouyahya, Morocco
Célia Cabral , Portugal
Nunzio Antonio Cacciola , Italy
Gioacchino Calapai , Italy
Francesco Cardini , Italy
María C. Carpinella , Argentina
Isabella Cavalcanti , Brazil
Shun-Wan Chan , Hong Kong
Harish Chandra , India
Calvin Yu-Chian Chen , China
Guang Chen, China
Jianping Chen , China
Kevin Chen, USA
Mei-Chih Chen, Taiwan
Xiaojia Chen , Macau
Evan P. Cherniack , USA
Giuseppina Chianese , Italy
Kok-Yong Chin , Malaysia
Lin China, China
I. Chinou , Greece
Salvatore Chirumbolo , Italy
Hwi-Young Cho , Republic of Korea
Jeong June Choi , Republic of Korea
Jun-Yong Choi, Republic of Korea




















Kathrine Bisgaard Christensen , Denmark
Shuang-En Chuang, Taiwan
Ying-Chien Chung , Taiwan
Francisco José Cidral-Filho, Brazil
Ian Cock , Australia
Guy Cohen , Israel
Daniel Collado-Mateo , Spain
Lisa A. Conboy , USA
Kieran Cooley , Canada
Edwin L. Cooper , USA
José Otávio do Amaral Corrêa , Brazil
Maria T. Cruz , Portugal
Huantian Cui , China
Giuseppe D'Antona , Italy
Ademar A. Da Silva Filho , Brazil
Chongshan Dai, China
Nawab Dar , USA
Laura De Martino , Italy
Josué De Moraes, Brazil
Arthur De Sá Ferreira , Brazil
Nunziatina De Tommasi , Italy
Rocío De la Puerta , Spain
Marinella De leo , Italy
Gourav Dey , India
Dinesh Dhamecha, USA
Claudia Di Giacomo , Italy
Antonella Di Sotto , Italy
Gabriel O. Dida , Japan
Mario Dioguardi, Italy
Vishal Diwan, Australia
Lin-Rui Duan , China
Jeng-Ren Duann , USA
Thomas Efferth , Germany
Abir El-Alfy, USA
Mohamed Ahmed El-Esawi , Egypt
Mohd Ramli Elvy Suhana, Malaysia
Talha Bin Emran, Japan
Roger Engel , Australia
Karim Ennouri , Tunisia
Giuseppe Esposito , Italy
Tahereh Eteraf-Oskouei, Iran
Robson Xavier Faria , Brazil
Mohammad Fattahi , Iran
Keturah R. Faurot , USA
Piergiorgio Fedeli , Italy

Nianping Feng , China
Yibin Feng , Hong Kong
Laura Ferraro , Italy
Antonella Fioravanti , Italy
Carmen Formisano , Italy
Harquin Simplicie Foyet , Cameroon
Hua-Lin Fu , China
Huiying Fu , China
Liz G Müller , Brazil
Dolores García Giménez , Spain
Gabino Garrido , Chile
Safoora Gharibzadeh, Iran
Muhammad N. Ghayur , USA
Angelica Gomes , Brazil
Elena González-Burgos, Spain
Susana Gorzalczany , Argentina
Jiangyong Gu , China
Maruti Ram Gudavalli , USA
Jian-You Guo , China
Shanshan Guo, China
Shuzhen Guo , China
Narcís Gusi , Spain
Svein Haavik, Norway
Fernando Hallwass, Brazil
Gajin Han , Republic of Korea
Ihsan Ul Haq, Pakistan
Md. Areeful Haque , India
Hicham Harhar , Morocco
Mohammad Hashem Hashempur , Iran
Muhammad Ali Hashmi , Pakistan
Waseem Hassan , Pakistan
Sandrina A. Heleno , Portugal
Pablo Herrero , Spain
Soon S. Hong , Republic of Korea
Md. Akil Hossain , Republic of Korea
Muhammad Jahangir Hossen , Bangladesh
Shih-Min Hsia , Taiwan
Changmin Hu , China
Tao Hu , China
Weicheng Hu , China
Wen-Long Hu, Taiwan
Xiao-Yang (Mio) Hu, United Kingdom
Sheng-Teng Huang , Taiwan
Ciara Hughes , Ireland

Attila Hunyadi , Hungary
Liaqat Hussain , Pakistan
Tarique Hussain , Pakistan
Maria-Carmen Iglesias-Osma , Spain
Elisha R. Injeti , USA
H. Stephen Injeyan , Canada
Amjad Iqbal , Pakistan
Chie Ishikawa , Japan
Angelo A. Izzo, Italy
Mohieddin Jafari , Finland
Satveer Jagwani , USA
Rana Jamous , Palestinian Authority
Muhammad Saeed Jan , Pakistan
G. K. Jayaprakasha, USA
Kamani Ayoma Perera Wijewardana
Jayatilaka , Sri Lanka
Kyu Shik Jeong, Republic of Korea
Qing Ji , China
Hualiang Jin , China
Yanxia Jin, China
Leopold Jirovetz , Austria
Jeeyoun Jung , Republic of Korea
Sleman Kadan , Israel
Nurkhalida Kamal , Saint Vincent and the
Grenadines
Atsushi Kameyama , Japan
Kyungsu Kang, Republic of Korea
Wenyi Kang , China
Shao-Hsuan Kao , Taiwan
Juntra Karbwang , Japan
Nasiara Karim , Pakistan
Morimasa Kato , Japan
Kumar Katragunta , USA
Deborah A. Kennedy , Canada
Asaad Khalid , Saudi Arabia
Haroon Khan , Pakistan
Washim Khan, USA
Bonglee Kim , Republic of Korea
Dong Hyun Kim , Republic of Korea
Junghyun Kim , Republic of Korea
Kibong Kim , Republic of Korea
Kyungho Kim, Republic of Korea
Yun Jin Kim , Malaysia
Woojin Kim, Republic of Korea

Yoshiyuki Kimura , Japan
Nebojša Kladar , Serbia
Mi Mi Ko , Republic of Korea
Toshiaki Kogure , Japan
Malcolm Koo , Taiwan
Yu-Hsiang Kuan , Taiwan
Robert Kubina , Poland
Chan-Yen Kuo , Taiwan
Kuang C. Lai , Taiwan
King Hei Stanley Lam, China
Fanuel Lampiao, Malawi
Ilaria Lampronti , Italy
Chou-Chin Lan , Taiwan
Mario Ledda , Italy
Byung-Cheol Lee , Republic of Korea
Dong-Sung Lee , Republic of Korea
Gihyun Lee , Republic of Korea
Harry Lee , China
Jeong-Sang Lee , Republic of Korea
Ju Ah Lee , Republic of Korea
Kyu Pil Lee , Republic of Korea
Namhun Lee , Republic of Korea
Sang Yeoup Lee , Republic of Korea
Yun Jung Lee , Republic of Korea
Ankita Leekha , USA
Christian Lehmann , Canada
Marivane Lemos , Brazil
George B. Lenon , Australia
Marco Leonti, Italy
Hua Li , China
Min Li , China
Xing Li , China
Xuqi Li , China
Yi-Rong Li , Taiwan
Vuanghao Lim , Malaysia
Bi-Fong Lin, Taiwan
Ho Lin , Taiwan
Shih-Chao Lin, Taiwan
Shuibin Lin, China
Kuo-Tong Liou , Taiwan
I-Min Liu, Taiwan
Suhuan Liu , China
Xiaosong Liu , Australia
Yujun Liu , China

Emilio Lizarraga , Argentina
Monica Loizzo , Italy
Nguyen Phuoc Long, Republic of Korea
Victor López , Spain
Zaira López, Mexico
Chunhua Lu , China
Ángelo Luís , Portugal
Anderson Luiz-Ferreira , Brazil
Ivan Luzardo Luzardo-Ocampo, Mexico
Michel Mansur Machado , Brazil
Filippo Maggi , Italy
Juraj Majtan , Slovakia
Toshiaki Makino , Japan
Nicola Malafronte, Italy
Giuseppe Malfa , Italy
Francesca Mancianti , Italy
Subashani Maniam , Australia
Carmen Mannucci , Italy
Juan M. Manzanque , Spain
Fatima Martel , Portugal
Simona Martinotti , Italy
Carlos H. G. Martins , Brazil
Stefania Marzocco , Italy
Maulidiani Maulidiani, Malaysia
Andrea Maxia , Italy
Avijit Mazumder , India
Isac Medeiros , Brazil
Ahmed Mediani , Malaysia
Lewis Mehl-Madrona, USA
Ayikoé Guy Mensah-Nyagan , France
Oliver Micke , Germany
Maria G. Miguel , Portugal
Luigi Milella , Italy
Roberto Miniero , Italy
Letteria Minutoli, Italy
Prashant Modi , India
Daniel Kam-Wah Mok, Hong Kong
Changjong Moon , Republic of Korea
Albert Moraska, USA
Mark Moss , United Kingdom
Yoshiharu Motoo , Japan
Yoshiki Mukudai , Japan
Sakthivel Muniyan , USA
Laura Muñoz-Bermejo , Spain

Saima Muzammil , Pakistan
Benoit Banga N'guessan , Ghana
Massimo Nabissi , Italy
Siddavaram Nagini, India
Takao Namiki , Japan
Srinivas Nammi , Australia
Krishnadas Nandakumar , India
Vitaly Napadow , USA
Edoardo Napoli , Italy
Derek Tantoh Ndinteh , South Africa
Pratibha V. Nerurkar , USA
Jorddy Neves Cruz , Brazil
Marcello Nicoletti , Italy
Eliud Nyaga Mwaniki Njagi , Kenya
Cristina Nogueira , Brazil
Sakineh Kazemi Noureini , Iran
Rômulo Dias Novaes, Brazil
Martin Offenbaecher , Germany
Oluwafemi Adeleke Ojo , Nigeria
Olufunmiso Olusola Olajuyigbe , Nigeria
Luís Flávio Oliveira, Brazil
Mozaniel Oliveira , Brazil
Atolani Olubunmi , Nigeria
Abimbola Peter Oluyori , Nigeria
Timothy Omara, Austria
Vahidreza Ostadmohammadi , Iran
Chiagoziem Anariochi Otuechere , Nigeria
Mustafa Ozyurek , Turkey
Sokcheon Pak , Australia
Antônio Palumbo Jr, Brazil
Zongfu Pan , China
Siyaram Pandey , Canada
Niranjan Parajuli, Nepal
Gunhyuk Park , Republic of Korea
Wansu Park , Republic of Korea
Rodolfo Parreira , Brazil
Mohammad Mahdi Parvizi , Iran
Matheus Pasquali , Brazil
Luiz Felipe Passero , Brazil
Visweswara Rao Pasupuleti, Malaysia
Mitesh Patel, India
Bhushan Patwardhan , India
Claudia Helena Pellizzon , Brazil
Cheng Peng, Australia

Weijun Peng , China
Shagufta Perveen , Saudi Arabia
Sonia Piacente, Italy
Andrea Pieroni , Italy
Richard Pietras , USA
Haifa Qiao , USA
Cláudia Quintino Rocha , Brazil
DANIELA RUSSO , Italy
Nor Fadilah Rajab , Malaysia
Manzoor Rather , India
Miguel Rebollo-Hernanz , Spain
Julita Regula , Poland
Gauhar Rehman, Pakistan
Kanwal Rehman , Pakistan
Man Hee Rhee , Republic of Korea
Daniela Rigano , Italy
José L. Rios, Spain
Francisca Rius Diaz, Spain
Eliana Rodrigues , Brazil
Maan Bahadur Rokaya , Czech Republic
Barbara Romano , Italy
Mariangela Rondanelli , Italy
Antonietta Rossi , Italy
Mi Heon Ryu , Republic of Korea
Bashar Saad , Palestinian Authority
Abdul Sadiq , Pakistan
Sabiuh Saheed, South Africa
Mohamed Z.M. Salem , Egypt
Avni Sali, Australia
Andreas Sandner-Kiesling, Austria
Manel Santafe , Spain
José Roberto Santin , Brazil
Antonietta Santoro , Italy
Tadaaki Satou , Japan
Roland Schoop, Switzerland
Sindy Seara-Paz, Spain
Veronique Seidel , United Kingdom
Vijayakumar Sekar , China
Terry Selfe , USA
Senthamil R. Selvan , USA
Arham Shabbir , Pakistan
Suzana Shahr, Malaysia
Wen-Bin Shang , China
Xiaofei Shang , China




Ali Sharif , Pakistan
Karen J. Sherman , USA
Ronald Sherman , USA
San-Jun Shi , China
Insop Shim , Republic of Korea
Maria Im Hee Shin, China
Yukihiro Shoyama, Japan
Morry Silberstein , Australia
Samuel Martins Silvestre , Portugal
Moganavelli Singh , South Africa
Rajeev K Singla , China
Kuttulebbai N. S. Sirajudeen , Malaysia
Slim Smaoui , Tunisia
Eun Jung Sohn , Republic of Korea
Maxim A. Solovchuk , Taiwan
Young-Jin Son , Republic of Korea
Chengwu Song , China
Yanting Song , China
Klaokwan Srisook , Thailand
Vanessa Steenkamp , South Africa
Annarita Stringaro , Italy
Dan Su , China
Keiichiro Sugimoto , Japan
Valeria Sulsén , Argentina
Zewei Sun , China
Sharifah S. Syed Alwi , United Kingdom
Eryvaldo Sócrates Tabosa do Egito , Brazil
Orazio Tagliatela-Scafati , Italy
Shin Takayama , Japan
Takashi Takeda , Japan
Gianluca Tamagno , Ireland
Jun Jie Tan , Malaysia
Hongxun Tao, China
Jun-Yan Tao , China
Hamid Tebyaniyan , Iran
Lay Kek Teh , Malaysia
Norman Temple , Canada
Kamani H. Tennekoon , Sri Lanka
Seong Lin Teoh, Malaysia
Mencherini Teresa , Italy
Mayank Thakur , Germany
Menaka Thounaojam , USA
Jinhui Tian, China
Zipora Tietel, Israel

Loren Toussaint , USA
Md. Sahab Uddin , Bangladesh
Riaz Ullah , Saudi Arabia
Philip F. Uzor , Nigeria
Patricia Valentao, Portugal
Luca Vanella , Italy
Antonio Vassallo , Italy
Cristian Vergallo, Italy
Miguel Vilas-Boas , Portugal
Aristo Vojdani , USA
Yun WANG , China
QIBIAO WU , Macau
Abraham Wall-Medrano , Mexico
Chunpeng (Craig) Wan , China
Jin-Yi Wan , USA
Almir Gonçalves Wanderley , Brazil
Chong-Zhi Wang , USA
Guang-Jun Wang , China
Jinan Wang , China
Qi-Rui Wang , China
Ru-Feng Wang , China
Shu-Ming Wang , USA
Ting-Yu Wang , China
Xue-Rui Wang , China
Youhua Wang , China
Kenji Watanabe , Japan
Jintanaporn Wattanathorn , Thailand
Silvia Wein , Germany
Meng-Shih Weng , Taiwan
Katarzyna Winska , Poland
Sok Kuan Wong , Malaysia
Christopher Worsnop, Australia
Jih-Huah Wu , Taiwan
Sijin Wu , China
Xian Wu, USA
Xu Wu , China
Zuoqi Xiao , China
Rafael M. Ximenes , Brazil
Guoqiang Xing , USA
JiaTuo Xu , China
Mei Xue , China
Yong-Bo Xue , China
Haruki Yamada , Japan
Nobuo Yamaguchi, Japan

Jing-Wen Yang , China
Junqing Yang, China
Longfei Yang , China
Mingxiao Yang , Hong Kong
Qin Yang , China
Sheng-Li Yang , China
Wei-Hsiung Yang, USA
Swee Keong Yeap , Malaysia
Albert S. Yeung , USA
Ebrahim M. Yimer , Ethiopia
Yoke Keong Yong , Malaysia
Fadia S. Youssef , Egypt
Zhilong Yu, Canada
Yanggang Yuan , China
RONGJIE ZHAO , China
Sultan Zahiruddin, USA
Hilal Zaid , Israel
Paweł Zalewski , Poland
Armando Zarrelli , Italy
Xiaobin Zeng , China
Y Zeng , China
Bimeng Zhang , China
Fangbo Zhang , China
Jianliang Zhang , China
Jiu-Liang Zhang , China
Mingbo Zhang , China
Jing Zhao , China
Zhangfeng Zhong , Macau
Guoqi Zhu , China
Yan Zhu , USA
Suzanna M. Zick , USA
Stephane Zingue , Cameroon




Contents




Pharmacology, Toxicology, and Therapeutics of Minerals in Traditional Medicine 2021

Jie Liu , Uma Maheswari Krishnan , and Lixin Wei 

Editorial (3 pages), Article ID 9823746, Volume 2023 (2023)





Inhibitory Effects of *Euphorbia ebracteolata* Hayata Extract ECB on Melanoma-Induced Hyperplasia of Blood Vessels in Zebrafish Embryos

Wenjing Dong , Xinyue Han , Chao Bao, Saijilahu Tai, Yuxia Bai , Liang Xu, Jingfeng Yang,

TinChung Leung , Wuliji Ao , and Wu Dong 

Research Article (10 pages), Article ID 5543259, Volume 2021 (2021)

The Herbal Constituents in An-Gong-Niu-Huang Wan (AGNH) Protect against Cinnabar- and Realgar-Induced Hepatorenal Toxicity and Accumulations of Mercury and Arsenic in Mice

Songsong Wang , Xiao Xiao , Ao Li , and Peng Li 

Research Article (9 pages), Article ID 5566078, Volume 2021 (2021)




Changes of Mineralogical Properties and Biological Activities of Gypsum and Its Calcined Products with Different Phase Structures

Kaiyang Liu , Shu Han , Wei Gao, Ya'nan Tang , Xitao Han , Ziqin Liu , Liyuan Bao, Meiru

Zhi , Hongyue Wang , Yingli Wang, and Hong Du 


Research Article (14 pages), Article ID 6676797, Volume 2021 (2021)

Arsenic Content, Speciation, and Distribution in Wild *Cordyceps sinensis*

Yuancan Xiao , Cen Li, Wei Xu, Yuzhi Du, Ming Zhang, Hongxia Yang, Lixin Wei , and Hongtao Bi 

Research Article (9 pages), Article ID 6651498, Volume 2021 (2021)

RNA-Seq Expression Analysis of Chronic Asthmatic Mice with Bu-Shen-Yi-Qi Formula Treatment and Prediction of Regulated Gene Targets of Anti-Airway Remodeling

Jie Cui , Zexi Lv, Fangzhou Teng, La Yi, Weifeng Tang, WenQian Wang, Wuniqiemu Tulake, Jingjing

Qin, Xueyi Zhu, Ying Wei , and Jingcheng Dong 



Research Article (9 pages), Article ID 3524571, Volume 2021 (2021)


Rutaecarpine Ameliorates Pressure Overload Cardiac Hypertrophy by Suppression of Calcineurin and Angiotensin II

Shujun Li , Bo Huang , Changfei Zhou , Jingshan Shi , Qin Wu , and Qingsong Jiang 

Research Article (8 pages), Article ID 8857329, Volume 2021 (2021)










Purification, Detoxification, and Incineration Methods of Minerals and Metals in Traditional Medicine Formulations of Sri Lanka

Horadugoda Gamage Sujatha Pushpakanthi Hewageegana , Ayuma Uththami Hewageegana , and




Liyana Dona Ashanthi Menuka Arawwawala 

Review Article (8 pages), Article ID 6634553, Volume 2021 (2021)



***Ulmus parvifolia* Jacq. Exhibits Antiobesity Properties and Potentially Induces Browning of White Adipose Tissue**

Yuan Yee Lee , Minki Kim , Muhammad Irfan , Heung Joo Yuk , Dong-Seon Kim , Seung Eun Lee, Seung-Hyung Kim , Suk Kim , Sung-Dae Kim , and Man Hee Rhee 
Research Article (14 pages), Article ID 9358563, Volume 2020 (2020)

Mode of Action of Shan-Zhu-Yu (*Cornus officinalis* Sieb. et Zucc.) in the Treatment of Depression Based on Network Pharmacology

Ping Liu , Ping Yang , and Lan Zhang 
Research Article (10 pages), Article ID 8838888, Volume 2020 (2020)

Potential Molecular Target Prediction and Docking Verification of Hua-Feng-Dan in Stroke Based on Network Pharmacology

Ping Yang , Haifeng He, Shangfu Xu, Ping Liu , and Xinyu Bai 
Research Article (12 pages), Article ID 8872593, Volume 2020 (2020)

Advances in the Study of the Potential Hepatotoxic Components and Mechanism of *Polygonum multiflorum*

He-Shui Yu, Lin-Lin Wang, Ying He, Li-Feng Han , Hui Ding, Xin-Bo Song, Xiu-Mei Gao , Nai-Ru Yun , and Zheng Li 
Review Article (12 pages), Article ID 6489648, Volume 2020 (2020)

Editorial

Pharmacology, Toxicology, and Therapeutics of Minerals in Traditional Medicine 2021

Jie Liu ¹, Uma Maheswari Krishnan ², and Lixin Wei ³

¹Key Lab for Basic Pharmacology of Ministry of Education and Joint International Research Laboratory of Ethnomedicine, Zunyi Medical University, Zunyi, China

²Centre for Nanotechnology & Advanced Biomaterials, School of Chemical & Biotechnology, SASTRA Deemed University, Thanjavur 613 401, Tamil Nadu, India

³Qinghai Key Lab of Tibetan Medicine Pharmacology and Safety Evaluation, Northwest Institute of Plateau Biology, Chinese Academy of Sciences, Xining 810008, China

Correspondence should be addressed to Jie Liu; jie@liuonline.com

Received 30 June 2022; Accepted 30 June 2022; Published 20 September 2023

Copyright © 2023 Jie Liu et al. This is an open access article distributed under the Creative Commons Attribution License, which permits unrestricted use, distribution, and reproduction in any medium, provided the original work is properly cited.

Minerals have been used in traditional medicine since ancient times and are still used in Indian Ayurveda and Chinese medicines including Tibetan medicine [1–4]. The processing/preparation procedures distinguish minerals used in traditional medicines from environmental toxic metals such as mercury-based Ayurveda [1], Zuotai, and various Bhasmas [3]. Minerals are not used alone but as polyherbal-metallic preparations for oral administration [1, 2, 4]. The aim of this Special Issue is to collate original research and review articles dealing with minerals in traditional medicines.

A review paper [5] summarized 10 herbo-mineral preparations used in Sri Lanka regarding the purification, detoxification, or incineration techniques. The minerals included in the 10 traditional medicines are copper sulphate, aluminum sulphate, borax powder, sulphur, cinnabar (HgS), realgar (As₂S₂), orpiment (As₂O₃), ammonium chloride, magnesium silicate, zinc oxide, and mercury (*Parada*). It should be noted that only sulfide and oxide forms of metals are used in oral traditional medicines, and these detailed methods highlight the importance of mineral processing techniques before addition to traditional medicines. Processing gypsum could change its mineral properties and biological activities when used in traditional medicines [6]. The preparations of minerals used in traditional medicines such as Zuotai and Bhasmas are very important and are needed for quality control [1, 3, 7, 8].

Quality control is an important issue for mineral-containing/contaminated traditional medicines. In this regard, Xiao et al. [9] used HPLC-ICP-MS to detect arsenic content, speciation, and distribution in wild *Cordyceps sinensis*, a famous traditional medicine, to provide scientific basis of quality control. Fu et al. [10] used ICP-MS to detect 18 element contents across 10 batches of Qishiwei Zhenzhu pills (QSW) produced by 5 pharmaceuticals. QSW is a famous Tibetan medicine listed in Pharmacopeia of China for many diseases. To establish a quality control for toxic elements (Hg, Pb, As, and Cd), essential elements with potential toxicity (Cu, Mn, Cr, and Co) and elements with medicinal use (Li and Au) could be used to ensure its efficacy and reduce adverse effects and toxicity.

Oral administration is the main route for using herbo-mineral preparations. Song et al. [11] determined 18 elements in QSW for absorption and distribution to the liver, kidney, and brain and excretion by feces, urine, and hair in rats with middle cerebral artery occlusion (MACO). The majority of minerals were excreted by feces implying the long-term stay of elements in the gut that could affect the gut-microbiota-brain axis in QSW-induced protective effects against cerebral ischemia-reperfusion injury [12].

QSW is effective against cerebral ischemia stroke in animal models. Mechanistic studies revealed QSW indeed affected gut microbiota in rats with MACO. At the phylum level, it can regulate the abundance of Firmicutes and

Proteobacteria; at the genus level, it can adjust the abundance of *Escherichia* and *Shigella*; and at the species level, it can adjust the abundance of *Lactobacillus johnsonii* and *Lactobacillus reuteri*. QSW can also decrease inflammatory factor IL-1 β , TNF- α , and IL-6 expression in the hippocampus of MACO rats, thus reducing oxidative damage caused by ischemia and reperfusion [12]. Cerebral ischemia injury can also be alleviated by cinnabar (HgS) and realgar (As₄S₄) containing An-Gong-Niu-Huang Wan (AGNH), and cinnabar and realgar are shown to be essential ingredients in the recipe [13]. The entire AGNH formulae can also protect against the hepatorenal toxicity produced by cinnabar and realgar alone and reduce Hg and As accumulation in tissues, implying herbal constituents in polyherbo-mineral preparations could offset the toxic effects of minerals [14, 15].

New approaches are attempted to explore the pharmacological basis of herbo-mineral preparations. The mechanism of arsenic trioxide against hepatocellular carcinoma (HCC) was examined through network pharmacology, and various pathways including TNF signaling pathway, AMPK signaling pathway, NF-kappa B signaling pathway, and several targets-pathways-HCC network molecules could be potential molecular targets for arsenic against HCC [16]. Modulation of gut microbiota could be an important target for QSW [12] to produce neuroprotective effects but also for Hua-Feng-Dan to produce neuroprotective effects [17] fortifying the role of metal composition and herbal interactions in herbo-mineral preparations. RNA-Seq technology was also employed to analyze the adaptive mechanism of hepatoprotection with cinnabar and realgar-containing Hua-Feng-Dan [18] and antihepatic fibrotic mechanism with Ganxianfang formula [19].

Thus, with contributions from investigators from different countries, this Special Issue presented recent experimental findings and reviews on pharmacology, toxicology, and therapeutics of minerals in traditional medicines. In this Special Issue, there are more valuable manuscripts besides those given above. We hope the readers will be interested in approaching minerals in traditional medicines from “processing,” “formulae,” quality control, pharmacokinetics, pharmacology, toxicology, and bioinformatics.

Conflicts of Interest

The editors declare that they have no conflicts of interest.

Jie Liu
Uma Maheswari Krishnan
Lixin Wei

Acknowledgments

The editors thank Dr. Swaminathan Sethuraman as an initial Guest Editor and thank all authors of the articles and all reviewers for their valuable contributions to this Special Issue.

References

- [1] S. U. Kamath, B. Pemiah, R. K. Sekar, S. Krishnaswamy, S. Sethuraman, and U. M. Krishnan, “Mercury-based traditional herbo-metallic preparations: a toxicological perspective,” *Archives of Toxicology*, vol. 86, no. 6, pp. 831–838, 2012.
- [2] J. Liu, L. X. Wei, Q. Wang et al., “A review of cinnabar (HgS) and/or realgar (As(4)S(4))-containing traditional medicines,” *Journal of Ethnopharmacology*, vol. 210, pp. 340–350, 2018.
- [3] J. Liu, F. Zhang, V. Ravikanth, O. A. Olajide, C. Li, and L. X. Wei, “Chemical compositions of metals in Bhasmas and Tibetan Zuotai are a major determinant of their therapeutic effects and toxicity,” *Evidence Based Complementary Alternative Medicine*, vol. 2019, Article ID 1697804, 13 pages, 2019.
- [4] M. Zhao, Y. Li, and Z. Wang, “Mercury and mercury-containing preparations: history of use, clinical applications, pharmacology, toxicology, and pharmacokinetics in traditional Chinese medicine,” *Frontiers in Pharmacology*, vol. 13, Article ID 807807, 2022.
- [5] H. G. Sujatha Pushpakanthi Hewageegana, A. U. Hewageegana, and L. D. Ashanthi Menuka Arawwawala, “Purification, detoxification, and incineration methods of minerals and metals in traditional medicine formulations of Sri Lanka,” *Evidence-Based Complementary and Alternative Medicine*, vol. 2021, Article ID 6634553, 8 pages, 2021.
- [6] K. Liu, S. Han, W. Gao et al., “Changes of mineralogical properties and biological activities of gypsum and its calcined products with different phase structures,” *Evidence-Based Complementary and Alternative Medicine*, vol. 2021, Article ID 6676797, 14 pages, 2021.
- [7] A. Pareek and N. Bhatnagar, “Physico-chemical characterization of traditionally prepared Yashada bhasma,” *Journal of Ayurveda and Integrative Medicine*, vol. 11, no. 3, pp. 228–235, 2020.
- [8] P. K. Mukherjee, R. K. Harwansh, S. Bahadur et al., “Development of Ayurveda - tradition to trend,” *Journal of Ethnopharmacology*, vol. 197, pp. 10–24, 2017.
- [9] Y. Xiao, C. Li, W. Xu et al., “Arsenic content, speciation, and distribution in Wild Cordyceps sinensis,” *Evidence-Based Complementary and Alternative Medicine*, vol. 2021, Article ID 6651498, 9 pages, 2021.
- [10] K. Fu, Y. Song, D. Zhang et al., “Determination of 18 trace elements in 10 batches of the Tibetan medicine Qishiwei Zhenzhu pills by direct inductively coupled plasma-mass spectrometry,” *Evidence-Based Complementary and Alternative Medicine*, vol. 2022, Article ID 8548378, 10 pages, 2022.
- [11] Y. Song, K. Fu, D. Zhang et al., “The absorption, distribution, and excretion of 18 elements of Tibetan medicine Qishiwei Zhenzhu pills in rats with cerebral ischemia,” *Evidence-Based Complementary and Alternative Medicine*, vol. 2021, Article ID 4508533, 11 pages, 2021.
- [12] K. Fu, D. Zhang, Y. Song et al., “Tibetan medicine Qishiwei Zhenzhu pills can reduce cerebral ischemia-reperfusion injury by regulating gut microbiota and inhibiting inflammation,” *Evidence-Based Complementary and Alternative Medicine*, vol. 2021, Article ID 2251679, 13 pages, 2021.
- [13] B. Tsoi, S. Wang, C. Gao et al., “Realgar and cinnabar are essential components contributing to neuroprotection of Angong Niu Huang Wan with no hepatorenal toxicity in transient ischemic brain injury,” *Toxicology and Applied Pharmacology*, vol. 377, Article ID 114613, 2019.
- [14] S. Wang, X. Xiao, A. Li, and P. Li, “The herbal constituents in an-gong-niu-huang wan (AGNH) protect against cinnabar- and realgar-induced hepatorenal toxicity and accumulations of mercury and arsenic in mice,” *Evidence-Based*

- Complementary and Alternative Medicine*, vol. 2021, Article ID 5566078, 9 pages, 2021.
- [15] F. Xia, A. Li, Y. Chai et al., "UPLC/Q-TOFMS-Based metabolomics approach to reveal the protective role of other herbs in an-gong-niu-huang wan against the hepatorenal toxicity of cinnabar and realgar," *Frontiers in Pharmacology*, vol. 9, p. 618, 2018.
- [16] X. Wang, L. Cao, J. Wu et al., "Exploring the mechanisms of arsenic trioxide (pishuang) in hepatocellular carcinoma based on network pharmacology," *Evidence-Based Complementary and Alternative Medicine*, vol. 2021, Article ID 5773802, 9 pages, 2021.
- [17] C. Chen, B. B. Zhang, A. L. Hu, H. Li, J. Liu, and F. Zhang, "Protective role of cinnabar and realgar in Hua-Feng-Dan against LPS plus rotenone-induced neurotoxicity and disturbance of gut microbiota in rats," *Journal of Ethnopharmacology*, vol. 247, Article ID 112299, 2020.
- [18] J. J. Liu, Y. Liang, Y. Zhang et al., "GC-MS profile of Hua-Feng-Dan and RNA-Seq analysis of induced adaptive responses in the liver," *Frontiers in Pharmacology*, vol. 13, Article ID 730318, 2022.
- [19] Z. Liu, H. Xiang, D. Xiang et al., "Revealing potential anti-fibrotic mechanism of Ganxianfang formula based on RNA sequence," *Chinese Medicine*, vol. 17, no. 1, p. 23, 2022.

Research Article

Inhibitory Effects of *Euphorbia ebracteolata* Hayata Extract ECB on Melanoma-Induced Hyperplasia of Blood Vessels in Zebrafish Embryos

Wenjing Dong ¹, Xinyue Han ¹, Chao Bao,¹ Saijilahu Tai,² Yuxia Bai ³, Liang Xu,⁴ Jingfeng Yang,¹ TinChung Leung ⁵, Wuliji Ao ³, and Wu Dong ¹

¹Inner Mongolia Key Laboratory of Toxicant Monitoring and Toxicant and Toxicology, College of Animal Science and Technology, Inner Mongolia University for Nationalities, Tongliao, Inner Mongolia 028000, China

²Mongolian State University of Education, Ulaanbaatar 210648, Mongolia

³Inner Mongolia Research Institute of Traditional Mongolian Medicine Engineering Technology/College of Mongolian Medicine and Pharmacy, Inner Mongolia University for Nationalities, Tongliao 028000, China

⁴Inner Mongolia Key Laboratory for the Natural Products Chemistry and Functional Molecular Synthesis, College of Chemistry and Chemical Engineering, Inner Mongolia University for Nationalities, Tongliao, Inner Mongolia 028000, China

⁵Julius L. Chambers Biomedical Biotechnology Research Institute, Dept of Biological & Biomedical Sciences, North Carolina Central University, Kannapolis, NC 28081, USA

Correspondence should be addressed to TinChung Leung; tleung@nccu.edu, Wuliji Ao; wuliji@126.com, and Wu Dong; dongwu2002@hotmail.com

Received 24 January 2021; Revised 25 March 2021; Accepted 5 April 2021; Published 27 April 2021

Academic Editor: Jie Liu

Copyright © 2021 Wenjing Dong et al. This is an open access article distributed under the Creative Commons Attribution License, which permits unrestricted use, distribution, and reproduction in any medium, provided the original work is properly cited.

Melanoma is a serious malignant form of skin cancer. Euphorbiaceae compound B (ECB, 2,4-dihydroxy-6-methoxy-3-methylacetophenone) is an acetophenone compound that is isolated from *Euphorbia ebracteolata* Hayata (EEH), an herbaceous perennial, and has antitumor activity. Here, we transplanted human melanoma cells into zebrafish embryos to establish a zebrafish/melanoma model. We showed that this model can be used to evaluate the therapeutic effect of EEH and ECB and discussed its potential mechanism of action. The results showed that ECB was an active ingredient of EEH in inhibiting melanoma-induced hyperplasia of blood vessels in zebrafish embryos, similar to the angiogenic inhibitor vatalanib. ECB inhibited the number and length of subintestinal veins ($p < 0.05$), as well as the distribution of melanoma in zebrafish embryos ($p < 0.05$). More importantly, unlike vatalanib, ECB only inhibited melanoma-induced abnormal and excessive growth of blood vessels in xenografts. In addition, ECB inhibited the mRNA expression of *vegfr2* and *vegfr3* in zebrafish. Both *vegfr2* and *vegfr3* are essential genes that regulate blood vessel formation and upregulate the expression of *p53* and *casp3a* genes in zebrafish. Together, the above-mentioned results indicate that ECB has a potential antimelanoma effect *in vivo*, which may be mediated by inhibiting vascular endothelial growth factor receptors.

1. Introduction

Malignant melanoma is the most serious type of skin cancer, which is caused by hyperplasia of melanocytes in the skin. In the body, melanoma cells can rapidly metastasize, and patients with metastatic melanoma have a survival of no more than five years [1]. Euphorbiaceae compound B (ECB, 2, 4-

dihydroxy-6-methylbenzoidone) is a compound of benzene ketones in the *Euphorbia ebracteolata* Hayata (EEH) and *Euphorbia fischeriana* Steud [2, 3]. Studies that focused on the anticancer effects of diterpenoids in Euphorbiaceae have been reported; however, studies on ECB are limited. Blocking the pathway underlying tumor angiogenesis may be a unique way to block the growth of blood vessels that

support tumor growth [4]. The zebrafish model can be used as a viable model for whole-animal screening using small molecules that affect tumor angiogenesis [5]. In particular, the subintestinal vein (SIV) of zebrafish/tumor xenografts can be visualized noninvasively in real time using vascular-specific transgenic zebrafish or can be stained using blood vessel dye and visualized under a microscope [6]. Koenig et al. showed that *vegfaa* was expressed at the site of intestinal vascularization and might provide a guiding signal and that *vegfc* overexpression could lead to SIV overgrowth. The authors suggested that (1) Vegfaa signaling might regulate endothelial cells to migrate out of the existing vasculature and subsequently merge to form intestinal blood vessels and that (2) Vegfc could induce growth of the SIV [7]. PTK787, a potent angiogenic inhibitor, inhibits vascular endothelial growth factor receptors (VEGFR) and platelet-derived growth factor receptor (PDGFR) tyrosine kinase and blocks cell proliferation and cell survival, resulting in cell death and reduced blood vessel density in leiomyosarcoma cells, as well as in zebrafish xenografts [8, 9]. The potent B-raf inhibitor PLX4720 (PLX) that acts against melanoma reduced the binding of C-MYC to the *VEGF* promoter to reduce the expression of VEGF in melanoma cells and increased the infiltration of adoptively transferred T cells, thereby leading to an antitumor effect [10].

As a model for high-throughput screening of anticancer drugs, zebrafish have been shown to be a potential model. In this study, we used *Tg(flk1:GFP)* transgenic zebrafish as a model to quantify fluorescent blood vessels after transplantation of melanoma cells into zebrafish embryos. We aimed to use this model for screening the antimelanoma effect of ECB through tumor-induced angiogenesis and metastasis. The potential underlying mechanisms involved were also studied (see Graphic abstract).

2. Materials and Methods

2.1. Chemicals and Reagents. Human melanoma cells (A2058 cells), originated from a 43-year-old Caucasian adult male, were obtained from the American Type Culture Collection (ATCC, Manassas, VA, USA). Human umbilical vein endothelial cells (HUVECs) were extracted from human umbilical cord vein tissue and obtained from ScienCell (San Diego, CA, USA). The Vybrant™ CM-DiI cell-labeling solution (CM-DiI) was purchased from Invitrogen (Carlsbad, CA, USA). Vatalanib (PTK) and PLX-4720 (PLX) were purchased from MedChemExpress (Monmouth Junction, NJ, USA). ECB was purchased from the National Institutes for Food and Drug Control (Beijing, China). Other compounds and reagents were purchased from Sigma-Aldrich (St. Louis, MO, USA).

2.2. Preparation and High-Performance Liquid Chromatography Analysis of EEH. *Euphorbia ebracteolata* Hayata (EEH) was provided by Liang Xu's Lab, and EEH was authenticated and analyzed by Dr. Liang Xu from the Inner Mongolia Key Laboratory for the Natural Products Chemistry and Functional Molecular Synthesis, College of

Chemistry and Chemical Engineering, Inner Mongolia University for Nationalities (Tongliao, China). A total of 10 g EEH powder was soaked into 100 mL of 90% ethanol at room temperature for 24 hours. The supernatant was concentrated to 10 mL after the mixture was refluxed for 3 hours, filtered through a 0.22 μ m filter, and used as a 1 g/mL stock solution. ECB is a major ingredient of EEH (Figure S1) [11].

2.3. Zebrafish Breeding. *Tg(flk1:GFP)* zebrafish were donated by the Chinese Academy of Sciences and raised in a zebrafish breeding system (Environ Science, Beijing, China) at a water temperature of 28.5°C and a 14 : 10-hour day-night cycle. The zebrafish breeding and testing process was approved by the Animal Protection Association of Inner Mongolia University for Nationalities (Tong Liao, China).

2.4. Establishment of a Zebrafish/Melanoma Xenograft Model. Melanoma cells were labeled with a fluorescence dye (CM-DiI), and zebrafish/melanoma xenografts were cultured in a 35°C incubator for 2 h, then transferred to a 28.5°C incubator until 24 hours after injection (hpi) and 48 hpi. After 6 h of culture (6 hpi), zebrafish/melanoma xenografts that showed the same amount of melanoma cells under a fluorescence microscope were selected for further analysis.

2.5. EEH or ECB Treatment and Calculation of Blood Vessel Number, Length, and CM-DiI Labeling (Melanoma Cells) Area in Zebrafish. Zebrafish embryos were imaged using an inverted fluorescence microscope (Olympus IX73, Tokyo, Japan) at 24 hpi to capture SIV blood vessels and melanoma fluorescence in zebrafish embryos. ImageJ software (NIH, Bethesda, MD, USA) was used to measure the length of SIV ectopic blood vessels, the CM-DiI labeling area, and the number of ectopic blood vessels. After imaging at 24 hpi, 10 zebrafish xenografts were placed in a 6-well plate and treated with EEH, ECB, PTK, PLX, or buffer for the control group. Zebrafish xenografts were cultured for an additional 24 h prior to a second round of fluorescence imaging at 48 hpi for quantification.

2.6. Cell Culture and Labeling. A2058 cells and/or HUVECs were cultured in a 37°C cell culture incubator at 5% CO₂. Tumor cells at a confluency of 60%–70% were labeled with CM-DiI for 20 min at 37°C, washed 3 times, 10 minutes with HBSS, and cultured overnight at 37°C. The next day, cells were trypsinized and collected for microinjection.

2.7. Total RNA Isolation and Quantitative Real-Time Polymerase Chain Reaction. Total RNA was extracted using the TRIzol reagent [12]; *vegfa*, *vegfr2*, *vegfr3*, *p53*, *casp3a*, and *18s* (supplemental data: Table S1) genes were used for quantitative real-time PCR. As an internal reference, 18S rRNA was used. The delta-delta Ct ($2^{-\Delta\Delta C_T}$) method was used to calculate the relative change in gene expression.

2.8. Statistical Analysis. For statistical analysis, GraphPad Prism 5 software (GraphPad Software Inc., La Jolla, CA, USA) was used. Differences between groups were analyzed using one-way analysis of variance (ANOVA) followed by Tukey's post hoc test. Significance levels were set to * $p < 0.05$; ** $p < 0.01$; and *** $p < 0.001$.

3. Results

3.1. Inhibitory Effect of EEH or ECB on Melanoma-Induced Hyperplasia of Blood Vessels in Zebrafish Embryos. A2058 cells were microinjected beneath the surface of the yolk area at the 48 hpf stage in transgenic *Tg(flk1:GFP)* zebrafish embryos. At 24 hpi, 50 $\mu\text{g}/\text{mL}$ of EEH was added to the embryo medium of the zebrafish/melanoma xenograft, containing the injected cells labeled with red fluorescent dye (CM-DiI, Invitrogen). Tumor-induced angiogenesis was quantified by evaluating the number and length of ectopic vessels in the SIV of zebrafish/tumor xenografts at 24 and 48 h after injection (24 and 48 hpi) (Figure 1). The length of the SIV ectopic blood vessels in control HUVECs and A2058 cells was measured. Our data showed that the length of SIV ectopic blood vessels in the A2058 group was significantly higher than that in the control group at both 24 and 48 hpi ($p < 0.001$). In addition, treatment of xenografts with 50 $\mu\text{g}/\text{mL}$ EEH reduced the length of SIV ectopic blood vessels of A2058 xenografts. To verify the results on ectopic vessel length, we also quantified the number of ectopic vessels in each xenograft and found that EEH had a more clear effect on the inhibition of tumor angiogenesis in A2058 xenografts at 48 hpi ($p < 0.05$).

Similar to EEH experiments at 24 hpi, 20 $\mu\text{g}/\text{mL}$ of ECB and 1 μM of PTK were added to the embryo medium of the zebrafish/melanoma xenograft, and tumor-induced angiogenesis was quantified by evaluating the number and length of ectopic vessels in the SIV of zebrafish/tumor xenografts at 24 and 48 hpi (Figure 2). The length of SIV ectopic blood vessels in control HUVECs and A2058 cells was measured. Our data showed that the length of SIV ectopic blood vessels in the A2058 group was significantly higher than that in the control group at both 24 and 48 hpi ($p < 0.01$). In addition, treatment of xenografts with 20 $\mu\text{g}/\text{mL}$ ECB or 1 μM PTK, which is antiangiogenic, significantly reduced the length of SIV ectopic blood vessels of A2058 xenografts ($p < 0.001$). Compared with control HUVECs, the length of ectopic vessels in both of ECB or PTK groups was not significantly different ($p > 0.05$) (Figure 2). Because the number of ectopic vessels was very small, it would be unable to compare the differences between treatments. To verify the results on ectopic vessel length, we also quantified the number of ectopic vessels in each xenograft and found that both ECB and PTK had a similar effect on the inhibition of tumor angiogenesis in A2058 xenografts at 48 hpi ($p < 0.05$). No significant differences were observed between A2058 cells and control HUVECs.

In embryos that were treated with different concentrations of ECB and PTK, no significant differences were observed at 72 hpf in perimeters or the area of the SIV between ECB groups and the control group. However, the

positive control group that was treated with 1 μM PTK showed reduction in both area and perimeter (length) of SIV blood vessels of the SIV compared with the control group/or the 20 $\mu\text{g}/\text{mL}$ ECB-treated group ($p < 0.05$). In addition, intersegment vessels (ISVs), as well as trunk artery and veins, were mostly missing in the 1 μM PTK-treated group. Therefore, our findings suggested that ECB treatment did not affect normal angiogenesis in zebrafish embryos (Figure 3). This contrasted with the anti-angiogenic molecule VEGK that showed to be a potent inhibitor of all known VEGFRs (VEGFR-1, VEGFR-2, and VEGFR-3).

3.2. Effect of ECB on the Metastasis of Melanoma Cells in Zebrafish Xenografts. The same number of melanoma cells (3×10^7 cells/mL) was injected into the superficial region of the yolk sac after the zebrafish developed for 48 h. The metastatic effect of A2058 cells was observed in the zebrafish embryos at 6 hpi, 24 hpi, and 48 hpi (Figure 4). At 24 hpi, 20 $\mu\text{g}/\text{mL}$ ECB and the melanoma inhibitor PLX were added and zebrafish/tumor xenografts were analyzed after 24 h. The data showed that the area of CM-DiI labeling (melanoma cells) at 6 hpi, 24 hpi, and 48 hpi in zebrafish embryos was 0.009 mm^2 , 0.012 mm^2 , and 0.013 mm^2 , respectively. In zebrafish, the area of A2058 cells was reduced to 0.005 mm^2 after treatment with 20 $\mu\text{g}/\text{mL}$ ECB, and the area of A2058 cells was reduced to 0.004 mm^2 after treatment with 1 μM PLX for 24 h ($p < 0.001$) (Figure 4(g)).

3.3. Effect of ECB on Blood Vessels and the Expression of Apoptosis-Associated Genes in a Zebrafish/Melanoma Xenograft Model. A2058 cells were labeled with CM-DiI, injected into zebrafish embryos at 48 hpf, and treated with 0 (Control) or 20 $\mu\text{g}/\text{mL}$ ECB or 1 μM PTK for 24 h from 72 hpf (24 hpi). Embryos were collected for the quantification of mRNA expression of *vegfa*, *vegfr2*, and *vegfr3* at 96 hpf (48 hpi) (Figure 5). The data showed that ECB or the vascular inhibitor PTK downregulated the mRNA expression of *vegfa*. Furthermore, PTK significantly downregulated the mRNA expression of *vegfr2*, which was 0.6-fold compared with that of the control group. Compared with the control group, ECB or PTK significantly downregulated the mRNA expression of *vegfr3* by 0.5-fold and 0.38-fold, respectively ($p < 0.05$). Furthermore, compared with the A2058 cells-injected group, ECB significantly increased the mRNA expression of *p53* by 2.3-fold and increased that of *casp3a* by 2.9-fold ($p < 0.05$). No significant changes were observed for PLX groups ($p > 0.05$) (Figure 6).

4. Discussion

To evaluate the inhibitory effect of EEH and ECB on melanoma, *Tg(flk1:GFP)* transgenic zebrafish embryos were used as an *in vivo* model. In brief, A2058 cells were labeled with red fluorescent dye and microinjected into 48 hpf zebrafish embryos. Therefore, the labeled cancer cells can be monitored for tumor growth and tumor-induced neovascularization in developmental zebrafish embryos.

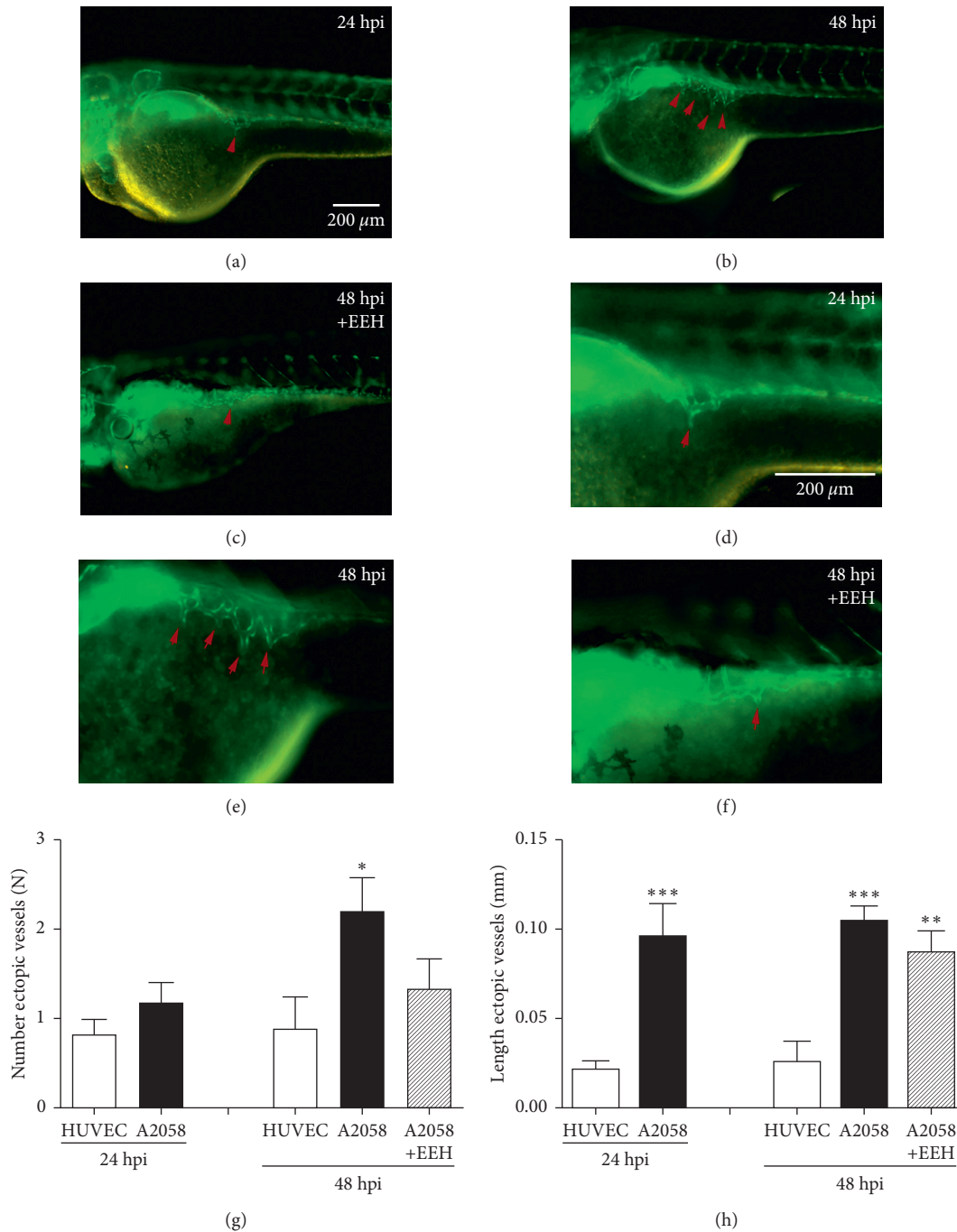


FIGURE 1: *Euphorbia ebracteolata* Hayata (EEH) inhibited SIV ectopic hyperplasia induced by melanoma cells in transgenic *Tg (flk1:GFP)* zebrafish embryos. Human melanoma cells were microinjected into zebrafish embryos at 48 hpf, and the resulting xenografts were imaged with a fluorescence microscope after 24 and 48 h (hpi), respectively. (a, d) SIV ectopic vessels in green fluorescence (red arrows) at 24 hpi zebrafish embryo (control). (b, e) SIV ectopic vessels (red arrows) at 48 hpi in zebrafish embryo (control). (c, f) SIV ectopic vessels after treatment with 50 μg/mL EEH for 48 (h). (g) The length of ectopic blood vessels in A2058 or HUVEC xenografts at 24 and 48 hpi and the effects after treatment with *Euphorbia ebracteolata* Hayata (EEH) (* $p < 0.05$). (h) The number of ectopic blood vessels in A2058 or HUVEC xenografts at 24 hpi and 48 hpi and the effects after treatment with EEH (* $p < 0.05$). Scale bar = 200 μm.

Injection of melanoma cells into zebrafish embryos not only resulted in the metastatic spread of melanoma cells but also induced angiogenesis (SIV) in zebrafish/tumor xenografts (Figure 1). Together, these results suggested that transplanted melanoma cells induced neovascularization in

zebrafish/tumor xenografts. First, we found that EEH significantly inhibited the increase in length and number of ectopic blood vessels of the SIV. Next, we confirmed that ECB was the active ingredient of EEH and was more potent in inhibiting the length and number of ectopic blood vessels

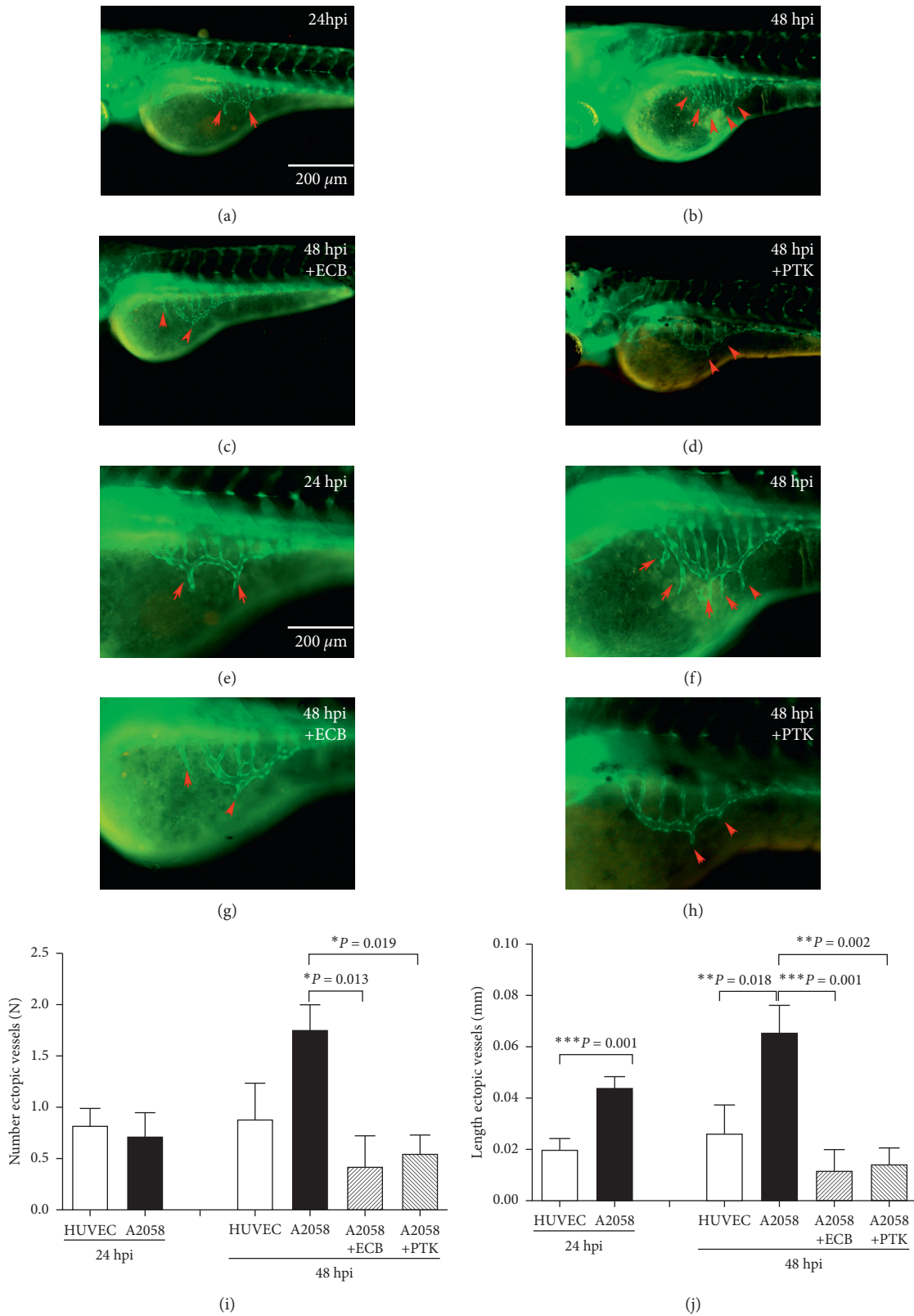


FIGURE 2: Euphorbiaceae compound B (ECB) inhibited SIV ectopic hyperplasia induced by melanoma cells in transgenic *Tg (flk1:GFP)* zebrafish embryos. Human melanoma cells were microinjected into zebrafish embryos at 48 hpf, and the resulting xenografts were imaged with a fluorescence microscope after 24 and 48 h (hpi), respectively. (a, e) SIV ectopic vessels in green fluorescence (red arrows) at 24 hpi zebrafish embryo (control). (b, f) SIV ectopic vessels (red arrows) at 48 hpi zebrafish embryo (control). (c, g) SIV ectopic vessels after treatment with 20 $\mu\text{g}/\text{mL}$ ECB for 48 h. (d, h) SIV ectopic vessels after treatment with 1 μM PTK for 48 h. (i) The length of ectopic blood vessels in A2058 or HUVEC xenografts at 24 and 48 hpi and the effects after treatment with ECB and PTK ($*p < 0.05$). (j) The number of ectopic blood vessels in A2058 or HUVEC xenografts at 24 hpi and 48 hpi and the effects after treatment with ECB or PTK ($*p < 0.05$). Scale bar = 200 μm .

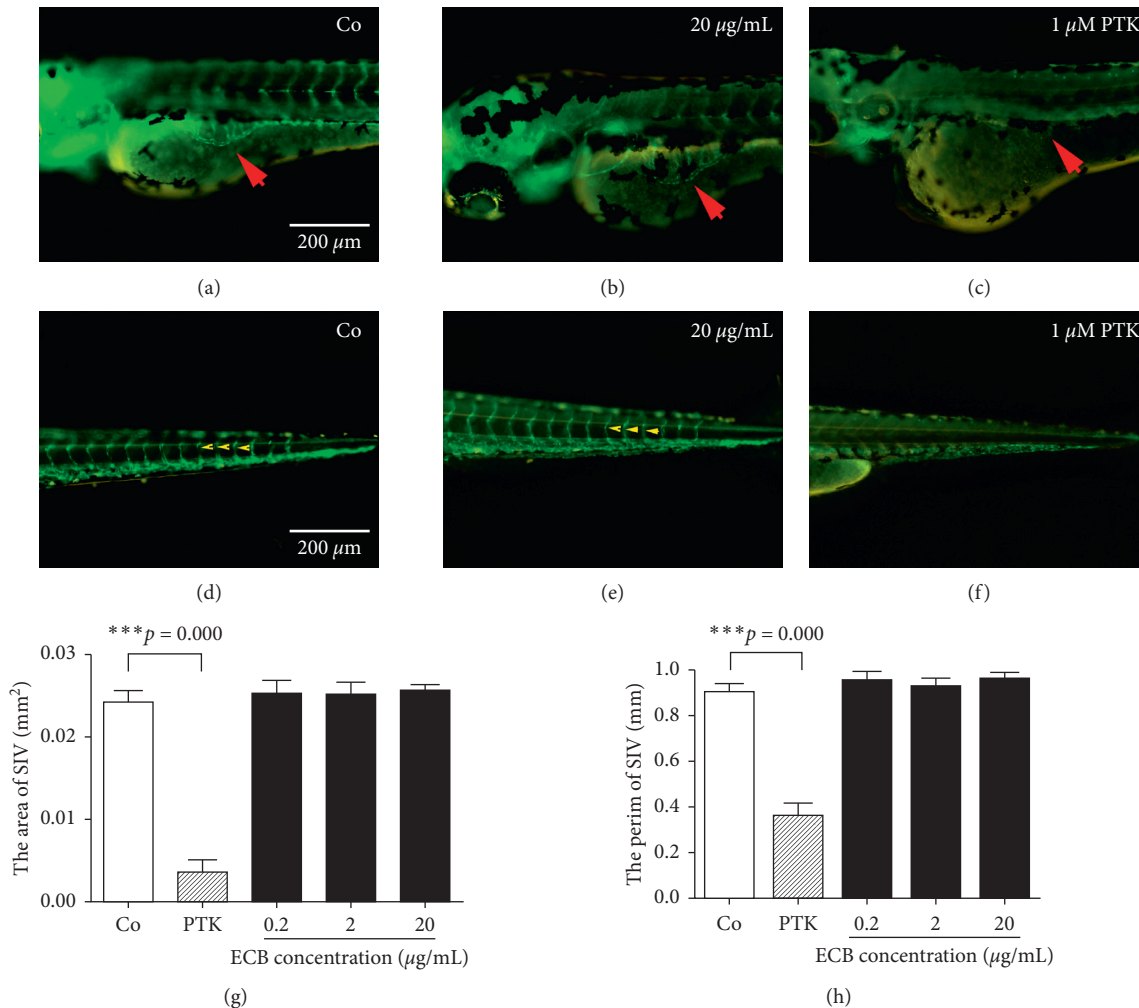


FIGURE 3: Effect of ECB on SIV and ISV angiogenesis in zebrafish embryos. Zebrafish embryos were imaged after treatment with ECB or PTK from 4 hpf to 72 hpf. (a, b) Control group. (b, e) ECB group. (c, f) PTK group. Red arrows point to SIV vessels above the yolk region (a-c). Yellow arrows show ISVs in the tail region (d-f). (g) The area covered by SIV vessels in zebrafish embryos (** $p < 0.001$). (h) The perimeter (length) of SIV vessels in zebrafish embryos (** $p < 0.001$). Scale bar = 200 µm.

of the SIV and inhibited the migration of A2058 cells in zebrafish/melanoma xenografts. Furthermore, ECB reduced the mRNA expression of zebrafish *vegfa*, *vegfr2*, and *vegfr3* and induced the mRNA expression of zebrafish *p53* and *casp3a* in xenografts.

Remodeling of the vascular network was required to support the tissues needed for oxygen and nutrients during embryonic development [13]. The occurrence and metastasis of tumors increased the proliferation of blood vessels. Therefore, many anticancer drugs suppressed cancer by inhibiting angiogenesis [14]. Even for short-term treatment (1 h), the angiogenesis inhibitor SU5416 prevented new angiogenesis and angiogenic blood vessel formation. However, TNP470 required continuous exposure to block formation of the SIV and had no obvious effect on angiogenesis [15]. To screen chemical compounds, Manfred et al. made *mitf::xmrk* transgenic medaka. This was a stable transgenic melanoma model in which tumor development was observed in all gene carriers [16]. Here, we used a zebrafish/melanoma xenograft model to evaluate tumor-

induced angiogenesis of the SIV in zebrafish embryos and showed that EEH or ECB inhibited the length of SIV ectopic blood vessels and reduced the number of blood vessels. Lenard et al. believed that the decrease in blood vessels was caused by cell self-fusion [13]. In addition, Koenig et al. suggested that *Vegfa* signaling can guide endothelial cells to migrate out of the existing vasculature and merge to form intestinal blood vessels. A similar mechanism may be used during angiogenesis in other organs [7]. Zhou et al. used the VEGFR1 antagonistic peptide F56 as an inhibitor to act on blood vessels and found that F56 did not affect VEGF-A-induced endothelial cell proliferation but did reduce endothelial cell migration and angiogenesis. In addition, F56 inhibited angiogenesis of the chorioallantoic membrane in chicken embryos and the SIV in zebrafish embryo. Monomeric peptide F56 has significant antitumor activity by inhibiting angiogenesis [17]. Ponatinib is a vascular inhibitor that is used for FDA-approved cancer treatment [18] and can also inhibit the formation of ISVs and the SIV in zebrafish embryos. The antiangiogenic effect of

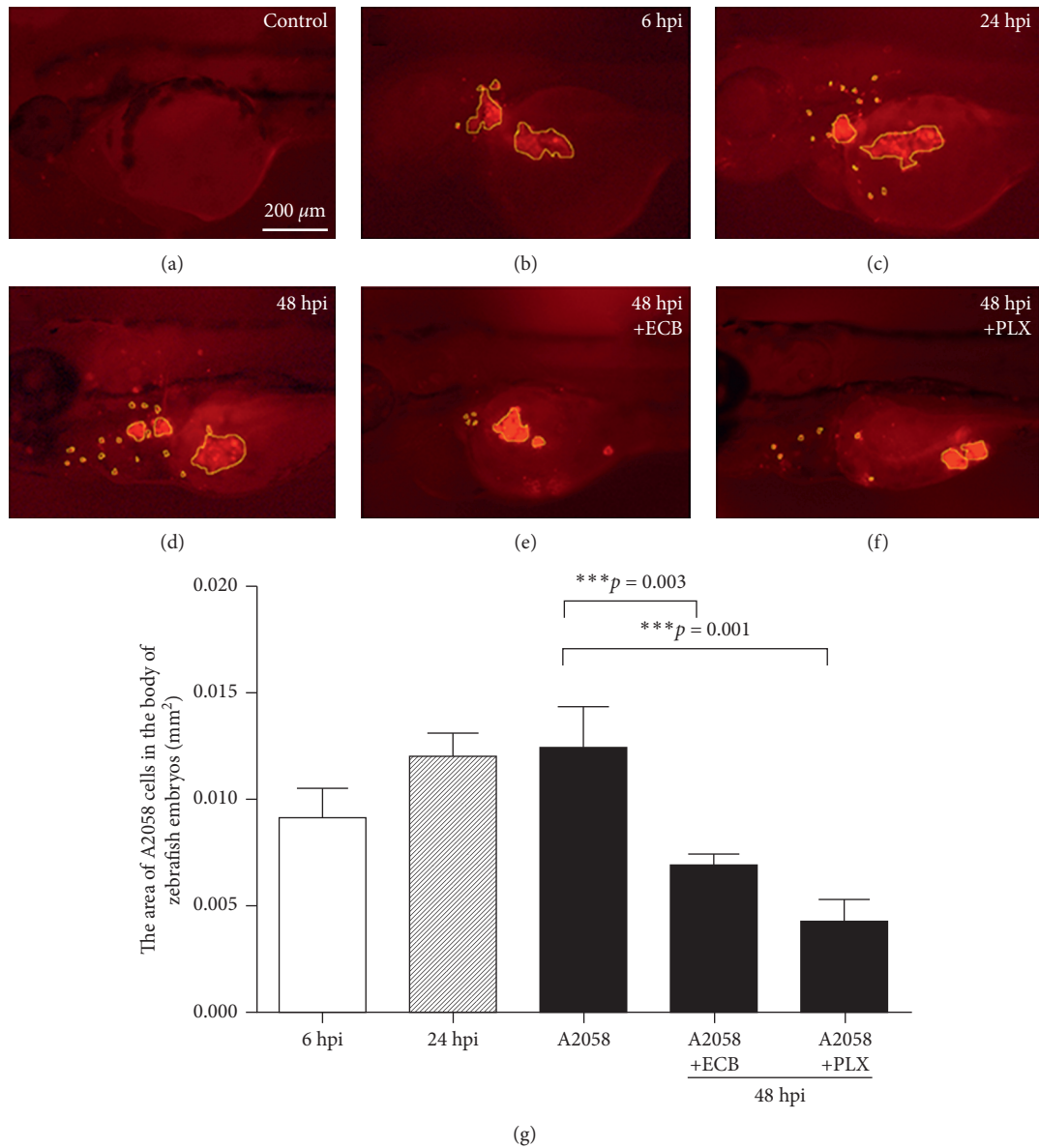


FIGURE 4: Effect of Euphorbiaceae compound B (ECB) on metastasis of melanoma cells in zebrafish xenografts. Zebrafish embryos were injected with A2058 cells at 48 hpf and observed at 6 hpi, 24 hpi, and 48 hpi, respectively. (a) Not injected. (b–d) A2058 cells were injected into zebrafish embryos at 48 hpf and observed at 6 hpi, 24 hpi, and 48 hpi, respectively. (e) A2058 cells were injected into zebrafish embryos and treated with 20 $\mu\text{g}/\text{mL}$ ECB for 24 h and observed at 48 hpi. (f) A2058 cells were injected into zebrafish embryos and treated with 1 μM PLX4720 (PLX) for 24 h and observed at 48 hpi. (g) The area of CM-DiI labeling (melanoma cell) in the zebrafish embryos. Scale bar = 200 μm . *** indicates a significant difference ($p < 0.001$).

Ponatinib on HUVECs was evaluated using cell proliferation and migration, angiogenesis, and wound-healing assays. Ponatinib inhibited Vegf-induced phosphorylation of Vegfr2 and its downstream signaling, including the Akt/eNOS/NO pathway and the MAPK pathway (ERK and p38MAPK) [12]. In addition, 12-deoxyphorbol 13-palmitate in *Euphorbia fischeriana* Steud inhibited the Vegfr-2 signaling pathway, reduced microvessel density, inhibited VEGF, and blocked the PI3K/Akt/mTOR signaling pathway, thereby resulting in inhibition of MCF-7 breast cancer cell proliferation in mice [19, 20]. Similar to these findings, we found that ECB significantly inhibited the ectopic

vascular length of the SIV in zebrafish and inhibited the mRNA expression of *vegfr2*, *vegfr3*, and *vegfr1* in zebrafish xenografts.

Jolkinolide B isolated from *Euphorbia fischeriana* Steud induced apoptosis in a B16F10 mouse melanoma model by altering glycolysis. In addition, jolkinolide B treatment increased mRNA expression of the apoptosis gene *Bax*, *Casp3*, and *Casp9*, reduced mRNA expression of antiapoptosis genes *Bcl2*, reduced the mitochondrial membrane potential of B16F10 cells, and increased the level of reactive oxygen species (ROS), thereby having antitumor effects [21]. Moreover, 12-deoxyphorbol 13-palmitate isolated from

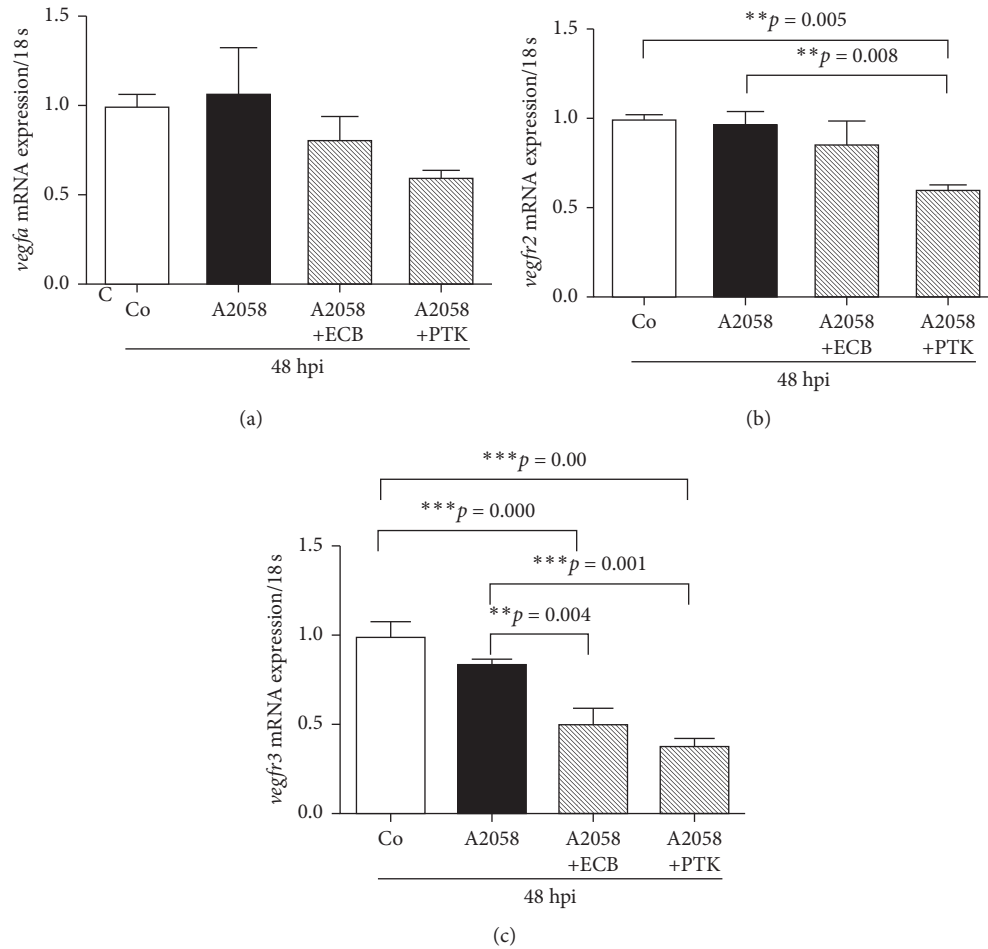


FIGURE 5: Effect of Euphorbiaceae compound B (ECB) on zebrafish *vegfa*, *vegfr2*, and *vegfr3* mRNA expression in xenografts using real-time PCR: (a) *vegfa* mRNA expression, (b) *vegfr2* mRNA expression, and (c) *vegfr3* mRNA expression. ** and *** indicate a significant difference (** $p < 0.01$; *** $p < 0.001$).

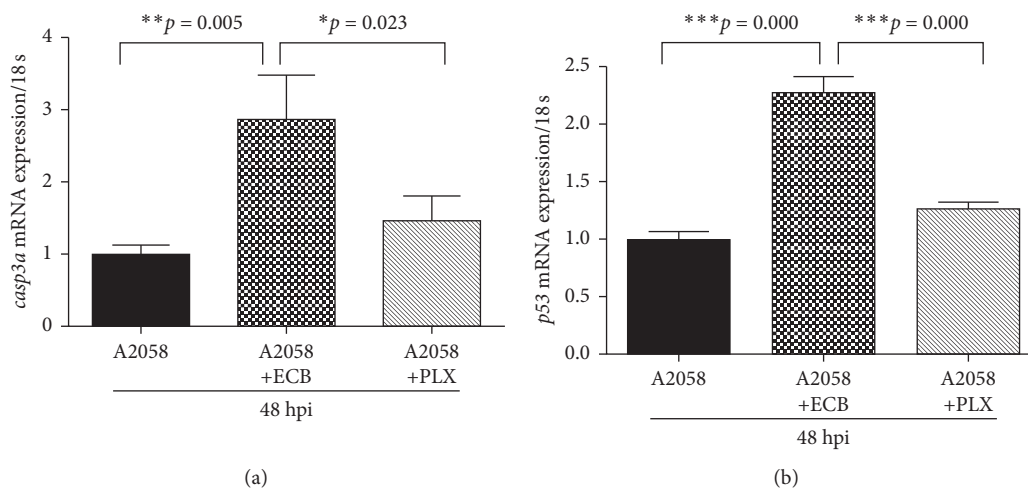


FIGURE 6: Euphorbiaceae compound B (ECB) affected the expression of zebrafish *casp3a* and *p53* mRNA in xenografts using real-time PCR. A2058 cells were labeled with CM-DiI, injected into zebrafish embryos at 48 hpf, and treated with 20 $\mu\text{g}/\text{mL}$ ECB and 1 μM PLX or the medium only control at 72 hpf (24 hpi), respectively. *Casp3a* (a) and *p53* (b) mRNA expressions were quantified. * $p < 0.05$, ** $p < 0.01$, and *** $p < 0.001$.

Euphorbia fischeriana Steud induced cell cycle arrest at the G2-M checkpoint of BGC823 cells and upregulated the expression of *p53*, *p21*, and *IκB-α* in tumor cells, leading to tumor cell apoptosis and the inhibition of tumor growth [22]. In this study, a zebrafish/melanoma xenograft model was established to demonstrate that ECB from *Euphorbia ebracteolata* treatment also inhibited proliferative blood vessels, which was associated with increased mRNA expression of *casp3a* and *p53* in zebrafish.

In this study, we investigated the inhibitory effect of EEH or ECB on hyperplasia of blood vessels caused by human melanoma cells in zebrafish embryos. EEH and ECB inhibited melanoma-induced vascular proliferation of the SIV in zebrafish. This inhibitory effect may be achieved by blocking zebrafish *vegfa* and mRNA expression of the Vegf receptors *vegfr2* and *vegfr3* that regulate blood vessels. The decrease in blood vessels may be affected by the apoptotic pathway. It is noteworthy that ECB treatment only inhibited abnormal blood vessel development induced by melanoma, which is different from vascular inhibitors that universally inhibit blood vessel growth, including normal angiogenesis. Taken together, these data show that ECB may have potential therapeutic value for anticancer treatment.

Data Availability

The study data are available from the corresponding author upon request.

Conflicts of Interest

The authors declare no conflicts of interest.

Acknowledgments

This study was funded by the National Natural Science Foundation of China (81360508 and 82060672) to Jingfeng Yang; Inner Mongolia University for Nationalities, China (MDXK008), to Wu Dong; Inner Mongolia Grassland Talent Project, China (2020), to Wu Dong; Natural Science Foundation of Inner Mongolia Autonomous Region of China (2018MS08033 to Jingfeng Yang, 2020MS08103 to Wu Dong); Open Project Program of Inner Mongolia Key Laboratory of Toxicant Monitoring and Toxicology, China (MDK2018027), to Wenjing Dong; and Open Project Program of Inner Mongolia Research Institute of Traditional Mongolian Medicine Engineering Technology, China (MDK2019051 and MDK2020002), to Wu Dong. TL is partially supported by grants U54MD012392 from NIH/NIMHD and U54CA156735 from NIH/NCI.

Supplementary Materials

Graphic abstract: Scheme for EEH or ECB inhibition of SIV ectopic hyperplasia induced by melanoma cells in transgenic *Tg(flk1:GFP)* zebrafish/tumor xenograft embryos. Table S1. Primer for quantitative real-time PCR. Figure S1. HPLC chromatogram of EEH. A: EEH extracts, peak 8: ECB, 2,4-

dihydroxy-6-methylbenzoidone, and B: Reference substance (EBC) (Bao, Y, 2014). (*Supplementary Materials*)

References

- [1] S. Singh, A. Zafar, S. Khan, and I. Naseem, "Towards therapeutic advances in melanoma management: an overview," *Life Sciences*, vol. 174, pp. 50–58, 2017.
- [2] Y. Ma, H. Wang, and M. Guo, "Stainless steel wire mesh supported molecularly imprinted composite membranes for selective separation of ebracteolata compound B from *Euphorbia fischeriana*," *Molecules*, vol. 24, p. 3, 2019.
- [3] A. Wang, X. Gao, X. Huo et al., "Antioxidant acetophenone glycosides from the roots of *Euphorbia ebracteolata* Hayata," *Natural Product Research*, vol. 32, no. 18, pp. 2187–2192, 2018.
- [4] R. Zhou, J. M. Curry, L. D. Roy et al., "A novel association of neuropilin-1 and MUC1 in pancreatic ductal adenocarcinoma: role in induction of VEGF signaling and angiogenesis," *Oncogene*, vol. 35, no. 43, pp. 5608–5618, 2016.
- [5] K. S. Moshal, K. F. Ferri-Lagneau, and T. Leung, "Zebrafish model: worth considering in defining tumor angiogenesis," *Trends in Cardiovascular Medicine*, vol. 20, no. 4, pp. 114–119, 2010.
- [6] K. S. Moshal, K. F. Ferri-Lagneau, J. Haider, P. Pardhanani, and T. Leung, "Discriminating different cancer cells using a zebrafish in vivo assay," *Cancers*, vol. 3, no. 4, pp. 4102–4113, 2011.
- [7] A. L. Koenig, K. Baltrunaite, N. I. Bower et al., "Vegfa signaling promotes zebrafish intestinal vasculature development through endothelial cell migration from the posterior cardinal vein," *Developmental Biology*, vol. 411, no. 1, pp. 115–127, 2016.
- [8] J. Dreves, R. Müller-Driver, C. Wittig et al., "PTK787/ZK 222584, a specific vascular endothelial growth factor-receptor tyrosine kinase inhibitor, affects the anatomy of the tumor vascular bed and the functional vascular properties as detected by dynamic enhanced magnetic resonance imaging," *Cancer Research*, vol. 62, no. 14, pp. 4015–4022, 2002.
- [9] A. K. A. Gaumann, H. C. A. Drexler, S. A. Lang et al., "The inhibition of tyrosine kinase receptor signalling in leiomyosarcoma cells using the small molecule kinase inhibitor PTK787/ZK222584 (Vatalanib)," *International Journal of Oncology*, vol. 45, no. 6, pp. 2267–2277, 2014.
- [10] C. Liu, W. Peng, C. Xu et al., "BRAF inhibition increases tumor infiltration by T cells and enhances the antitumor activity of adoptive immunotherapy in mice," *Clinical Cancer Research*, vol. 19, no. 2, pp. 393–403, 2013.
- [11] Y. Bao, *Analysis of HPLC Chromatographic Fingerprint of Mongolian Medicine Euphorbia Fischeriana Steud and HPLC-MSn Analysis of its Different Processing Products*, Inner Mongolia University for Nationalities, Tongliao, China, 2014.
- [12] N. Ai, C.-M. Chong, W. Chen et al., "Ponatinib exerts anti-angiogenic effects in the zebrafish and human umbilical vein endothelial cells via blocking VEGFR signaling pathway," *Oncotarget*, vol. 9, no. 62, pp. 31958–31970, 2018.
- [13] A. Lenard, S. Daetwyler, C. Betz, E. Ellertsdottir, H. G. Belting, and J. Huisken, "Endothelial cell self-fusion during vascular pruning," *PLoS Biology*, vol. 13, no. 4, Article ID e1002126, 2015.
- [14] H. Luo, C. T. Vong, H. Chen, Y. Gao, P. Lyu, and L. Qiu, "Naturally occurring anti-cancer compounds: shining from Chinese herbal medicine," *Chinese Medicine*, vol. 14, p. 48, 2019.

- [15] G. N. Serbedzija, E. Flynn, and C. E. Willett, "Zebrafish angiogenesis: a new model for drug screening," *Angiogenesis*, vol. 3, no. 4, pp. 353–359, 1999.
- [16] S. Manfred, W. Brigitta, A. G. C. L. Juliette, T. Yoshihito, T. Shunichi, and M. Svenja, "A mutated EGFR is sufficient to induce malignant melanoma with genetic background-dependent histopathologies," *Journal of Investigative Dermatology*, vol. 130, no. 1, pp. 249–258, 2010.
- [17] Z. Zhou, C. Zhao, L. Wang et al., "A VEGFR1 antagonistic peptide inhibits tumor growth and metastasis through VEGFR1-PI3K-AKT signaling pathway inhibition," *American Journal of Cancer Research*, vol. 5, no. 10, pp. 3149–3161, 2015.
- [18] J. Kim, A. Nair, P. Keegan et al., "Evaluation of serious postmarket safety signals within 2 Years of FDA approval for new cancer drugs," *The Oncologist*, vol. 25, no. 4, pp. 348–354, 2019.
- [19] H.-Y. Xu, Y.-M. Pan, Z.-W. Chen et al., "12-Deoxyphorbol 13-palmitate inhibit VEGF-induced angiogenesis via suppression of VEGFR-2-signaling pathway," *Journal of Ethnopharmacology*, vol. 146, no. 3, pp. 724–733, 2013.
- [20] Y. Yang, H. Cong, C. Han, L. Yue, H. Dong, and J. Liu, "12-Deoxyphorbol 13-palmitate inhibits the expression of VEGF and HIF-1 α in MCF-7 cells by blocking the PI3K/Akt/mTOR signaling pathway," *Oncology Reports*, vol. 34, no. 4, pp. 1755–1760, 2015.
- [21] C. Gao, X. Yan, B. Wang, L. Yu, J. Han, and D. Li, "Jolkinolide B induces apoptosis and inhibits tumor growth in mouse melanoma B16F10 cells by altering glycolysis," *Science Reports*, vol. 6, p. 36114, 2016.
- [22] H.-Y. Xu, Z.-W. Chen, H. Li et al., "12-Deoxyphorbol 13-palmitate mediated cell growth inhibition, G2-M cell cycle arrest and apoptosis in BGC823 cells," *European Journal of Pharmacology*, vol. 700, no. 1-3, pp. 13–22, 2013.

Research Article

The Herbal Constituents in An-Gong-Niu-Huang Wan (AGNH) Protect against Cinnabar- and Realgar-Induced Hepatorenal Toxicity and Accumulations of Mercury and Arsenic in Mice

Songsong Wang ¹, Xiao Xiao ^{2,3}, Ao Li ³, and Peng Li ¹

¹State Key Laboratory of Quality Research in Chinese Medicine, Institute of Chinese Medical Sciences, University of Macau, Macao 999078, China

²College of Pharmacy and Bioengineering, Chongqing University of Technology, Chongqing 400054, China

³Clinical Research Center, Affiliated Hospital of Guangdong Medical University, Zhanjiang 524001, Guangdong, China

Correspondence should be addressed to Ao Li; ao_livip@gdmu.edu.cn and Peng Li; pli1978@hotmail.com

Received 14 January 2021; Revised 19 March 2021; Accepted 24 March 2021; Published 2 April 2021

Academic Editor: Jie Liu

Copyright © 2021 Songsong Wang et al. This is an open access article distributed under the Creative Commons Attribution License, which permits unrestricted use, distribution, and reproduction in any medium, provided the original work is properly cited.

An-Gong-Niu-Huang Wan (AGNH) has been a well-known cinnabar- and realgar-containing compound recipe for cerebral diseases. Unfortunately, its clinical practice is often restrained by the specific hepatorenal toxicity of cinnabar and realgar (C + R). In previous research studies, we have found that the antioxidative and anti-inflammatory effects of its herbal constituents could mitigate the risks from the toxicity. The underlying detoxification mechanisms are still unsolved. The present study investigated the protective effects of AGNH's herbal constituents on hepatorenal injury induced by C + R. For the mice treated with C + R, the increased expression levels of sensitive biomarkers of metal exposure and hepatorenal toxicity, including metallothionein (MT) in both hepatorenal tissues and kidney induced molecule-1 (KIM-1) in the kidney, were simultaneously reduced when C + R coadministered with other herbal medicines. In addition, the contents of trivalent As (As^{III}), pentavalent As (As^V), and mercury (Hg) in hepatorenal tissues of mice were also significantly reduced benefiting from the herbal constituents in AGNH. Further mechanism studies showed that the herbal constituents in AGNH could downregulate the expressions of uptake transporters (AQP9 and OAT1) and upregulate the expressions of efflux transporters (P-gp, MRP2, and MRP4) in mice intoxicated by C + R. Our results suggested that AGNH's herbal constituents protect the body against C + R-induced hepatorenal toxicity and accumulations of Hg and As, which could be associated with the reestablishment of heavy metal homeostasis and the detoxification system.

1. Introduction

An-Gong-Niu-Huang Wan (AGNH) has been a renowned compound recipe for treating cerebral diseases [1]. Mineral medicinal materials cinnabar and realgar (C + R) (with 96% of HgS and 90% of As_4S_4) are contained, accounting for 12.5% by weight in the formula [2]. In recent years, realgar-induced hepatic injury and cinnabar-induced renal toxicity have been reported [3–5], which are often associated with overdose or prolonged exposure. Furthermore, it is evident that AGNH contains multiple herbal ingredients, which are deemed to function in delivering drugs to target tissues as

well as eliminating the harmful influences of the metallic ingredients including mercury (Hg) and arsenic (As) [6].

Various metabolizing enzymes and transporters mediate heavy metal compounds' metabolism and secretion. As a family of phase-2 detoxification enzymes *in vivo*, glutathione S-transferases (GST) could catalyze the conjugation of reduced glutathione (GSH) to mercuric and arsenical species [7, 8]. The generated Hg- and As- glutathione S-conjugates were transported across the canalicular membrane into the bile by the basolateral efflux transporters, such as P-glycoprotein (P-gp) and members of the multidrug resistance-associated protein family (MRP) [9]. These glutathione

S-conjugates may also traverse the cell membrane at the apical end of renal proximal tubular epithelial cells (RPTECs) into urine assisted by the transporters akin to those expressed in hepatocytes [10]. On the other hand, drugs extracted from the blood into hepatocytes and renal tubular cells are mediated by basolateral uptake transporters, including organic anion and cation transporter (OAT/OCT) family members [11, 12]. The coordinated action of efflux and uptake transporters regulates the amount of mercuric and arsenical glutathione S-conjugates that transverse out of or return to hepatocytes and renal tubular cells. Our previous studies have shown that the combination of herbal medicine in AGNH can mitigate inflammation and injury in the liver and kidney tissues of mice induced by C + R [13, 14]. However, little is known about how AGNH's herbal ingredients act on phase-2 sulfotransferases and phase-3 uptake and efflux transporters induced by C + R.

In the present study, we wanted to compare the toxicity of AGNH with C + R in mice, focusing on the content of total As, water-soluble As including trivalent As (As^{III}) and pentavalent As (As^{V}) in sera, hepatorenal tissues, and the expressions of both metallothionein (MT) and kidney-induced molecule-1 (KIM-1), and sensitive biomarkers of metal exposure and hepatorenal toxicity. Furthermore, we further investigated whether the alleviating effects of other herbal medicines in AGNH to hepatorenal damage resulted from the overload of Hg and As are mediated, at least in part, by the drug-processing enzymes and transports in hepatorenal tissues of mice.

2. Materials and Methods

2.1. Chemicals and Animals. AGNH pill (weighted 3 g for each), cinnabar (containing 96% of HgS), as well as realgar (containing 90% of As_4S_4) were all provided by Guangzhou Bai-Yun-Shan Zhong-Yi Pharmaceutical Company Ltd. (Guangzhou, China). Methanol (Chromatographic grade) was purchased from Sigma Chemical Company (St. Louis, MO, USA), and ammonium carbonate (99.999%) was purchased from Aladdin Industrial Corporation (Shanghai, China). The As^{III} , As^{V} , and Hg standard solutions (1000 mg/L) were purchased from Sigma-Aldrich company, using as the standard curve solution. The production of ultrapure water (UPW) at 25°C depended on the Milli-Q® lab water purifying system (Merck, MA, USA). Specific antigens for the primary antibodies were as follows: GST α 1, GSTmu, OCT1, OCT2, MRP1, aquaporin-9 (AQP-9), and β -actin (Bioworld Technology Co, Ltd., MN, USA); Na⁺-K⁺-ATPase, and MT-1 (Santa Cruz, CA, USA); KIM-1, GSTpi, MRP2, MRP4, P-gp, and OAT1 (Boster Biological Technology Co, Ltd., Hubei, China).

2.2. Animals and Experimental Design. Thirty-six Kunming (KM) mice (20 ± 2 g bodyweight, half of male and female) were provided by the Center of Experimental Animals of the Army military Medical University in Chongqing, China, and randomly assigned into 3 groups, with 12 in each group. All mice were housed in an environment with the controlled

temperature of 22 ± 1°C and the humidity of 50 ± 2% under a 12 : 12 h light/dark (L/D) cycle. Before experiments, the mice were acclimatized to standard rodent diet and free access to water for 1 week. Mice were then treated with saline (vehicle), AGNH (2.5 g/kg), and equal amounts (0.14 g/kg + 0.14 g/kg) of C + R by intragastric administration once daily for 4 weeks, respectively. According to the Chinese Pharmacopoeia (2020 edition), the daily dosage of AGNH is 3 g/day for adults. In the present study, the dosage chosen for the mice (2.5 g/kg/day) is equal to five times the clinical equivalent dose. Since equal amounts (0.056 g) of cinnabar and realgar were contained in per gram AGNH, one group of mice was treated by oral administration of cinnabar (0.14 g/kg) and realgar (0.14 g/kg) per day for comparison. The details of the dosing regimen were described in our previous report [13, 14]. At 1 h after the last dosing, mice were anesthetized by pentobarbital sodium (50 mg/kg) intraperitoneally and sacrificed by cervical dislocation after collection of blood samples from the eyeballs. Hepatorenal tissues of mice were also collected and reserved for further analysis. All animal procedures were carefully approved by the Institutional Ethics Committee of the Chongqing University of Technology and performed in complete accordance with the National Institutes of Health Guidelines for the Care and Use of Laboratory Animals (8th Edition, 2011).

2.3. Analysis of the Speciation of As and the Content of Hg in the Sera and Hepatorenal Tissues of Mice. Serum samples (55 μ l) were added to 0.3 ml of mixture of methanol-water (v/v, 1 : 1), fully mixed using vortex for 30 sec. Subsequently, the mixture was extracted in the ultrasonic waterbath (10 min) and centrifugated (10 min, 15,000 g). Then, ion chromatography inductively coupled plasma mass spectrometry (IC-ICP-MS, Thermo Fisher Scientific, MA, USA) was applied for the analysis of As speciation in the supernatant of the mixture (180 μ l). The supernatant (150 μ l) left was diluted to 1.5 ml in purified water for the Hg content assay using the ICP-MS system (Thermo Fisher Scientific).

Hepatorenal tissues weighing 35 mg were mixed with 2 ml ultrapure water, followed by homogenization, bath in the ultrasonic waterbath (10 min) as well as centrifugation (15,000 g, 50 min, 4°C). The supernatant of the mixture was filtered through a 0.22 μ m polytetrafluoroethylene (PTFE) membrane prior to IC-ICP-MS and ICP-MS analyses.

The ICP-MS (ICAP-Q) was programmed to detect the speciation of As and the content of Hg in our study, mainly including the parameters of forward radiofrequency (RF) power (1550 W), auxiliary gas flow rate of argon (12.9 l/min), gas flow rate of nebulizer argon (0.70 l/min), and dwell time (200 ms). Chromatographic separation of As speciation was carried out using the Thermo Scientific Dionex ICS-5000 IC system coupled with Thermo Scientific Dionex IonPac AS7 Specialty Anion-Exchange (AE) Column (4 × 250 mm for pore size, 10 μ m for bead diameter). The mobile phase was composed of ammonium carbonate (mobile phase A, 5 mM) and ammonium carbonate (mobile phase B, 200 mM). Besides, the gradient elution system was programmed as 0% B for 0–2.0 min, 0–100% B for 2.0–2.1 min, 100% B for

2.1–5.5 min, 100–0% B for 5.5–5.6 min, and 0% B for 5.6–10 min, setting the flow rate of the mobile phase to 1.0 ml/min as well as the injected sample volume to 25 μ l. In addition, linearity, accuracy, precision, LOD (limit of detection), and LOQ (limit of quantitation) of IC-ICP-MS were fully verified by characteristic indicators.

2.4. Immunohistochemical Examination. Paraffin-embedded sections of hepatorenal tissues were dewaxed with xylene and hydrated with gradient ethanol. For antigen retrieval, the slices were then put into a boiled citrate buffer for 20 min (pH 6.0, 10 mM). Afterwards, H₂O₂ of 3% (v/v) was adopted for the inactivation of endogenous enzymes such as peroxidase. Subsequently, sections were probed with the primary antibody (dilution, 1:150) against MT-1 or KIM-1 overnight at 4°C. Secondary antibody incubation was performed with a Polink-2 polymer conjugated with horseradish peroxidase (HRP, Beijing Zhongshan Golden Bridge Biotechnology Co., Ltd., Beijing, China). Positive reactions in 3, 3'-diaminobenzidine- (DAB-) stained areas were then visualized. Hematoxylin was further adopted for counterstaining the nuclei. Images for immunohistochemistry staining ($n=5$ per mice) were acquired on a bright-field Olympus microscope (BX51) at a magnification of $\times 200$. The expression levels of MT-1 and KIM-1 were quantified using the integrated optical density (IOD) for immunoreactive regions. Five random fields were collected from each section, and their IOD values were determined by the image analysis software of Image-Pro[®] Plus (Version 6.0, Media Cybernetics Inc., USA).

2.5. Western Blotting (WB) Analysis. The extraction of the total protein from hepatorenal tissues of mice was performed using RIPA buffer (Beyotime Biotechnology, Jiangsu, China) plus protease inhibitors (Solarbio, Beijing, China). Then, the bicinchoninic acid (BCA) protein assay was available in kit (Beyotime) to further quantify the concentrations of protein. Proteins (30 μ g) were resolved by sodium dodecyl sulfate polyacrylamide gel (SDS-PAGE) electrophoresis and transblotted to PVDF membranes, which were subsequently blocked with skimmed milk (5% w/v) in Tris-buffered saline with Tween 20 (TBST) for 1 h. The desired primary antibodies against KIM-1, MT-1, GST α 1, GST μ , GST π , OCT1, OCT2, MRP1, MRP2, MRP4, P-gp, OAT1, AQP-9, and β -actin were probed onto the membranes overnight at the temperature of 4°C. After washing in TBST, membranes were further incubated for 1 h with specific secondary antibodies at the dilution of 1:10000 (Bioworld). Besides, β -actin or Na⁺-K⁺-ATPase was referred as an loading control. An enhanced chemiluminescence kit (Millipore, MA, USA) was adopted for the visualization of immunoprobed proteins. The capture of immunosignals depended on Amersham[™] Imager 600 (Amersham Biosciences-GE Healthcare, UK). In addition, the quantification of band intensities was performed using the software of Quantity One for WB analysis (Version 4.62, Bio-Rad Laboratories, Inc., USA). Defining the level in the saline

control group as 1-fold, the variations in the band intensity were presented as changes of fold.

2.6. Statistical Analysis. The statistical analysis was conducted with IBM[®] SPSS[®] statistical software package for Windows (Version 18.0, Chicago, IL, USA). Values for continuous variables were described as mean \pm standard deviation (SD). One-way analysis of variance (ANOVA) was used to compare the significance of variation among the 3 groups, applying $P < 0.05$ as the level of statistical significance in all cases.

3. Results

3.1. Toxicity-Related Protein Expressions in Hepatorenal Tissues of Mice. Hepatorenal tissues are the major target tissues of As and Hg toxicity. MT plays a key part in the detoxification of As and Hg, and therefore, this protein is often considered to be one of the sensitive biomarkers to evaluate the injury to the hepatorenal tissues [15]. Immunohistochemical analysis showed both hepatocytes and RPTECs stained strongly positive for MT-1 when mice were treated with cinnabar combined with realgar for 28 days (Figures 1(a) and 1(b)), whereas positive staining for MT-1 was weak in the sections of hepatorenal tissues in mice treated with saline or AGNH. Besides, results obtained from WB analysis also revealed that MT-1 expression levels in hepatorenal tissues of mice were unchanged between groups of AGNH and saline (Figures 1(d) and 1(e)), but combined administration of C + R exerted a significant increasing effect on MT-1 protein levels in hepatorenal tissues of mice.

KIM is another biomarker whose expression is highly increased in the renal proximal tubule in mice after kidney injury [16]. By immunohistochemical staining, almost all RPTECs from mice coexposed to C + R were strongly stained positive for KIM-1 (Figures 1(a) and 1(c)); whereas, few KIM-1-positive RPTECs were found in the mice groups of saline and AGNH. By WB analysis, we also found that compared to that of the saline group, exposed to C + R markedly increased the KIM-1 expression level in the kidney of mice (Figures 1(d) and 1(f)); whereas, no significant difference of KIM-1 expression was detected between the mice treated with AGNH and those treated with saline.

3.2. As and Hg Quantification in the Sera, Liver, and Kidneys of Mice. As^{III} and As^V are well separated by optimization of mobile phase and gradient, and representative ion chromatograms of As speciation in the sera, liver, and kidneys of mice are shown in Supplemental Figure 1. Linearity, R^2 and linearity range, LOD, LOQ, precision, and the accuracy of the IC-ICP-MS method for the analysis of As^{III} and As^V were tested. The precision of IC-ICP-MS was tested by relative standard deviation (RSD) in percentage. Detailed information is shown in Supplemental Table 1.

As shown in Figure 2(a), hepatic Hg content reached 0.12 ng per mg liver in the C + R group when compared to 0.004 ng per mg liver in the AGNH group, which was slightly higher than the saline control group (0.002 ng per mg liver).

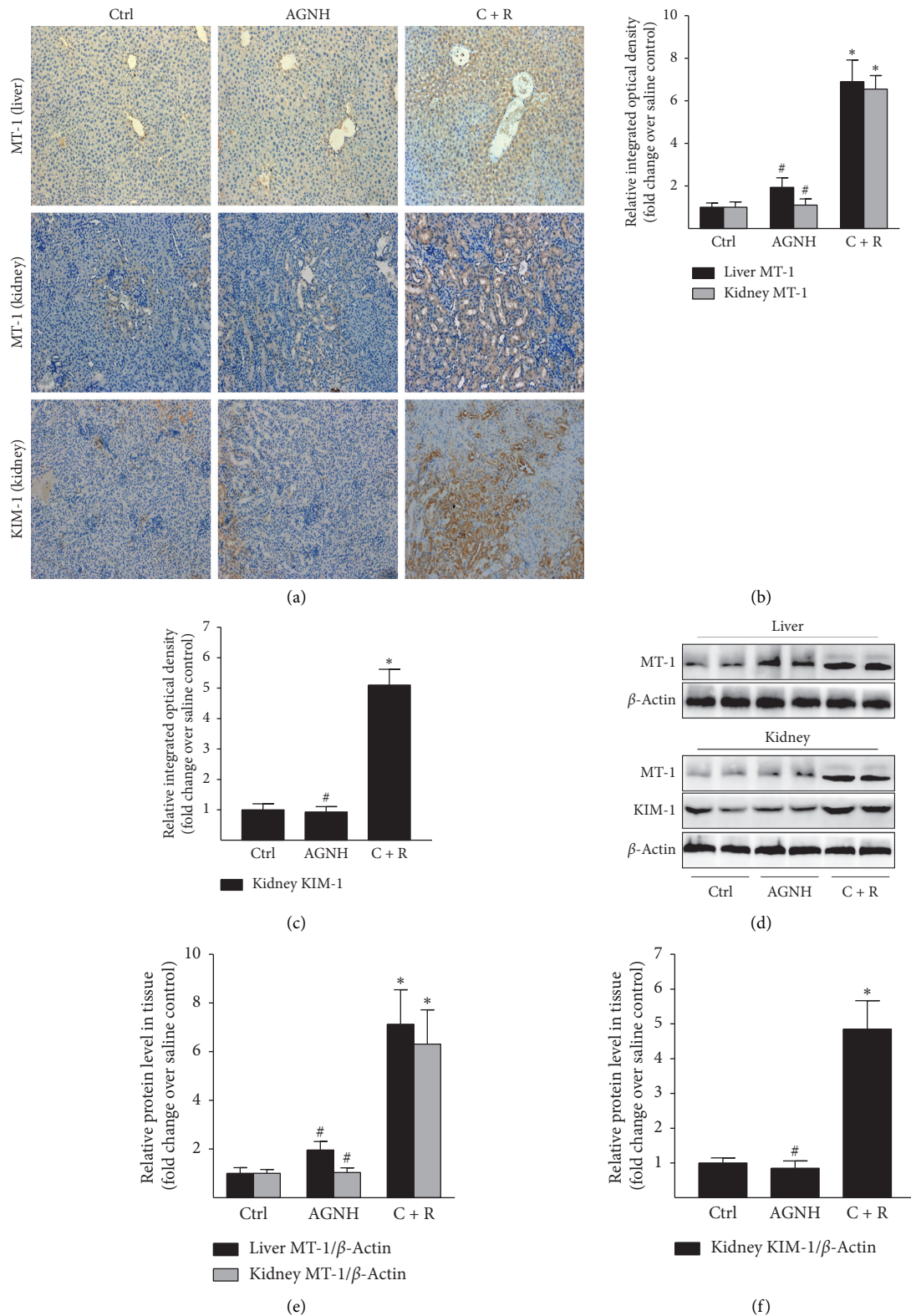


FIGURE 1: AGNH's herbal constituents alleviate hepatorenal impairment induced by cinnabar and realgar (C + R) in mice. Mice received saline (vehicle), AGNH (2.5 g/kg), as well as C + R (0.14 g/kg + 0.14 g/kg) orally once daily for 4 weeks, respectively. (a) Representative immunostaining images of MT-1 and KIM-1 in the hepatic and renal sections of mice. Scale bar: 100 μ m. (b), (c) Semiquantitative immunohistochemical analysis of MT-1 and KIM-1 in the respective group. (d) WB analysis of MT-1 and KIM-1 levels in the hepatorenal tissues. The level of housekeeping protein β -actin was referred as a control for equal protein loading. (e), (f) Band intensities were converted to arbitrary densitometric units (ADUs), normalized by the value of β -actin, and finally expressed according to the levels in saline-treated mice (defined as 1-fold). Each bar represents mean \pm standard deviation (SD) from six mice. * $P < 0.05$ compared to the saline control group; # $P < 0.05$ compared to the C + R coadministration group.

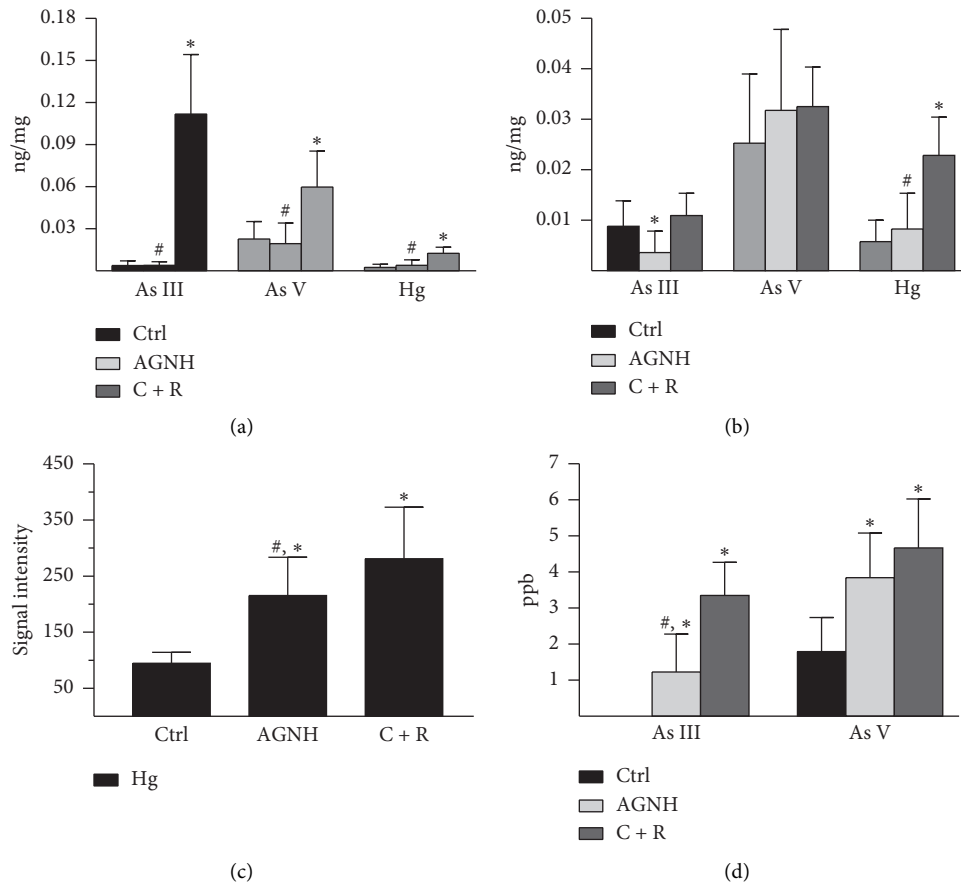


FIGURE 2: AGNH's herbal constituents prevented Hg and As accumulation induced by C + R in the hepatorenal tissues and sera of mice. Mice received saline (vehicle), AGNH (2.5 g/kg), as well as C + R (0.14 g/kg + 0.14 g/kg) orally once daily for 4 weeks, respectively. (a) Hepatic and (b) renal tissues from mice were obtained on day 28. As (As^{III} and As^{V}) and Hg contents in the hepatorenal tissues from mice were analyzed by IC-ICP-MS. (c) Blood specimens from mice were also obtained on day 28. The signal intensity of Hg in the sera from mice was measured by ICP-MS. (d) As (As^{III} and As^{V}) contents in the sera from mice were analyzed by IC-ICP-MS. Values for continuous variables are described as mean \pm standard deviation (SD), $n = 12$. * $P < 0.05$ compared to the saline control group; # $P < 0.05$ compared to the C + R coadministration group.

Similar results were obtained with the As^{III} and As^{V} content assay in the liver of mice, where the As^{III} and As^{V} contents in the C + R coadministered mice were found to be significantly increased when compared with the saline-treated group, whereas there was no difference with statistical significance in contents of both As^{III} and As^{V} between the mice treated with AGNH and those treated with saline.

Renal Hg content in the mice after C+R coadministration was 3-4 folds higher than those in the mice treated with vehicle and AGNH (Figure 2(b)). Interestingly, the content of As^{III} in the kidneys of mice was even less in the group treated with AGNH than in the group treated with saline. Moreover, no obvious difference was detected concerning As^{V} content in the kidneys among the groups of mice.

Since Hg of the sera could be detected only in trace amount, we selected signal intensity from ICP-MS to evaluate the differences in Hg content between different groups. Results showed that the average signal intensity of sera from C + R cotreated mice was 2.9 times higher than that from the saline control group (Figure 2(c)).

Coadministration of other herbal medicines with C + R in AGNH led to signal intensity that was only 76.70% of the intensity from C + R cotreated mice, despite having stronger signal intensity than that from the saline control group. Besides, similar results were discovered in the As^{III} and As^{V} content assay (Figure 2(d)).

3.3. Phase-2 Conjugation Enzyme and Transporter Expressions in the Hepatorenal Tissues of Mice. The potential detoxification mechanisms involved in metal-herb interactions in AGNH are further explored. GST catalyzes the conjugation of GSH with Hg and As and convert them to water-soluble glutathione S-conjugates, which are easily excreted to the bile with the help of the basolateral efflux transporters, including MRP2 and P-gp. The Hg- and As-glutathione S-conjugates may also traverse the luminal plasma membrane of RPTECs into urine by MRP2 and 4 [17]. WB analysis revealed that compared with the saline group, coadministration of C + R upregulated the expressions of GST family members (GST α 1, GSTmu, and GSTpi) in the livers of

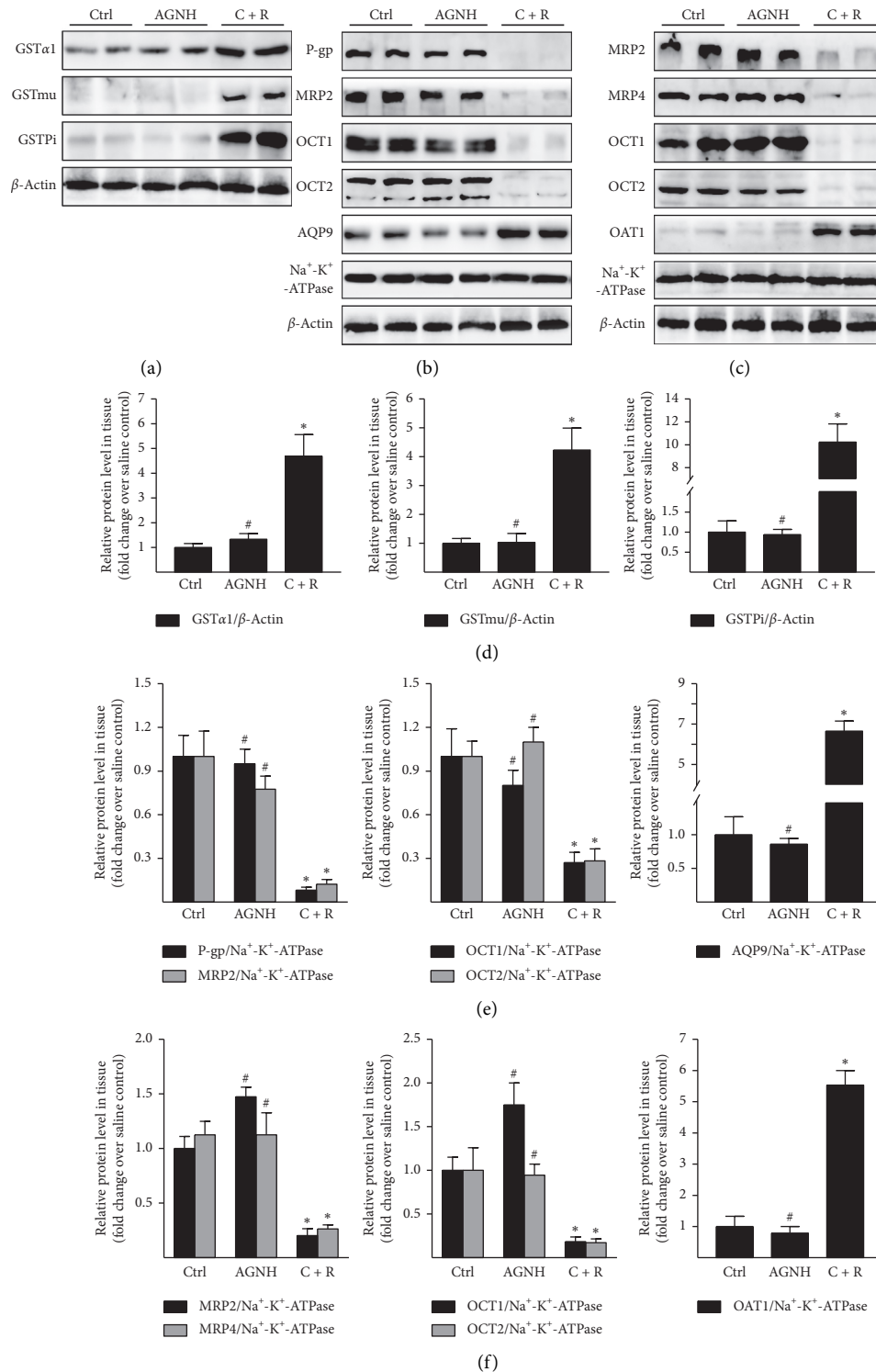


FIGURE 3: AGNH's herbal constituents inhibited expressions of GST and uptake transporters induced by C + R but enhanced the expressions of efflux transporters in the hepatorenal tissues of mice. Mice received saline (vehicle), AGNH (2.5 g/kg), as well as C + R (0.14 g/kg + 0.14 g/kg) orally once daily for 4 weeks, respectively. Hepatorenal tissues from mice were obtained on day 28. WB analysis of GST- α 1, GSTmu, GSTpi, P-gp, MRP2, MRP4, OCT1/2, AQP9, and OAT1 in (a, b) hepatic and (c) renal tissues. The protein level of β -actin or Na⁺-K⁺-ATPase was referred as a loading control. (d-f) Band intensities were measured in arbitrary densitometric units (ADUs), normalized by the value of β -actin or Na⁺-K⁺-ATPase and finally expressed according to the levels in saline-treated mice (defined as 1-fold). Values for continuous variables are described as mean \pm standard deviation (SD), $n = 6$. * $P < 0.05$ compared to the saline control group; # $P < 0.05$ compared to the C + R coadministration group.

mice (Figures 3(a) and 3(d)). In contrast, expressions of efflux family proteins including P-gp and MRP2 in the livers (Figures 3(b) and 3(e)) and MRP2 and 4 in the kidneys were downregulated after treating mice with C + R (Figures 3(c) and 3(f)). However, no significant differences in the expressions of GST and efflux family members were detected between the mice groups treated with AGNH and saline.

AQP9, an aquaglyceroporin protein, facilitates hepatic uptake of As from the portal blood and accelerates hepatocellular injury in the liver [18]. Furthermore, basolateral uptake transporters at RPTECs, including the members of OAT/OCT, extract the Hg-glutathione S-conjugates from the bloodstream, causing renal tubular injury [19]. WB analysis revealed that compared with the saline control group, C + R coadministration induced a marked increase in the protein expressions of AQP9 in the livers and OAT1 in the kidneys of mice (Figures 3(b), 3(c), 3(e), and 3(f)). Unexpectedly, C + R coadministration caused an obvious decrease in the protein expressions of OCT1 and 2 in the hepatorenal tissues of mice (Figures 3(b), 3(c), 3(e), and 3(f)). However, the protein expressions of AQP9, OAT1, OCT1, and OCT2 did not differ significantly between the mice groups treated with AGNH and saline.

4. Discussion

Our previous study has shown that the hepatorenal toxicity induced by C + R could be mitigated when used in combination with other herbs in AGNH [13]. Consecutive 28-day intragastric administration of C + R merely increased the aspartate aminotransferase (AST) activity as well as the alanine aminotransferase (ALT) activity in liver homogenates. However, it did not significantly influence blood biochemical parameters, suggesting routine serum biochemical markers may not be sensitive indices of hepatorenal impairment induced by C + R [14]. MTs are a family of cysteine-rich intracellular proteins with a well-known metal-binding ability that participate in heavy metal detoxification. MTs have been widely used as specific biomarkers reflecting heavy metal-induced tissue injury [20]. In addition, KIM-1 is a reliable histological biomarker to detect the progression of renal tubular injury [16]. Currently, compared with the saline group, MT-1 expressions in hepatorenal tissues and KIM-1 expression in the kidney were significantly higher in the C + R group, while levels of MT-1 and KIM-1 protein were similar after treatment with AGNH to the levels after coexposed to vehicle alone. The aforementioned studies further confirmed that the combined use of other herbal medicine in AGNH could attenuate the hepatorenal damage induced by C + R.

It is generally assumed that the hepatorenal toxicity induced by C + R relies on the amount and the diverse chemical forms of heavy metals in the target tissues; we next examined the As and Hg accumulation in the blood and hepatorenal tissues of mice. Treatment of C + R increased As (As^{III} and As^{V}) and Hg levels in the liver, suggesting cinnabar- and realgar-induced hepatotoxicity may be initiated by As (As^{III} and As^{V}) and Hg deposition. The changes of the As (As^{III} and As^{V}) level in the kidney were different from

those in the liver. Although C + R failed to increase the level of As (As^{III} and As^{V}), this does not exclude the possibility that the oxidase and methylase in the kidney catalyzed the ingested As^{III} and As^{V} to form monomethyl arsenic acid (MMA^{V} and MMA^{III}) and dimethyl arsenic acid (DMA^{V}), which could be important sources of chronic nephrotoxicity in mice intoxicated by C + R [21]. In contrast, compared with the saline control group, AGNH, an Hg and As-containing traditional Chinese compound prescription, did not induce any significant Hg and As accumulation in hepatorenal tissues, suggesting that other herbal constituents in AGNH might promote Hg and As elimination from the hepatorenal tissues of mice. Further studies in future are necessary for exploring the potential mechanisms.

GST is an important phase-2 drug-metabolizing enzyme, which conjugates Hg and As with GSH to accelerate their biliary excretion [7]. The current study found that coadministration of C + R potentially upregulated the hepatic expression of GST α 1, GSTmu, and GSTpi, while treatment of AGNH had little effect on the expression of GST family members. This increase in the GST protein level facilitates biliary excretion of Hg and As-GSH conjugates, which might be an adaptive mechanism aimed at protecting the body against Hg and As overload in hepatocytes.

Xenobiotic transporters in the hepatorenal tissues have been found to be essential for the bile/urinary secretion and reabsorption of heavy metals [22]. As one of the most predominant mechanisms of Hg and As accumulation in hepatorenal tissues, C + R coadministration reduced Hg and As excretion via urine and bile, as reflected by a simultaneous decrease in the expressions of efflux transporters (P-gp, MRP2, and MRP4) and increase in the expressions of uptake transporters (AQP9 and OAT1), relative to those in saline-treated mice. However, no significant difference between the mice groups treated with AGNH and saline was discovered. There have been numerous reports that multiple herbal constituents in AGNH, such as curcumin, baicalin, berberine, and quercetin, possess a wide range of pharmacological activities including anti-inflammatory, antioxidative, and detoxifying activities [23–26]. In addition, they could interfere with the hepatobiliary and urinary elimination of drugs through affecting the major uptake and efflux transporters [23, 27–30]. Thus, it is reasonable to speculate that herbal constituents in AGNH could alleviate hepatorenal toxicity induced by C + R, probably by the decreased reabsorption and enhanced excretion of Hg and As in hepatorenal tissues.

5. Conclusion

In short, this study demonstrates that AGNH's herbal constituents protect against the accumulations of Hg and As and hepatorenal toxicity induced by C + R by decreasing expressions of uptake transporters and increasing expressions of efflux transporters in the hepatorenal tissues. These findings provide the first detailed detoxification metabolism regarding the herbal constituents in AGNH that protect from hepatic and renal injuries initiated by Hg and As deposition. Notably, blood Hg and As levels were

significantly increased in the AGNH group than in the saline group. Thus, long-term consumption of AGNH at the higher dose should be considered with caution.

Data Availability

The data used to support the findings of this study are included within the article.

Conflicts of Interest

The authors declare there are no conflicts of interest.

Authors' Contributions

Songsong Wang and Xiao Xiao contributed equally to this work and should be considered co-first authors. A Li and P Li codesigned this study and should be considered co-corresponding authors. SS Wang and X Xiao carried out the experiments. A Li and SS Wang made the draft of the manuscript. SS Wang and X Xiao conducted the data analysis. All of the authors revised and improved the manuscript.

Acknowledgments

This work was sponsored by the Research Committee of the University of Macau (MYRG2018-00239-ICMS), the Macao Science and Technology Development Fund (0147/2019/A3), Guangzhou International Science and Technology Cooperation Project (201807010044), the Chongqing Natural Science Foundation (cstc2019jcyjmsxmX0045), and the TCM project of Chongqing Municipal Health and Family Planning Commission (ZY201702122).

Supplementary Materials

Supplementary material includes methodology validation of AsIII, AsV, and Hg detection in Supplemental Table 1 and representative ion chromatograms of arsenic speciation in the sera, liver, and kidneys from mice administered by oral gavage with An-Gong-Niu-Huang Wan in Supplemental Figure 1. (*Supplementary Materials*)

References

- [1] Y. Guo, S. H. Yan, and L. P. Xu, "Use of angong niuhuang in treating central nervous system diseases and related research," *Evidence-Based Complementary and Alternative Medicine*, vol. 2014, p. 9, Article ID 346918, 2014.
- [2] Y.-F. Lu, Q. Wu, J.-W. Yan, J.-Z. Shi, J. Liu, and J.-S. Shi, "Realgar, cinnabar and An-Gong-Niu-Huang Wan are much less chronically nephrotoxic than common arsenicals and mercurials," *Experimental Biology and Medicine*, vol. 236, no. 2, pp. 233–239, 2011.
- [3] Y. Wang, D. P. Wang, and J. Wu, "Cinnabar-induced sub-chronic renal injury is associated with increased apoptosis in rats," *BioMed Research International*, vol. 2015, Article ID 278931, , 2015.
- [4] L. Wei, P. Liao, H. Wu et al., "Metabolic profiling studies on the toxicological effects of realgar in rats by 1H NMR spectroscopy," *Toxicology and Applied Pharmacology*, vol. 234, no. 3, pp. 314–325, 2009.
- [5] H. Wang, G. Su, G. Chen, J. Bai, and Y. Pei, "1H NMR-based metabolomics of the protective effect of Curcuma longa and curcumin on cinnabar-induced hepatotoxicity and nephrotoxicity in rats," *Journal of Functional Foods*, vol. 17, pp. 459–467, 2015.
- [6] J. Liu, L.-X. Wei, Q. Wang et al., "A review of cinnabar (HgS) and/or realgar (As₄S₄)-containing traditional medicines," *Journal of Ethnopharmacology*, vol. 210, pp. 340–350, 2018.
- [7] S. F. Xu, Q. Wu, B. B. Zhang et al., "Comparison of mercury sulfides with mercury chloride and methylmercury on hepatic P450, phase-2 and transporter gene expression in mice," *Journal of Trace Elements in Medicine and Biology*, vol. 37, pp. 37–43, 2016.
- [8] M. Farina and M. Aschner, "Glutathione antioxidant system and methylmercury-induced neurotoxicity: an intriguing interplay," *Biochimica et biophysica acta*, "General Subjects", vol. 1863, no. 12, Article ID 129285, 2019.
- [9] N. H. Hendrikse, F. Kuipers, C. Meijer et al., "In vivo imaging of hepatobiliary transport function mediated by multidrug resistance associated protein and P-glycoprotein," *Cancer Chemotherapy and Pharmacology*, vol. 54, no. 2, pp. 131–138, 2004.
- [10] L. H. Lash, "Role of glutathione transport processes in kidney function," *Toxicology and Applied Pharmacology*, vol. 204, no. 3, pp. 329–342, 2005.
- [11] N. Ballatori, C. L. Hammond, J. B. Cunningham, S. M. Krance, and R. Marchan, "Molecular mechanisms of reduced glutathione transport: role of the MRP/CFTR/ABCC and OATP/SLC21A families of membrane proteins," *Toxicology and Applied Pharmacology*, vol. 204, no. 3, pp. 238–255, 2005.
- [12] M. F. Fromm, "Transporters and drug-drug interactions: important determinants of drug disposition and effects," *Toxicology Letters*, vol. 238, p. S49, 2013.
- [13] A. Li, J.-Y. Zhang, X. Xiao et al., "Hepatorenal protective effects of medicinal herbs in An-Gong-Niu-Huang Wan (AGNH) against cinnabar- and realgar-induced oxidative stress and inflammatory damage in mice," *Food and Chemical Toxicology*, vol. 119, pp. 445–456, 2018.
- [14] F. B. Xia, A. Li, and Y. S. Chai, "UPLC/Q-TOFMS-based metabolomics approach to reveal the protective role of other herbs in An-Gong-Niu-Huang Wan against the hepatorenal toxicity of cinnabar and realgar," *Frontiers in Pharmacology*, vol. 9, p. 618, 2018.
- [15] Y. F. Lu, J. W. Yan, and Q. Wu, "Realgar-and cinnabar-containing An-Gong-Niu-Huang Wan (AGNH) is much less acutely toxic than sodium arsenite and mercuric chloride," *Chemico-Biological Interactions*, vol. 189, no. 1-2, pp. 134–140, 2011.
- [16] W. K. Han, V. Bailly, R. Abichandani, R. Thadhani, and J. V. Bonventre, "Kidney injury molecule-1 (KIM-1): a novel biomarker for human renal proximal tubule injury," *Kidney International*, vol. 62, no. 1, pp. 237–244, 2002.
- [17] C. C. Bridges, L. Joshee, and R. K. Zalups, "MRP2 and the DMPS- and DMSA-mediated elimination of mercury in TR- and control rats exposed to Thiol S-conjugates of inorganic mercury," *Toxicological Sciences*, vol. 105, no. 1, pp. 211–220, 2008.
- [18] Z. Liu, J. Shen, J. M. Carbrey, R. Mukhopadhyay, P. Agre, and B. P. Rosen, "Arsenite transport by mammalian aquaglyceroporins AQP7 and AQP9," *Proceedings of the National Academy of Sciences*, vol. 99, no. 9, pp. 6053–6058, 2002.

- [19] B. C. Burckhardt and G. Burckhardt, "Transport of organic anions across the basolateral membrane of proximal tubule cells," *Reviews of Physiology, Biochemistry and Pharmacology*, vol. 146, pp. 95–158, 2003.
- [20] R. Brandão, F. W. Santos, and M. Farina, "Antioxidants and metallothionein levels in mercury-treated mice," *Cell Biology and Toxicology*, vol. 22, no. 6, pp. 429–438, 2007.
- [21] J. Y. Luo, X. Han, and X. W. Dou, "Accumulation of arsenic speciation and in vivo toxicity following oral administration of a Chinese patent medicine Xiao-Er-Zhi-Bao-Wan in rats," *Frontiers in Pharmacology*, vol. 8, p. 491, 2017.
- [22] B.-B. Zhang, W.-K. Li, W.-Y. Hou et al., "Zuotai and HgS differ from HgCl₂ and methyl mercury in Hg accumulation and toxicity in weanling and aged rats," *Toxicology and Applied Pharmacology*, vol. 331, pp. 76–84, 2017.
- [23] W. R. García-Niño and J. Pedraza-Chaverri, "Protective effect of curcumin against heavy metals-induced liver damage," *Food and Chemical Toxicology*, vol. 69, pp. 182–201, 2014.
- [24] P. Hasanein, M. Ghafari-Vahed, and I. Khodadadi, "Effects of isoquinoline alkaloid berberine on lipid peroxidation, antioxidant defense system, and liver damage induced by lead acetate in rats," *Redox Report*, vol. 22, no. 1, pp. 42–50, 2017.
- [25] J.-Y. Wan, X. Gong, L. Zhang, H.-Z. Li, Y.-F. Zhou, and Q.-X. Zhou, "Protective effect of baicalin against lipopolysaccharide/D-galactosamine-induced liver injury in mice by up-regulation of heme oxygenase-1," *European Journal of Pharmacology*, vol. 587, no. 1-3, pp. 302–308, 2008.
- [26] G. Zhang, J.-L. He, X.-Y. Xie, and C. Yu, "LPS-induced iNOS expression in N9 microglial cells is suppressed by geniposide via ERK, p38 and nuclear factor- κ B signaling pathways," *International Journal of Molecular Medicine*, vol. 30, no. 3, pp. 561–568, 2012.
- [27] N. R. Srinivas, "Baicalin, an emerging multi-therapeutic agent: pharmacodynamics, pharmacokinetics, and considerations from drug development perspectives," *Xenobiotica*, vol. 40, no. 5, pp. 357–367, 2010.
- [28] P.-L. Tsai and T.-H. Tsai, "Hepatobiliary excretion of berberine," *Drug Metabolism and Disposition*, vol. 32, no. 4, pp. 405–412, 2004.
- [29] A. T. Nies, E. Herrmann, M. Brom, and D. Keppler, "Vectorial transport of the plant alkaloid berberine by double-transfected cells expressing the human organic cation transporter 1 (OCT1, SLC22A1) and the efflux pump MDR1 P-glycoprotein (ABCB1)," *Naunyn-Schmiedeberg's Archives of Pharmacology*, vol. 376, no. 6, pp. 449–461, 2008.
- [30] C. C. Wong, Y. Akiyama, T. Abe, J. D. Lippiat, C. Orfila, and G. Williamson, "Carrier-mediated transport of quercetin conjugates: involvement of organic anion transporters and organic anion transporting polypeptides," *Biochemical Pharmacology*, vol. 84, no. 4, pp. 564–570, 2012.

Research Article

Changes of Mineralogical Properties and Biological Activities of Gypsum and Its Calcined Products with Different Phase Structures

Kaiyang Liu ¹, Shu Han ¹, Wei Gao,² Ya'nan Tang ¹, Xitao Han ¹, Ziqin Liu ¹,
Liyuan Bao,¹ Meiru Zhi ¹, Hongyue Wang ¹, Yingli Wang,³ and Hong Du ¹

¹School of Chinese Materia Medica, Beijing University of Chinese Medicine, Beijing 102488, China

²School of Traditional Chinese Medicine, Beijing University of Chinese Medicine, Beijing 102488, China

³Shanxi University of Chinese Medicine, Jinzhong, Shanxi 030619, China

Correspondence should be addressed to Hong Du; duhong@vip.163.com

Received 16 December 2020; Revised 11 February 2021; Accepted 24 February 2021; Published 10 March 2021

Academic Editor: Jie Liu

Copyright © 2021 Kaiyang Liu et al. This is an open access article distributed under the Creative Commons Attribution License, which permits unrestricted use, distribution, and reproduction in any medium, provided the original work is properly cited.

Raw gypsum (RG) and calcined gypsum (CG) are widely used in traditional Chinese medicine (TCM). RG is usually taken orally to resolve heat and diminish inflammation, while CG is only used externally to treat ulcerations and empyrosis. Calcination at different temperatures, three phase CG structures, namely, bassanite, anhydrite III, and anhydrite II, may be generated. We herein investigated the relationship between the phase structure and the efficacy of CG and the optimum phase structure for CG. RG has a compact structure, small pore size, weak anti-inflammatory effect, but no antibacterial effect, and has almost no effect on the repair of scalds. CG150 (bassanite) has a loose texture, large pore size and specific surface area, and certain antibacterial and anti-inflammatory effects, but it has a poor repair effect on scalds. CG750 (anhydrite II) has a compact structure, small pore size and specific surface area, and low antibacterial and anti-inflammatory effects, but it has a certain repair effect on scalds. Only CG350 (anhydrite III) has good performance in texture, pore size, specific surface area, antibacterial, anti-inflammatory, and scald repair. Our research has proved that the mineral properties and biological activities of CG are different due to different phase structures. CG350, namely, anhydrite III, is considered by our research to be the optimal phase structure as CG.

1. Introduction

Gypsum is a monoclinical crystal mineral. Its main component is $\text{CaSO}_4 \cdot 2\text{H}_2\text{O}$ [1]. Referred to as “Shi Gao” in Chinese, it has been used as a mineral medicine in China for thousands of years. Gypsum was first recorded in China’s earliest materia medica book called “Shen Nong’s Classic Materia Medica” (“Han” dynasty), and it is still widely used in the clinical practice of traditional Chinese medicine in modern times.

In TCM, gypsum can be used in two forms: raw gypsum (RG) and calcined gypsum (CG) [2], which are very different in their functions and usage. RG is usually used in decoction for oral administration, treating high fever, headache, and various inflammations [3, 4]. However, CG is the only medicine for external application, treating empyema, ulcers, and empyrosis [2]. According to Chinese Pharmacopoeia

requirements, CG should be calcined at a high temperature until it is crispy and easily crushed. However, the optimal calcination temperature for preparing CG is not specified. Studies have shown that three different phase structures, namely, bassanite, anhydrite III, or anhydrite II [5–7], will be produced when calcined at different temperatures. Previous studies only focused on changes of Ca^{2+} or whether the crystal water was utterly removed before and after calcination [8]. As far as we know, the changes of mineral properties of CGs with different phase structures or their antibacterial, anti-inflammatory, and scald treatment effects have never been studied hitherto.

CG is usually used to treat scald, with exudate absorption, wound healing, and muscle regeneration. According to TCM theory, CG needs to be calcined to opaque, crisp, and reddish. In the process of producing CG, colour and texture are essential appearance indexes to control product quality.

Microstructure and pore size are often considered as mineralogical properties related to the exudate absorption ability of CG. When the scald occurs, wounds often suffer from microbial infections in untreated situations. After wounds infection, toxic molecules and metabolites produced by persistent inflammatory and bacterial and immune responses adversely affect wound repair [9]. According to related studies, *E. coli*, as a Gram-negative bacterium, is a relatively common strain of scald infection, which secretes toxins (exotoxins) that affect tissue repair [10]. During the inflammatory reaction stage of scald, there are often many overexpressed inflammatory factors, such as interleukin-1 β (IL-1 β) and nitric oxide (NO), which inhibit wound healing [11]. So, inhibiting microbial infection and alleviating inflammation can promote wound healing. Therefore, in this study, the efficacy of CG can be comprehensively evaluated by *in vitro* bacteriostatic and anti-inflammatory experiments and the expression of growth factor (transforming growth factor, TGF) related to animal scald.

To clarify which phase structure is most suitable for being included in the clinical practice, we investigated the mineralogical properties and biological activities of CGs calcined at different temperatures (150°C, 350°C, and 750°C) and RG. Fourier transform infrared spectroscopy (FTIR) and X-ray diffraction (XRD) were used to confirm the phase structure and phase composition. Scanning electron microscopy (SEM) was applied to detect the variation of microstructure. A surface area porosity analyzer (SAPA) was used to measure the pore volume and surface area, and a colorimeter was conducted to qualify the colour. *In vitro*, the bacterial experiment was carried out to detect the bacteriostatic activity, and a cell experiment was implemented to detect the anti-inflammatory activity. *In vivo*, a scald animal model was constructed to detect the repairing effect of CGs with different phase structures on scaled skin.

2. Materials and Methods

2.1. Preparation of Samples. Gypsum (license number: 1903137) was purchased from Beijing Shengshilong Pharmaceutical Co., Ltd. and identified by Professor Jingjuan Wang, an expert at Beijing University of Chinese Medicine.

Preparation of RG samples: crushing GF by ultrafine pulverizer and then sieved through a 200-mesh to obtain fine powder (particle size less than 0.074 mm).

Preparation of CG samples: 10 g of RG was put into a muffle furnace (KSW-6-12 ASP, Beijing Kewei Yongxing Instrument Co., Ltd.) and calcined at 150°C, 350°C, and 750°C for 1.5 hours, respectively, to obtain CG samples named CG150, CG350, and CG750, respectively.

2.2. Determination of Phase Structure

2.2.1. FTIR Analysis. To reveal changes in the molecular structure of RG, CG150, CG350, and CG750, RG, CG150, CG350, and CG750 were mixed with KBr at the ratio of 1 : 100 and pressed into transparent sheets, respectively. FTIR spectroscopic characterization was determined using a FTIR spectrometer equipped with a DTGS detector (MB104, ABB

Bomen Co., Quebec, Canada) in the range of 4000–400 cm⁻¹. Each spectrum was recorded at the resolution of 4 cm⁻¹ with 64 coadded scans. Spectrum Version 5.0 software (PerkinElmer Company) was used to collect all sample data. The data were processed by OMNIC 6.0 software (Thermo Electron Corporation, Madison, WI, USA).

2.2.2. XRD Analysis. To analyze the phase composition of RG, CG150, CG350, and CG750, we detected all samples by using XRD. XRD patterns were collected on a diffractometer (Rigaku D/max 2500) with a detector voltage of 30 kV and 30 mA using a CuK α radiation source, and the scan speed was 8° min⁻¹ with the 2 θ range of 10–80°.

2.3. Mineralogical Properties Analysis

2.3.1. SEM Observation. The samples' microstructure was observed utilizing field emission scanning electron microscopy (FESEM) (JSM-7001F, Japan). The powders of RG, CG150, CG350, and CG750 were evenly dispersed on the sample table with double-sided adhesive tape and then were sputter-coated with gold (Au) and observed using FESEM. Measurement conditions: scanning electron microscope resolution, 2 nm (30 KV)/3.0 nm (1 KV); acceleration voltage, 20 KV.

2.3.2. Textural Properties. The nitrogen isotherms at the liquid nitrogen temperature were measured on SAPA (3H-2000, Beishide, China). The Brunauer–Emmett–Teller (BET) model [12] was used to obtain the surface area. Pore size distribution curves and average pore sizes were calculated by analyzing the adsorption branches of isotherms, based on the Barrett–Joyner–Halenda (BJH) algorithm [13].

2.3.3. Colour Quantification. The colors of RG, CG150, CG350, and CG750 sample powders were measured by a colorimeter (Konica Minolta Japan, CM-5). The colorimeter consists of a measuring head, white calibration board, black calibration board, and colour management software (SpectraMagic NX). Six random measurements were taken on the samples and values of 3 reflectance coordinates: L^* (lightness), a^* (redness), and b^* (yellowness) [14] were determined. The average values of 6 consecutive measurements were calculated separately.

2.4. Anti-Inflammatory Activity

2.4.1. Preparation of Samples. Samples of RG, CG150, CG350, and CG750, 20 g each, were soaked in 100 mL of distilled water for 30 min, stirring with a glass rod, decocted for 30 min before filtration. The first portion of water extract was collected. The residue material then underwent the second and third extractions with boiling water, each for 30 minutes, and the second and third portions of the extract were collected. The three portions were combined and concentrated through rotary evaporation at 45°C. Finally,

the extract was concentrated to 20 ml. The sample extract with a concentration of 1 g/ml was prepared.

2.4.2. RAW264.7 Cells Culture. The RAW264.7 cells were purchased from the National Infrastructure of Cell Line Resource. The cells were cultured in Dulbecco's Modified Eagle's Medium (DMEM) medium containing 10% fetal bovine serum, 1% penicillin and streptomycin, and grown in incubators at 37°C and 5% CO₂. DMEM was replaced every two days, and cells were allowed to subculture when they reached 80%–90% confluency.

2.4.3. RAW264.7 Cells Viability Assay. Raw 264.7 cells were treated with extract solution of different concentrations of RG, CG150, CG350, and CG750 (100, 250, 500, 750, 1000, 1500, 2000, or 2500 mg/ml). After 24 h incubation, the medium was removed following incubation, and 20 µL of MTT (5 mg/mL) was added into the wells and incubated for another 4 h. Finally, 150 µL of DMSO was added, and the absorbance at 490 nm was determined. The experiments were repeated three times independently. Cell viability = (experimental pore/blank pore) × 100%.

2.4.4. NO Determination. RAW264.7 cells were seeded on 96-well plates at a density of 1 × 10⁵ cells/ml. The cells were incubated at 37°C and 5% CO₂. RAW264.7 cells were treated with LPS (1 µg/mL), LPS + quercetin (5 µg/mL), LPS + RG (100, 250, or 500 mg/ml), LPS + CG150 (100, 250, or 500 mg/ml), LPS + CG350 (100, 250, or 500 mg/ml), and LPS + 750 (100, 250, or 500 mg/ml). All the agents were added at the same time, and the groups were treated for 24 h. The supernatant of cells was mixed with an equal volume of Griess reagent, and the absorbance of the mixture was measured at 540 nm. The experiments were repeated three times independently.

2.5. Bacteriostatic Activity

2.5.1. *E. coli* Viability Assay. *E. coli* (ATCC 8739) was placed in a triangular flask containing 100 ml Luria–Bertani broth medium and cultured for 20 h in a constant temperature rotary shaker at 37°C. All samples were sterilized in an autoclave (121°C, 15 min) before microbial testing to remove any environmental bacteria. After sterilization, cool to room temperature. 1 ml of bacterial suspension (~10⁸ CFU/ml) was added to media containing 20 g sterilized samples and cultured for 20 h at a rate of 150 r/min at a constant temperature in a rotary shaker at 37°C. The mixture of bacteria and samples cultured in Luria–Bertani medium was continuously diluted to 10⁸ times, and 100 µl was taken and evenly coated on Luria–Bertani agar plate and incubated in an incubator for 20 hours. Finally, the number of colonies on the agar plate was observed.

2.5.2. Morphology Observation of *E. coli*. On treatment with RG, CG150, CG350, and CG750, specific morphological changes of *Escherichia coli* (ATCC 8739) were observed by

FESEM (JSM-7001F, Japan). *E. coli* was cultured in 250 ml triangular flasks with 5 g/ml RG, CG150, CG350, and CG750 for 7 and 14, respectively. At 7 and 14, respectively, 1 ml of bacterial liquid was sucked, centrifuged, and separated (8000 rpm, 10 min) to obtain the bacterial bodies, washed three times with PBS, and finally fixed with 2.5% glutaraldehyde fixative for 4 h. Then, the samples were then dehydrated by increasing ethanol concentrations (30, 50, 70, 80, 90, 95, and 100%) for 10 min each time. *E. coli* grown in the blank medium was employed as a control. The bacterial morphology was fixed with 2.5% glutaraldehyde fixation fluid. After being dried in air at room temperature and coated by gold sputter, samples were examined with FESEM.

2.6. Scald Healing Assay

2.6.1. Animals. 126 SPF male Kun Ming (KM) mice weighing 20–25 g were purchased from Beijing Vital River Laboratory Animal Technology Co., Ltd. (License number: SCXK (Jing) 2016002, Beijing, China). The mice were raised in the animal feeding room of BUCM under specified conditions, i.e., temperature: 22 ± 2°C; relative humidity: 50 ± 5%; and 12/12 h light-dark cycle. All the methods and procedures of animal experiments were audited and approved by the Animal Experimental Welfare Ethics Committee of BUCM (BUCM-4-2019051002-2100).

2.6.2. Treatment and Assessment of Scald Healing. The scald model was created using the method described by Said et al. [15] with some modifications. For scald wound infliction, the animals were first anesthetized with pentobarbital sodium (50 mg/kg, b. w.), followed by removal of hairs from the dorsal area of mice using a hair trimmer. The model was established by heating copper sheets to induce skin scald (200°C, 3 s) with a wound diameter of 1.5 cm on the back of mice.

Preparation of ointment: RG, CG150, CG350, and CG750 were mixed with sesame oil in the ratio of 4:6, respectively, and RG ointment, CG150 ointment, CG350 ointment, and CG750 ointment were prepared.

A total of 126 animals were used and divided into 7 different groups (normal group, model group, RG group, CG150 group, CG350 group, CG750 group, and positive control group, *n* = 18, respectively), each having 6 animals. The model group was treated with sesame oil and considered as vehicle control. The RG group was topically treated with RG ointment; the CG150 group was topically treated with CG150 ointment; the CG350 group was topically treated with CG350 ointment; and the CG750 group was topically treated with CG750 ointment. The positive control group was topically treated with Jingwanhong Scald Ointment (JSO) purchased from Tianjin Darentang Jingwanhong Pharmaceutical Co., Ltd. (batch number: Z12020440, Tianjin, China). The treatment was given two times a day for 21 days.

On 5, 10, and 15 days after injury, 6 animals in each group were anesthetized and euthanized by intraperitoneal pentobarbital sodium injection (150 mg/kg, b. w.). Then, the

skin tissues from the wound site were excised for histological observation and immunohistochemical study. For histological and immunohistochemical analyses, tissues were fixed in 10% formalin at room temperature, and unbound fixative was removed by washing in PBS.

2.6.3. Histopathological Observation. The formalin-fixed tissue specimens were dehydrated by passing through gradient alcohol of 90%, 95%, and then absolute alcohol for 5, 5, and 5 min, respectively. This was followed by removing alcohol in the xylene solution and, finally, embedded in hot paraffin to prepare blocks. Blocks of a tissue section of $5\ \mu$ thickness were cut with a microtome. Hematoxylin and eosin (H&E) staining was used to show the morphology of skin tissue. Slice images were captured and digitized by a microscope (Nikon Eclipse Ti-SR, Nikon, Japan).

2.6.4. Immunohistochemical Analysis. On 5, 10, and 15 days after injury, the expression of IL-1 β and TGF was detected by immunohistochemistry in wound tissue sections. Immunohistochemical reactions were performed and incubated overnight at 4°C. Then, they were incubated with a secondary antibody (DAKO, China) for 50 minutes. After adequate diaminobenzidine staining and hematoxylin counterstaining, the positive expression can be observed and recorded under the microscope. The integrated optical density (IOD) was quantitatively analyzed using ImagePro Plus software (Media Cybernetics, USA).

2.7. Statistical Analysis. SPSS 16.0 software was used for statistical analysis, and one-way ANOVA and Student's *t*-test were used. All data were expressed as the mean \pm standard deviation. $P < 0.05$ was considered significant, and $P < 0.01$ was considered extremely significant.

3. Results

3.1. FTIR Spectroscopy Analysis. As shown in Figure 1(A), the main phase composition of RG is gypsum. It is conclusive that the IR absorption bands of RG are located at around $1620\ \text{cm}^{-1}$ and $1687\ \text{cm}^{-1}$ (bending vibration H_2O), $3405\ \text{cm}^{-1}$ and $3545\ \text{cm}^{-1}$ (stretching vibration H_2O), $601\ \text{cm}^{-1}$ and $668\ \text{cm}^{-1}$ (bending vibration SO_4^{2-}), and $1115\ \text{cm}^{-1}$ and $1141\ \text{cm}^{-1}$ (stretching vibration SO_4^{2-}) [1, 16].

As revealed in Figure 1(B), compared with RG, the intensity of the IR absorption peak of CG150 for bending vibration ($1620\ \text{cm}^{-1}$, $1687\ \text{cm}^{-1}$) and stretching vibration ($3405\ \text{cm}^{-1}$ and $3545\ \text{cm}^{-1}$) of H_2O decreased, corresponding to bassanite [17]. For CG350 (Figure 1(C)), there was a great deal of loss in absorbance at bending vibration and stretching vibration of H_2O . CG350 FTIR peaks at $673\ \text{cm}^{-1}$ and $1155\ \text{cm}^{-1}$ were attributed to anhydrite III [7]. For CG750, as shown in Figure 1(D), any bending vibration and stretching vibration of H_2O were not detected, and the IR absorption peak of CG750 was located at $594\ \text{cm}^{-1}$, $613\ \text{cm}^{-1}$, and $676\ \text{cm}^{-1}$, demonstrating that the main phase of CG750 was anhydrite II [7].

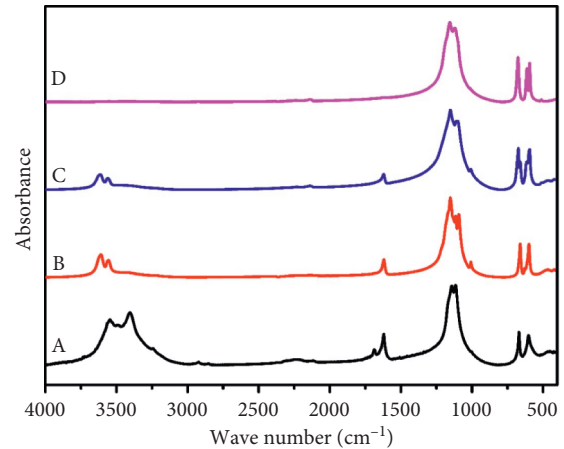


FIGURE 1: The infrared spectrum of RG (a), CG150 (b), CG350 234 (c), and CG750 (d).

3.2. XRD Spectroscopy Analysis. XRD was employed to analyze the phase composition changes of samples. XRD data were further processed by Jade 9 software for phase analysis. In Figure 2, the diffraction pattern of RG is consistent with the PDF file no.04-008-9805 (gypsum), showing that the main crystal structure of RG is gypsum; three prominent diffraction peaks correspond to (020), (040), and (041) crystal faces of the standard peak. The diffraction pattern of CG150 is consistent with the PDF file no. 97-038-0286 (bassanite), and four weak peaks correspond to (200), (020), (220), and (204) crystal faces, indicating that the main crystal structure of CG150 is bassanite. CG350 pattern matches the PDF file no. 04-011-1764 (anhydrite III); four weak peaks correspond to (110), (310), (400), and (112) crystal faces, illustrating that the main crystal structure of CG350 is anhydrite III. The diffraction pattern of CG750 is in keeping with the PDF file no. 04-008-2486 (anhydrite II); four weak peaks corresponding to (020), (210), (202), (220), and (212) crystal faces, illustrating that the main crystal structure of CG750 is anhydrite II. The results are in good agreement with those of FTIR.

Integrating FTIR and XRD detection results, we confirmed that the phase structures of RG, CG150, CG350, and CG750 are gypsum, bassanite, anhydrite III, and anhydrite II in order. In the next study, we will explore these four different phase structures' mineralogical properties, their antibacterial and anti-inflammatory effects, and their healing effects on scald injuries.

3.3. SEM Observation. SEM images clearly showed differences in texture among RG, CG150, CG350, and CG750 (Figure 3). As shown in Figure 3(a), no defects were observed on RG particles' surface, and the surface is plate-like and overlapped. While, small cracks appeared on the outside of CG150, as shown in Figure 3(b). For CG350, there are many pore structures with faults, and the marks are arranged longitudinally parallel. However, interestingly, the surface of CG750 began to appear as small and dense cracks instead of becoming looser.

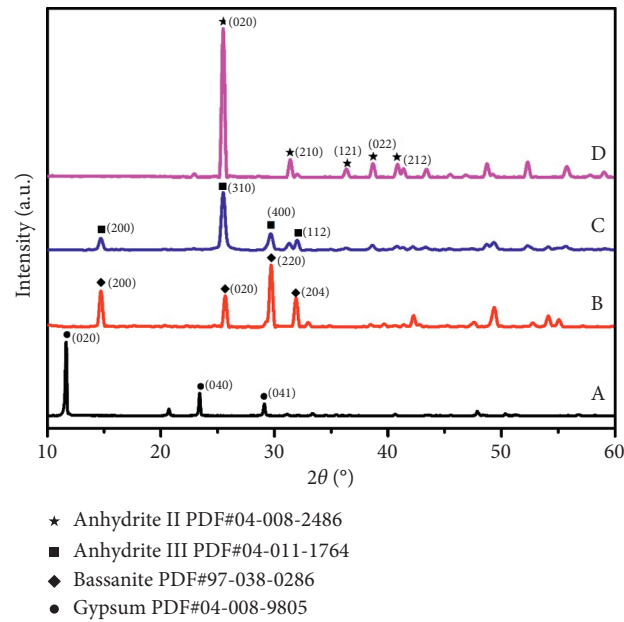


FIGURE 2: The XRD patterns of RG (A), CG150 (B), CG350 (C), and CG750 (D).

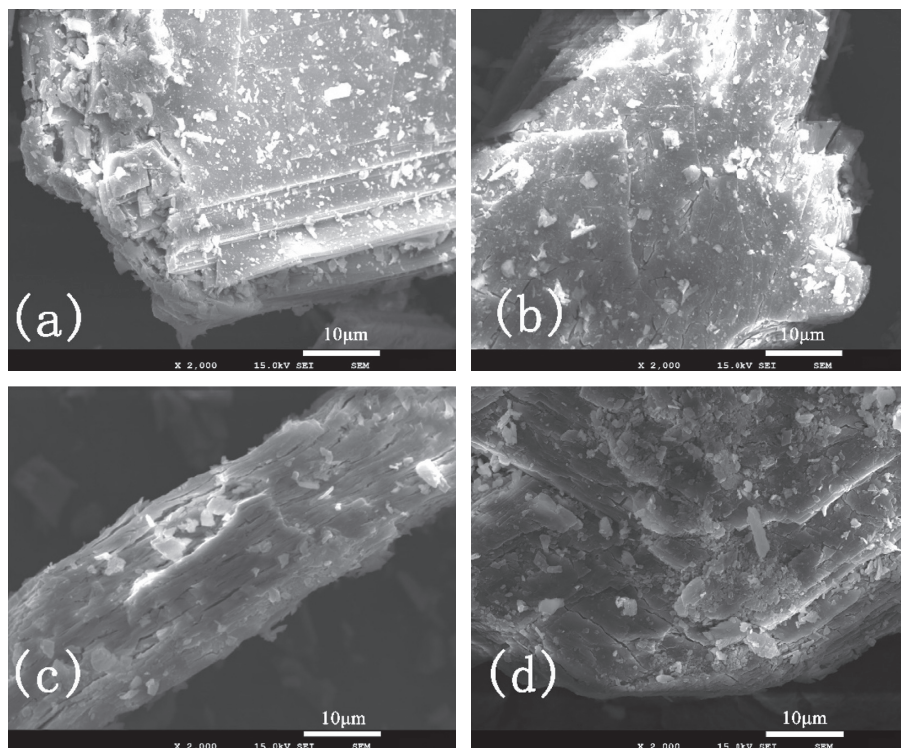


FIGURE 3: The SEM images of (a) RG, (b) CG150, (c) CG350, and (d) CG750.

According to the description of CG [2], loose and fragile means better quality. From our results, we can see that the order of the cracks on CGs from large to small is CG350, CG150, CG750, and RG; the corresponding phase structures are anhydrite III, bassanite, anhydrite II, and gypsum.

3.4. SAPA Measurement. The N_2 adsorption-desorption isotherms of RG, CG150, CG350, and CG750 powders are shown in Figure 4. The N_2 adsorption-desorption isotherms of RG and CG750 followed type III with an H1 hysteresis loop [18] in the relative pressure range of 0.8–1.0, which

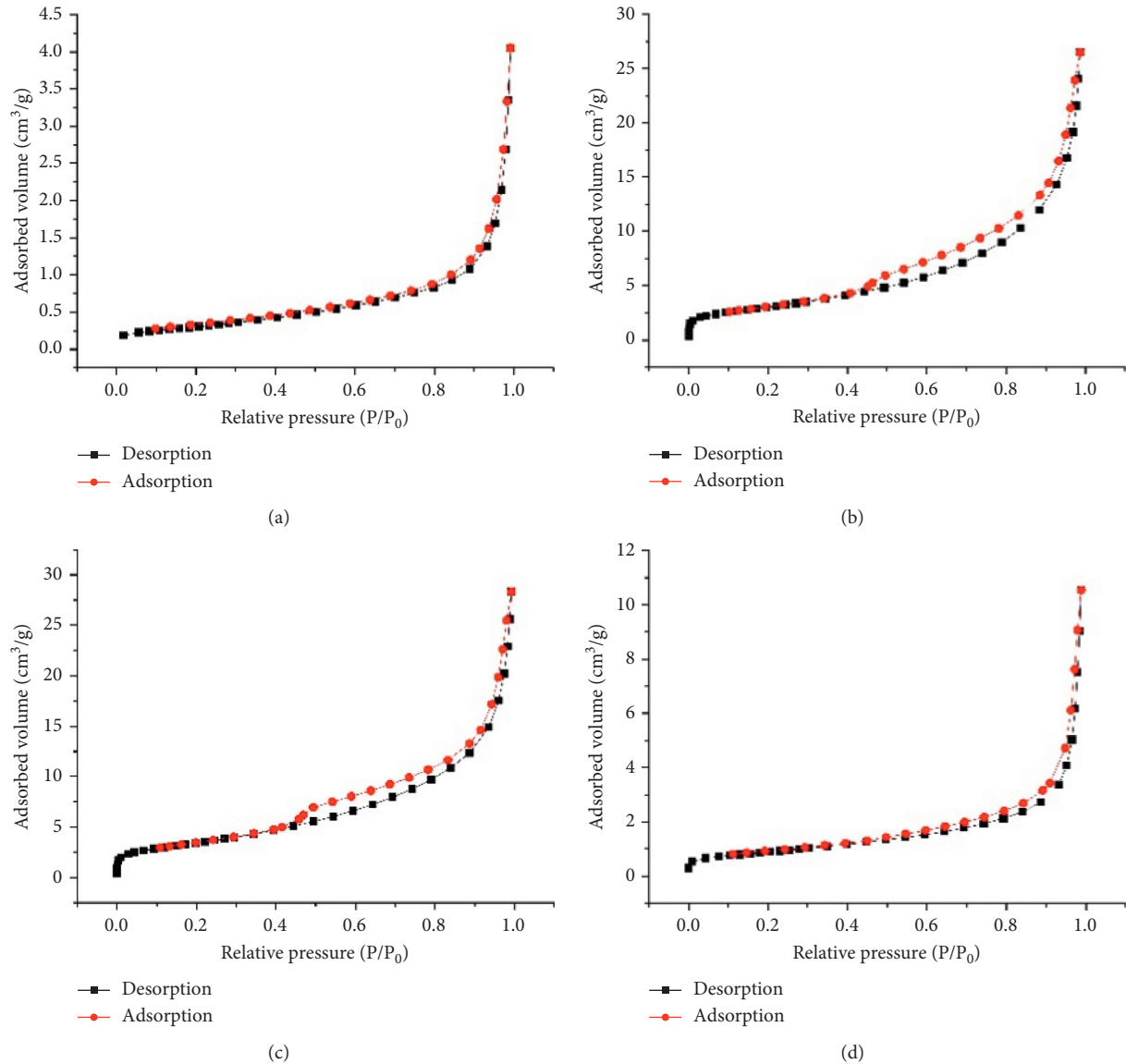


FIGURE 4: Nitrogen adsorption-desorption isotherms of (a) RG, (b) CG150, (c) CG350, and (d) CG750 powder.

means that the powder has macroporous characteristics. The N_2 adsorption-desorption isotherms of CG150 and CG350 were consistent with type IV with an H3 hysteresis loop [18] in the relative pressure range of 0.4–1.0, which means that the characteristics of the materials are mesoporous [19].

It can be seen from Table 1, as the calcination temperature of RG rises from 150°C to 750°C, the specific surface area and pore volume of the calcined products first increase and then decrease. Among RG, CG150, CG350, and CG750, CG150 and CG350 had the larger specific surface area and pore volume. The increase of the specific surface area and pore volume of CG150 and CG350 may be due to dehydration and dehydroxylation reactions in gypsum with the increase of calcination temperature [20]. When the calcination temperature is set at 750°C, due to the influence of high temperature, the internal chemical bonds of CG750 are broken, and the molecular structure is rearranged, resulting in smaller pore volume and specific surface area [21]. The

relatively large surface area and pore volume mean more space to absorb exudate and keep the wound surface dry for external use. The experimental results are consistent with those of SEM observation.

3.5. Colour Measurement. The colorimetric characteristics, lightness (L^*), redness (a^*), and yellowness (b^*) values are presented in Figure 5(b). The L^* value results showed that the colour of all the calcined samples is lighter than the gypsum. From the detected a^* value results, it can be found that the colour of gypsum gradually turns to red after calcination: the colour of CG750 is redder than that of CG350 and CG150, and the colour of CG350 is redder than that of CG150. CG750, CG350, and CG150's b^* value measured with the colorimeter was significantly higher than that of RG, meaning that the colour of calcined samples was yellow, and the order of yellowness was CG350 > CG750 > CG150.

TABLE 1: The textural properties of RG, CG150, CG350, and CG750 powder.

| Sample | RG | CG150 | CG350 | CG750 |
|--------------------------------------|---------|---------|---------|---------|
| BET surface area (m ² /g) | 1.1215 | 11.0159 | 12.5437 | 3.1734 |
| Pore volume (ml/g) | 0.0063 | 0.0409 | 0.0438 | 0.0163 |
| Average pore size (nm) | 22.4699 | 14.8513 | 13.9672 | 20.5458 |

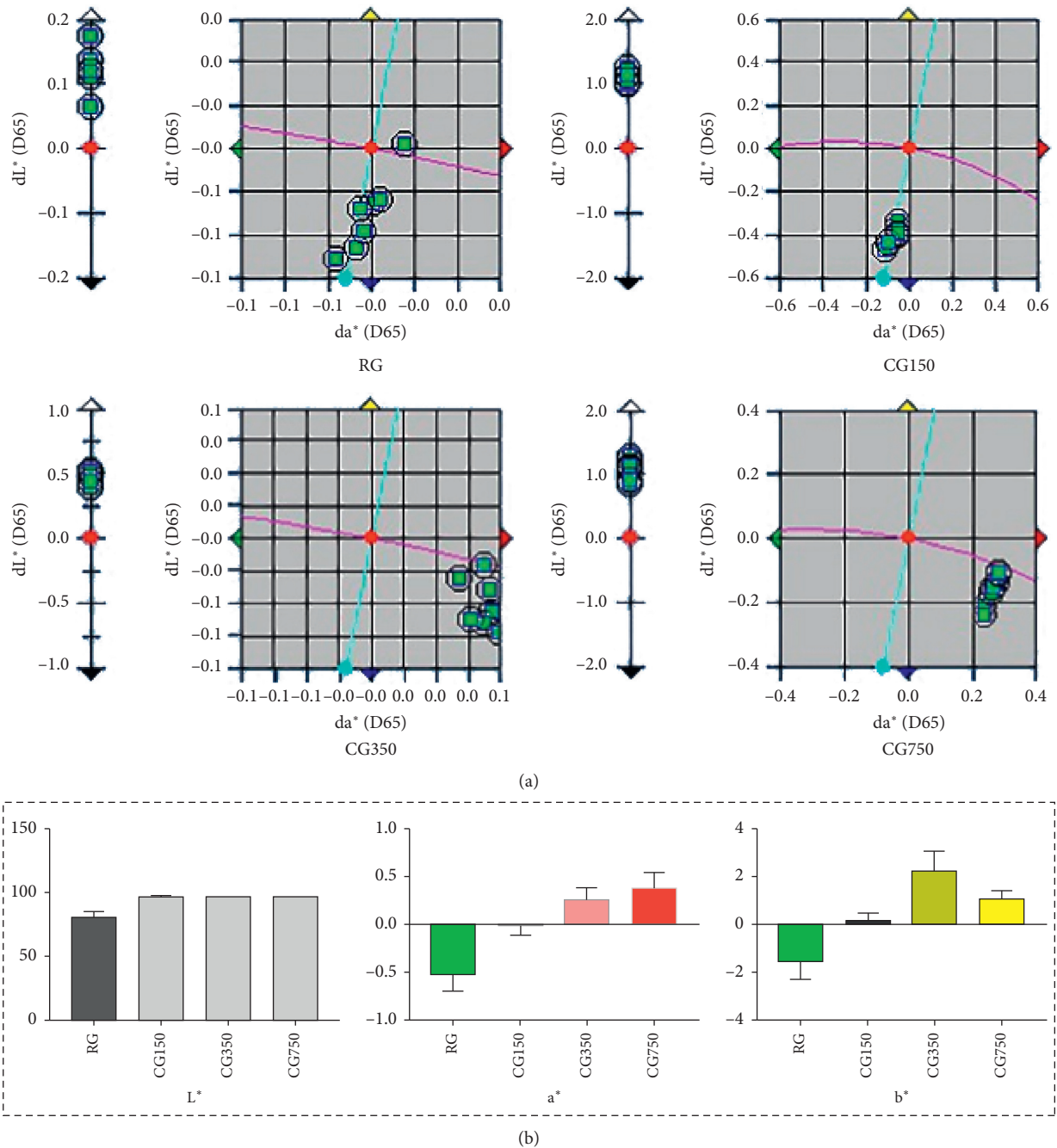


FIGURE 5: (a) Instrumental colour dL^* values, da^* values, and db^* values' scatter diagram of RG, CG150, CG350, and CG750. (b) Instrumental colour L^* values, a^* values, and b^* values of RG, CG150, CG350, and CG750 (values within each column with different letters are significantly different ($P < 0.05$)).

Shape, colour, smell, and texture are the traditional indicators commonly used to evaluate the quality of Chinese medicine. However, the application of them is limited due to

the difficulty of quantification and the high dependence on experience. Many evaluation methods based on colour measurement have been developed in modern times to

evaluate the quality of traditional Chinese medicine [22]. According to the Chinese Pharmacopoeia, CG should be white and opaque with red lustre [2]. However, it is difficult to distinguish the difference between samples with the naked eye. Colour as an appearance indicator of CG has not been determined by a quantitative method. Our colour measurement results also provide a reference for the quality control of CG.

3.6. Cell Experiment Results

3.6.1. Effect on the Viability of RAW 264.7 Cells. The effects of RG, CG150, CG350, and CG750 on RAW264.7 cell viability are shown in Figure 6. On treatment with 100, 250, or 500 mg/ml, the cell viability was above 90%, implying that RG, CG150, CG350, and CG750 did not produce harmful toxicity. The LD50 of the RG group was 2853 mg/ml, that of the CG150 group was 1933 mg/ml, that of the CG350 group was 1304 mg/ml, and that of the CG750 group was 1685 mg/ml. Samples significantly decreased the cell viability at 1000 mg/ml and 2000 mg/ml ($P < 0.01$). Therefore, concentrations of 100, 250, and 500 mg/ml of samples were selected for further investigation.

3.6.2. Effects on NO Production in LPS-Induced RAW264.7 Cells. To evaluate the effect of RG, CG150, CG350, and CG750 on inflammation, the LPS-induced inflammation model was successfully established. As shown in Figure 7, compared with the LPS model group, the NO expression level in the quercetin-positive group was significantly decreased ($P < 0.01$). All samples had inhibitory effects on NO production in LPS-induced RAW264.7 cells ($P < 0.01$). The inhibitory effects of CG150 and CG350 on the release of NO were stronger than those of RG and CG750 ($P < 0.01$), and there was no significant difference between the effects of CG150 and CG350 ($P > 0.05$).

NO can be stimulated by a variety of harmful stimuli, such as pathogens, damaged cells, or irritants [23]. Excessive production of NO can induce chronic inflammation in macrophages [24, 25]. Our results showed that RG, CG150, CG350, and CG750 could dose-dependently inhibit the production of NO produced by LPS-stimulated cells, while CG350 and CG150 have a stronger effect. All these indicate that CG150 and CG350 will perform better in the inflammatory response induced by injuries such as burns or ulcers, compared with RG and CG750.

3.7. Bacteriostatic Experiment Results

3.7.1. Antibacterial Activity. In Figure 8, there was no significant difference in the number of colonies in the RG group compared with the control group, which implied that RG has no inhibitory effect on *E. coli*. It is worth noting that the inhibition rate of CG350 on *E. coli* was $91.26 \pm 7.33\%$. However, CG750 exhibited lower antibacterial activity, with its inhibition rate at $35.54 \pm 0.57\%$, and the inhibition rate of CG150 was $65.50 \pm 12.43\%$. So, CG350 performs obvious bacteriostatic advantages on *E. coli*, compared to RG,

CG150, and CG750 ($P < 0.05$). The differences in the bacteriostatic effect between samples were unexpected. Our results indicated that all CG samples exhibit bacteriostatic effects after calcination, while CG samples with different phase structures showed a different antibacterial effect.

Bacterial infections are very common in burns and other traumas [26]. European Wound Management Association (2005) described that *E. coli* is an important organism causing wound infections [27]. Our results showed that CG350 has an excellent effect in inhibiting *E. coli*, which provides a piece of evidence for CG350 as a better phase structure for external use. However, the antibacterial effects of CG with different phase structures on other bacteria still need to be further studied to support this conclusion.

3.7.2. Bacterial Morphological Changes. The morphology of *E. coli* after being cultured with RG, CG150, CG350, and CG750 for 7 h and 14 h is shown in Figure 9. Under normal conditions, *E. coli* is short rod-shaped and have a smooth surface; their diameter is about 800 nm. Compared with the control group, RG showed no effect on the cell membrane of *E. coli* at both 7 h and 14 h, while CG150, CG350, and CG750 excreted different degrees of damage to the cell membrane. Compared with normal *E. coli*, the shape of *E. coli* that interacted with CG150 and CG350 became irregular. The cell membrane was damaged and could not be kept intact. The membrane and structure of *E. coli* interacted with CG350 were more seriously damaged and broken compared with CG150 and CG750. The results of the influence on the morphology of *E. coli* are consistent with those of the antibacterial effect on *E. coli*.

Infection is one of the severe complications of trauma [28]. Over the past decades, many studies have confirmed this view that microorganisms are critical causes of delayed healing and infection of acute or chronic burn wounds [29, 30]. *E. coli* is the most common pathogen causing wound infection [31]. However, most pathogenic bacteria's resistance increases year by year with the widespread use of antibiotics [32]. It is urgent to find nontoxic materials to resist bacterial infection. CG is a widely used external medicine for wound healing in Chinese medicine. Pathogenic bacteria easily infect wounds after formation, so inhibiting the growth of bacteria is an important indicator to evaluate the efficacy of CG. In this experiment, CG showed a strong antimicrobial effect.

3.8. Results of Histopathological Analysis

3.8.1. Histopathological Examinations. As shown in Figure 10, histological observations of wounds in different groups are presented. The normal anatomy of skin tissues stained with H&E showed healthy granulation, hair follicles, epithelial cells, fibroblast cells, blood vessels, epithelial, epidermal, and dermal layers (Figure 10).

On the 5th day, in the RG group and CG150 group, skins had more severe damage to the epidermal tissue, a large number of necrotic tissue debris, pus cells, adipocyte cavities, and exudates formed by the crust structure covering,

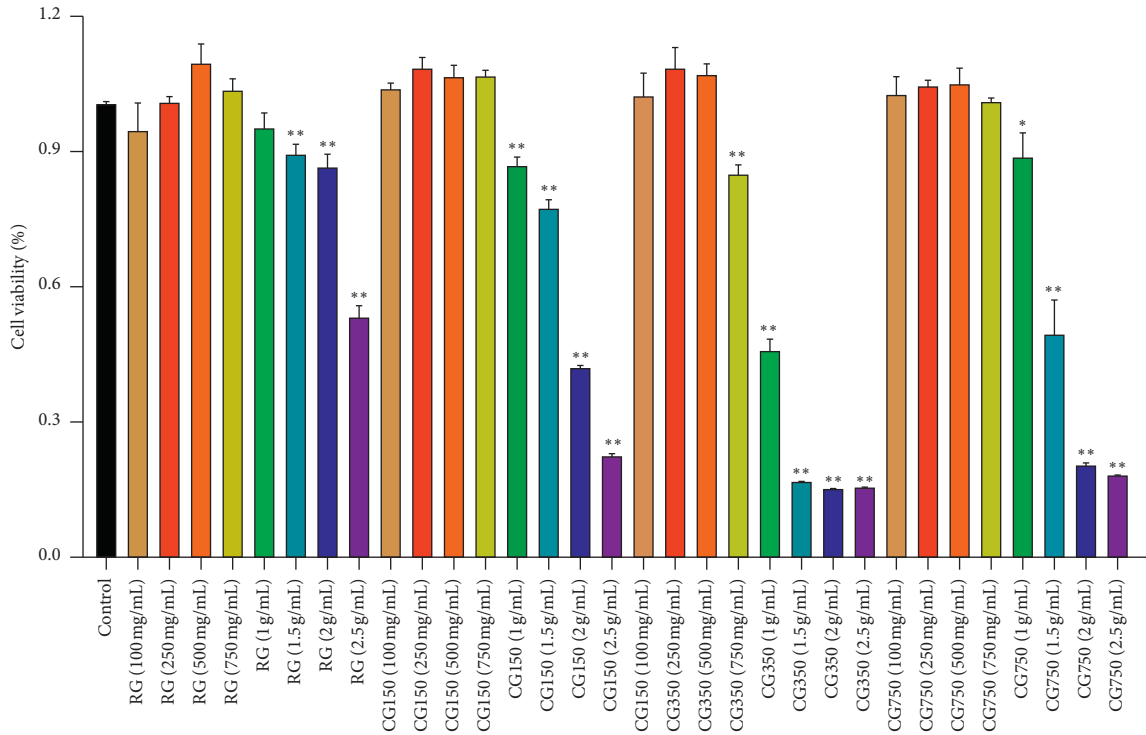


FIGURE 6: RAW264.7 cell viability. Cells were treated with different concentrations of RG, CG150, CG350, and CG750 for 24 h, and cell viability was measured using an MTT assay (** $P < 0.01$ and * $P < 0.05$ vs. control).

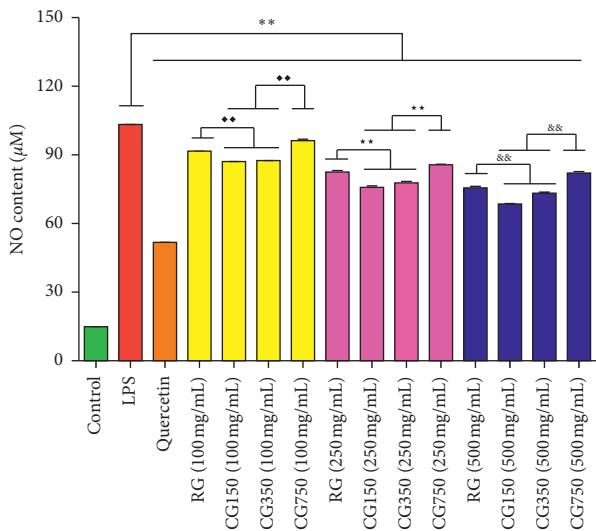


FIGURE 7: NO content of RG, CG150, CG350, and CG750. NO assay using the cells treated with LPS ($1 \mu\text{g/ml}$) in the absence or presence of RG, CG150, CG350, and CG750 at different concentrations (100, 250, and 500 mg/ml, respectively) for 24 h (** $P < 0.01$ vs. LPS; ♦♦ $P < 0.01$ vs. CG150 (100 mg/mL) and CG350 (100 mg/mL); ** $P < 0.01$ vs. CG150 (250 mg/mL) and CG350 (250 mg/mL); && $P < 0.01$ vs. CG150 (500 mg/mL) and CG350 (500 mg/mL)).

with a large number of inflammatory cell infiltration and more bleeding phenomenon. The damaged skin of the CG150 group had signs of exfoliation. In the CG350, CG750, and positive drug groups, the necrotic epidermal tissues

began to recover, with tiny scabs, a small number of inflammatory cells scattered around, a small number of fibroblasts and new capillaries visible, as well as mature granulation tissue proliferation and repair, and more fibroblasts and collagen fibres visible.

On day 10, the skin of CG350, CG750, and positive drug groups recovered well and generated a large amount of mature hair follicle tissue, fat vacuoles, and arranged complete muscle tissue. The model group, RG group, and CG150 group had worse skin recovery. The model group and RG group had early hair follicle tissue generation, while the CG150 group had no hair follicle tissue generation and muscular tissue of which was also irregularly arranged.

On day 15, the skin in other groups except the CG150 group grew more mature granulation tissue, fibroblasts, collagen fibres, and many mature hair follicle tissues. Compared with other groups, the CG350 and positive drug groups had more new well-arranged hair follicle tissues and well-recovered skin blood vessels.

It is surprising in the experimental results that the effect of CG150 on wound healing is worse than that of the model group. The reason for this result may be that CG150, whose main phase structure is bassanite with strong water absorption [33], leads to excessive dryness of the wound, resulting in a secondary pus discharge from the wound [34].

3.8.2. Immunohistochemical Analysis. The expression of IL- β and TGF in the wound site was detected by immunohistochemistry. Immunohistochemical examination of the vital wound is summarized in Figures 11 and 12. On the 5th,

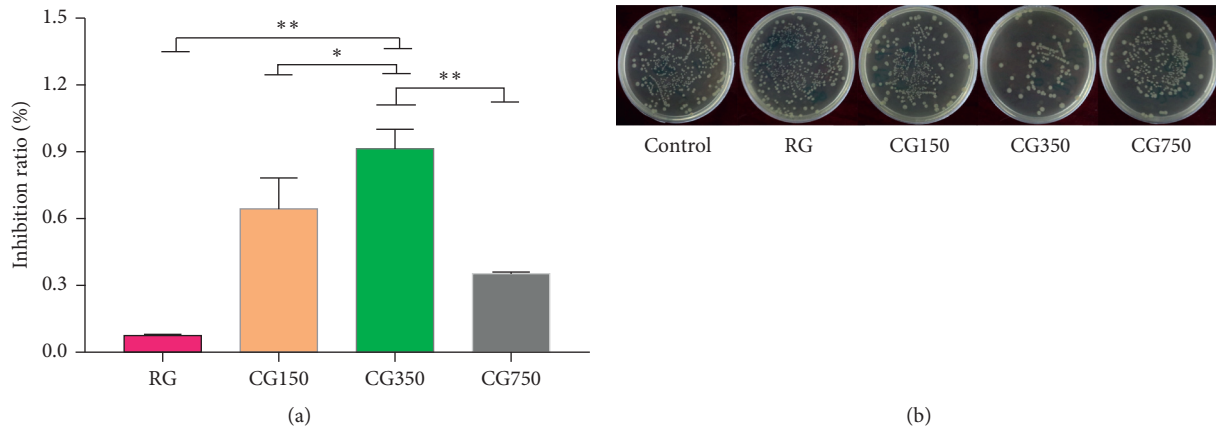


FIGURE 8: (a) Inhibition ratio of RG, CG150, CG350, and CG750 measured by a plate counting method. (b) Number of live bacteria of *E. coli* treated with culture medium, with 5 g/mL of RG, CG150, CG350, and CG750 (** $P < 0.01$ and * $P < 0.05$ vs. CG350).

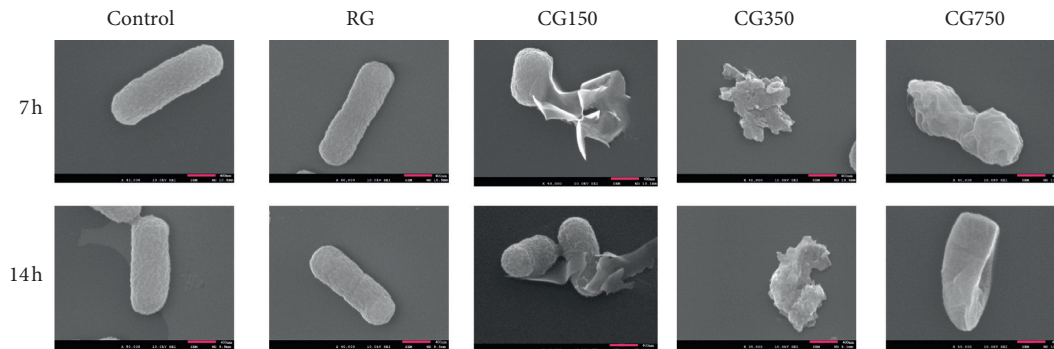


FIGURE 9: FESEM images of bacterial morphology. (a) The bacteria morphology at 7 h. (b) The bacteria morphology at 14 h.

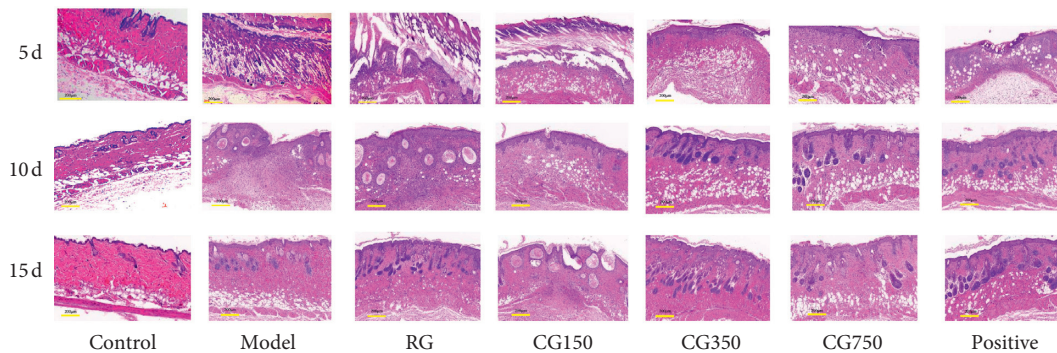


FIGURE 10: Histological appearance of scald wounds stained with hematoxylin and eosin (20x magnification, the scale is marked in the lower left corner).

10th, and 15th day, compared with the control group, the content of IL-1 β in the model group was high ($P < 0.01$). On the 10th day, compared with the model group, the IL-1 β expression levels of CG350, CG750, and the positive groups decreased significantly ($P < 0.01$). Compared with the CG350 group, the IL-1 β expression levels of the model, RG, CG150, and CG750 groups increased significantly ($P < 0.05$). On the 15th day, compared with the model group, the IL-1 β expression levels of CG350 and the positive group decreased

significantly ($P < 0.01$). There was no significant difference between CG350 and the positive group ($P > 0.05$). Compared with the CG350 group, the IL-1 β expression levels of the model, CG150, RG, and CG750 groups increased significantly ($P < 0.05$).

In terms of TGF expression, on the 5th, 10th and 15th day, compared with the control group, the content of TGF in the model group was high ($P < 0.01$). On the 5th day, compared with the model group, the expression of TGF in the CG350

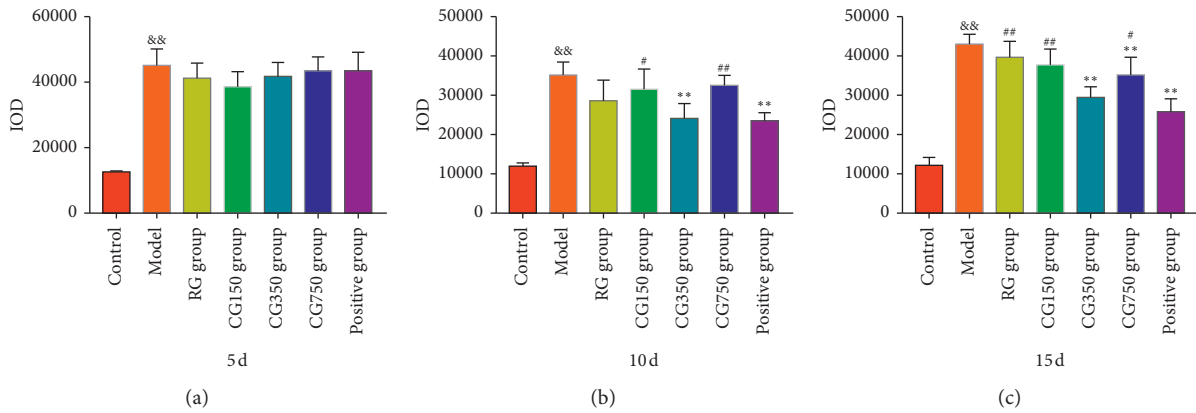


FIGURE 11: IL-1 β expression levels in RG, CG150, CG350, and CG750 groups (&& $P < 0.01$ vs. the control group. ** $P < 0.01$ vs. the model group. ## $P < 0.01$ and # $P < 0.05$ vs. the CG350 group).

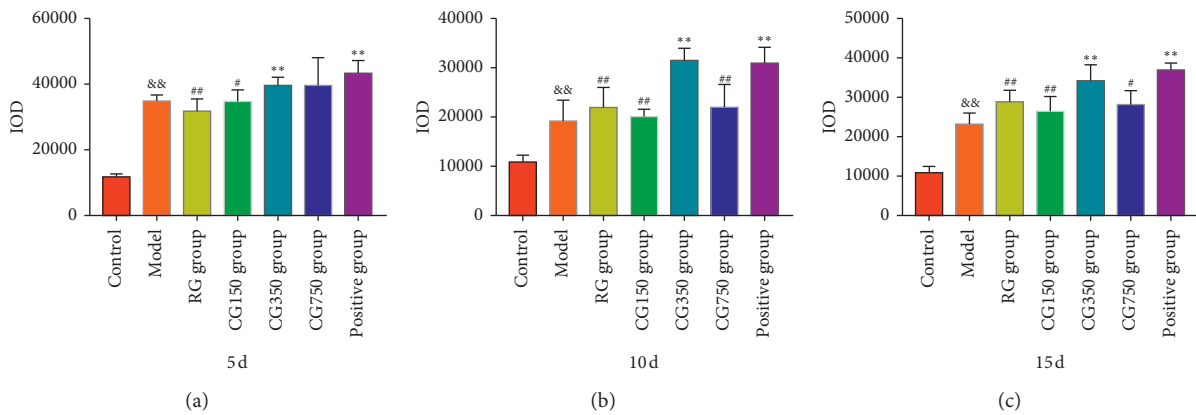


FIGURE 12: TGF expression levels in RG, CG150, CG350, and CG750 groups (&& $P < 0.01$ vs. the control group. ** $P < 0.01$ and * $P < 0.05$ vs. the model group. ## $P < 0.01$ and # $P < 0.05$ vs. the CG350 group).

group and positive group was significantly higher ($P < 0.01$). Compared with the CG350 group, the TGF content of RG, CG150, and model groups was decreased ($P < 0.05$). On the 10th day, compared with the model group, the TGF content of CG350 and positive groups was increased ($P < 0.05$). Compared with the CG350 group, the TGF content of RG, CG150, CG750, and model groups was decreased ($P < 0.01$). On the 15th day, compared with the model group, the TGF expression of the CG350 group and positive group increased significantly ($P < 0.01$). Compared with the CG350 group, the TGF content of RG, CG150, CG750, and model groups was decreased ($P < 0.05$).

After scald injuries, a natural repair process is initiated, consisting of hemostasis, inflammation, proliferation, and remodelling [35]. High levels of proinflammatory cytokines and mediators, such as IL-1 β , delayed wound healing [36]. TGF is the primary growth factor responsible for epithelial-mesenchymal transitions and has a generous contribution to skin fibrosis [37].

Our study results corroborated that CG350 had a repair effect on scalded skin. More notably, CG350 significantly downregulated the expression of IL-1 β and upregulated the expression of TGF to improve scald wound healing.

4. Discussion

CG is commonly used to treat scalds and has the effects of secretion absorption, wound healing, and muscle regeneration [38]. According to traditional trait requirements, CG needs to be calcined to be opaque, brittle, and reddish [39]. During calcination, colour and texture are essential appearance indicators to control product quality. Microstructure and pore size are generally considered to be mineralogical properties related to the exudate absorbing capacity of CG. When scalds occur, wounds tend to become infected with microorganisms without treatment [40]. Following wound infection, toxic molecules and metabolites produced by persistent inflammation, bacteria, and immune responses adversely affect wound repair [41]. So far, it is still unclear how the material phase structure of CG impacts the treatment of scald wounds.

In this study, three kinds of phase structures are produced after gypsum calcination: CG150, CG350, and CG750 correspond to bassanite, anhydrite III, and anhydrite II, respectively. CG350 was the most brittle with the largest specific surface area and pore volume, followed by CG150 and CG750. RG's main component is CaSO₄•2H₂O;

when the calcination temperature rises to 150°C, the internal water molecules spill from the structure, the molecular structure stabilized by RG is destroyed, the spatial structure is unstable, the internal pores increase, and bassanite is generated. A larger crack appeared on the surface of CG150, and the specific surface area and pore volume increased correspondingly. When the calcination temperature was 350°C, anhydrite III without crystallographic water was formed. CG350 showed a larger surface crack, larger specific surface area, and pore volume. Nevertheless, when the temperature increased to 750°C, anhydrite II was formed, the structure was compact, and the specific surface area and pore volume became small. The reason is that high temperature makes CG350 internal sintering, and stable state molecules (or atoms) attract each other [42], thus forming particle binding and powder strength. In turn, the crack, specific surface area, and pore volume of CG750 are smaller than CG350. After scalding, abscesses are easily formed on the skin surface, CG350 has a large pore structure, and its phase structure is anhydrite III, which has a strong water absorption capacity [43]. Thus, CG350 can better absorb exudation in wound abscess, promoting the disappearance of the abscess, which is conducive to scald healing.

Our research group found that the calcium dissolution of RG, CG150, CG350, and CG750 was 3.17%, 3.25%, 4.76%, and 3.19%, respectively. The dissolution of calcium ions in samples is closely related to the pore structure. When CG150, CG350, and CG750 were in contact with water, the water molecules then moved along the channel towards the crystal's interior and interacted with the surrounding ions. After interacting with the surrounding ions, the crystal structure is destroyed, further expanding the contact surface between the crystal and water molecules, accelerating the crystal breaking and forcing Ca^{2+} and SO_4^{2-} to move to water [44]. CG350 has the most extensive porosity, specific surface area, and pore volume, so calcium ion dissolution is the highest. Studies have shown that calcium ion plays a vital role in scald healing [45] and the anti-inflammatory effect [46]. Cadherin is a kind of cell adhesion glycoprotein with the characteristics of convergence and calcium dependence. It plays an essential role in cell recognition, migration, tissue differentiation, and adult tissue and organ composition [47]. Therefore, it is speculated that the different degrees of dissolution of calcium ions caused by the phase structure may be an important factor causing the difference in biological activity.

Based on the above analysis, the biological activity exerted by CG is closely related to the phase structure, which affects the mineralogical properties and the dissolution of calcium ions. The experimental results showed that CG350, the main phase structure of anhydrite III, exhibited more advantages in texture, pore size, specific surface area, antibacterial, anti-inflammatory, and scald repairing. FTIR and XRD are the most common and reliable methods to determine the phase structure [48, 49]. In the process of calcining gypsum, FTIR and XRD are suggested to identify the phase structure of CG, which is of great significance for the quality control of CG.

5. Conclusions

In summary, RG, CG150, CG350, and CG750 are different in mineral properties and biological activities. RG has a dense structure, small pore size, a weak anti-inflammatory effect, but no antibacterial effect, and has almost no effect on the repair of scalds. CG150 has a loose texture, large pore size, and specific surface area and has a unique antibacterial and anti-inflammatory effect, but it has a low repair effect on scalds. CG750 has a compact structure, small pore size and specific surface area, and low antibacterial and anti-inflammatory effects, but it has a specific repair effect on scalds. Only CG350 has good properties in texture, pore size, specific surface area, antibacterial, anti-inflammatory, and scald repair. Our research has proved that, on the one hand, it is reasonable to not use RG for external use to treat trauma. On the other hand, the mineral properties and biological activities of CG are different due to different phase structures; an appropriate temperature should be selected in order to prepare CG with a better curative effect. CG350, namely, anhydrite III, is considered by our research to be the optimal phase structure for CG. Our research provides a reference for determining the best temperature for preparing CG and evaluating CG quality.

Data Availability

The data used to support the findings of this study are available from the corresponding author upon request.

Ethical Approval

Experiments were approved by the Experimental Animal Ethics Committee of Beijing University of Chinese Medicine, Beijing.

Conflicts of Interest

The authors declare that they have no conflicts of interest.

Authors' Contributions

Kaiyang Liu performed the experiments, data processing, and manuscript writing. Shu Han performed the experiments and data analysis. Wei Gao carried out experimental design and performed the experiments. Ya'nan Tang, Xitao Han, and Ziqin Liu participated in the collection and processing of tissue samples. Liyuan Bao, Meiru Zhi, and Hongyue Wang participated in mineralogical analysis. Yingli Wang carried out mineralogical experiment. Hong Du designed the study and wrote the manuscript.

Acknowledgments

This work was supported by grants from the Beijing Municipal Natural Science Foundation (BJNSF, 7182093), the National Natural Science Foundation of China (NSFC, 81774004), and the National Key Research and Development Plan (2018YFC1706303).

References

- [1] P. K. Mandal and T. K. Mandal, "Anion water in gypsum (CaSO₄·2H₂O) and hemihydrate (CaSO₄·1/2H₂O)," *Cement and Concrete Research*, vol. 32, no. 2, pp. 313–316, 2002.
- [2] National Pharmacopoeia Committee, *Pharmacopoeia of People's Republic of China*, China Medical Science and Technology Press, vol. 2, p. 98, Beijing, China, 2020.
- [3] C. Song, Z. J. Zhang, and B. L. Bian, "The hypothesis of medicinal gypsum cooling material," *Spectroscopy and Spectral Analysis*, vol. 40, no. 6, pp. 1716–1721, 2020.
- [4] J. Zhang, M. Zhu, H. X. Xue et al., "Effect of ginseng and gypsum decoction combined with lomefloxacin hydrochloride on patients with liver-yang-hyperactivity migraine," *China Journal of Pharmaceutical Economics*, vol. 12, no. 11, pp. 109–111, 2017.
- [5] S. Seufert, C. Hesse, F. Goetz-Neunhoffer, and J. Neubauer, "Quantitative determination of anhydrite III from dehydrated gypsum by XRD," *Cement and Concrete Research*, vol. 39, no. 10, pp. 936–941, 2009.
- [6] D. Gazdič, I. Hájková, and R. Magrla, "Monitoring of calcium sulphate phase transformations using high-temperature X-ray diffraction," *Advanced Materials Research*, vol. 864–867, pp. 621–624, 2014.
- [7] N. Prieto-Taboada, O. Gómez-Laserna, I. Martínez-Arkarazo, M. Á. Olazabal, and J. M. Madariaga, "Raman spectra of the different phases in the CaSO₄-H₂O system," *Analytical Chemistry*, vol. 86, no. 20, pp. 10131–10137, 2014.
- [8] Y. Li, Y. L. Wang, S. Liu et al., "The effect of temperature and time factors on the quality of calcined gypsum," *Beijing Journal of Traditional Chinese Medicine*, vol. 36, no. 4, pp. 368–370+372, 2017.
- [9] J. M. Duke, S. M. Randall, J. H. Boyd et al., "A retrospective cohort study to compare post-injury admissions for infectious diseases in burn patients, non-burn trauma patients and uninjured people," *Burns & Trauma*, vol. 6, no. 2, pp. 129–139, 2018.
- [10] G. L. Rodgers, J. Mortensen, M. C. Fisher, A. Lo, A. Cresswell, and S. S. Long, "Predictors of infectious complications after burn injuries in children," *The Pediatric Infectious Disease Journal*, vol. 19, no. 10, pp. 990–995, 2000.
- [11] D.-m. Liu, B.-w. Sun, Z.-w. Sun, Q. Jin, Y. Sun, and X. Chen, "Suppression of inflammatory cytokine production and oxidative stress by CO-releasing molecules liberated CO in the small intestine of thermally-injured mice," *Acta Pharmacologica Sinica*, vol. 29, no. 7, pp. 838–846, 2008.
- [12] S. Brunauer, P. H. Emmett, E. Teller et al., "Adsorption of gases in multimolecular layers," *Journal of the American Chemical Society*, vol. 60, no. 2, pp. 309–319, 1938.
- [13] E. P. Barrett, L. G. Joyner, and P. P. Halenda, "The determination of pore volume and area distributions in porous substances. I. Computations from nitrogen isotherms," *Journal of the American Chemical Society*, vol. 73, no. 1, pp. 373–380, 1951.
- [14] K. León, D. Mery, F. Pedreschi, and J. León, "Color measurement in L*a*b* units from RGB digital images," *Food Research International*, vol. 39, no. 10, pp. 1084–1091, 2006.
- [15] A. Said, N. Naeem, S. Siraj et al., "Mechanisms underlying the wound healing and tissue regeneration properties of *Cheopodium album*," *3 Biotech*, vol. 10, no. 10, p. 452, 2020.
- [16] M. D. Lane, "Mid-infrared emission spectroscopy of sulfate and sulfate-bearing minerals," *American Mineralogist*, vol. 92, no. 1, pp. 1–18, 2007.
- [17] F. Rosi, A. Daveri, B. Doherty et al., "On the use of overtone and combination bands for the analysis of the CaSO₄-H₂O system by mid-infrared reflection spectroscopy," *Applied Spectroscopy*, vol. 64, no. 8, pp. 956–963, 2010.
- [18] S. W. K. Sing, "Reporting physisorption data for gas/solid systems with special reference to the determination of surface area and porosity (Recommendations 1984)," *Pure & Applied Chemistry*, vol. 57, no. 4, 2013.
- [19] Y. Zhang, M. Yuan, B. Jiang, P. Li, and X. Zheng, "Effect of mesoporous structure on Bi_{3.25}La_{0.75}Ti₃O₁₂ powder for humidity sensing properties," *Sensors and Actuators B: Chemical*, vol. 229, no. 28, pp. 453–460, 2016.
- [20] S. U. Qiucheng, Z. Shaohong, C. Peili, L. I. Xinjun, F. U. Juan, and M. A. Longlong, "In situ characterization and analysis on the thermal transformation of boehmite," *Chinese Journal of Inorganic Chemistry*, vol. 28, no. 11, pp. 2280–2284, 2012.
- [21] S. H. Liu, "Effect of calcination time and temperature on three phases of gypsum," *Sichuan Building Materials*, vol. 40, no. 4, pp. 25–28, 2014.
- [22] X. Min, Y. Shi-Long, P. Wei et al., "A novel method for the discrimination of semen arecae and its processed products by using computer vision, electronic nose, and electronic tongue," *Evidence-Based Complementary and Alternative Medicine*, vol. 2015, Article ID 753942, 10 pages, 2015.
- [23] P. L. Arroyo, V. Hatch-Pigott, H. F. Mower, and R. V. Cooney, "Mutagenicity of nitric oxide and its inhibition by antioxidants," *Mutation Research Letters*, vol. 281, no. 3, p. 193, 1992.
- [24] G. Aliev, M. E. Obrenovich, S. Tabrez et al., "Link between cancer and Alzheimer disease via oxidative stress induced by nitric oxide-dependent mitochondrial DNA overproliferation and deletion," *Oxidative Medicine and Cellular Longevity*, vol. 2013, Article ID 962984, 19 pages, 2013.
- [25] Y.-C. Yang, H.-Y. E. Chou, T.-L. Shen, W.-J. Chang, P.-H. Tai, and T.-K. Li, "Topoisomerase II-mediated DNA cleavage and mutagenesis activated by nitric oxide underlie the inflammation-associated tumorigenesis," *Antioxidants & Redox Signaling*, vol. 18, no. 10, pp. 1129–1140, 2013.
- [26] N. Pallua, P. C. Fuchs, B. Hafemann, U. Völpel, M. Noah, and R. Lütticken, "A new technique for quantitative bacterial assessment on burn wounds by modified dermabrasion," *Journal of Hospital Infection*, vol. 42, no. 4, p. 329, 1999.
- [27] European Wound Management Association (EWMA), *Position Document: Identifying Criteria for Wound Infection*, MEP Ltd, London, UK, 2005.
- [28] L. Danielsen, E. Balslev, G. Döring et al., "Ulcer bed infection," *APMIS*, vol. 106, no. 7–12, pp. 721–726, 1998.
- [29] S. Tejiram and J. W. Shupp, "Infections in burn patients: innovations in infection prevention and treatment," *Surgical Infections*, vol. 22, 2021.
- [30] R. Reid, J. W. Simcock, L. Chisholm, B. Dobbs, and F. A. Frizelle, "Postdischarge clean wound infections: incidence underestimated and risk factors overemphasized," *ANZ Journal of Surgery*, vol. 72, no. 5, pp. 339–343, 2002.
- [31] M. A. Saeed, A. Haque, A. Ali et al., "A profile of drug resistance genes and integrons in *E. coli* causing surgical wound infections in the Faisalabad region of Pakistan," *The Journal of Antibiotics*, vol. 62, no. 6, pp. 319–323, 2009.
- [32] M. Raviglione, "XDR-TB: entering the post-antibiotic era?" *The International Journal of Tuberculosis and Lung Disease: The Official Journal of the International Union Against Tuberculosis and Lung Disease*, vol. 10, no. 11, pp. 1185–1187, 2006.
- [33] G. D. Mou, "A study on the phase transformation of the bassanites during hydration," *Journal of the Chinese Ceramic Society*, vol. 4, pp. 532–536, 2002.

- [34] J. H. Zhang, "Purulent wounds should not be smeared with purple potions," *Xin Nong Cun*, vol. 4, p. 26, 2003.
- [35] V. Kanikireddy, K. Varaprasad, T. Jayaramudu, C. Karthikeyan, and R. Sadiku, "Carboxymethyl cellulose-based materials for infection control and wound healing: a review," *International Journal of Biological Macromolecules*, vol. 164, pp. 963–975, 2020.
- [36] Y. Lim, M. A. Levy, and T. M. Bray, "Dietary supplementation of N-acetylcysteine enhances early inflammatory responses during cutaneous wound healing in protein malnourished mice," *The Journal of Nutritional Biochemistry*, vol. 17, no. 5, pp. 328–336, 2006.
- [37] F. Caiado, T. Carvalho, F. Silva et al., "The role of fibrin E on the modulation of endothelial progenitors adhesion, differentiation and angiogenic growth factor production and the promotion of wound healing," *Biomaterials*, vol. 32, no. 29, pp. 7096–7105, 2011.
- [38] T. Xu, Y. J. Xu, X. X. Xu et al., "Effects of gypsum and saimei'an powder on wound healing," *Guide of China Medicine*, vol. 9, no. 36, pp. 251–252, 2011.
- [39] J. Y. Yue and L. Zhang, "Research progress on medicinal gypsum fibrosum," *Guangzhou Chemical Industry*, vol. 6, no. 44, pp. 4–6, 2016.
- [40] Z. Kopecki, "Development of next-generation antimicrobial hydrogel dressing to combat burn wound infection," *Bioscience Reports*, vol. 41, 2021.
- [41] R. M. Huebinger, D. H. Stones, M. D. S. Santos et al., "Infection following burn injury," *Scientific Reports*, vol. 6, p. 39341, 2016.
- [42] I.-W. Chen and X. H. Wang, "Sintering dense nanocrystalline ceramics without final-stage grain growth," *Nature*, vol. 404, no. 6774, pp. 168–171, 2000.
- [43] S. C. Zheng, Q. Yu, P. Ning et al., "Effect of soluble anhydrite III on hydration process of hemihydrate gypsum," *Yunnan Chemical Technology*, vol. 43, no. 3, pp. 1–5, 2016.
- [44] H. Fan, X. F. Song, Y. X. Xu et al., "Effect of calcination on stabilization of calcium sulfate hemihydrate whiskers," *Huadong Ligong Daxue Xuebao, Ziran Kexueban*, vol. 45, no. 3, pp. 388–395, 2019.
- [45] C. L. YueShan, Q. L. YongzhiWu, and J. Liao, "Hybrid cellulose nanocrystal/alginate/gelatin scaffold with improved mechanical properties and guided wound healing," *RSC Advances*, vol. 9, 2019.
- [46] J. Desousa, M. Tong, J. Wei, L. Chamley, P. Stone, and Q. Chen, "The anti-inflammatory effect of calcium for preventing endothelial cell activation in preeclampsia," *Journal of Human Hypertension*, vol. 30, 2016.
- [47] M. Kuwahara, M. Hatoko, H. Tada, and A. Tanaka, "E-cadherin expression in wound healing of mouse skin," *Journal of Cutaneous Pathology*, vol. 28, no. 4, pp. 191–199, 2010.
- [48] R. N. A. H. Lewis and R. N. Mcelhaney, "Membrane lipid phase transitions and phase organization studied by Fourier transform infrared spectroscopy," *Biochimica Et Biophysica Acta*, vol. 1828, no. 10, pp. 2347–2358, 2016.
- [49] U. Sarac, M. C. Baykul, and Y. Uguz, "Differences observed in the phase structure, grain size–shape, and coercivity Field of electrochemically deposited Ni–Co thin films with different Co contents," *Journal of Superconductivity & Novel Magnetism*, vol. 28, no. 10, pp. 1–6, 2015.

Research Article

Arsenic Content, Speciation, and Distribution in Wild *Cordyceps sinensis*

Yuancan Xiao ^{1,2,3} Cen Li,^{1,2} Wei Xu,⁴ Yuzhi Du,^{1,2} Ming Zhang,^{1,2} Hongxia Yang,^{1,2} Lixin Wei ^{1,2} and Hongtao Bi ^{1,2}

¹Qinghai Provincial Key Laboratory of Tibetan Medicine Pharmacology and Safety Evaluation, Northwest Institute of Plateau Biology, Chinese Academy of Sciences, Xining 810008, China

²Key Laboratory of Tibetan Medicine Research, Chinese Academy of Sciences, Xining 810008, China

³University of Chinese Academy of Sciences, Beijing 10049, China

⁴Beijing Synchrotron Radiation Facility, Institute of High Energy Physics, Chinese Academy of Sciences, Beijing 100049, China

Correspondence should be addressed to Lixin Wei; lxwei@nwipb.cas.cn and Hongtao Bi; bihongtao@hotmail.com

Received 9 October 2020; Revised 21 January 2021; Accepted 1 February 2021; Published 19 February 2021

Academic Editor: Adolfo Andrade-Cetto

Copyright © 2021 Yuancan Xiao et al. This is an open access article distributed under the Creative Commons Attribution License, which permits unrestricted use, distribution, and reproduction in any medium, provided the original work is properly cited.

The excessive arsenic content in wild *Cordyceps sinensis* has caused great concerns on human health. The toxicity of arsenic depends on its concentration, chemical form, and valence. The source studies of arsenic in *C. sinensis* are essential for safety evolution and quality control. We used ICP-MS and HPLC-ICP-MS methods to determine the total arsenic amount and the arsenic speciation. Synchrotron-based XANES and micro-XRF imaging techniques were used to characterize arsenic valence and distribution. The total arsenic amount range in wild *C. sinensis* samples was 5.77–13.20 $\mu\text{g/g}$ with an average of $8.85 \pm 2.5 \mu\text{g/g}$. As(III) and As(V) were the main species in wild *C. sinensis* samples. The iAs only accounts for 4.47–11.42% of the extracted arsenic. Trivalent and pentavalent forms were the dominant chemical forms of arsenic. Besides, we found that arsenic was accumulated at the digestive tract of the host larva.

1. Introduction

Cordyceps sinensis (*C. sinensis*) is a traditional medicine in China and eastern Asia. It is a complex of *C. sinensis* fungus and host larva that grow well at altitudes 3000–5000 m [1, 2]. *C. sinensis* occurs in the Qinghai-Tibet plateau and surrounding areas, including Tibet, Qinghai, Sichuan, Gansu, and Yunnan provinces [3]. Yushu and Guoluo prefecture of Qinghai province and Naqu region of Tibet are the core natural distribution areas [4, 5]. *C. sinensis* medicinal benefits include lung protection and kidney improvement [1, 2], immunomodulation [2, 6], antitumour effects [7], hepatoprotection [8], and increased endurance [9].

Some wild *C. sinensis* samples have a high arsenic content [10, 11] and some samples do not comply with the limit standard of BS ISO 18664:2015 [12]. Arsenic is a common element in air, soil, and groundwater [13]. Acute and chronic human exposure to arsenic causes a series of

adverse health effects. These include pulmonary and respiratory, cardiovascular and hematological, gastrointestinal, hepatic, renal, neurological, immunologic, developmental, and reproduction diseases and cancer [14–16]. Arsenic is a harmful element, and most countries have established arsenic limits for drinking water, food, and medicine. The pharmacopoeia of China [1] requires the total arsenic content for most Chinese traditional medicines to be lower than 2 mg kg^{-1} .

The toxicity of arsenic depends upon its concentration, chemical form, and valence. The chemical speciation of arsenic greatly affects its toxicity. Different arsenic speciations vary in their toxicity to humans. Inorganic arsenic, including arsenate and arsenite, is more toxic than organic forms like arsenosugars and arsenolipids [16]. The valence of arsenic affects its toxicity, and trivalent arsenicals are more toxic than the pentavalent forms for inorganic arsenic (iAs), monomethylarsonic acid (MMA), and dimethylarsinic acid

(DMA) in vitro [16, 17]. Naranmandura [18] calculated LC50 values for human cells as 571, 843, 5.49, and $2.16 \mu\text{M}$ for iAs^{V} , DMA^{V} , iAs^{III} , and DMA^{III} .

Arsenic in *C. sinensis* remains a serious problem for users. Questions to be addressed are the following: (1) What is the range of the total arsenic concentration in wild *C. sinensis*? (2) What are the chemical speciation and valence of arsenic in wild *C. sinensis*? (3) What is the arsenic distribution in *C. sinensis* and where does the arsenic originate?

The total arsenic of *C. sinensis* samples has been documented [11, 19–22], and some studies have reported the arsenic speciation analysis of wild *C. sinensis* [21–25]. However, valence analysis and in vivo arsenic distribution in wild *C. sinensis* are rare. Basic research on the content, form, and valence of arsenic in *C. sinensis* is critical for understanding *C. sinensis*. The arsenic distribution in medicinal *C. sinensis* is important for arsenic source investigation. The arsenic source can be inferred from the distribution results of arsenic, and it provides data related to the accumulation and mechanism of arsenic in *C. sinensis*. Therefore, it is important and necessary to study the distribution of arsenic in *C. sinensis*.

Inductively coupled plasma-mass spectrometry (ICP-MS) [26] is a powerful technique for element detection with very low detection limits and wide linear dynamic range. ICP-MS hyphenated with chromatographic separation techniques such as liquid chromatography, gas chromatography, and capillary electrophoresis was used in elemental speciation analysis in clinical, environmental, food, and life sciences [26–28]. ICP-MS and HPLC-ICP-MS methods are useful tools for arsenic content determination and arsenic chemical species studies [29] and are applied in plant hyperaccumulation studies [30] and environmental and health studies [31].

Synchrotron-based X-ray techniques, including X-ray absorption near-edge structure spectroscopy (XANES) and micro X-ray fluorescence spectroscopy (μ -XRF), can provide molecular-level information and spatial imaging capabilities [32]. Synchrotron-based X-ray techniques are widely used in physics, chemistry, earth and environmental sciences, and life and agricultural sciences [32–36].

The aim of this research was to acquire information of the total arsenic content, arsenic speciation, arsenic valence, and distribution of arsenic in wild *C. sinensis* by ICP-MS, HPLC-ICP-MS, SXANS, and μ -XRF techniques. The data reveal the chemical form and distribution of arsenic in wild *C. sinensis*, suggest the sources of arsenic, and provide a reference for additional safety assessments of wild *C. sinensis*.

2. Materials and Methods

2.1. Chemicals and Reagents. Element reference standard solutions of arsenic (As, GBW(E)080117, $1000 \mu\text{g}/\text{ml}$), arsenite ($\text{As}(\text{III})$, GBW08666, $75.7 \pm 1.2 \mu\text{g}/\text{g}$), arsenate ($\text{As}(\text{V})$, GBW08667, $17.5 \pm 0.4 \mu\text{g}/\text{g}$), monomethylarsonic acid (MMA, GBW08668, $25.1 \pm 0.8 \mu\text{g}/\text{g}$), dimethylarsinic acid (DMA, GBW08669, $52.9 \pm 1.8 \mu\text{g}/\text{g}$), arsenobetaine (AsB , GBW08670, $38.8 \pm 1.1 \mu\text{g}/\text{g}$), arsenocholine (AsC ,

GBW08671, $28.0 \pm 1.1 \mu\text{g}/\text{g}$), and standard reference material GBW09588 (*Atractylodes macrocephala*) were obtained from the National Institute of Metrology (Beijing, China), with their concentrations guaranteed. Working mixture standard solutions of arsenic speciation were prepared daily by diluting the source standard solutions to proper concentrations with pure water. Tune solution and mixed internal standard were provided by PerkinElmer (MA, USA). Na_3AsO_4 , NaAsO_2 , and $\text{As}(\text{Cys})_3$ were also provided by the National Institute of Metrology (Beijing, China).

Nitric acid (HNO_3 , 68%, ultrapure) and hydrogen peroxide (H_2O_2 , 30%, ultrapure) were purchased from Suzhou Crystal Clear Chemical Co., Ltd. (Suzhou, China). High purity argon (Ar, 99.999 %) was obtained from Jinxin Gas Co., Ltd. (Xining, China). HPLC grade methanol (Merck, Germany), HPLC grade ammonium dihydrogen phosphate, and aqueous ammonia were obtained from ANPEL Laboratory Inc. (Shanghai, China). Ultrapure water ($18.2 \text{ M}\Omega$) prepared with a Milli-Q system (Millipore, Co., USA) was used for all solution preparations. The glassware and plasticware used in this experiment were soaked in 20% HNO_3 solution for 24 h prior to use.

2.2. Sample Collection and Preparation. Six wild *C. sinensis* samples (C1–C6) (each 20 g) were purchased from native habitats, Zaduo, Chengdu, Yushu, Nangqian, Zhiduo, and Qumalai county, Yushu prefecture, Qinghai province, China. Samples were authenticated by professor Yuzhi Du, a certified pharmacist of traditional Chinese medicine.

Samples were rinsed with deionized water to remove dust and soil from surface, dried at 40°C for 48 h, and then stored at -20°C before use. Before experiments, the samples were ground into powder and passed through a 40 mesh sieve.

2.3. Instrumentation. A NexION™ 350D ICP-MS (PerkinElmer, Waltham, MA, USA) and A-30 UPLC (PerkinElmer, Waltham, MA, USA) were used. The separation of arsenic species was performed on a PerkinElmer Altus A-30 UPLC system, equipped with a solvent delivery module (quaternary pump) and sampling module. Separation was achieved using a Hamilton PRP100 column ($250 \text{ mm} \times 4.6 \text{ mm id}$, $5 \mu\text{m}$) (Hamilton, Sweden). The ICP-MS was operated on the standard mode. The pH values were measured using a Mettler Toledo FiveEasy Plus pH meter (Mettler Toledo Co., Shanghai, China). Milli-Q purified water was obtained from a Milli-Q (reference) purified water apparatus (Millipore Co., USA). A microwave oven (MASTER 40 Digestion/Extraction/Synthesis Microwave Labstation) equipped with forty 70 ml TFM Teflon vessels, with an energy output of 3600W, was used to digest samples. The maximum digestion temperature and pressure were 220°C and 3 Mpa, respectively. An ECH-20 digital temperature control heater was used for evaporating excess nitric acid. The microwave oven and ECH-20 digital temperature control heater were products of Sineo Microwave Chemistry Technology Co., Ltd. (Shanghai, China).

The XAFS experiment end station 1W1B, Beijing Synchrotron Radiation Facility (Beijing, China); micro X-ray fluorescence beamline BL15U at Shanghai Synchrotron Radiation; infrared tablet presser (HY-12, Tianjin Skylight Optical Instrument Co., Ltd); vacuum freeze dryer (FD-1D-50, Beijing Boyikang Laboratory Instrument Co., Ltd); frozen microtome (CM 1950, Leica Co., Ltd, Germany); and positive optical microscope imaging system (E200, Sony Co., Ltd., Japan) were used.

2.4. Determination of Total Arsenic

2.4.1. Sample Ingestion. An ICP-MS system coupled with the microwave digestion technique was used for sample preparation and detection. *C. sinensis* powder, 0.25 g, was decomposed using microwave equipment with a mixture of HNO₃ (4.0 mL) and H₂O₂ (2.0 mL). The operating program of the microwave system was as follows: the samples were heated to 120°C from room temperature in 5 min and held for 5 min, then heated to 160°C in 5 min and held for 10 min, and heated to 200°C in 15 min and held for 15 min. During the digestion process the wave power was set to 1800 W. After digestion, the samples were cooled to room temperature. Excess HNO₃ was removed by heating the sample solution at 120°C for 20 min. The digestion sample solutions were cooled to room temperature and diluted with ultrapure water up to 50 mL.

2.4.2. Conditions and Methods. The analysis conditions, including RF power, plasma gas flow, auxiliary gas flow, nebulizer gas flow, sampling depth, and peristaltic pump rate, were 1250 W, 18 L/min, 1.2 L/min, 0.72 L/min, 6 mm, and 35 r/min, respectively. Besides, selected isotope m/z 75 was detected ion. Samples were quantified with external calibration curve As standards (calibration points: 1, 5, 10, 20, and 50 ng/mL), and internal standards (40 ng/mL of ⁷²Ge) were used for metal determination by ICP-MS. Before determination, the status of ICP-MS was adjusted to optimum with the tuning solution. The internal standard was used, and internal standard solution was introduced into the sample flow with a T shape pipe online. Triplicate analyses were performed for each sample. The corresponding digestion blanks (reagent blanks) were also measured. The arsenic of CRM GBW09588 (*Atractylodes macrocephala*) was determined and used for quality control purposes using the same methods.

2.5. Arsenic Speciation Analysis

2.5.1. Sample Preparation. The extraction methods were performed with reference to the method of Guo et al. [21] and Zhou et al. [23]. Approximately 0.5 g of each powder sample of *C. sinensis* was added to 10 mL of 0.15 mol/L dilute nitric acid solution and soaked in the mixture overnight. Then, the mixtures were heated in an incubator for 150 min at 90°C and shaken for 1 min every 30 min. The mixtures were cooled to room temperature and centrifuged at 8000 r/min after heat extraction. The supernatants were

removed, and 5 mL of 0.15 mol/L dilute nitric acid solution was added to the residue. The extraction was repeated using the procedure described above. The combined supernatants from the two rounds of extraction were analyzed immediately after filtration with a 0.22 μm PTEF membrane. A corresponding reagent blank was made, and the procedure was performed in triplicate.

2.5.2. Arsenic Speciation Analysis Method. The different species of arsenic were separated by HPLC and detected by ICP-MS. An anion-exchange column (Hamilton RPR 100 column, 250 mm × 4.6 mm, 5 μm) was used for separation with a gradient system of eluent A, 10 mmol/L NH₄H₂PO₄ (containing 1% methanol V/V, NH₃·H₂O adjusted pH 9.7), and eluted with B, 40 mmol/L NH₄H₂PO₄ (containing 1% methanol V/V, NH₃·H₂O adjusted pH 6.7) solution, at a flow rate of 1.0 mL/min. The HPLC elution condition was achieved using the following procedures. For eluent A, 100.0% initial proportion, 100.0% maintained for 4.0 min; linear decrease to 0.0% at 4.5 min and 0.0% maintained for 13.5 min; linear increase to 100.0% at 14.0 min; equilibrium maintained for 4.0 min. The total sample injection time was 18.0 min, and the acquisition time was 14 min. The injection volume was 10.0 μL.

The method of arsenic speciation analysis was validated by the standard addition method, and the recoveries of each arsenic speciation were used for evaluating the method feasibility. The total arsenic in the extraction solution and the residue of the extracted sample were ingested by microwave digestion method, and the total arsenic was determined by the method in Section 2.4. Then, total arsenic results of extraction solution and residue of extraction were compared with the results of sum of six arsenic species in *C. sinensis*.

2.6. Arsenic Valance Analysis In Vivo

2.6.1. Sample Preparation and Reference Materials. *C. sinensis* samples were ground into fine powder and then pressed into round tablet with 1 cm diameter. All samples were coded and examined by X-ray absorption spectroscopy. The reference materials Na₃AsO₄ and As (Cys)₃ were used.

2.7. Arsenic Distribution in Wild *C. sinensis*

2.7.1. Sample Preparation. A *C. sinensis* sample from Zhiduo county was frozen, and sections of 50 μm thickness were made from the stroma, head, thorax, and abdomen (the location of the thin slices of the samples is shown in Figure 1) and pasted on the XRF tape (TF-500) for μ-XRF imaging.

2.7.2. Facility Conditions. The distribution of As in *C. sinensis* samples was analyzed with μ-XRF at the beamline BL15U at the Shanghai Synchrotron Radiation Facility (SSRF, Shanghai, China). The continuous synchrotron X-rays were monochromatized by a Si(111) double-crystal monochromator. A monochromatic X-ray beam with photon energy of 13 keV was used to excite the samples. The

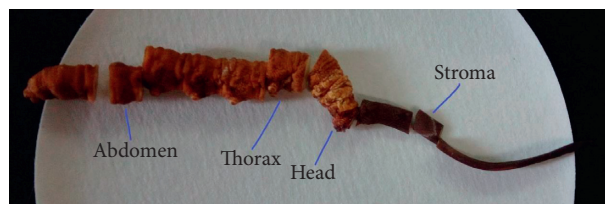


FIGURE 1: The location of thin slice on *C. sinensis*.

cross section of the beam irradiation on the samples was adjusted to about $200 \times 200 \text{ mm}^2$ with an about 10^{11} phs/s photon flux. The sample was placed at a 45° angle to the incident X-ray beam, and X-ray fluorescence was detected with a 50 mm^2 silicon drift detector (Vortex, USA) oriented at a 90° angle to the incident beam. A light microscope was coupled to a computer for sample viewing. The sample platform was moved by a motorized x-y mapping stage. The As distributions in the sections of different parts of the caterpillar were continuously scanned at a step of $125 \mu\text{m}$ for both x and y directions. Each spot was irradiated for 5 s.

2.7.3. Data Analysis. The X-ray spectra were analyzed by the AXIL program (Canberra Benelux, Belgium), and all the element fluorescence intensities and the Compton scattering intensity were normalized to the collecting time and the changes in I_0 , which was measured by an upstream ion chamber. The relative quantitative images of metals were obtained using software IGOR Pro 6 (WaveMetrics Inc., USA).

3. Results

3.1. Total Arsenic Content of Wild *C. sinensis* Samples. The amount of total arsenic in wild *C. sinensis* was determined by microwave digestion coupled with the ICP-MS method. Total arsenic content of the six *C. sinensis* samples ranged from 5.77 to $13.20 \mu\text{g/g}$, with RSD of 2.1–5.4% and mean of $8.85 \pm 2.5 \mu\text{g/g}$ (details are provided in Table 1 and Supplementary Table 1).

The ^{75}As standard curve was $Y = 0.010X + 0.002$ with a correlation coefficient (r) of 0.9999, and the detection limit was 0.011 ng/ml . The total As of CRM GBW09588 was $0.202 \pm 0.005 \mu\text{g/g}$ ($n = 3$). This result was similar to the certificate value of $0.211 \pm 0.008 \mu\text{g/g}$.

3.2. Arsenic Speciation of Wild *C. sinensis*. The arsenic speciation analysis was performed on a HPLC-ICP-MS using the established method. The representative chromatograms for typical separation of arsenic species are shown in Figure 2. The analysis methodology data including regression equations, correlation coefficients, linear ranges, detection limits, and recoveries are shown in Table 2. The recoveries of As(III), As(V), MMA, DMA, AsC, and AsB were 94.4%, 79.6%, 95.6%, 96.7%, 93.7%, and 94.9%, respectively. Accordingly, we can state that the results of recovery of HPLC-ICP-MS method are reliable. The contents of different arsenic species in the samples are shown in Table 3 and Figure 3.

3.3. Arsenic Valence of Wild *C. sinensis*. The raw XAFS data of *C. sinensis* samples and the references were preprocessed through conventional procedures by normalizing to the unit edge jump after removing the atomic background as implemented in the IFEFFIT package, shown in Figure 4. The Fourier transforms of k^2 -weighted EXAFS were conducted over the k range [$3\text{--}10 \text{ \AA}^{-1}$] for all samples. Speciation analysis was conducted on the XANES region, the 20 eV below and 50 eV above the absorption edge, for all samples using the selected standards. Due to the limitation of the standards library, the useful standards were selected by comparing the spectral fingerprint of the sample and that of the standards. We narrowed the fingerprint to two compounds, i.e., $\text{Na}_3\text{AsO}_4\text{-As}^{5+}$ and As-Cys-As^{3+} , each of which showed distinctive fingerprints in the XANES region (details are provided in Supplementary Figure 1).

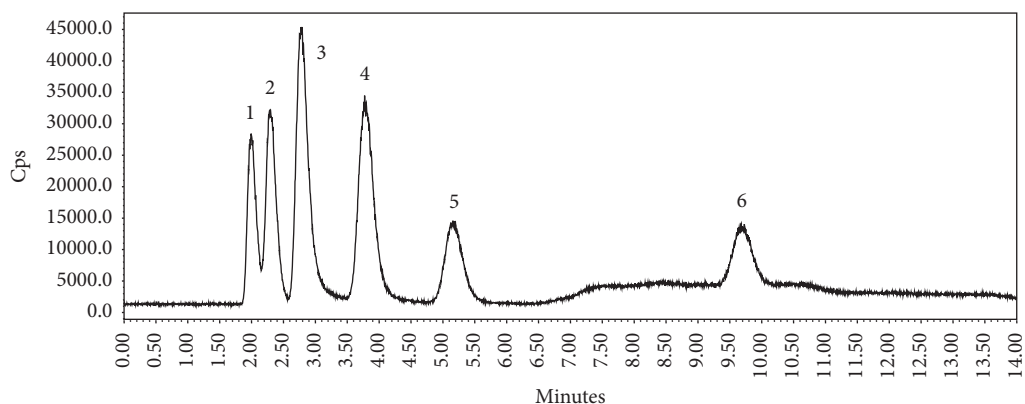
3.4. Distribution of Arsenic in Wild *C. sinensis*. The different *C. sinensis* sections of stroma, larva head, larva thorax, and larva abdomen were imaged using the synchrotron radiation μ -XRF method. Sampling location is shown in Figure 1, and As distribution is shown in Figure 5. The relative level of arsenic is represented by the intensity or counts of fluorescence photons. Figure 5 shows the As micro distribution in the host body of *C. sinensis*. The micro distribution of As shows that As exists in the larva and is concentrated in the mid-thorax and the abdomen. We speculated that it was the digestive tract according to the location and shape of As focusing. Compared to the larval thorax and abdomen, the stroma and head had low photon counts, indicating their low As content.

4. Discussion

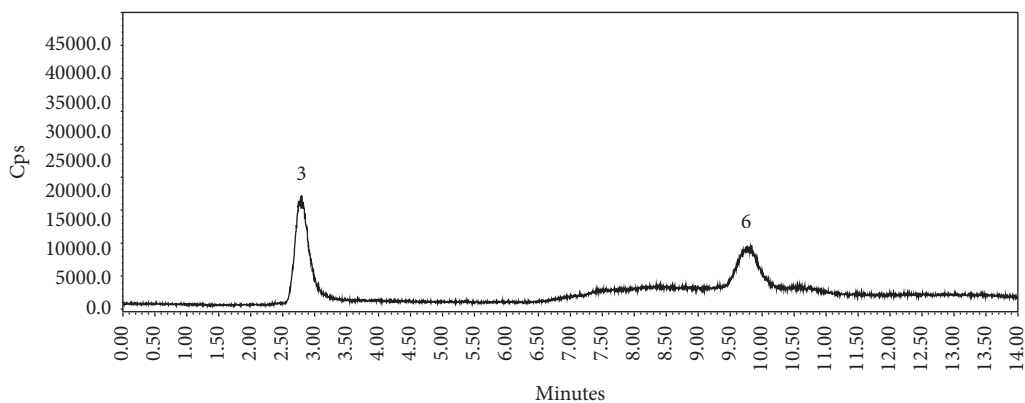
4.1. Total Arsenic Content of Wild *C. sinensis*. The total As results in this study were consistent with previous studies of wild *C. sinensis*. The total arsenic results of Guo [21] were 4.00–5.25 mg/kg in *C. sinensis* samples from Litang, Naqu, and Yushu. They were 2.560–5.590 mg/kg with mean of $1.032 \pm 0.989 \text{ mg/kg}$ in 45 samples from a Beijing market that were collected from major origins of wild *C. sinensis* in Lu's studies [19]. Li [20] documented 5.9–12.5 mg/kg of five samples from Qinghai, Tibet, and Gansu provinces. Zuo et al. [22] found $8.53 \pm 3.49 \text{ mg/kg}$ in 34 samples from Qinghai, Tibet, Sichuan, Gansu, and Yunnan provinces. Zhou et al. [23] found $9.70 \pm 0.62 \text{ mg/kg}$ in a sample from Qinghai province.

TABLE 1: Total arsenic content of wild *C. sinensis*.

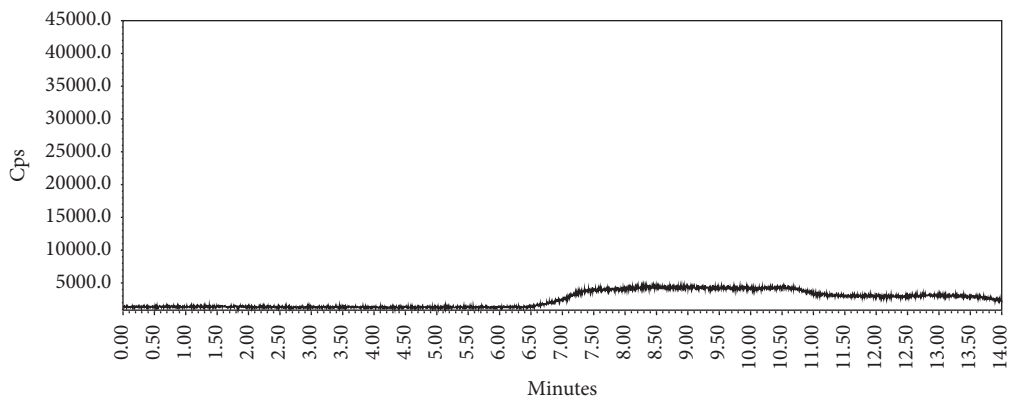
| No. | Sample | Origin | As (mg/kg) | RSD (%) (n = 3) |
|---------|--------|-----------------|------------|--------------------|
| 1 | C1 | Yushu city | 8.08 | 2.8 |
| 2 | C2 | Nangqian county | 5.77 | 2.2 |
| 3 | C3 | Qumalai county | 9.18 | 2.9 |
| 4 | C4 | Chengdu county | 9.38 | 4.4 |
| 5 | C5 | Zhiduo county | 7.49 | 2.1 |
| 6 | C6 | Zaduo county | 13.20 | 5.4 |
| Average | | | 8.85 | |
| SD | | | 2.50 | |



(a)



(b)



(c)

FIGURE 2: Chromatogram of arsenic speciation analysis of wild *C. sinensis* using the HPLC-ICP-MS method: (a) mixed standard of six arsenic species; (b) sample of wild *C. sinensis*; (c) blank (0.15 mol/L HNO₃). 1: AsC; 2: AsB; 3: As(III); 4: DMA; 5: MMA; 6: As(V).

TABLE 2: Regression equations, correlation coefficients, linear ranges, detection limits, and recoveries of HPLC-ICP-MS method.

| Analyte | Linear equation | R | Linear range ($\mu\text{g/L}$) | LOD ($\mu\text{g/L}$) | Recovery (%) |
|---------|-----------------------|--------|----------------------------------|-------------------------|--------------|
| AsC | $Y = 11589X - 10045$ | 0.9999 | 4.13–264.01 | 0.41 | 93.7 |
| AsB | $Y = 12052X + 19812$ | 0.9998 | 5.05–322.95 | 1.35 | 94.9 |
| As(III) | $Y = 9814.4X + 28579$ | 0.9997 | 10.77–689.02 | 0.35 | 94.4 |
| DMA | $Y = 12006X + 34041$ | 0.9996 | 7.98–510.86 | 0.80 | 96.7 |
| MMA | $Y = 10794X + 13051$ | 0.9993 | 3.76–240.38 | 1.51 | 95.6 |
| As(V) | $Y = 12410X - 15367$ | 0.9991 | 2.75–176.27 | 2.06 | 79.6 |

TABLE 3: As speciation analysis in wild *C. sinensis* preparations by 0.15 mol/L HNO_3 .

| No. | AsC | AsB | As(III) ^a | DMA | MMA | As(V) ^a | iAs | ETAs ^b | RTAs ^c | iAs ^d (%) |
|-----|-----|-----|----------------------|-----|-----|--------------------|-------|-------------------|-------------------|----------------------|
| C1 | ND | ND | 0.127 ± 0.007 | ND | ND | 0.180 ± 0.006 | 0.307 | 6.858 | 1.103 | 4.47 |
| C2 | ND | ND | 0.202 ± 0.004 | ND | ND | 0.263 ± 0.017 | 0.465 | 4.073 | 1.546 | 11.42 |
| C3 | ND | ND | 0.126 ± 0.002 | ND | ND | 0.191 ± 0.013 | 0.316 | 5.231 | 3.722 | 6.05 |
| C4 | ND | ND | 0.215 ± 0.001 | ND | ND | 0.208 ± 0.025 | 0.422 | 8.415 | 0.917 | 5.02 |
| C5 | ND | ND | 0.194 ± 0.043 | ND | ND | 0.196 ± 0.000 | 0.391 | 4.949 | 2.435 | 7.89 |
| C6 | ND | ND | 0.473 ± 0.058 | ND | ND | 0.265 ± 0.016 | 0.738 | 6.745 | 5.984 | 10.94 |

Note. ND: not detected. ^aData are the mean \pm SD, $\mu\text{g/g}$. ^bTotal arsenic of sample extracted solution, $\mu\text{g/g}$. ^cArsenic content of residues after the extraction, $\mu\text{g/g}$. ^dPercentage of inorganic arsenic in extracted solution (%).

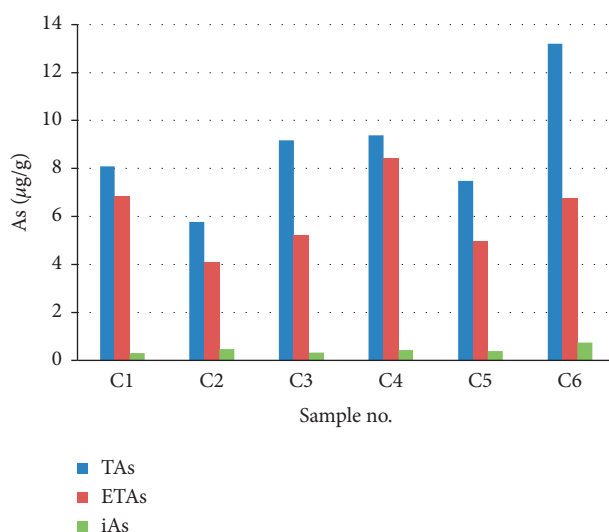


FIGURE 3: Content of TAs, ETAs, and iAs in wild *C. sinensis*. TAs represent total arsenic of *C. sinensis*, ETAs represent total extracted arsenic with 0.15 mol/L HNO_3 of *C. sinensis*, and iAs represents the sum of As(III) and As(V) of extracted solution.

4.2. Arsenic Speciation Concentration of Wild *C. sinensis*.

For six arsenic species, AsC, AsB, As(III), MMA, DMA, and As(V), were separated well in 14 min (Figure 2). Performance parameters of established methods (Table 2) showed that the detection limits for the six arsenic species ranged from 0.41 $\mu\text{g/L}$ to 2.06 $\mu\text{g/L}$. The standard curve prepared for each arsenic species was linear, and the correlation coefficients were 0.9991 to 0.9999. The relative standard deviations (RSDs %) were less than 5%.

The arsenic speciation results showed that AsC, AsB, MMA, and DMA were not detected in the six samples of wild *C. sinensis* from Yushu prefecture. Two inorganic arsenic species, As(III) and As(V), were the major species in wild *C. sinensis*. Their concentration ranged from $0.126 \pm 0.002 \mu\text{g/g}$ to $0.473 \pm 0.058 \mu\text{g/g}$, and $0.180 \pm 0.006 \mu\text{g/g}$ to $0.265 \pm 0.016 \mu\text{g/g}$,

respectively. The total iAs was 0.307–0.738 $\mu\text{g/g}$ and amounted to 4.47–11.42% of the total arsenic. Compared with the total arsenic result of *C. sinensis* (Table 1), the extracted arsenic was less than the former.

The total arsenic results of extraction solution and residue of extraction were compared with the results of the total arsenic of *C. sinensis* samples by microwave digestion method (Tables 1 and 3). The sum of total arsenic in the extraction and residue is basically consistent with the total arsenic content of each *C. sinensis* sample.

Using the same extraction solution of 0.15 mol/L HNO_3 and temperature of 90°C, the arsenic speciation results of the present study were in partial agreement with the results of Guo et al. [21] who discovered AsB in *C. sinensis* samples from Litang, Naqu, and Yushu, and the iAs content ranged

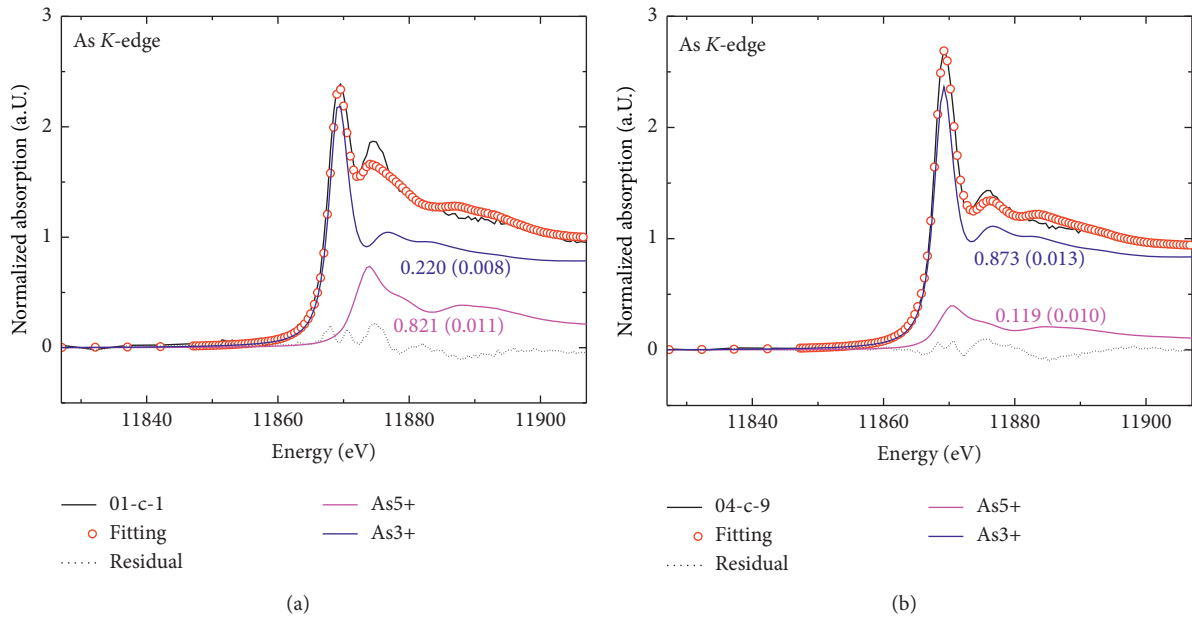


FIGURE 4: Experimental and fitted spectra of two samples (C1 and C4).

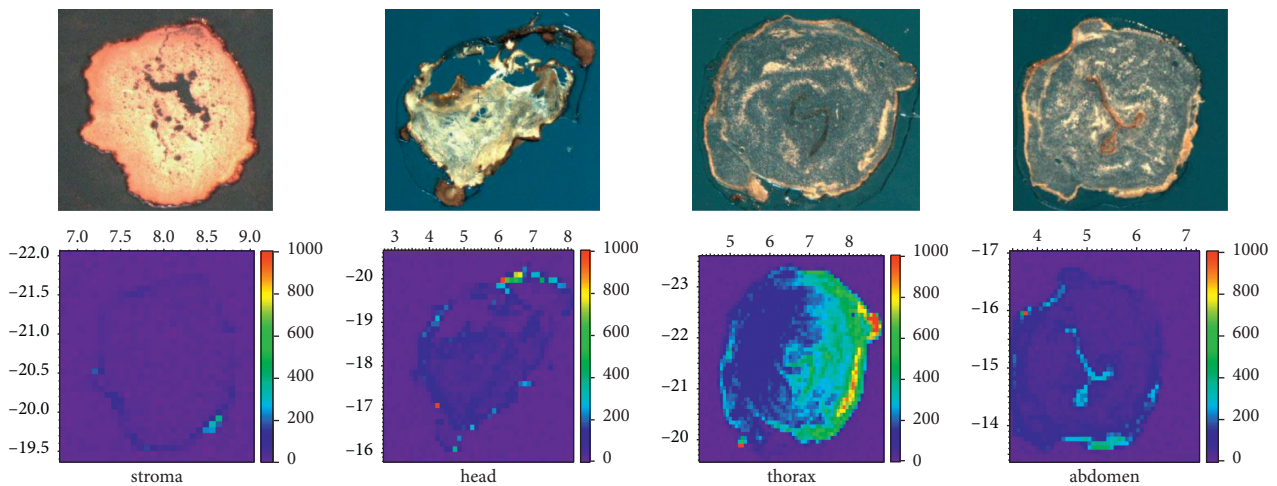


FIGURE 5: Arsenic distribution in wild *C. sinensis*.

from 0.31 to 0.38 $\mu\text{g/g}$ (6.0– 8.3%). The extraction time for these two studied samples differed, with 12 hours for Guo et al. [21] and 2.5 hours for the present study. Guo et al. [21] had an extraction efficiency of 92.3–104% for total arsenic, which is higher than that in the present study (51.1–89.7%).

In arsenic speciation analysis, different extraction methods produce different results. HNO_3 solution is superior for recovery of iAs compared to simulated gastrointestinal juice. The results of Guo et al. [21], Zuo et al. [22], Zhou et al. [23], Li et al. [24], and the present research all support this conclusion.

Unknown arsenic species exist in wild *C. sinensis* based on the present study and published results [22–24, 37]. Other studies indicate that the unknown arsenic species were in organic form and Guo's results [22] supported this conclusion using an H_2O_2 oxidation test. Li et al. [24]

showed that unknown organic arsenic was abundant in wild *C. sinensis* using SEC-HPLC- ICP- MS and continuous extraction methods. Arsenic is distributed in lipids, proteins, polysaccharides, and other chemical compositions [24].

4.3. Arsenic Valence. The speciation of the samples was analyzed using linear combination fitting (LCF), which is implemented in the ATHENA-IFEFFIT package. By carefully calibrating the energy and allowing a small shift of energy as a fitting parameter, the proportion of constituent species can be obtained by linear combinations of the selected standards. The acceptable criterion for LCF is to obtain fitting with minimum residual and full physical meaning, shown in Figure 4.

The LCF was conducted for the XANES region: -20 eV to $+60\text{ eV}$ from the edge. We did not constrain the sum of the individual weights, because there should be some missing references that are not included in the standards library. Fortunately, the major constituents are included in the analysis. There are spectral features that cannot be fully reproduced, considering the difference between the natural/complex samples and the synthesized/simpler standards.

4.4. Arsenic Distribution and Source of Arsenic. Arsenic was concentrated in the larva digestive tract, which indicates that the arsenic source is the larval food. This is likely because the host larva spends most of its life in the soil, and soil humus is documented as a larval food. The results of stable isotope composition showed that [38] soil humus is one of the foods for the host of *C. sinensis* in the Qinghai-Tibet plateau. Additionally, the levels of As in *Cordyceps* are correlated with the soil samples from their collection locations [39], suggesting that As in *C. sinensis* likely originates from the soil.

5. Conclusion

The study documented high total arsenic concentrations in wild *C. sinensis* with most levels exceeding 2 mg/kg . Most arsenic detected was inorganic, and it existed in trivalent and pentavalent forms. The soil and food of the host larva of caterpillar of *C. sinensis* were the source of arsenic. Unknown organic arsenic species exist in a large amount in *C. sinensis*; therefore, the chemical properties and toxicity of the unknown organic arsenic speciation decide the health risk of *C. sinensis*.

Data Availability

The data are included within the article.

Conflicts of Interest

The authors declare that they have no conflicts of interest.

Acknowledgments

This study was supported by the Development Program of Qinghai Provincial Key Laboratory of Tibetan Medicine Pharmacology and Safety Evaluation (2017-ZJ-Y08). The XAS experiments were granted by the BL15U beamline at Shanghai Synchrotron Radiation Facility (SSRF, Shanghai, China). The staff members (such as Lili Zhang and Yu Zhang) of SSRF are acknowledged for their assistance in measurements and data reduction. The authors thank LetPub (<http://www.letpub.com>) for its linguistic assistance during the preparation of this manuscript.

Supplementary Materials

Supplementary Figure 1: XAFS data of six *Cordyceps sinensis* samples. Supplementary Table 1: total arsenic content of wild *Cordyceps sinensis* samples. (*Supplementary Materials*)

References

- [1] Pharmacopoeia, *Pharmacopoeia of the People Republic of China*, Vol. 1, Chinese Medical Press, Beijing, China, 2015.
- [2] X. Zhou, Z. Gong, Y. Su, J. Lin, and K. Tang, "Cordyceps fungi: natural products, pharmacological functions and developmental products," *Journal of Pharmacy And Pharmacology*, vol. 61, no. 3, pp. 279–291, 2009.
- [3] Y. Li, X.-L. Wang, L. Jiao et al., "A survey of the geographic distribution of ophiocordyceps sinensis," *The Journal of Microbiology*, vol. 49, no. 6, pp. 913–919, 2011.
- [4] F. Li, Z. F. Wu, C. Xu, Y. D. Xu, and L. B. Zhang, "The spatial distribution of Ophiocordyceps sinensis suitability in sanjiangyuan region," *Acta Ecologica Sinica*, vol. 34, no. 5, pp. 1318–1325, 2014.
- [5] K. S. Zhou, J. C. Zhang, X. Q. Huang et al., "Suitability and regionalization of ophiocordyceps sinensis in the Tibetan plateau," *Acta Ecologica Sinica*, vol. 38, no. 8, pp. 2768–2779, 2018.
- [6] B. Shi, Z. Wang, H. Jin, Y. W. Chen, Q. Wang, and Y. Qian, "Immunoregulatory cordyceps sinensis increases regulatory T cells to Th17 cell ratio and delays diabetes in NOD mice," *International Immunopharmacology*, vol. 9, no. 5, pp. 582–586, 2009.
- [7] K. Nakamura, K. Shinozuka, and N. Yoshikawa, "Anticancer and antimetastatic effects of cordycepin, an active component of cordyceps sinensis," *Journal of Pharmacological Sciences*, vol. 127, no. 1, pp. 53–56, 2015.
- [8] B.-S. Wang, C. P. Lee, Z.-T. Chen, H. M. Yu, and P.-D. Duh, "Comparison of the hepatoprotective activity between cultured cordyceps militaris and natural cordyceps sinensis," *Journal of Functional Foods*, vol. 4, no. 2, pp. 489–495, 2012.
- [9] R. Kumar, P. S. Negi, B. Singh, G. Ilavazhagan, K. Bhargava, and N. K. Sethy, "Cordyceps sinensis promotes exercise endurance capacity of rats by activating skeletal muscle metabolic regulators," *Journal of Ethnopharmacology*, vol. 136, no. 1, pp. 260–266, 2011.
- [10] G. L. Wang, H. Y. Jin, X. P. Han, Y. Shi, J. G. Tian, and R. C. Lin, "Quality study and problems of Cordyceps sinensis," *Chinese Traditional and Herbal Drugs*, vol. 39, no. 1, pp. 115–118, 2008.
- [11] L. Zhou, Q. X. Hao, S. Wang et al., "Study on distribution of five heavy metal elements in different parts of cordyceps sinensis by microwave digestion ICP-MS," *China Journal of Chinese Material Medica*, vol. 42, no. 15, pp. 2934–2938, 2017.
- [12] Traditional Chinese Medicine, "Determination of heavy metals in herbal medicines used in traditional Chinese medicine," *ISO*, vol. 2015, p. 18664, 2015.
- [13] B. Mandal, K. T. Suzuki, and "Suzuki, "Arsenic round the world: a review," *Talanta*, vol. 58, no. 1, pp. 201–235, 2002.
- [14] J. C. Saha, A. K. Dikshit, M. Bandyopadhyay, and K. C. Saha, "A review of arsenic poisoning and its effects on human health," *Critical Reviews in Environmental Science and Technology*, vol. 29, no. 3, pp. 281–313, 1999.
- [15] R. N. Ratinaike, "Acute and chronic arsenic toxicity," *Postgraduate Medical Journal*, vol. 79, pp. 391–396, 2003.
- [16] V. K. Sharma and M. Sohn, "Aquatic arsenic: toxicity, speciation, transformations, and remediation," *Environment International*, vol. 35, no. 4, pp. 743–759, 2009.
- [17] M. J. Mass, A. Tennant, B. C. Roop et al., "Methylated trivalent arsenic species are genotoxic†," *Chemical Research in Toxicology*, vol. 14, no. 4, pp. 355–361, 2001.
- [18] H. Naranmandura, K. Iyata, and K. T. Suzuki, "Toxicity of dimethylmonothioarsinic acid toward human epidermoid

- carcinoma A431 cells,” *Chemical Research in Toxicology*, vol. 20, no. 8, pp. 1120–1125, 2007.
- [19] H. Lu, N. Xu, and F. Y. Meng, “Determination and health risk assessment of heavy metals in *Cordyceps sinensis* (Berk.) Sacc,” *Environmental Chemistry*, vol. 36, no. 5, pp. 103–1008, 2017.
- [20] Y. L. Li, J. Xu, H. Y. Jin, X. Han, L. P. An, and S. C. Ma, “Pollution assessment of five heavy metals and harmful element in cordyceps and its habitat’s soil,” *China Journal of Pharmaceutical Analysis*, vol. 39, no. 4, pp. 677–674, 2019.
- [21] L.-X. Guo, G.-W. Zhang, J.-T. Wang, Y.-P. Zhong, and Z.-G. Huang, “Determination of arsenic species in ophiocordyceps sinensis from major habitats in China by HPLC-ICP-MS and the edible hazard assessment,” *Molecules*, vol. 23, no. 5, pp. 1012–1026, 2018.
- [22] T. T. Zuo, Y. L. Li, H. Y. Jin et al., “HPLC-ICP-MS speciation analysis and risk assessment of arsenic in cordyceps,” *Chinese Medicine*, vol. 13, no. 19, 2018.
- [23] L. Zhou, S. Wang, Q. X. Hao et al., “Bioaccessibility and risk assessment of heavy metals, and analysis of arsenic speciation in cordyceps sinensis,” *Chinese Medicine*, vol. 13, p. 40, 2018.
- [24] Y. L. Li, Y. Liu, X. Han, H. Y. Jin, and S. C. Ma, “Arsenic species in cordyceps sinensis and its potential health risks,” *Frontiers in Pharmacology*, vol. 10, p. 1471, 2019.
- [25] J. S. Shao, Y. J. Hu, S. L. Liu, and Z. X. Ji, “Speciation of arsenic in cordyceps sinensis,” *Journal of Analytical Science*, vol. 36, no. 2, pp. 229–234, 2020.
- [26] D. Beauchemin, “Inductively coupled plasma mass spectrometry,” *Analytical Chemistry*, vol. 82, no. 12, pp. 4786–4810, 2010.
- [27] D. Profrock and A. Prange, “Inductively coupled plasma-mass spectrometry (ICP-MS) for quantitative analysis in environmental and life sciences: a review of challenges, solutions, and trends,” *Applied Spectroscopy*, vol. 66, no. 8, pp. 843–868, 2012.
- [28] E. Prange and B. Wagner, “Quantitative aspects of inductively coupled plasma mass spectrometry,” *Philosophical Transactions Royal Society A*, vol. 374, Article ID 20150369, 2016.
- [29] M.-L. Chen, L.-Y. Ma, and X.-W. Chen, “New procedures for arsenic speciation: a review,” *Talanta*, vol. 125, pp. 78–86, 2014.
- [30] E. M. Kroukamp, T. Wondimu, and P. B. C. Forbes, “Metal and metalloid speciation in plants: overview, instrumentation, approaches and commonly assessed elements,” *TrAC Trends in Analytical Chemistry*, vol. 77, pp. 87–99, 2016.
- [31] Q. Liu, X. Lu, H. Peng et al., “Speciation of arsenic—a review of phenylarsenicals and related arsenic metabolites,” *TrAC Trends in Analytical Chemistry*, vol. 104, pp. 171–182, 2018.
- [32] P. M. Bertsch and D. B. Hunter, “Applications of synchrotron-based X-ray microprobes,” *Chemical Reviews*, vol. 101, no. 6, pp. 1809–1842, 2001.
- [33] S. Majumdar, J. R. Peralta-Videa, H. Castillo-Michel, J. Hong, C. M. Rico, and J. L. Gardea-Torresdey, “Applications of synchrotron μ -XRF to study the distribution of biologically important elements in different environmental matrices: a review,” *Analytica Chimica Acta*, vol. 755, pp. 1–16, 2012.
- [34] D. C. Pearce, K. Dowling, A. R. Gerson et al., “Arsenic microdistribution and speciation in toenail clippings of children living in a historic gold mining area,” *Science of the Total Environment*, vol. 408, no. 12, pp. 2590–2599, 2010.
- [35] T. I. Savchenko, O. V. Chankina, A. V. Bogatov, and K. P. Koutzenogii, “SR XRF used to establish pedigree and species differences in the elements accumulated in the hair of aurochs and valuable strains of cattle endemic to the altai mountains,” *Bulletin of the Russian Academy of Sciences: Physics*, vol. 77, no. 2, pp. 172–175, 2013.
- [36] J. Schaller, I. Koch, G. Caumette, M. Nearing, K. J. Reimer, and B. Planer-Friedrich, “Strategies of *Gammarus pulex* L. to cope with arsenic - results from speciation analyses by IC-ICP-MS and XAS micro-mapping,” *Science of the Total Environment*, vol. 531, pp. 430–433, 2015.
- [37] X. G. Cao, J. Wang, J. M. Li, and S. Z. Wang, “Analysis of arsenic speciations in cordyceps sinensis in Tibet by HPLC-HG-AFS,” *Chinese Traditional Patent Medicine*, vol. 37, no. 9, pp. 1985–1989, 2015.
- [38] D. Chen, J. Yuan, S. Xu et al., “Stable carbon isotope evidence for tracing the diet of the host *Hepialus* larva of *Cordyceps sinensis* in the Tibetan Plateau,” *Science in China Series D: Earth Sciences*, vol. 52, no. 5, pp. 655–659, 2009.
- [39] H.-L. Zuo, S.-J. Chen, D.-L. Zhang, J. Zhao, F.-Q. Yang, and Z.-N. Xia, “Quality evaluation of natural cordyceps sinensis from different collecting places in China by the contents of nucleosides and heavy metals,” *Analytical Methods*, vol. 5, no. 20, pp. 5450–5456, 2013.

Research Article

RNA-Seq Expression Analysis of Chronic Asthmatic Mice with Bu-Shen-Yi-Qi Formula Treatment and Prediction of Regulated Gene Targets of Anti-Airway Remodeling

Jie Cui ^{1,2}, Zexi Lv,^{1,2} Fangzhou Teng,^{1,2} La Yi,^{1,2} Weifeng Tang,^{1,2} WenQian Wang,^{1,2} Wuniquemu Tulake,^{1,2} Jingjing Qin,^{1,2} Xueyi Zhu,^{1,2} Ying Wei ^{1,2} and Jingcheng Dong ^{1,2}

¹Department of Integrative Medicine, Huashan Hospital, Fudan University, Shanghai, China

²Institute of Integrative Traditional Chinese and Western Medicine, Fudan University, Shanghai, China

Correspondence should be addressed to Ying Wei; weiyiing_acup@126.com and Jingcheng Dong; jcdong2004@126.com

Received 9 July 2020; Revised 3 December 2020; Accepted 7 January 2021; Published 18 January 2021

Academic Editor: Jie Liu

Copyright © 2021 Jie Cui et al. This is an open access article distributed under the Creative Commons Attribution License, which permits unrestricted use, distribution, and reproduction in any medium, provided the original work is properly cited.

Airway remodeling is one of the typical pathological characteristics of asthma, while the structural changes of the airways in asthma are complex, which impedes the development of novel asthma targeted therapy. Our previous study had shown that Bu-Shen-Yi-Qi formula (BSYQF) could ameliorate airway remodeling in chronic asthmatic mice by modulating airway inflammation and oxidative stress in the lung. In this study, we analysed the lung transcriptome of control mice and asthmatic mouse model with/without BSYQF treatment. Using RNA-sequencing (RNA-seq) analysis, we found that 264/1746 (15.1%) of transcripts showing abnormal expression in asthmatic mice were reverted back to completely or partially normal levels by BSYQF treatment. Additionally, based on previous results, we identified 21 differential expression genes (DEGs) with fold changes (FC) > (±) 2.0 related to inflammatory, oxidative stress, mitochondria, PI3K/AKT, and MAPK signal pathways which may play important roles in the mechanism of the anti-remodeling effect of BSYQF treatment. Through inputting 21 DEGs into the IPA database to construct a gene network, we inferred Adipoq, SPP1, and TNC which were located at critical nodes in the network may be key regulators of BSYQF's anti-remodeling effect. In addition, the quantitative real-time polymerase chain reaction (qRT-PCR) result for the selected four DEGs matched those of the RNA-seq analysis. Our results provide a preliminary clue to the molecular mechanism of the anti-remodeling effect of BSYQF in asthma.

1. Introduction

Asthma, a chronic inflammatory respiratory disease, is caused by complex factors and affects approximately 300 million people of all ages worldwide [1]. The pathogenesis of asthma is characterized by airway inflammation and airway hyperresponsiveness (AHR), and airway remodeling is the main pathophysiological feature [1, 2]. Airway remodeling is usually observed in asthma and can be driven by pathways that are partly independent of airway inflammation. It includes airway smooth muscle (ASM) mass, peribronchial collagen deposition, goblet cell, and glandular hyperplasia and angiogenesis [3, 4]. The progression of asthma is associated with the functional changes of the airways [5], whereas the complexity of airway function and structure

changes in asthma has impeded the development of novel asthma targeted therapy.

Asthma-related morbidity results from immune imbalances caused by the release of inflammatory mediators including reactive oxygen species (ROS), cytokines, and growth factors [4]. ROS could induce cell damage, change the physiological function of structural cells, and play a key role in initiation as well as amplification of inflammation in asthma [6, 7]. Meanwhile, accumulating evidence has suggested that ROS is involved in airway remodeling in asthma. ROS can enhance release of transforming growth factor- β 1 (TGF- β 1) and vascular endothelium growth factor (VEGF), which contribute to subepithelial fibrosis and airway remodeling [6]. Mitochondria are one of the important sources of basal endogenous ROS production in the lung [8].

Furthermore, airway abnormalities, particularly secretion of various cytokines, leads to the activation of intracellular signaling pathways which are involved in airway inflammation as well as remodeling process. The PI3K/AKT pathway has been proved to play an important role in regulating cell proliferation, growth, differentiation, and metabolism [9]. As well, the mitogen-activated protein kinase (MAPK) pathway is known to regulate a variety of biological processes like cell growth and proliferation, chemotaxis, degranulation, and other processes [10]. Therefore, PI3K/AKT and MAPKs signal pathways are considered as therapeutic targets in airway remodeling of asthma.

Traditional Chinese medicines (TCMs) were derived from thousands of years of clinical use in China. TCMs containing multiple bioactive ingredients are potential novel resources for asthma treatment drugs. BSYQF is used in the clinical treatment of asthma in China and is composed of *Astragalus membranaceus* (Fisch.) Bunge, *Rehmannia glutinosa* Libosch, and *Epimedium brevicornu* Maxim. The chemical fingerprint of BSYQF contains at least 16 chemical components including icariin, acteoside, catalpol, leonuride, calycosin, and epimedin A. This indicates that multiple compounds in BSYQF may deliver an integrated anti-asthma effect through multiple targets and their associated molecular pathways.

The anti-remodeling effects of BSYQF including the inhibition of ASMC proliferation and peribronchial collagen deposition in chronic asthmatic mice have been demonstrated in our previous study [11]. We also preliminarily explored the anti-remodeling mechanism of BSYQF, which may be related to its anti-inflammatory, antioxidant, and mitochondrial structure restoration. To further investigate the molecular mechanism of BSYQF, we used lung samples obtained from previous experiments and took advantage of high-throughput whole-transcriptome analyses to explore molecular mechanisms targeted by BSYQF. BSYQF is a multicomponent formula with wide molecular mechanisms. Given this complexity of multiple targets and their associated molecular pathways, increased understanding of the mechanisms of BSYQF might be best derived from the available experimental results. Hence, according to our previous result, we mainly focused on inflammatory, oxidative stress, and mitochondria in GO enrichment and PI3K/AKT and MAPKs signal pathways which are thought to play an important role in asthma airway remodeling to identify differentially expressed genes (DEGs) which may be therapeutic targets of BSYQF.

2. Materials and Methods

2.1. Animals. Lung tissue samples were obtained from our recently published study that tested the effects of BSYQF on airway remodeling in murine chronic asthma [11]. Female BALB/c mice were sensitized and challenged with ovalbumin for 8 weeks to establish chronic asthmatic model as described previously [11]. BSYQF was prepared as described previously [12]. Briefly, *Astragalus membranaceus* (Fisch.) Bunge, *Rehmannia glutinosa* Libosch, and *Epimedium*

brevicornu Maxim were decocted in the ratio of 3 : 2 : 1.5 (w/w). From day 14, mice in BSYQF group were oral administered 20g raw herbs/kg body weight, and mice in control and asthma groups were oral administered with saline. At the end of experimental period, mice were euthanized and lung tissues used to extract RNA were harvested immediately and frozen in liquid nitrogen.

2.2. Tissue Sample RNA Isolation. For RNA-seq, we used 3 lung tissue samples from control mice, 3 from asthmatic mice, and 3 from BSYQF treatment mice. Total RNA was isolated using Trizol reagent as described previously [13]. The quality of RNA was checked by 1% agarose gels electrophoresis, and quantity was determined with NanoPhotometer spectrophotometer (IMPLEN, CA, USA). Optical density values were confirmed an $A_{260} : A_{280}$ ratio above 1.9. RNA integration number (RIN) was measured using the RNA Nano 6000 Assay Kit of the Bioanalyzer 2100 system (Agilent Technologies, CA, USA) to confirm RIN above 7.

2.3. Library Preparation and Transcriptome Sequencing. We used NEBNext[®] Ultra[™] RNA Library Prep Kit for Illumina (NEB, USA) to construct sequencing libraries according to the manufacturer's recommendations. Briefly, using poly-T oligo beads, the mRNA was purified from total RNA. In NEBNext First-Strand Synthesis Reaction Buffer, fragmentation was performed using divalent cations. M-MuLV Reverse Transcriptase (RNase H) was used to synthesize the first strand cDNA, and DNA polymerase I and RNase H were used to synthesize the second-strand cDNA. Via exonuclease/polymerase activities, and remaining overhangs were transformed into blunt ends. The NEBNext adaptor with the hairpin loop structure was ligated and prepared for hybridization after the 3'-end of the DNA fragment was identified. Using AMPure XP system (Beckman Coulter, Beverly, USA), we purify the library fragments and the cDNA fragment with length of 250–300 bp was selected preferentially. Finally, PCR products were purified using AMPure XP system, and on the Agilent Bioanalyzer 2100 system, the library quality was evaluated. TruSeq PE Cluster Kit V3 -cBot-HS (Illumina, San Diego, CA, USA) was performed to cluster the index coded samples according to the manufacturer's protocol on the cBot Cluster generation system. After cluster generation, sequenced library was prepared on Illumina Novaseq6000 platform to generate 150 bp paired end reads.

2.4. Quality Control, Mapping, and Quantification of RNA-Seq Reads. Firstly, clean reads were obtained by removing reads containing adapter or ploy-N as well as low quality reads from raw reads. Meanwhile, the Q20, Q30, and GC contents of clean data were calculated. All downstream data were analysed on the basis of high quality cleaning readings. STAR was performed to align clean reads to reference genome. In the mapping speed, STAR outperformed other aligners by a factor of >50 and improved alignment

sensitivity and precision [14]. The HTSeq V0.6.0 count was mapped to the reading for each gene. The value of the FPKM (number of segments per thousand base exon; mapping per million segments) is calculated based on the length of the gene as well as the read count mapped to the gene.

2.5. Differential Expression Analysis. After the significant analysis and FDR analysis, only genes under $|\log_2\text{FC}| > 1$ and p value < 0.05 criteria were included in the analysis. DESeq2 algorithm was applied to filter the differentially expressed genes.

2.6. Functional Analysis. The gene ontology (GO) and Kyoto Encyclopedia of Genes and Genomes (KEGG) analysis were performed to describe the function of each DEGs. We applied the ingenuity pathway analysis (IPA, Redwood City, CA, USA) to construct gene interaction network.

2.7. Real-Time PCR. The primers used in this study were purchased from BioTNT (Shanghai, China). Total RNA from treated, asthma, and control lung samples was extracted by the TRIZOL method. cDNA synthesis was performed using cDNA Reverse Transcription Kit (Takara) according to the manufacturer's instructions. qRT-PCR was performed using TB Green Premix Ex Taq Kit (Takara). We used GAPDH gene as an internal reference to normalize the expression of target genes. Reactions were run on the 7500 Real-time PCR system (ABI, USA), and the data were analysed using its software. Ct (threshold cycle) was used to determine the target gene expression levels.

2.8. Statistical Analysis. Intergroup differences were analysed using one-way ANOVA. Data in the experiments are expressed as mean \pm SD. All statistical analyses were accomplished by using PRISM version 7.0 (GraphPad). A p value of < 0.05 was considered statistically significant.

3. Results

3.1. Gene Expression Analysis. DEGseq analysis results applied on RNA-seq FPKM. The RNA expression result in lung tissue showed significant differences among control (C, control), asthma (M, model), and BSYQF treatment in the mouse model of asthma (T, treatment). As shown in Figure 1(a), clustering analysis was used to detect overexpressed genes and underexpressed genes.

3.2. Gene Expression Regulated by Asthma and BSYQF. Gene expression differences between the asthmatic compared to control (A vs C) and asthma compared to BSYQF treatment (A vs T) groups were shown in the Venn diagram in Figure 1(b) and Table 1. As the Venn diagram shown, changes in expression levels were observed in 1,899 transcripts in the lung. 271 (180 + 7 + 84 + 0) of these were regulated by both asthma and treatment. As shown in Table 1, 1,746 transcripts were regulated by asthma with \log_2 fold changes (FC) ranging from -8.6 to 11.7 , $p < 0.05$. Of these,

1,025 were upregulated and 721 were downregulated by asthma. BSYQF treatment alters the expression of 424 transcripts with FC between -5.5 and 7.8 ($p < 0.05$). Among these, 325 were upregulated and 99 were downregulated. By BSYQF treatment, a total of 264/1746 (15.1%) transcripts including 180 upregulated and 84 downregulated transcripts, and their expression levels were reversed to normal levels.

3.3. Volcano Results. In Figure 1 C/D, the volcano plot shows transcriptome changes in asthmatic compared to control (A vs C) and asthma compared to BSYQF treatment (A vs T) groups in the lung tissues of mice. The scatter plot showed that the distribution of genes in significance (y axis, $-\log_{10}$ (p value)) vs fold changes (x axis, \log_2 (normalized fold change (FC))). As shown in Figure 1 C/D, genes are outside the midline of the absolute normalized FC $\geq (\pm)1$, and $-\log_{10}$ (p value) ≥ 1.3 are colored red for overexpressed genes and blue for underexpressed genes. The underlying key genes in asthma pathogenesis and those regulated by treatment including Adipoq, HMOX1, SPP1, Cyp2e1, TNC, MB, MPO, Col9a1, Ckmt2, and Erbb4 were taken as examples to illustrate the positions and relationships with other points and midline in the figure. There were small changes in the expression levels of many genes in both directions, but only the FC $\geq (\pm)1$ and $p < 0.05$ genes that met our screening criteria were meaningful in this study.

3.4. BSYQF Treatment Normalized Gene Expression Altered in Asthma. From this analysis (Table 1 A/B), we found a small group of genes that showed significant (above 50%) or complete reversal of changes in asthma during BSYQF therapy. These genes are listed in Table 1 C and rank-ordered by FC $\geq (\pm)5$ ($p < 0.05$). These DEGs were regulated by both asthma and BSYQF and may be closely related to the mechanism of BSYQF's anti-asthma.

3.5. Key Gene Interaction Network Identification. Based on the gene expression analysis and our previous results, 21 genes were selected from DEGs between asthma group and treatment group according to their relevant functions with inflammatory, oxidative stress, mitochondria, PI3K/AKT, and MAPKs signal pathways which are thought to be related to the action mechanism of BSYQF (Table 2). Then, we applied IPA software to identify gene networks about 21 DEGs (Figure 2). 11 of 21 input genes could be located in this network including Adipoq, HMOX1, SPP1, Cyp2e1, TNC, MB, MPO, Col9a1, Ckmt2, Erbb4, and MAPK10. In the network, Adipoq, HMOX1, SPP1, and TNC appeared to be key components which directly or indirectly interact with multiple genes and participate in multiple biological functions.

3.6. Verification of Selected DEGs. According to IPA analysis result, Adipoq, HMOX1, SPP1, and TNC were selected for further validation. We performed qRT-PCR analysis on the four genes to confirm the results of DEGs in the lung. As

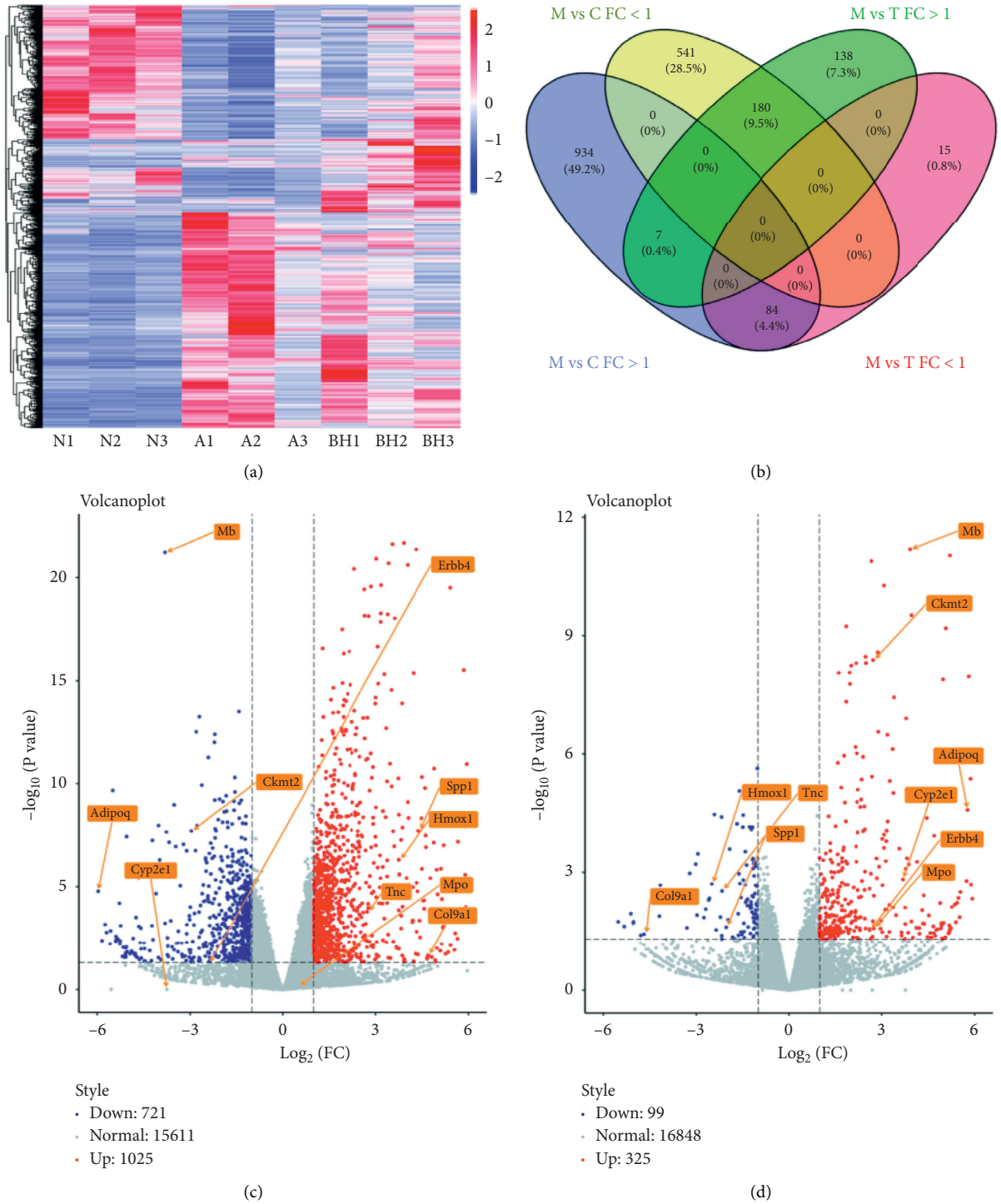


FIGURE 1: (a) The clustering heat maps of gene expressions. Red represents the upregulation expressions; blue represents the downregulation expressions. The color brightness is associated with differences in multiples. (b) The Venn diagram shows RNA-seq data for all genes that were regulated in asthma compared to control (M vs C) and by BSYQF treated compared to non-treated asthma controls (T vs M). FC: fold changes. Blue: M vs C, positive FC (FC > 1). Yellow: M vs C, negative FC (FC < 1). Green: M vs T, positive FC (FC > 1). Pink: M vs T, negative FC (FC < 1). (c) Volcano plot (M vs C). (d) Volcano plot (M vs T). Genes of interest are labeled as examples to show changes in expression levels. Horizontal dashed line represents expression value $p = 0.05$. Genes outside the midline have FC > 1.

shown in Figure 3, a significant reduction of adiponectin (Adipoq) gene expressions in asthma group compared with control group were observed. In addition, the expressions of heme oxygenase 1 (HMOX1), tenascin C (TNC), and

secreted phosphoprotein 1 (SPP1) in asthma group compared with control group genes were significantly elevated, while BSYQF treatment completely or partially reversed asthma-induced expression changes of Adipoq, HMOX1,

TABLE 1: Differently expressed genes showing the highest fold changes (in either direction) in lung samples of the mice in the control (C), asthmatic model (M), and BSYQF treatment (T) groups.

| A. M vs C | | B. T vs M | | C | | |
|------------------|-------------|------------------|-------------|---------------|--------|--------|
| Gene | Fold change | Gene | Fold change | Gene | M vs C | T vs M |
| <i>Increased</i> | | <i>Increased</i> | | Timp1 | 6.22 | -3.01 |
| Chil4 | 11.74 | A530016L24Rik | 7.79 | Reg1 | 6.20 | -3.30 |
| Sprr2a3 | 11.18 | Tmem179 | 7.17 | Dmp1 | 5.65 | -4.15 |
| Clca1 | 9.86 | Serp1nb11 | 7.01 | Glod5 | 5.55 | -5.52 |
| Mcp1 | 8.71 | Ebf2 | 6.85 | Rnf17 | 5.35 | -5.33 |
| Rnase2a | 8.43 | Htr3a | 6.59 | Dspp | 5.14 | -5.11 |
| Capn9 | 7.48 | Lep | 6.52 | Lep | -8.64 | 6.52 |
| Saa3 | 7.42 | Glycam1 | 6.43 | A530016L24Rik | -8.36 | 7.79 |
| Saa1 | 7.23 | Syt4 | 6.39 | Tmem179 | -7.57 | 7.17 |
| Saa4 | 7.18 | Lrtm1 | 5.95 | Lctl | -7.36 | 5.20 |
| Retnlb | 7.09 | Nalcn | 5.91 | Ebf2 | -6.77 | 6.85 |
| A | 6.93 | Slc5a8 | 5.89 | Nalcn | -6.42 | 5.91 |
| Cd209e | 6.93 | Dsc3 | 5.84 | Adipoq | -5.97 | 5.80 |
| Mmp12 | 6.84 | Adipoq | 5.80 | Htr3a | -5.58 | 6.59 |
| Timd2 | 6.78 | Lsmem1 | 5.76 | Myh1 | -5.57 | 4.94 |
| Retnla | 6.64 | Ugt2b34 | 5.57 | Car3 | -5.50 | 5.10 |
| Cbln1 | 6.47 | Cartpt | 5.54 | Gm10382 | -5.40 | 4.72 |
| Mrgprg | 6.32 | Dnmt3c | 5.51 | Lrtm1 | -5.39 | 5.95 |
| Prss32 | 6.27 | Nefm | 5.46 | Slc5a8 | -5.29 | 5.89 |
| Timp1 | 6.22 | Slc38a3 | 5.42 | Hist1h4k | -5.27 | 5.29 |
| Reg1 | 6.20 | Pnoc | 5.39 | Kcnq3 | -5.26 | 5.22 |
| Fgl1 | 6.18 | Hist1h4k | 5.29 | Pnoc | -5.18 | 5.39 |
| Btbd16 | 6.12 | Krt6a | 5.26 | Dnmt3c | -5.16 | 5.51 |
| Nuggc | 6.11 | Serpina1e | 5.24 | Retn | -5.09 | 4.96 |
| <i>Decreased</i> | | Acp7 | 5.24 | Cfd | -5.06 | 5.01 |
| Lep | -8.64 | Krt5 | 5.23 | Lsmem1 | -5.03 | 5.76 |
| A530016L24Rik | -8.36 | Kcnq3 | 5.22 | | | |
| Tmem179 | -7.57 | BC117090 | 5.21 | | | |
| Lctl | -7.36 | Lctl | 5.20 | | | |
| Ebf2 | -6.77 | BC016579 | 5.19 | | | |
| Gys2 | -6.69 | Car3 | 5.10 | | | |
| Ebf3 | -6.58 | Gm5416 | 5.09 | | | |
| Nalcn | -6.42 | Dync1i1 | 5.03 | | | |
| | | Cfd | 5.01 | | | |
| | | <i>Decreased</i> | | | | |
| | | Glod5 | -5.52 | | | |
| | | Rnf17 | -5.33 | | | |
| | | Dspp | -5.11 | | | |
| | | Gm49320 | -5.03 | | | |
| | | Azgp1 | -5.03 | | | |

A, all genes with increased or decreased expression levels by $FC > (\pm)6$ ($p < 0.05$) in the asthma group (M) relative to the control group (C); B, all genes upregulated or downregulated by the BSYQF treatment group (T) with $FC > =(\pm)5$ ($p < 0.05$) relative to the asthma group (M). C, all genes with $FC > (\pm)5$ ($p < 0.05$) that were reverted in their expression towards normal levels by BSYQF treatment. Genes are ranked orderly by FC (positive or negative values).

SPP1, and TNC. The results showed that the expression of the four genes from qRT-PCR was consistent with the RNA-seq analysis pattern.

4. Discussion

In this research, we identified a set of transcriptome changes in the lung of chronic asthmatic mice with and without BSYQF treatment. Lung tissues were taken from our recently published study in which we have demonstrated that BSYQF treatment could ameliorate airway remodeling in asthmatic mice by reducing airway inflammation and oxidative stress in the lung [11]. The results from this study provided us

insight into the molecular mechanism of BSYQF's anti-airway remodeling in chronic asthmatic mice.

We identified genes whose expression in asthmatic mice were impacted by BSYQF treatment. 264/1746 (15.1%) of genes showing abnormal expression in asthma group were reverted back to completely or partially to normal levels by BSYQF treatment. These included Adipoq, also known as Adiponectin, which in this study was found to be one of the most prominently downregulated genes in asthma and completely reversed back by BSYQF treatment. It has been shown that Adiponectin is an anti-inflammatory adipokine [15]. Since BSYQF has been shown to effectively regulate many pathological processes in asthma, we proposed that

TABLE 2: Differently expressed gene with FC > (±) 2.0 in asthma group (M) relative to treatment group (T) related to inflammatory, oxidative stress, mitochondria, PI3K/AKT, and MAPK signal pathways.

| Gene name | Description | log2 fold change (A vs T) |
|-----------|---|---------------------------|
| Adipoq | Adiponectin C1Q and collagen domain containing | 5.80 |
| Nefm | Neurofilament medium polypeptide | 5.46 |
| Car3 | Carbonic anhydrase 3 | 5.10 |
| Mb | Myoglobin | 3.94 |
| Krt15 | Keratin 15 | 3.99 |
| Cyp2e1 | Cytochrome P450 family 2 subfamily e polypeptide 1 | 3.71 |
| Gdap1 | Ganglioside induced differentiation associated protein 1 | 3.66 |
| Cyp4a12b | Cytochrome P450 family 4 subfamily a polypeptide 12B | 3.10 |
| Cacna2d2 | Calcium channel voltage dependent alpha 2 delta subunit 2 | 2.77 |
| Mpo | Myeloperoxidase | 2.77 |
| Ckmt2 | Creatine kinase mitochondrial 2 | 2.75 |
| ErbB4 | Erb-B2 receptor tyrosine kinase 4 | 2.63 |
| Mapk10 | Mitogen-activated protein kinase 10 | 2.47 |
| Pln | Phospholamban | 2.42 |
| Obscn | Obscurin cytoskeletal calmodulin and titin interacting RhoGEF | 2.24 |
| Cox8b | Cytochrome c oxidase subunit VIIIb | 2.23 |
| Col9a1 | Collagen type IX alpha 1 | -4.69 |
| Mt-Nd4l | Mitochondrially encoded NADH dehydrogenase 4L | -2.94 |
| Hmox1 | Heme oxygenase 1 | -2.48 |
| Tnc | Tenascin C | -2.16 |
| Spp1 | Secreted phosphoprotein 1 | -2.02 |

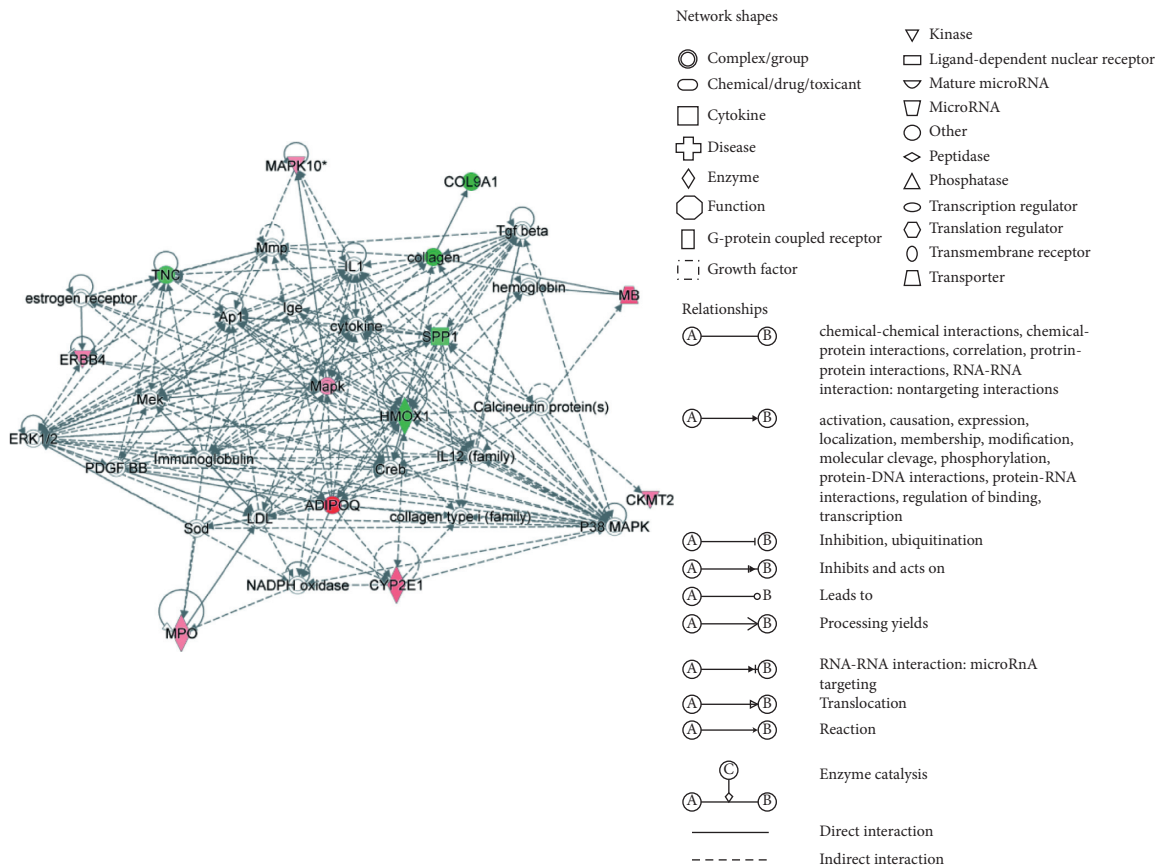


FIGURE 2: The gene networks by IPA. The intensity of green or red coloured shapes indicates the degree of down- or upregulation, respectively.

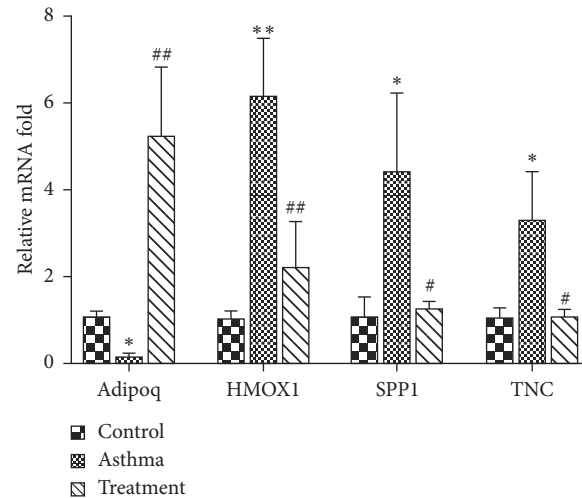


FIGURE 3: qRT-PCR validation of Adipoq, HMOX1, SPP1, and TNC results. * $p < 0.05$, ** $p < 0.01$ vs control; # $p < 0.05$, ## $p < 0.01$ vs asthma.

this core set of genes may be related to the pathology of asthma and represent key BSYQF targets.

Based on previous result, we identified a set of genes related to inflammatory, oxidative stress, mitochondria, PI3K/AKT, and MAPKs signal pathways which may play important roles in the mechanism of BSYQF's anti-remodeling. We screened 21 DEGs with $FC > (\pm) 2.0$ that were differentially expressed between asthma and treatment. Additionally, 21 DEGs were input into IPA database to obtain gene networks related to regulatory functions. Gene network analyses by IPA are based on current known pathways. We used IPA because we aimed to elucidate the interaction of the gene expression found in specific functions and pathways which are thought to be related to BSYQF's anti-remodeling. Furthermore, we identified the possible key targets of BSYQF through IPA. In the gene network analyses by IPA, we found that Adipoq, HMOX1, SPP1, and TNC are genes at critical nodes. We also verified the four DEGs selected through qRT-PCR and confirmed that their variation trend were consistent with the RNA-seq analysis.

Adipoq, also known as diponectin, is an important adipokine with anti-inflammatory and antioxidative effects [16]. Adiponectin plays a physiological role by activating receptors such as AdipoR1, AdipoR2, and T-cadherin which are expressed on airway epithelial and endothelial pulmonary cells playing functional roles on lung physiology [17, 18]. AdipoRs mediate pleiotropic adiponectin actions through signaling mechanisms including AMPK, AKT, ERK1/2, and P38 [19]. Previous study reported that adiponectin was reduced in the asthmatic murine model [20]. Additionally, adiponectin attenuated the airway inflammation and AHR in asthmatic mice [20]. Another study has also shown that adiponectin can reduce inflammation and suppress oxidative stress in vivo [21]. Adiponectin not only downregulates proinflammatory cytokines including TNF- α , IL-6, and NF- κ B but also upregulates anti-inflammatory cytokines such as IL-10 [22]. Benjamin D et al. found that adiponectin deficiency

increased allergic airway inflammation and pulmonary vascular remodeling [23]. In our RNA-seq result, Adipoq was significantly downregulated more than five-fold in asthma group and reversed completely after BSYQF treatment which drew our attention. The qRT-PCR results further confirmed the result of RNA-seq. Furthermore, in the gene network analysed by IPA, Adipoq interacted with multiple genes and participated in multiple cellular functions. Hence, the mechanism related to Adipoq expression might provide a new understanding for illustrating the therapeutic target of BSYQF's anti-remodeling.

HOMX1, known as HO-1, is a rate-limiting enzyme that catalyzes the degradation of heme into biliverdin, ferrous ion, and carbon monoxide [24]. Studies have shown that HO-1 has anti-inflammatory, excessive cell proliferation and interstitial fibrosis effects [25]. Previous study has shown that HO-1 could ameliorate airway inflammation by downregulating the tumor necrosis factor receptor (TNFR)1 dependent oxidative stress [26]. In asthma, increased HO-1 expression and activity are considered protective. The expression level of HO-1 was associated with its anti-asthma effect. Our results turned out that HO-1 gene expression was increased in asthmatic mice which was consistent with that in the previous study [27]. However, there are conflicting results about the role of BSYQF in regulating the HO-1 expression. We observed BSYQF treatment reduced HO-1 gene expression by using RNA-seq analysis and qRT-PCR. This implies that it is possible that the effect of BSYQF on HO-1 expression differs between gene and protein levels and further studies are needed.

SPP1 (secreted phosphoprotein 1, also known as osteopontin) is a phosphorylated glycoprotein secreted by activated macrophages, leucocytes, and activated T lymphocytes [28]. It is recognized as a key cytokine involved in Th1 cytokine expression and immune cell recruitment at sites of inflammation [28, 29]. It is also a mediator of tissue repair and remodeling [30, 31]. According to RNA-seq and qRT-PCR results, we found the SPP1 expression increased in asthma and decreased after BSYQF

treatment which suggested that SPP1 might play important effect on the mechanism of BSYQF's anti-remodeling.

TNC is considered an important gene in asthma pathogenesis [32] and known as an extracellular matrix (ECM) protein whose expression is increased in asthma [32]. TNC plays important roles in cell communication and signal transduction and regulates cell adhesion, migration, proliferation, and differentiation [32, 33]. Study in TNC knockout (KO) mice showed that lung disease phenotype was largely attenuated in the absence of TNC in OVA-induced asthma [34]. Our RNA-seq and qRT-PCR results confirmed that TNC up-regulation in asthma. Additionally, we found that TNC mRNA expression decreased after BSYQF treatment. These results provided that BSYQF may have a beneficial effect on asthma by reducing the TNC expression.

5. Conclusion

In this study, we used RNA-seq analysis to obtain the differentially expressed genes. We found expressions of a group of coding genes were altered in asthmatic mice. Treatment with BSYQF reversed the expressions of a specific subset of these genes in asthmatic mice. As BSYQF was previously shown to ameliorate airway remodeling by reducing airway inflammation and oxidative stress in asthmatic mice, we enriched a group of genes related to inflammatory, oxidative stress, mitochondria, PI3K/AKT, and MAPKs signal pathways and used IPA to construct gene network. Based on gene network, we inferred that Adipoq, SPP1, and TNC may be key regulators of BSYQF's anti-remodeling effect. While RNA-seq analysis could not show protein levels and the precise role of these genes needs further verification, they provided initial clues to explore the mechanisms of BSYQF's anti-remodeling in asthma.

Data Availability

The data used to support the findings of this study are available from the corresponding author upon request.

Conflicts of Interest

The authors declare that they have no conflicts of interests.

Authors' Contributions

JC and ZXL contributed equally to this study.

Acknowledgments

This work was supported by grants from the National Natural Science Foundation of China (Grant nos. 8170150685 and 8177140514), Shanghai Science and Technology Commission (Grant nos. 17401930300 and 18401971300), and Young Elite Scientists Sponsorship Program by China Association for Science and Technology (Grant no. 2018QNRC001).

References

- [1] B. N. Lambrecht, H. Hammad, and J. V. Fahy, "The cytokines of asthma," *Immunity*, vol. 50, no. 4, pp. 975–991, 2019.
- [2] U. Katwa and S. K. Kabra, "Advances in asthma," *The Indian Journal of Pediatrics*, vol. 85, no. 8, pp. 641–642, 2018.
- [3] F. L. M. Ricciardolo, G. Folkerts, A. Folino, and B. Mognetti, "Bradykinin in asthma: modulation of airway inflammation and remodelling," *European Journal of Pharmacology*, vol. 827, pp. 181–188, 2018.
- [4] L.-P. Boulet, "Airway remodeling in asthma," *Current Opinion in Pulmonary Medicine*, vol. 24, no. 1, pp. 56–62, 2018.
- [5] C. Y. Yick, A. H. Zwinderman, P. W. Kunst et al., "Transcriptome sequencing (RNA-Seq) of human endobronchial biopsies: asthma versus controls," *European Respiratory Journal*, vol. 42, no. 3, pp. 662–670, 2013.
- [6] C. H. Wiegman, C. Michaeloudes, G. Haji et al., "Oxidative stress-induced mitochondrial dysfunction drives inflammation and airway smooth muscle remodeling in patients with chronic obstructive pulmonary disease," *Journal of Allergy and Clinical Immunology*, vol. 136, no. 3, pp. 769–780, 2015.
- [7] U. M. Sahiner, E. Birben, S. Erzurum, C. Sackesen, and O. Kalayci, "Oxidative stress in asthma: part of the puzzle," *Pediatric Allergy Immunology*, vol. 29, 2018.
- [8] L. Aguilera-Aguirre, A. Bacsi, A. Saavedra-Molina, A. Kurosky, S. Sur, and I. Boldogh, "Mitochondrial dysfunction increases allergic airway inflammation," *The Journal of Immunology*, vol. 183, no. 8, pp. 5379–5387, 2009.
- [9] X. Li, L. Zhou, Z. Zhang, Y. Liu, J. Liu, and C. Zhang, "IL-27 alleviates airway remodeling in a mouse model of asthma via PI3K/Akt pathway," *Experimental Lung Research*, vol. 46, no. 3–4, pp. 98–108, 2020.
- [10] P. S. Chauhan, D. K. Singh, D. Dash, and R. Singh, "Intranasal curcumin regulates chronic asthma in mice by modulating NF- κ B activation and MAPK signaling," *Phytomedicine*, vol. 51, pp. 29–38, 2018.
- [11] J. Cui, F. Xu, Z. Tang et al., "Bu-Shen-Yi-Qi formula ameliorates airway remodeling in murine chronic asthma by modulating airway inflammation and oxidative stress in the lung," *Biomedicine & Pharmacotherapy*, vol. 112, Article ID 108694, 2019.
- [12] Y. Wei, Q.-L. Luo, J. Sun, M.-X. Chen, F. Liu, and J.-C. Dong, "Bu-Shen-Yi-Qi formulae suppress chronic airway inflammation and regulate Th17/Treg imbalance in the murine ovalbumin asthma model," *Journal of Ethnopharmacology*, vol. 164, pp. 368–377, 2015.
- [13] Q. Guan, X. Wang, Y. Jiang, L. Zhao, Z. Nie, and L. Jin, "RNA-seq expression analysis of enteric neuron cells with rotenone treatment and prediction of regulated pathways," *Neurochemical Research*, vol. 42, no. 2, pp. 572–582, 2017.
- [14] A. Dobin, C. A. Davis, F. Schlesinger et al., "STAR: ultrafast universal RNA-seq aligner," *Bioinformatics*, vol. 29, no. 1, pp. 15–21, 2013.
- [15] Y. Ding, H. Yang, H. He et al., "Plasma adiponectin concentrations and adiponectin gene polymorphisms are associated with bronchial asthma in the Chinese Li population," *Iranian Journal of Allergy, Asthma, and Immunology*, vol. 14, no. 3, pp. 292–297, 2015.
- [16] M. Dogru, S. Ozde, A. Aktas, and E. Yuksel Karatoprak, "The adiponectin levels and asthma control in non-obese children with asthma," *Journal of Asthma*, vol. 52, no. 8, pp. 772–776, 2015.

- [17] A. S. Williams, D. I. Kasahara, N. G. Verbout et al., "Role of the adiponectin binding protein, T-cadherin (Cdh13), in allergic airways responses in mice," *PLOS ONE*, vol. 7, no. 7, Article ID e41088, 2012.
- [18] M. Miller, J. Y. Cho, A. Pham, J. Ramsdell, and D. H. Broide, "Adiponectin and functional adiponectin receptor 1 are expressed by airway epithelial cells in chronic obstructive pulmonary disease," *The Journal of Immunology*, vol. 182, no. 1, pp. 684–691, 2009.
- [19] L. Zhu, X. Chen, L. Chong et al., "Adiponectin alleviates exacerbation of airway inflammation and oxidative stress in obesity-related asthma mice partly through AMPK signaling pathway," *International Immunopharmacology*, vol. 67, pp. 396–407, 2019.
- [20] S. A. Shore, R. D. Terry, L. Flynt, A. Xu, and C. Hug, "Adiponectin attenuates allergen-induced airway inflammation and hyperresponsiveness in mice," *Journal of Allergy and Clinical Immunology*, vol. 118, no. 2, pp. 389–395, 2006.
- [21] T. Yamauchi, Y. Nio, T. Maki et al., "Targeted disruption of AdipoR1 and AdipoR2 causes abrogation of adiponectin binding and metabolic actions," *Nature Medicine*, vol. 13, no. 3, pp. 332–339, 2007.
- [22] S.-H. Kim, E. R. Sutherland, and E. W. Gelfand, "Is there a link between obesity and asthma?" *Allergy, Asthma & Immunology Research*, vol. 6, no. 3, pp. 189–195, 2014.
- [23] B. D. Medoff, Y. Okamoto, P. Leyton et al., "Adiponectin deficiency increases allergic airway inflammation and pulmonary vascular remodeling," *American Journal of Respiratory Cell and Molecular Biology*, vol. 41, no. 4, pp. 397–406, 2009.
- [24] A. Grochot-Przeczek, J. Dulak, and A. Jozkowicz, "Haem oxygenase-1: non-canonical roles in physiology and pathology," *Clinical Science*, vol. 122, no. 3, pp. 93–103, 2012.
- [25] M. Li, Z. Li, X. Sun et al., "Heme oxygenase-1/p21WAF1 mediates peroxisome proliferator-activated receptor- γ signaling inhibition of proliferation of rat pulmonary artery smooth muscle cells," *Febs Journal*, vol. 277, no. 6, pp. 1543–1550, 2010.
- [26] I.-T. Lee, S.-F. Luo, C.-W. Lee et al., "Overexpression of HO-1 protects against TNF- α -mediated airway inflammation by down-regulation of TNFR1-dependent oxidative stress," *The American Journal of Pathology*, vol. 175, no. 2, pp. 519–532, 2009.
- [27] J. Xu, Y.-t. Zhu, G.-z. Wang et al., "The PPAR γ agonist, rosiglitazone, attenuates airway inflammation and remodeling via heme oxygenase-1 in murine model of asthma," *Acta Pharmacologica Sinica*, vol. 36, no. 2, pp. 171–178, 2015.
- [28] S. Ashkar, G. F. Weber, V. Panoutsakopoulou et al., "Eta-1 (osteopontin): an early component of type-1 (cell-mediated) immunity," *Science*, vol. 287, no. 5454, pp. 860–864, 2000.
- [29] D. Chabas, S. E. Baranzini, D. Mitchell et al., "The influence of the proinflammatory cytokine, osteopontin, on autoimmune demyelinating disease," *Science*, vol. 294, no. 5547, pp. 1731–1735, 2001.
- [30] L. Liaw, D. E. Birk, C. B. Ballas, J. S. Whitsitt, J. M. Davidson, and B. L. Hogan, "Altered wound healing in mice lacking a functional osteopontin gene (spp1)," *Journal of Clinical Investigation*, vol. 101, no. 7, pp. 1468–1478, 1998.
- [31] N. A. Trueblood, Z. Xie, C. Communal et al., "Exaggerated left ventricular dilation and reduced collagen deposition after myocardial infarction in mice lacking osteopontin," *Circulation Research*, vol. 88, no. 10, pp. 1080–1087, 2001.
- [32] R. Chiquet-Ehrismann and M. Chiquet, "Tenascins: regulation and putative functions during pathological stress," *The Journal of Pathology*, vol. 200, no. 4, pp. 488–499, 2003.
- [33] H. C. Hsia and J. E. Schwarzbauer, "Meet the tenascins: multifunctional and mysterious," *Journal of Biological Chemistry*, vol. 280, no. 29, pp. 26641–26644, 2005.
- [34] H. Nakahara, E. C. Gabazza, H. Fujimoto et al., "Deficiency of tenascin C attenuates allergen-induced bronchial asthma in the mouse," *European Journal of Immunology*, vol. 36, no. 12, pp. 3334–3345, 2006.

Research Article

Rutaecarpine Ameliorates Pressure Overload Cardiac Hypertrophy by Suppression of Calcineurin and Angiotensin II

Shujun Li ¹, Bo Huang ², Changfei Zhou ², Jingshan Shi ², Qin Wu ²,
and Qingsong Jiang ³

¹Department of Burn and Plastic Surgery, The first Affiliated Hospital of Zunyi Medical University, Zunyi, Guizhou 563000, China

²Key Laboratory of Basic Pharmacology of Ministry of Education and Joint International Research Laboratory of Ethnomedicine of Ministry of Education, Zunyi Medical University, Zunyi, Guizhou 563000, China

³Department of Pharmacology, Chongqing Key Laboratory of Biochemistry and Molecular Pharmacology, Chongqing Medical University, Chongqing 400016, China

Correspondence should be addressed to Qin Wu; wuqinzm@163.com and Qingsong Jiang; cqjiangqs@163.com

Received 8 October 2020; Revised 1 December 2020; Accepted 24 December 2020; Published 15 January 2021

Academic Editor: Lixin Wei

Copyright © 2021 Shujun Li et al. This is an open access article distributed under the Creative Commons Attribution License, which permits unrestricted use, distribution, and reproduction in any medium, provided the original work is properly cited.

Cardiac hypertrophy is a major pathological process to result in heart failure and sudden death. Rutaecarpine, a pentacyclic indolopyridoquinazolinone alkaloid extracted from *Evodia rutaecarpa* with multiple pharmacological activities, yet the underlying protective effects and the mechanisms on cardiac hypertrophy remain unclear. This study aimed to evaluate the potential effects of rutaecarpine on pressure overload cardiac hypertrophy. Cardiac hypertrophy in rat was developed by abdominal aortic constriction (AAC) for 4 weeks, which was improved by rutaecarpine supplementation (20 or 40 mg/kg/day, i.g.) for another 4 weeks. The level of angiotensin II was increased; the mRNA expression and the activity of calcineurin in the left ventricular tissue were augmented following cardiac hypertrophy. Rutaecarpine administration decreased angiotensin II content and reduced calcineurin expression and activity. Noteworthy, in angiotensin II-induced cardiomyocytes, rutaecarpine ameliorated the hypertrophic effects in a dose-dependent manner and downregulated the increased mRNA expression and activity of calcineurin. In conclusion, rutaecarpine can improve cardiac hypertrophy in pressure overload rats, which may be related to the inhibition of angiotensin II-calcineurin signal pathway.

1. Introduction

Cardiac hypertrophy is considered as a compensatory response to maintain cardiac output during various physiological and pathological conditions. However, prolonged hypertrophy often leads to decompensation, resulting in heart failure and sudden death. Many factors including mechanical stress and neurohumoral stimulation induce cardiac hypertrophy [1]. Among them, angiotensin II has been identified as one of the most powerful stimuli in inducing cardiac hypertrophy. It has been reported that angiotensin II-activated Ca^{2+} signaling pathway initiated the progress of cardiomyocytes hypertrophy. Angiotensin II activates G protein-dependent signaling pathways in cardiomyocytes that evokes Ca^{2+} entry [2]. The sustained

intracellular Ca^{2+} concentration ($[Ca^{2+}]_i$) increase induces pathological myocardial hypertrophy through activation of Ca^{2+} -dependent signaling pathway such as Ca^{2+} -calcineurin, which directly participates in several extracellular signal pathways causing myocardial hypertrophy.

Evodia rutaecarpa (Wu-Chu-Yu), a traditional Chinese herb, has been used to treat various diseases for centuries. Rutaecarpine, one of the main bioactive components of *Evodia rutaecarpa* and other related herbs, is a pentacyclic indolopyridoquinazolinone alkaloid with multiple pharmacological activities, including anticoagulation, vasodilation, and anticholinesterase [3]. Rutaecarpine has multifactorial cardiovascular actions, such as cardiotoxic responses, vasodilatory and blood-pressure lowering effects, endothelium protection, and antiplatelet activation.

Therefore, it can be used to treat various cardiovascular diseases, including atherosclerosis, myocardial injury, and hypertension [4]. It can also attenuate ventricular remodeling in rats induced by isoprenaline or hypoxia [5, 6]. Recently, Zeng et al. found that rutaecarpine could prevent hypertensive cardiac hypertrophy [7]. However, little is known about the potential therapeutic effect of rutaecarpine on pressure overload cardiac hypertrophy. It has been found that some mechanisms are involved in the antihypertrophic effect of rutaecarpine, such as the stimulation of calcitonin gene-related peptide (CGRP) [5, 6, 8] and the inhibition of NADPH oxidase 4 (Nox4) reactive oxygen species (ROS) via the disintegrin and metalloproteinase-17 (ADAM17) pathway [7]. In addition, rutaecarpine could inhibit angiotensin II-induced proliferation of vascular smooth muscle cells and senescence of endothelial progenitor cells [8, 9]. Nevertheless, the underlying mechanisms of rutaecarpine on angiotensin II-related signal pathways in cardiac hypertrophy have not been fully clarified, especially the effect on angiotensin II-calcineurin remains unknown.

In the present study, therefore, the therapeutic effect of rutaecarpine on pressure overload cardiac hypertrophy and the possible mechanisms related to angiotensin II-calcineurin were investigated *in vivo* and *in vitro*.

2. Materials and Methods

2.1. Chemicals and Reagents. Rutaecarpine (MW: 287.32; purity: HPLC \geq 98%) was purchased from Nanjing Zelang Biotechnology Co., Ltd. (Jiangsu, China); BCA assay kit was purchased from Beyotime Biotechnology Co. Ltd. (Jiangsu, China); α -actin and calcineurin antibodies were purchased from Abcam (Cambridge, MA, USA); 4', 6-diamidino-2-phenylindole (DAPI) was purchased from Sigma-Aldrich (St. Louis, MO, USA); angiotensin II radioimmunoassay kit was purchased from Beijing North Institute of Biological Technology (Beijing, China); calcineurin activity kit was purchased from Nanjing Jiancheng Biology Engineering Institute (Shanghai, China); RT-qPCR primers were custom-synthesized and purified by Invitrogen (Shanghai, China). All other reagents were from commercial suppliers and were of standard biochemical quality.

2.2. Induction of Cardiac Hypertrophy *In Vivo*. Healthy adult male Sprague-Dawley (SD) rats weighing between 190 and 220 g were purchased from Daping Experimental Animal Center of the Third Affiliated Hospital of Army Medical University (Chongqing, China, Animal qualified certificate: SCXK 2012-0005) and provided humanitarian care. Animals were housed in a temperature-controlled room ($25 \pm 2^\circ\text{C}$) with a 12 h light/dark cycle and were given free access to standard laboratory pellet diet and water. All experimental procedures were in accordance with the NIH Guide for Care and Use of Laboratory Animals and approved by the Animal Experiment Ethics Committee of Zunyi Medical University.

Pressure overload was produced by abdominal aortic constriction (AAC), which has primarily been used as a model of cardiac hypertrophy [9]. Briefly, rats ($n = 46$) were

anesthetized using 5% pentobarbital (60 mg/kg, ip) and the aorta was exposed through a midline abdominal incision. For the banding model, a blunt 21-gauge needle was placed adjacent to the abdominal aorta between the renal arteries just below the renal bifurcations, and a ligature was tightened around the aorta and adjacent needle. The sham procedure for the control rats included injection of the same dose of combination anesthesia, an incision of approximately the same size, and the placement of a loosely tied ligature at the same position on the abdominal aorta. The muscular layer was sutured, followed by the abdominal skin suture, and the animals were isolated in a cage for recovery. Each rat was given penicillin 120 000 units i.p. for 3 days to avoid infection.

Similar to the results of our previous [10] and other studies [11, 12], the left ventricular hypertrophy developed on the 4th week after AAC in rats, which was confirmed by pathological observation and atrial natriuretic factor (ANF) mRNA expression in six randomly selected AAC rats. The remaining AAC rats, that is, cardiac hypertrophy rats, were then randomly assigned to three groups ($n = 8$ per group), including untreated AAC rats (Model) and AAC rats treated with rutaecarpine 20 or 40 mg/kg/day i.g., respectively. Rutaecarpine was formulated freshly using 1% carboxy methyl cellulose (CMC) in distilled water and administered orally at different doses for another 4 weeks. The sham-operated rats and cardiac hypertrophy rats were given an equal volume of 1% CMC solution for 4 weeks.

Rats were sacrificed under anesthesia. Body weight (BW) was recorded and heart was separated into the left ventricle with septum (LV + S) and the right ventricle (RV) and weighed separately. Finally, the (LV + S)/RV and (LV + S)/BW were calculated to evaluate cardiac hypertrophy.

2.3. Pathological Examination in Left Ventricle. The left ventricular tissue was fixed with 10% formaldehyde solution for 48 h, then dehydrated with graded alcohol, and then embedded in paraffin and 3-5 μm thick sections were stained with H&E. The histopathological changes were examined with an optical microscopic (BX-43, Olympus Co. Ltd., Tokyo, Japan).

2.4. Induction of Cardiomyocytes Hypertrophy *In Vitro*. Ventricular myocytes from 1- to 3-day-old SD rats were prepared and cultured for 48 h in Dulbecco's modified Eagle's medium (DMEM) containing 20% fetal bovine serum and 0.1 mmol/L 5'-bromodeoxyuridine. The seeding density was about 1×10^5 cells/mL for measuring cell diameters or 1×10^6 cells/mL for evaluating cellular total protein content by BCA kits. The medium was replaced by serum-free DMEM for a further 48 h before pharmacological treatment. Angiotensin II at 1 $\mu\text{mol/L}$ was used to stimulate the cardiomyocytes. The antihypertrophic effects of rutaecarpine (dissolved in DMSO of the final concentration less than 0.1%) from 0.1 to 10 $\mu\text{mol/L}$ were studied.

Immunofluorescence staining was performed to identify the cardiomyocytes by α -actin antibody (red fluorescence) and DAPI (blue fluorescence). Cellular hypertrophy was

evaluated by the increase of cardiomyocytes diameter and protein level. The diameter of single cells was measured by a digital image analysis system (Leica QwinV3, Leica Microsystems Ltd., USA). Five random fields (with approximately 10 to 15 cells per field) from every sample were averaged and expressed as $\mu\text{m}/\text{cell}$. Collected cardiomyocytes protein was extracted with RIPA lysate and determined by BCA assay. The protein concentration per 10^6 cells was detected to calculate the amount of protein per cell. All experiments were repeated six times.

2.5. Measurement of ANF and Calcineurin mRNA by RT-qPCR. According to the instructions, Trizol was used to extract total RNA from left ventricle tissue or cultured cardiomyocytes. The real-time PCR reaction procedure (95°C for 30 s; 95°C for 5 s, 60°C for 30 s, 40 cycles) was carried out on a RT-qPCR instrument (Bio-Rad CFX96, CA, USA). The primer sequences used were shown in Table 1 and β -actin was used as an internal reference gene. The Ct value was used as the statistical parameter and the expression fold of mRNA was expressed as $2^{-\Delta\Delta\text{Ct}}$. All experiments were repeat four times for each group.

2.6. Measurement of Angiotensin II Level and Calcineurin Activity. The left ventricle tissue or cultured cardiomyocytes were homogenized with RIPA lysate and finally centrifuged at 4°C for 20 min at $13,000 \times g$. The protein concentration in the supernatant was detected with a BCA assay kit. Meanwhile, the level of angiotensin II in tissue was detected with an angiotensin II radioimmunoassay kit. The activity of calcineurin was detected with a calcineurin assay kit and was expressed as Pi produced by the calcineurin decomposition of substrate PNPP per hour from per mg of total protein ($\mu\text{mol pi/h mg pro}$). All experiments were repeated six times.

2.7. Statistical Analysis. Results were expressed as mean \pm SD and statistical analysis was performed using SPSS 20.0. The mean value among groups was analyzed by one-way analysis of variance (ANOVA) and $P < 0.05$ was considered statistically significant.

3. Results

3.1. Effects of Rutaecarpine on AAC-Induced Cardiac Hypertrophy. Figure 1 showed that there was no significant change in BW in every group ($P > 0.05$). However, (LV + S)/BW, (LV + S)/RV, and ANF mRNA expression significantly increased in model group ($P < 0.05$), in comparison with sham-operated group. The pathomorphology of the left ventricle showed that larger cardiomyocytes and irregular and disruptive fiber in model group were observed. Administration of rutaecarpine at 20 or 40 mg/kg/d could significantly improve cardiac hypertrophy in AAC-induced rats, which decreased (LV + S)/BW, (LV + S)/RV, and ANF mRNA expression in a dose-dependent manner and ameliorated the pathological changes of the left ventricle (Figure 1).

3.2. Effects of Rutaecarpine on Angiotensin II Level, Calcineurin mRNA Expression, and Activity in Left Ventricle of AAC-Induced Rats. The level of angiotensin II, the mRNA expression, and the activity of calcineurin in the left ventricle increased significantly in AAC-induced rats. Rutaecarpine administration decreased the elevated angiotensin II and calcineurin in the model rats ($P < 0.05$) (Figure 2).

3.3. Effects of Rutaecarpine on Cardiomyocytes Hypertrophy Induced by Angiotensin II. Angiotensin II ($1 \mu\text{mol/L}$) stimulation caused significant cardiomyocytes hypertrophy following 48 h incubation. Cell diameter and total protein content increased by 75.0% and 31.2%, respectively, while ANF mRNA increased 2.3-fold compared with the control group ($P < 0.05$) (Figure 3). Treatment with rutaecarpine (from 0.1 to $10 \mu\text{mol/L}$) significantly relieved the changes induced by angiotensin II in a concentration-dependent manner ($P < 0.05$).

3.4. Effects of Rutaecarpine on Calcineurin mRNA Expression and Activity in Angiotensin II-Induced Hypertrophic Cardiomyocytes. In angiotensin II-conditioned cardiomyocytes, calcineurin mRNA increased by 167.9%, while calcineurin activity increased by 56.5% after 48 h incubation ($P < 0.05$). Treatment with rutaecarpine (from 0.1 to $10 \mu\text{mol/L}$) significantly relieved the changes induced by angiotensin II in a concentration-dependent manner ($P < 0.05$) (Figure 4).

4. Discussion

Cardiac hypertrophy is an adaptive response of the heart to pressure or volume overload, myocardial infarction, and other cardiovascular stimuli [13]. Hypertension is the most important background of cardiac overload. In the response to long-standing arterial hypertension, heart function is maintained through enlarged cardiomyocytes and increased protein synthesis, accompanied by the reactivation of the fetal gene expression, such as ANF, which are the characteristics of cardiac hypertrophy. The abdominal aorta is constricted to increase cardiac pressure overload and induce cardiac hypertrophy, which is more clinically relevant and similar to the human form of the disease [9, 14]. Numerous studies have found that the left ventricular hypertrophy was developed on the 4th week after AAC in rats, which was similar to the results in the present study (data not shown). In the end of the experiment, the AAC-operated rats developed significantly cardiac hypertrophy, which manifested as increased (LV + S)/BW, (LV + S)/RV, and ANF mRNA expression, as well as the histopathological changes of left ventricle. Rutaecarpine has protective effects in different cardiac hypertrophy rats [8]. In hypertensive cardiac hypertrophy, rutaecarpine has also shown a preventive role [7]. Our results found that rutaecarpine treatment could improve the pathological changes and decrease the mRNA expression of ANF in a dose-dependent way in AAC-induced hypertrophy. The results suggested that rutaecarpine

TABLE 1: Primer sequences for real-time quantitative RT-PCR.

| Gene | Forward primer (5'-3') | Reverse primer (5'-3') |
|----------------|--------------------------|---------------------------|
| ANF | TGACAGGATTGGAGCCCAGAG | TCGAGCAGATTTGGCTGTTATCTTC |
| CaN | CTGAGATGCTGGTAAACGTCCTGA | TGCTCGGATCTTGTTCCTGATG |
| β -actin | GGAGATTACTGCCCTGGCTCCTA | GACTCATCGTACTCCTGCTTGCTG |

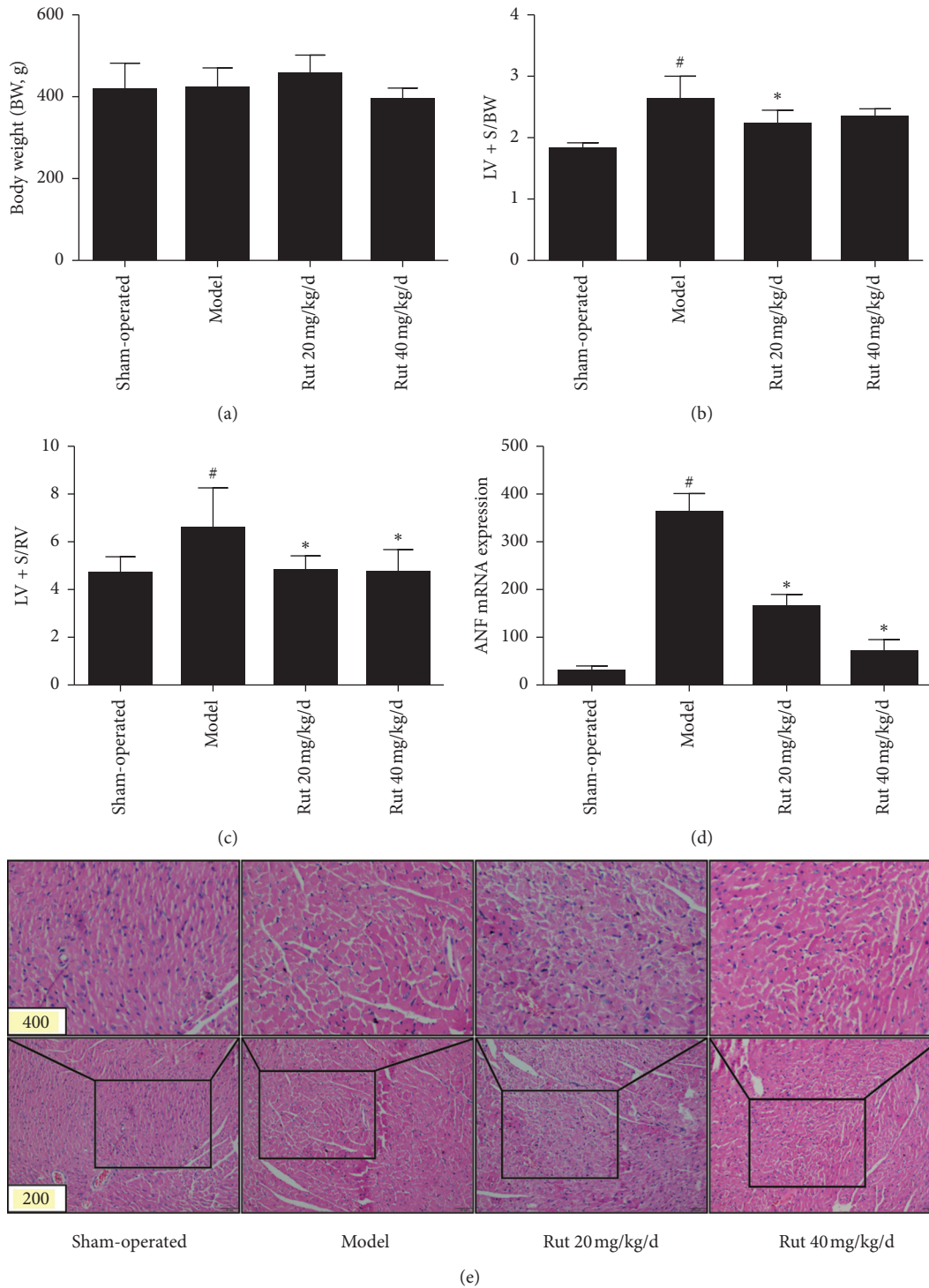


FIGURE 1: Effects of rutaecarpine on left ventricular hypertrophy induced by AAC. (a) Body weight (BW) ($n = 8$); (b) (LV + S)/BW ($n = 8$); (c) (LV + S)/RV ($n = 8$), (d) ANF mRNA expression ($n = 4$), and (e) myocardial morphological changes by H&E staining. [#] $P < 0.05$ versus sham-operated; ^{*} $P < 0.05$ versus model. LV + S: left ventricle with septum; RV: right ventricle.

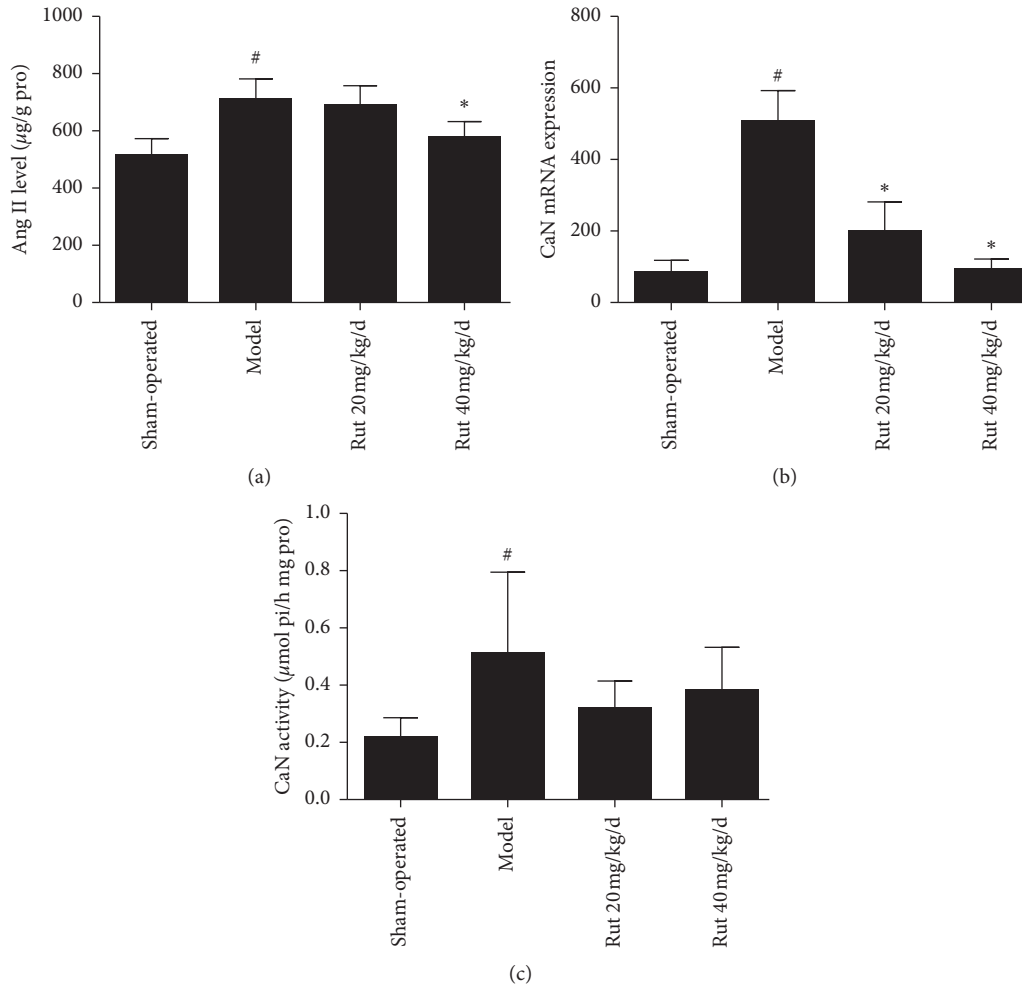


FIGURE 2: Effects of rutaecarpine (Rut) on angiotensin II (Ang II) level. (a) ($n = 6$) and calcineurin (CaN) mRNA expression, (b) ($n = 4$) and CaN activity, and (c) ($n = 6$) in left ventricle in AAC-induced rat. [#] $P < 0.05$ versus sham-operated; ^{*} $P < 0.05$ versus model.

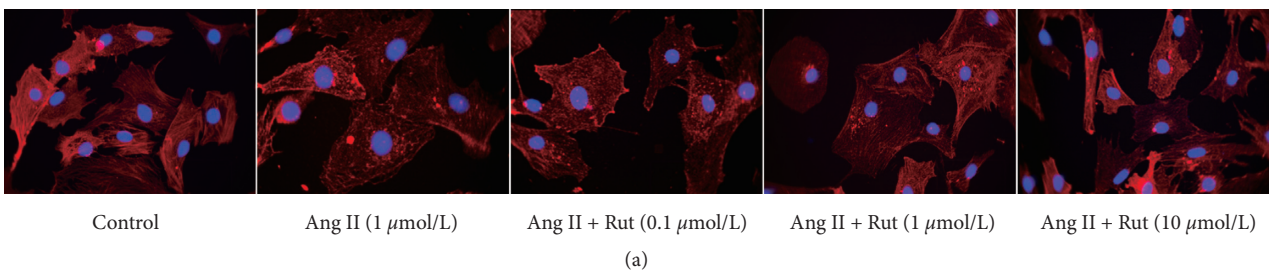


FIGURE 3: Continued.

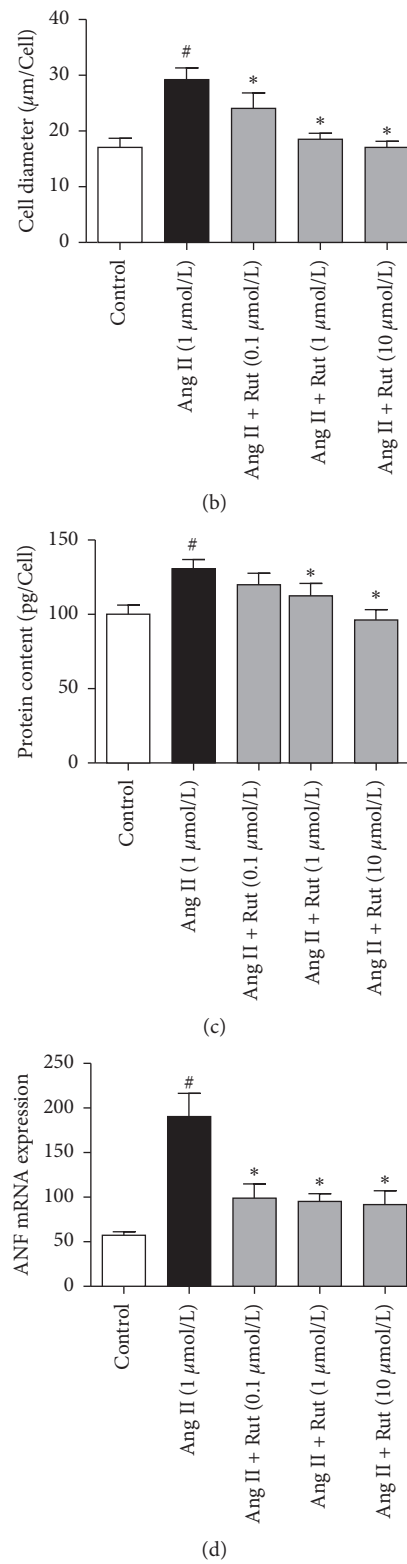


FIGURE 3: Effects of rutaecarpine (Rut) on hypertrophic cardiomyocytes induced by angiotensin II (Ang II). (a) Morphological changes of cardiomyocytes by immunofluorescence (400 \times), (b) cell diameter ($n=6$), (c) protein content ($n=6$), and (d) ($n=4$). [#] $P < 0.05$ versus control; ^{*} $P < 0.05$ versus Ang II.

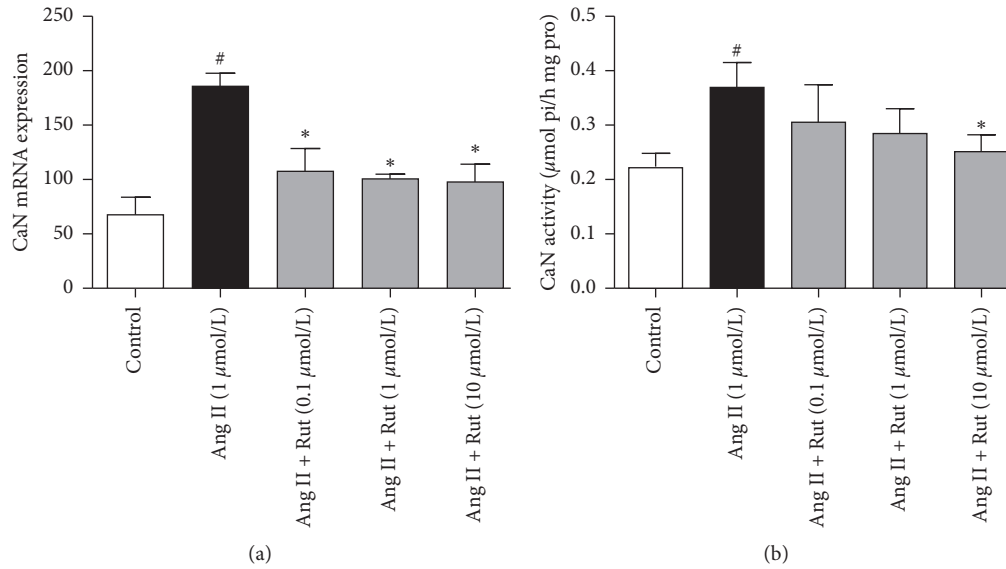


FIGURE 4: Effects of rutaecarpine (Rut) on calcineurin (CaN) level and CaN activity in angiotensin II- (Ang II-) induced cardiomyocytes. (a) mRNA expression ($n=4$) and (b) CaN activity ($n=6$). [#] $P < 0.05$ versus control; ^{*} $P < 0.05$ versus Ang II.

has also a beneficial therapeutic effect against ventricular hypertrophy induced by pressure overload.

Mechanical stress and neurohumoral mechanisms are known to stimulate the initiation of myocardial hypertrophy. Angiotensin II, an important active peptide from the renin-angiotensin system, has been defined as a powerful stimulus to induce cardiac hypertrophy [15]. Similar to the studies, angiotensin II was also increased in left ventricular tissue in AAC-induced rats. In cultured primary cardiomyocytes cultures, angiotensin II caused significant hypertrophy by increasing cell diameter, protein content, and ANF mRNA expression. Rutaecarpine is effective against angiotensin II-induced rat vascular smooth muscle cells proliferation [16]. It can also counteract angiotensin II-induced endothelial progenitor cells senescence [17]. Our results showed that the antihypertrophic effect of rutaecarpine was accompanied by the decrease of angiotensin II level in AAC-operated rats. In angiotensin II-induced primary cardiomyocytes, rutaecarpine also showed significant antihypertrophic effects in a concentration-dependent way. Combined with the results from *in vivo* and *in vitro*, the effect of rutaecarpine may be related to the inhibition of angiotensin II.

It has been reported that angiotensin II-activated Ca^{2+} signaling pathway initiated the progress of cardiomyocytes hypertrophy [18, 19]. Angiotensin II activates AT_1 receptor induces Ca^{2+} influx via complex interacting signaling pathways involving G protein-mediated activation of phospholipase C (PLC), which in turn generates diacylglycerol (DAG) and inositol 1,4,5-trisphosphate (IP_3) that are responsible for sustained increase in $[Ca^{2+}]_i$ [20]. The increasing $[Ca^{2+}]_i$ stimulates Ca^{2+} -related signal pathway, for example, calcineurin. The activation of calcineurin in cardiac cells is sufficient to induce cardiac hypertrophy [15]. However, little is known about the effect of rutaecarpine on angiotensin II-calcineurin pathway. In the present study, the

mRNA expression and the activity of calcineurin were up-regulated in AAC-model rats and in angiotensin II-induced cardiomyocytes. Rutaecarpine treatment could reduce the levels of calcineurin in AAC-operated model rats; notably, rutaecarpine could also downregulate the increases of calcineurin in angiotensin II-induced cardiomyocytes. These results suggested that the antihypertrophic effect of rutaecarpine is related to reducing the activity of angiotensin II-calcineurin signal pathway.

Taken together, the present study showed that rutaecarpine has potential therapeutic effect on pressure overload cardiac hypertrophy induced by AAC-operated rats, which may be, at least partly, related to the downregulation of calcineurin via the inhibition of angiotensin II pathway.

Abbreviations

| | |
|---------|-------------------------------|
| AAC: | Abdominal aortic constriction |
| ANF: | Atrial natriuretic factor |
| Ang II: | Angiotensin II |
| BW: | Body weight |
| BSA: | Bull serum albumin |
| CaN: | Calcineurin |
| LV + S: | Left ventricle with septum |
| RV: | Right ventricle |
| Rut: | Rutaecarpine. |

Data Availability

The data used to support the findings of this study are included within the article.

Disclosure

Shujun Li and Bo Huang should be considered co-first authors

Conflicts of Interest

The authors have no conflicts of interest to report.

Acknowledgments

This work was supported by a Guizhou Provincial Science and Technology Department Social Development Project, China (No. 2009-3074); 2011 Collaborative Innovation Center of Guizhou Province, China (No. CJ-926); Tutor Workshop of Guizhou Education Department, China (No. 99-030); Science and Technology Fund of Guizhou Province, China (No. 2014-7574); and Master Start-up Fund of Zunyi Medical University (No. F-772).

References

- [1] L. Schirone, M. Forte, S. Palmerio et al., "A review of the molecular mechanisms underlying the development and progression of cardiac remodeling," *Oxidative Medicine and Cellular Longevity*, vol. 2017, Article ID 3920195, 16 pages, 2017.
- [2] N. He, Q.-h. Gong, F. Zhang et al., "Evodiamine inhibits angiotensin II-induced rat cardiomyocyte hypertrophy," *Chinese Journal of Integrative Medicine*, vol. 24, no. 5, pp. 359–365, 2018.
- [3] I. Baburin, R. Varkevisser, A. Schramm et al., "Dehydroevodiamine and hortiamine, alkaloids from the traditional Chinese herbal drug *Evodia rutaecarpa*, are IKr blockers with proarrhythmic effects in vitro and in vivo," *Pharmacological Research*, vol. 131, pp. 150–163, 2018.
- [4] K.-m. Tian, J.-j. Li, and S.-w. Xu, "Rutaecarpine: a promising cardiovascular protective alkaloid from *Evodia rutaecarpa* (Wu Zhu Yu)," *Pharmacological Research*, vol. 141, pp. 541–550, 2019.
- [5] W.-Q. Li, X.-H. Li, J. Du et al., "Rutaecarpine attenuates hypoxia-induced right ventricular remodeling in rats," *Naunyn-Schmiedeberg's Archives of Pharmacology*, vol. 389, no. 7, pp. 757–767, 2016.
- [6] M.-H. Bao, W. Dai, Y.-J. Li, and C.-P. Hu, "Rutaecarpine prevents hypoxia-reoxygenation-induced myocardial cell apoptosis via inhibition of NADPH oxidases," *Canadian Journal of Physiology and Pharmacology*, vol. 89, no. 3, pp. 177–186, 2011.
- [7] S. y. Zeng, L. Yang, H. q. Lu, Q. j. Yan, L. Gao, and X. p. Qin, "Rutaecarpine prevents hypertensive cardiac hypertrophy involving the inhibition of Nox4-ROS-ADAM17 pathway," *Journal of Cellular and Molecular Medicine*, vol. 23, no. 6, pp. 4196–4207, 2019.
- [8] J.-Z. Li, J. Peng, L. Xiao et al., "Reversal of isoprenaline-induced cardiac remodeling by rutaecarpine via stimulation of calcitonin gene-related peptide production," *Canadian Journal of Physiology and Pharmacology*, vol. 88, no. 10, pp. 949–959, 2010.
- [9] Y. Xiao, J. Ye, Y. Zhou et al., "Baicalin inhibits pressure overload-induced cardiac fibrosis through regulating AMPK/TGF- β /Smads signaling pathway," *Archives of Biochemistry and Biophysics*, vol. 640, pp. 37–46, 2018.
- [10] J. Huang, D. Wang, J. Zheng, X. Huang, and H. Jin, "Hydrogen sulfide attenuates cardiac hypertrophy and fibrosis induced by abdominal aortic coarctation in rats," *Molecular Medicine Reports*, vol. 5, no. 4, pp. 923–928, 2012.
- [11] W.-j. Dai, Q. Dong, M.-s. Chen et al., "Alterations in cardiac structure and function in a modified rat model of myocardial hypertrophy," *Journal of Huazhong University of Science and Technology [Medical Sciences]*, vol. 34, no. 5, pp. 626–633, 2014.
- [12] W. Liu, J. Deng, W. Ding et al., "Decreased KCNE2 expression participates in the development of cardiac hypertrophy by regulation of calcineurin-NFAT (nuclear factor of activated T cells) and mitogen-activated protein kinase pathways," *Circulation Heart Failure*, vol. 10, 2017.
- [13] M. Nakamura and J. Sadoshima, "Mechanisms of physiological and pathological cardiac hypertrophy," *Nature Reviews Cardiology*, vol. 15, no. 7, pp. 387–407, 2018.
- [14] Y. Wu, F. Si, L. Luo et al., "The effect of melatonin on cardiac fibrosis in juvenile rats with pressure overload and deregulation of HDACs," *The Korean Journal of Physiology & Pharmacology*, vol. 22, no. 6, pp. 607–616, 2018.
- [15] Y. K. Tham, B. C. Bernardo, J. Y. Y. Ooi, K. L. Weeks, and J. R. McMullen, "Pathophysiology of cardiac hypertrophy and heart failure: signaling pathways and novel therapeutic targets," *Archives of Toxicology*, vol. 89, no. 9, pp. 1401–1438, 2015.
- [16] Y.-j. Li, F. Zhang, Q.-h. Gong, Q. Wu, L.-m. Yu, and A.-s. Sun, "Rutaecarpine inhibits angiotensin II-induced proliferation in rat vascular smooth muscle cells," *Chinese Journal of Integrative Medicine*, vol. 20, no. 9, pp. 682–687, 2014.
- [17] Z. Zhou, C.-P. Hu, C.-J. Wang, T.-T. Li, J. Peng, and Y.-J. Li, "Calcitonin gene-related peptide inhibits angiotensin II-induced endothelial progenitor cells senescence through up-regulation of klotho expression," *Atherosclerosis*, vol. 213, no. 1, pp. 92–101, 2010.
- [18] H. Jiang, C. Zhang, and W. He, "The effects of dracocephalum heterophyllum benth flavonoid on hypertrophic cardiomyocytes induced by angiotensin II in rats," *Medical Science Monitor*, vol. 24, pp. 6322–6330, 2018.
- [19] Q. L. Yan, W. Hua, and L. Z. Yu, "The functional changes in L-type Ca²⁺ channel of hypertrophied cardiomyocytes in neonatal rats induced by angiotensin II," *Zhongguo Ying Yong Sheng Li Xue Za Zhi*, vol. 29, no. 1, pp. 91–95, 2013.
- [20] C. Sunggip, K. Shimoda, S. Oda et al., "TRPC5-eNOS Axis negatively regulates ATP-induced cardiomyocyte hypertrophy," *Frontiers in Pharmacology*, vol. 9, p. 523, 2018.

Review Article

Purification, Detoxification, and Incineration Methods of Minerals and Metals in Traditional Medicine Formulations of Sri Lanka

Horadugoda Gamage Sujatha Pushpakanthi Hewageegana ¹,
Ayuma Uththami Hewageegana ², and Liyanage Dona Ashanthi Menuka Arawwawala ³

¹Department of Kayachikitsa, Institute of Indigenous Medicine, University of Colombo, Colombo, Sri Lanka

²Faculty of Science, University of Colombo, Colombo, Sri Lanka

³Industrial Technology Institute, Bauddhaloka Mawatha, Colombo 07, Sri Lanka

Correspondence should be addressed to Liyanage Dona Ashanthi Menuka Arawwawala; menuka@iti.lk

Received 9 October 2020; Revised 10 December 2020; Accepted 30 December 2020; Published 15 January 2021

Academic Editor: Lixin Wei

Copyright © 2021 Horadugoda Gamage Sujatha Pushpakanthi Hewageegana et al. This is an open access article distributed under the Creative Commons Attribution License, which permits unrestricted use, distribution, and reproduction in any medium, provided the original work is properly cited.

Background. Herbo-mineral therapies are very popular in traditional medical systems and formulations consisting of specific minerals or metals or mixture of both and mixed with organic components derived from plants. Purification/detoxification or incineration procedures play an important role to detoxify these and metals and minerals. **Objective.** In the present review, an attempt was made to gather herbo-mineral formulations which are used commonly in traditional medicinal systems in Sri Lanka and recapitulate the purification/detoxification or incineration techniques. **Method.** Commonly used herbo-mineral formulations are collected from a text book of Vatikaaprakarana. However, the purification/detoxification and incineration techniques for all minerals/metals are not mentioned in Vatikaaprakarana, and these techniques were collected from journal articles published between 1st January 2000 and 1st June 2020 through searching PubMed (US National Library of Medicine, USA), Science Direct (RELX Group, Netherlands), and Semantic Scholar (Allen Institute for Artificial Intelligence, USA). **Results.** Ten herbo-mineral formulations were selected, and purification/detoxification or incineration techniques were described in brief for copper sulphate, aluminum sulfate, borex powder, sulphur, sodium chloride, cinnabar, arsenicals, realgar, orpiment, ammonium chloride, magnesium silicate, zinc, and mercury. **Conclusion.** The review has demonstrated different types of purification/detoxification or incineration techniques of minerals used in herbo-mineral preparations. In addition, there is an urgent need for comprehensive survey or evaluation to check whether purification/detoxification or incineration techniques of metals/minerals are practiced properly in the country.

1. Introduction

Sri Lanka has its own indigenous scheme of healing systems including Ayurveda, Siddha, Unani, and traditional medicine. Sri Lankan traditional medical system is based on a series of prescriptions handed from generation to generation over 3000 years [1]. Herbo-mineral therapies are very popular in traditional medical systems of Sri Lanka specially for diseases which are related to neuromuscular disorders, malnutrition, different types of fever, and worm and digestive tract disorders, and herbo-mineral formulations

consist of specific minerals (e.g., mica, realgar (As₂S₂), orpiment (As₂S₃), chalk (CaCO₃), salts (NaCl or KCl), magnetite (Fe₃O₄), pyrite (FeS₂), etc.) [2] or metals (e.g., gold, copper, iron, zinc, mercury, etc.) [3] or mixture of both. In addition, some herbo-mineral formulations consist of plant/s along with minerals or metals or both. Herbo-mineral formulations are used in Rasayana therapy for several external and internal diseases [4]. It is claimed that herbo-minerals can become very less or nontoxic due to the purification and detoxification techniques during the drug preparation procedures. Many metals such as zinc [5, 6], copper [7, 8], and

iron [9, 10] exhibit many therapeutic benefits in humans. However, excess amounts of these metals may exhibit toxic effects. Therefore, metals/minerals present in herbo-mineral formulations should be subjected to purification/detoxification and/or incineration procedures.

Most of raw materials (metals/minerals) are collected from earth and there is a chance for mixing of impurities, toxins, and heterogeneous and unwanted substances to a large extent. Hence, these are subjected to various methods of purification and detoxification techniques (Shodhana) and incineration (*Marana*) to make them competent for medicinal use. Both purification/detoxification and incineration techniques are indicated to induce certain qualities, which are essential for making sure of the safe and easy assimilation of the material in the living body.

Most of the herbo-mineral recipes mentioned in traditional medicine in Sri Lanka are in the form of paste (kalka) or in pills (guli). Buddharaja kalka and Desadun kalka are used in the form of paste. Seetarama guliya, Koladavunde, Suranvidura guliya, Diyatarama guliya, and Krimiraja guliya are the common form of pills. These pastes or pills contain the minerals such as thurisi (copper sulphate), savindalunu (rock salt), sinakkaram (aluminium sulphate), pushkara (borax sodium biborate), nellikka gendagam (sulphur sublimatum), sivanguru (kaoliumbolerubja (china clay)), sadilingam (hydragyrisulphidum), haritala (trisulfide of arsenic), manosila (arsenigralar), galmada (rock alum), galnahara (asbestos), black salt (suwasa lunu), swarna makshika (ferri sulphuratum), and shilajathu (asphaltum/asphalt mineral). In this review, an attempt was made to gather the herbo-mineral formulations which are used commonly in traditional medicinal systems in Sri Lanka and display the purification/detoxification and incineration techniques.

2. Materials and Methods

In Sri Lanka, traditional herbo-mineral formulations are documented in the textbook known as Vatikaaprakarana [11]. In the present survey, some of the herbo-mineral preparations described in Vatikaaprakarana are costly and the processes of purification/detoxification and incineration techniques need much effort. Total numbers of 143 formulations (both herbal and herbo-mineral) are found in Vatikaaprakarana. In addition, all the purification/detoxification and incineration techniques for herbo-minerals are not mentioned in Vatikaaprakarana. Therefore, commonly used purification/detoxification and incineration techniques are followed whenever required. In the present survey, purification/detoxification and incineration techniques were collected from journal articles published between 1st January 2000 and 1st June 2020 through searching PubMed (US National Library of Medicine, USA), Science Direct (RELX Group, Netherlands), and Sementic Scholar (Allen Institute for Artificial Intelligence, USA). The keywords are “herbo-minerals and toxicity” and “herbo-minerals and purification and incineration”. From a total number of 165 results, 40 were excluded due to duplication or being irrelevant for the title. The frequently used traditional herbo-mineral formulations used in Sri Lanka are given in Table 1.

3. Purification/Detoxification and Incineration Techniques

Purification/detoxification and incineration of minerals and metals are very essential to avoid unwanted hazards caused by herbo-minerals.

3.1. Copper Sulphate-Palmanikkam

3.1.1. Method 1. Seven hundred and fifty grams of crude copper sulphate is dissolved in water, filtered through a cloth and dried in shade to remove external impurities. Dried copper sulphate is put into a mortar and 350 ml of *Citrus acida* Roxb juice is poured to make it sufficiently wet. Then, content is triturated manually using the paste under constant pressure for 6 h. The paste is allowed to dry and then preserved. Approximately 1% weight loss can be observed after purification of copper sulphate [12].

3.1.2. Method 2. Copper sulphate is converted into a powder form using “*khalva yantra*” (it is an instrument that can made up of good quality of stone useful for trituration and levigation). After that, copper sulphate powder is collected on a three-layered cloth and closed firmly by a tight knot. Subsequently, cow urine is collected and filtered to a steel vessel through a filter paper. Then, 8 L of cow urine is added to a special vessel called “*dolayantra*” and copper sulphate which is tightened with cloth which is dipped in three fingers above from the bottom of vessel. Then, “*dolayantra*” is kept on a stove and exposed to mild heat and the cow urine is left to boil for 9 hours. When the level of cow urine is decreased, extra 500 ml cow urine is added again to it. After completion, leave it to cool and allow it to settle down for re-crystallization for 24 hours under room temperature. The crystals of copper sulphate are formed at bottom of the “*dolayantra*” and supernatant liquid is removed. Copper sulphate crystals are collected and allowed to dry in shade [13].

3.2. Aluminum Sulfate/ $X Al(SO_4)_2 \cdot 12H_2O$ -Alum (Phitkari).

Formulation is $X Al(SO_4)_2 \cdot 12H_2O$, where X is a monovalent cation such as potassium or ammonium. Alum or phitkari is a transparent salt-like substance that is used in cooking as well as for medicinal purposes. In Ayurveda, alum (phitkari) is used in the form of Bhasma (Pure Ash) called Sphatika Bhasma.

Method: impure alum is dissolved in water and the insoluble impurities are removed through filtration. Then, the solution is concentrated and kept in a container with cooled water [14, 15].

3.3. Borax Powder (Sodium Borate)-Puskara/Tankana.

Puskara or tankana kshra ($[Na_2B_4O_5(OH)_4] \cdot 8H_2O$) is composed of boric acid and soda. Chemical name of borax is

TABLE 1: Traditional herbo-mineral formulations in Sri Lanka.

| Traditional preparation | Minerals/chemicals in nomenclature | Medicinal plants in number |
|-------------------------|--|--|
| 1 Buddharaja kalka | Cinnabar (Hydragryi sulphidum HgS)-sadilingam, Trisulfide of arsenic (As ₂ S ₃)-haritala (orpiment) Rock alum-galmada Asbestos-galnahara Copper sulphate-palmanikkam Arsenic sulfide- α -As ₂ S ₂ manosila Sodium chloride/rock salt-saindhava lavana | 16 |
| 2 Desandun kalka | Sodium chloride/rock salt-saindhava lavana | 7 |
| 3 Diyatarama | Copper sulphate-palmanikkam Aluminum sulfate [Al ₂ (SO ₄) ₃]-sinakkaram Borax powder (sodium borate)-puskara/tankana Ammonium chloride-navasaran Zinc oxide-ridiththam | 31 + ghee, bees' honey, neem oil (oil of <i>Azadirachta indica</i>) |
| 4 Koladavundaya | Borax powder (sodium borate)-puskara/tankana Copper sulphate-palmanikkam Sodium chloride/rock salt-saindhava lavana arsenic sulfide (α -As ₂ S ₂)-Manashila Aluminum sulfate-sinakkaram | 33 |
| 5 Mandam guliya | Sodium chloride/rock salt-saindhava lavana Aluminum sulfate [Al ₂ (SO ₄) ₃]-sinakkaram Borax powder (sodium borate)-puskara/tankana | 22 |
| 6 Mattupaha | Arsenic sulfide (α -As ₂ S ₂)-manashila Trisulfide of arsenic (As ₂ S ₃)-haritala (orpiment) Copper sulphate-palmanikkam Borax powder (sodium baborate)-puskara/tankana Aluminum sulfate [Al ₂ (SO ₄) ₃]-sinakkaram Rock alum-galmada Asbestos-galnahara Ammonium chloride-navasaran | 28 |
| 7 Ratnadi guliya | Arsenic trioxide, vitrious arsenic, arsenolite (As ₂ O ₃) (white arsenic)-gouripashana Cinnabar (hydragryi sulphidum HgS)-sadilingam | 7 |
| 8 Sanni gajankushaya | Murcury-rasadiya Borax powder (sodium baborate)-puskara/tankana Sodium chloride/rock salt-saindhava lavana Arsenic trioxide vitrious arsenic, arsenolite (As ₂ O ₃) (white arsenic)-gouripashana | 7 |
| 9 Seetarama guliya | Arsenic sulfide- α -As ₂ S ₂ -manosila Sodium chloride/rock salt-saindhava lavana Copper sulphate-palmanikkam Aluminum sulfate-sinakkaram Borax powder (sodium baborate)-puskara/tankana Rock alum-galmada Trisulfide of arsenic (As ₂ S ₃)-haritala (orpiment) Cinnabar (hydragryi sulphidum HgS)-sadilingam | 29 |
| 10 Suranvidura | Borax powder (sodium baborate)-puskara/tankana Aluminum sulfate-sinakkaram Copper sulphate-palmanikkam Sulpher sublimatum-gendagam Trisulfide of arsenic (As ₂ S ₃)-haritala (orpiment) Sodium chloride/rock salt-saindhava lavana China clay-siwanguru | 23 |

sodium tetraborate decahydrate. Scientific investigations have proven the antimicrobial [16] and anti-inflammatory activities [17] and wound healing [18] properties of borax powder.

3.3.1. *Method 1.* Borax powder is put into a clean and dry "khalva yantra" and crushed well to prepare powder. This powder is added to a clean earthen pot and heated under moderate heat to maximum heat until all the water content is

completely evaporated to obtain borax powder. This procedure should be repeated thrice to obtain pure borax and approximately 50% weight loss can be observed [19, 20].

3.3.2. *Method 2.* Raw borax is powdered, then put to a hot iron pot, and stirred till it intumescs. Finally, borax is taken out and ground to become fine powder [21].

3.3.3. *Method 3.* Borax is dissolved in water, strained through a cloth, and evaporated to dryness [22].

3.4. *Sulphur-Sulphur Sublimatum/Gandhaka.* Sulphur sublimatum or gandhaka is one of the members of Upa Rasa (one of the two groups of alchemical mineral agents, according to the Rasashashtra) by Rasa Vagbhata found and described in the Bible as brimstone [23]. The sulphur is extensively used in herbo-mineral preparations especially in various mercurial operations. There are several methods, which have been mentioned in different texts, for the Shodhana of gandhaka. It can purify blood, support for healthy digestion, and prevent build-up of toxic substances [24]. Gandhaka contains two kinds of impurities: (a) stone powder or clay (b) As, Pb, or both [25]. Therefore, it is important to remove physical and chemical impurities in sulphur.

3.4.1. *Method 1.* The commonest method consists of heating of sulphur with cows' ghee into its melting stage and filtering into a vessel containing cow milk through a cloth. Finally, it is washed with hot water and the whole procedure should be repeated three to seven times using fresh ghee and fresh cow milk. In the present process, chemical impurities bind with ghee and physical impurities are removed while filtering through the cloth [26, 27].

3.4.2. *Method 2.* Crude sulphur (100 g) is powdered and placed on an iron/steel spoon containing 25 ml of cow's ghee and subjected to mild heat while stirring the content using a glass rod. After all the solid particles are melted, the content is filtered through a cloth into a vessel containing freshly prepared *Eclipta prostrata* L. (Bhringaraja) juice. Sulphur becomes solidified with presence of *Eclipta prostrata* juice. Then, collected sulphur is washed with hot water to remove the traces of ghee and juice. This purification procedure should be repeated at least six times using the fresh juice of *Eclipta prostrata* [28].

3.4.3. *Method 3.* Cow milk (2 L) and ghee (150 ml) are added to an earthen vessel with wide mouth and covered by a cloth and tied with an iron wire. Approximately 500 g of coarse powder of gandhaka is applied on the inner surface of the cloth which covers the lower earthen vessel containing cow milk and ghee. Then, the lower pot is covered with another earthen vessel by placing in up-down position. The edges of both earthen vessels are sealed with a cloth applied with Fuller's earth and allowed to dry and kept inside a pit (1.5 feet from the upper surface of the earth) in a way that the

brim of the vessel should be at ground level. Then, cow dung cakes are kept on the brim of the vessel and fire is set and the sulphur is allowed to flow down into the vessel containing cow milk and ghee. Once it is cooled, whole vessel is taken out from the pit and opened. The purified sulphur is collected and washed with hot water to remove the traces of ghee and shade dried [29].

3.4.4. *Method 4.* The sulphur purification steps for heating, melting, and filtering are the same as method 2 [28]. In brief, *Millettia pinnata* L. oil (Karanja oil, 25 ml) and *Ricinus communis* oil (Erand oil, 25 ml) are mixed together and used instead of ghee. In addition, goat milk and *Datura metelis* L. (Dhattura patra) juice are used instead of *Eclipta prostrata* juice. Sulphur is filtered through the cloth into a vessel containing goat milk and *Datura metelis* juice thrice, respectively. Finally, sulphur is washed and dried [28].

3.5. *Sahindava Lavana-Sodium Chloride/Rock Salt/Bay Salt.* There are five types of lavana commonly used in treatments. Among the lavana, saindhava lavana is the best and considered as sodium chloride/rock salt/bay salt chemically. Rock salt is the purest form of salt, which is free from environmental pollutants and chemical components and does not require a refining process [30]. Rock salt is used to cure several disorders and ailments including rheumatic pains, herpes, inflammation, common cold, and cough [31].

3.6. *Cinnabar (Hydrargyri-HgS).* Sadilingam or hingula is an important drug in Ayurveda which is used as single remedy or as an ingredient in various herbo-mineral preparations. By most of the Ayurveda Rasa Shastra classics, it is grouped under Sadharana Rasa Varga. Hingula is the prime source of mercury. Chemically, it consists of mercury (86%) and sulphur (13.5%), with molecular formula HgS, called red mercury sulphide. Purified mercury is used in the treatment of eye diseases, disorders in liver and pancreas, rheumatoid arthritis, fever, and skin disorders [32].

3.6.1. *Method 1.* A paste of cinnabar is prepared by triturating with *Zingiber officinale* Roscoe. (Aardraka Swarasa) or *Citrus limon* L. (Nimbu Swarasa) or *Allium sativa* L. (Lakucha Swarasa) and applying on the inner surface of the upper pot. The lower pot filled with sufficient amount of water is buried in the earth with neck above. Then, the pot that cinnabar paste is applied to is placed in an up-down position and the edges of both earthen vessels are sealed. Then, cow dung cakes are kept on the top of the upper vessel and fire is set and allowed to heat for three hours. The purified mercury from base of upper pot gradually collected trickles down and gets collected at the base of the lower pot. After 24 h, the lower pot is taken out with mercury [32].

3.6.2. *Method 2.* Unpurified hingula is smashed into powder in mortar triturated with ginger juice (*Zingiber officinale*) seven times using a pestle. After seven times trituration,

hingula turns into a crystallized powder form bearing an acidic pH. Then, crystallized powder is washed with hot water until acidity is completely removed and dried in sun light [33].

3.6.3. *Method 3.* Hingula is soaked in *Citrus limon* juice until the colour of the powder becomes dark red, then it is washed with water at least seven times [34].

3.7. *Arsenicals.* α -As₂S₂ is structurally identical to realgar (*Manashila*) among the three distinct As₄S₄ polymorphs [35] and identified as a promising drug for cancer treatments [36, 37]. Realgar has been used as an ingredient in Chinese Traditional Medicine for many centuries and some of the Realgar contained in *Hong Ling San*, *Sha Yao*, *Qi Zhen Wan*, etc. [38]. Other two polymorphs are orpiment (haritala) and white arsenic (gouripasana) with chemical structures of As₂S₃ and As₂O₃, respectively [39]. Some of the therapeutic uses of three As₄S₄ polymorphs are listed in Table 2.

Arsenic is listed as the most hazardous element by Agency for Toxic Substances and Diseases Registry (ATSDR) among the top 20 hazardous substances [41]. Therefore, purification is essential.

3.7.1. *Realgar (Manashila, Arsenic Disulphide- α -As₂S₂).* Realgar is used only in purified and detoxified condition for the therapeutic purposes as internal as well as external medicine. The most of the formulation of Manahshila is used for external application, whereas fine powders of these processed minerals are used for both external and internal applications. Purification of realgar is generally carried out by trituration with *Sesbania grandiflora* L. (*Agastya*), *Zingiber officinale* (*Ardraka*) (*Rosc.*), *Citrus medica* (*Bijaura Nimbu*), *Sesbania sesban* L. (*Jayanti*), and *Eclipta alba* L. (*Bhringaraja*) juice [42].

(1) *Method 1.* Realgar is placed in a mortar and mixed with the *Zingiber officinalis* juice and triturated with a pestle manually until the material in the mortar dries. This is repeated seven times with fresh *Zingiber officinalis* juice. Finally, purified realgar is shade-dried and powdered [43].

(2) *Method 2.* Realgar is triturated to 120 mesh size for particle size reduction. Detoxification of realgar (400 g) is done by boiling it in *Eclipta alba* juice, *Sesbania grandiflora* juice, *Sesbania sesban* juice, and *Zingiber officinale* juice sequentially, each for 12 hours in *Dolayantra*. Detoxified realgar is then washed with *Kanjika* (sour liquid prepared with of rice grain, etc.) and kept in airtight container after drying [44].

3.7.2. *Orpiment (Haratala-As₂S₃)*

(1) *Method 1.* Orpiment is steamed (*Swedana*) followed by submerging the drug in liquid media for a whole night and during day time it is to be dried under sun light (*Bhavana*) or both [45]. The liquids like *Tilaksarajala*, *Salmali mula*

Kwatha, lime juice, and *Balamula Kwatha* are also used by one or two *Acharyas* for the purification of orpiment either for *Swedana* or *Bhavana*. *Swedana-Haritala churna* should be kept in a *pottali* and this *pottali* should be placed in *dolayantra* containing various types of liquids. The *dolayantra* should be subjected to fire for given time [46].

(2) *Method 2.* Haratala is powdered and subjected to *Bhavana* for twenty-one days with the juice of *Ficus religiosa* L. (*Asvattha*). Using a clean mortar, haratala is made into a ball and kept in a vessel where one half is filled with ashes. The vessel is closed with a basin and subjected to incineration for 12 h [47].

3.7.3. *White Arsenic (Gouripasana-As₂O₃).* It is a crystalline or amorphous substance. When heating with intense heat, it evaporates and gives garlic odour [48].

(1) *Method 1.* White Arsenic is kept inside a large fruit of *Momordica charantia* L. (*Bitter gourd*), then tied well, and subjected to steam *Dolayantra* (hanged in a big pot which is filled with water) for three hours. This process purifies the white arsenic [49].

(2) *Method 2.* White arsenic is kept inside a large fruit of *Momordica charantia* and tied well and subjected to steam in *Dolayantra* (hanged in a big pot which is filled with borex water or cow milk) for 24 hours [50].

Steaming of bitter gourd (filled with *Gouripashana*) is done in borex water (*tankana jala*) or cow's milk (*godugdha*) with the help of *dolayantra*, for one day. Cow's milk or borex water purifies the *gouripashana* [51].

(3) *Method 3.* Take purified (*Shuddha*) *gouripashana* in a mud pot. Put 15 g of Goat's milk and cover by a cloth. Place this in a pit and cover it by using mud by the width of middle phalanges of middle finger. Then, ignite using dried cowdung as the fuel. This procedure is repeated 21 times. For each burning, add 56 ml goat's milk and finally get purified yellow red *gouripasana* [52, 53].

3.8. *Sal-Ammoniac/Ammonium Chloride-NH₄Cl-Navasagara.* It is a crystalline, inorganic salt, white in colour and highly soluble in water [54].

3.8.1. *Method 1.* Water (three parts) is added to *navasara* (one part), stirred well, and filtered into a vessel using a cloth. Then, the vessel is heated until the solution is dried [55].

3.8.2. *Method 2.* Water is added to *navasara*, stirred well, and filtered to a pan and subjected to dry conditions in sun light [56].

3.9. *Magnesium Silicate (Asbestos)-Gal Nahara*

3.9.1. *Method.* Boil magnesium silicate using Buffalo urine for three hours. Then, wash it and dry properly [14].

TABLE 2: Medicinal uses of arsenicals.

| Name of the arsenicals | Medicinal uses | References |
|------------------------|--|------------|
| Realgar | Skin diseases, diarrhea, high fever, coma, heart stroke, abdominal pain, ulcers in tongue and mouth, sore throat, toothache | [38, 39] |
| Orpiment | Skin diseases, it increases appetite and cures leprosy | [39] |
| White arsenic | Hemicrania, headache, sinusitis, syphilis, elephantiasis, anemia, psoriasis, asthma, osteoarthritis, splenomegaly, impotency, cancer | [39, 40] |

3.10. *Rock Alum-Gal Mada*. No purification method is mentioned in texts though these ingredients are commonly mentioned in traditional recipes. Further, according to Ayurveda Pharmacopoeia in Sri Lanka [57], the materials gal mada and gal nahara can be used for medicinal preparations after removing the dirty particles.

3.11. *Zinc Oxide-Ridi Thuththam*. Zinc is a trace element and plays a vital role in all physiological processes in human. It has been introduced as a drug in the prevention and treatments of diseases for the last two decades. The Ayurvedic physicians have practiced both oral and topical applications of zinc after purification and calcification before 14th century A.D.

Rasaka or Kharpara (zinc ore or zinc carbonate), Yasada (zinc metal), Puspanjana (zinc oxide), and Pittala (brass) are zinc-containing minerals used as therapeutic agents in Ayurveda [58].

3.11.1. *Method 1*. Raw *Yashada* pieces are heated in an iron ladle till they melt completely and then poured into a mixture of sour gruel, butter milk, decoction of *Dolichus biflorus*, cow's urine, and oil of *Sesamum indicum*. This is repeated 3 times in each liquid medium, in the same order [59].

3.11.2. *Method 2*. Five hundred grams of zinc granules is kept in iron utensil and placed on a gas burner. Zinc granules are heated till they melt. The molten mass is poured in a container containing milk (200 ml). This exercise is repeated 21 times [60].

3.12. *Mercury-Parada*. Mercury (Parada) has many synonyms. Mercury is the best among all medicines which is effective in low dose and fast acting in the eradication of disease without causing anorexia or other side effects. Mercury in the form of one of its common ores, cinnabar, is used in various traditional medicines, especially in traditional Chinese and Indian medicine [57].

Mercury also undergoes extensive detoxification procedures before being used in medical formulations. Mercury obtained by all these procedures is an inorganic form of mercury (mainly sulphides). Studies have also validated this fact and showed that mercury used in Ayurveda is of inorganic form. Moreover, inorganic mercury does not cross the blood-brain barrier as well as placental barrier [58].

3.12.1. *Method 1*. Equal quantities of mercury (500 g) and Sudha churna (limestone-500 g) are taken into a mortar and triturated for 36 hours (3 hours for 12 days). Mercury is collected from limestone filtered through a cloth. The remaining mercury is obtained by washing it with warm water. The wet powder of limestone is allowed to dry. After drying of these carefully, mercury is collected from these trays. Then, equal quantity of Lashuna Kalka 439 g (paste of garlic) is added to the obtained mercury and half the quantity of saindhava lavana (219.5 g) is added and triturated for 8 hours. Washing of garlic paste is done with lukewarm water. The salt present in it dissolves in water leaving behind the garlic paste from which again mercury can be collected. Once again, drying of the remaining garlic paste into trays is done for 6 days and then triturated into fine powder and filtered through cloth to obtain the remaining mercury from the garlic paste to avoid the loss of mercury. The collected mercury is known as purified mercury [59].

3.12.2. *Method 2*. Mercury is taken with *Piper betel* L. (Nagavalli svarasa, 50 ml), *Zingiber officinalae* (Ardraka svarasa, 50 ml), and Trikshara (Yavakshara, Sarjika kshara and Tankana kshara, each of 50 g) in a clean *Khalva Yantra*. The above-said materials are rubbed in *Khalva Yantra* for eight hours per day for three days. The obtained material is washed and poured out with the help of lukewarm water several times until we get the pure mercury [57].

3.12.3. *Method 3*. Mercury is roasted in a covered crucible with asafetida (dried latex exuded from *Ficus oppositifolia* Roxb) [61].

3.12.4. *Method 4*. The seeds of *Achyranthes aspera* L and *Ricinus communis* L are pounded together and mercury is placed inside the powder. Then, the whole mass is subjected for incineration [61].

3.13. *Safety Studies on Herbo-Minerals*. Literature on evaluation of toxicity levels of metals/minerals in herbo-mineral preparations after purification/detoxification or incineration is limited. Some experiments were carried out to determine the overall toxicity of herbo-minerals using animal experiments in terms of hepatotoxicity, hemototoxicity, renal toxicity, etc. However, purification/detoxification or incineration techniques of herbo-minerals were not properly documented in those studies. Thus, one example is cited here

in order to get an idea about toxicity of herbo-minerals. Doddamani and co-workers [62] found that Tribhuvan Keerthi rasa (contains cinnabar), Swasakutara rasa (contains mercury and sulphur), Smritisagara rasa (contains orpiment), Sutashekara rasa (contains mercury), Lashunadi vati (contains sulphur), and Agnitundi vati and Arogya vardini vati (contain both mercury and sulphur) did not affect kidney functions in terms of urea and creatinine levels. More than one purification/detoxification or incineration technique are available for metals/minerals. Therefore, without knowing the purification/detoxification or incineration technique, there is a difficulty to interpret the suitability of the techniques towards safety studies of herbo-minerals.

4. Conclusion

In the present study, an attempt was done to collect the commonly used traditional herbo-mineral formulations and their purification/detoxification or incineration techniques. The review illustrated different types of purification/detoxification or incineration techniques of minerals used in herbo-mineral preparations. In addition, there is an urgent need for comprehensive survey or evaluation to check whether purification/detoxification or incineration techniques of minerals are practiced properly in the country.

Data Availability

Data are available on request to the corresponding author.

Conflicts of Interest

The authors declare that they have no conflicts of interest.










References

- [1] G. V. P. Samaranyake and A. A. J. Pushpakumara, "A literary review on traditional medical systems of cancer in Sri Lanka," in *Proceedings of the Conference on National Research Symposium at Gampaha Wickramarachchi Ayurveda Institute*, Yakkala, Sri Lanka, December 2016.
- [2] L. C. Mishra, *Scientific Basis for Ayurvedic Therapies*, CRS Press, Boca Raton, FL, USA, 2004.
- [3] S. Paul and A. Chugh, "Assessing the role of ayurvedic 'bhasms' as ethno-medicine in the metal based nanomedicine patent regime," *Journal of Intellectual Property*, vol. 16, no. 6, pp. 509–515, 2011.
- [4] A. Chaudhary and N. Singh, "Herbo mineral formulations (rasaoushadhies) of ayurveda an amazing inheritance of ayurvedic pharmaceuticals," *Ancient Science of Life*, vol. 30, no. 1, pp. 18–26, 2010.
- [5] D. Bhowmik, K. P. Chiranjib, and K. P. S. Kumar, "A potential medicinal importance of zinc in human health and chronic disease," *International Journal of Pharmaceutical and Biomedical Sciences*, vol. 1, no. 1, pp. 5–11, 2010.
- [6] N. Roohani, R. Hurrell, R. Kelishadi, and R. Schulin, "Zinc and its importance for human health: an integrative review," *Journal of Research in Medical Sciences*, vol. 18, no. 2, pp. 144–157, 2013.
- [7] M. Bost, S. Houdart, M. Oberli, E. Kalonji, J.-F. Huneau, and I. Margaritis, "Dietary copper and human health: current evidence and unresolved issues," *Journal of Trace Elements in Medicine and Biology*, vol. 35, pp. 107–115, 2016.
- [8] A. Hefnawy and H. Khaiat, "The importance of copper and the effects of its deficiency and toxicity in animal health," *International Journal of Livestock Research*, vol. 5, no. 12, pp. 1–20, 2015.
- [9] N. Abbaspour, R. Hurrell, and R. Kelishadi, "Review on iron and its importance for human health," *Journal of Research in Medical Sciences*, vol. 19, pp. 164–174, 2014.
- [10] B. Lönnerdal, "Excess iron intake as a factor in growth, infections, and development of infants and young children," *The American Journal of Clinical Nutrition*, vol. 106, no. Supplement 6, pp. 1681S–1687S, 2017.
- [11] EASA, *Illapperuma*, Vatikaaprakaranaya, Colombo, Sri Lanka, 2nd edition, 1903.
- [12] S. Sharma, *Rasatarangini*, pp. 542–543, Motilal Banarasidas, Varanasi, Uttar Pradesh, India, 1979.
- [13] K. Shastri, *Rasatarangini*, p. 534, Motilal Banarasi Das Publication, Varanasi, Uttar Pradesh, India, 2009.
- [14] Anonymous, *Ayurveda Aushadha Samgraha, Volume 1, Part 2*, State Printing Cooperation, Padukka, Sri Lanka, 1979.
- [15] K. Vignesh, S. J. Niresh, K. Saravanasingh, and A. P. Uma, "Padikaram (alum)-a unique drug and its utilization in Siddha medicine: a pharmacological review," *Siddha Papers*, vol. 14, no. 2, pp. 1–12, 2019.
- [16] T. R. Adhvaryu, K. S. Patel, V. K. Kori, S. Rajgopala, and R. Majusha, "In vitro antimicrobial activity of tankana," *European Journal of Biomedical and Pharmaceutical Sciences*, vol. 2, no. 7, pp. 210–213, 2015.
- [17] B. Srinivas, A. Kumar, G. S. Saran, A. Mouna, and C. N. Kumar, "In vitro anti-inflammatory activity of tankana churna," *Food and Feed Research*, vol. 40, no. 1, pp. 17–20, 2013.
- [18] R. Swati, "Development and study of wound healing activity of an ayurvedic formulation," *Asian Journal of Research in Pharmaceutical Science*, vol. 1, no. 1, pp. 26–28, 2011.
- [19] I. Sahoo, S. S. More, V. Jadhav, S. Dalai, and M. Sahoo, "Clinical Appraisal on therapeutic efficacy of tankana & Sphatika Bhasma with madhu pratisarana in tundikeri," *Journal of Drug Delivery and Therapeutics*, vol. 9, no. 6, pp. 130–134, 2019.
- [20] S. M. Shaikh, R. C. Doijad, A. S. Shete, and P. S. Sankpal, "A review on: physico-chemical evaluation of ayurvedic mineral drug tankan bhasma," *Pharma Tutor*, vol. 4, no. 4, pp. 23–27, 2016.
- [21] K. Nilesh, "Evaluation of prativisha properties (antidote properties) of tankana (borax) in vatsanabha vishaktata (aconite poisoning)," *International Ayurvedic Medical Journal*, vol. 3, no. 7, pp. 1991–1998, 2015.
- [22] R. Chopra, *Text Book of Chopra's Indigenous Drugs of Indiap*. 685, 2nd edition, Academic Publishers, Calcutta, India, 1994.
- [23] D. Panigrahi, "Sulphur (gandhaka) purification methods W. S. R. to rasa classics," *Journal of Biomedical and Pharmaceutical Research*, vol. 8, no. 6, pp. 92–98, 2019.
- [24] A. Singh, M. K. Yadav, and R. K. Mishra, "(Classical review of gandhaka (sulphure)-an ayurvedic perspective," *International Journal for Unani and Integrative Medicine*, vol. 3, no. 3, pp. 49–52, 2019.
- [25] B. Mukherjee, *Rasa Jala Nidhi*, Parimal Publications, vol. 2II, p. 99, 1st edition, New Delhi, India, 2001.
- [26] D. Panigrahi, "Pharmaceutico therapeutics of sulphur (Gandhaka): an ayurvedic review," *Journal of Biomedical and Pharmaceutical Research*, vol. 7, no. 2, pp. 54–60, 2018.

- [27] K. Pardeshi and V. Kadibagil, "Gandhaka shodhana (purification of sulphur)," *International Ayurvedic Medical Journal*, vol. 6, no. 9, pp. 1961–1966, 2018.
- [28] D. Joshi, "Concept of ayurvedic sodhana methods and its effects with reference to sulphur," *Ancient Science of Life*, vol. 1, no. 4, pp. 229–235, 1982.
- [29] B. Srinivasulu1, P. B. Dev, and P. H. C. Murthy, "Sodhana of gandhaka (Sulphur) with godugdha (cow s milk), gogrutha (cow s ghee): a chemical analysis," *Journal of Pharmaceutical and Scientific Innovation*, vol. 2, no. 1, pp. 70–72, 2013.
- [30] N. Khandelwal, S. Dhundi, P. Yadav, and P. K. Prajapati, "Lavana (salt): an ayurvedic outlook on saindhava (rock salt)," *Indian Journal of Ancient Medicine and Yoga*, vol. 5, no. 2, pp. 95–101, 2012.
- [31] Y. Kumar, "Uses of rock salt in diet with table salt: a wonderful combination for good health," *Journal of Biological and Chemical Research*, vol. 35, no. 1, pp. 75–79, 2018.
- [32] P. M. Asma, G. Krishna, and J. Shashidhar, "A conceptual review on hingula (Cinnabar-HgS)," *International Journal of Ayurveda and Pharma Research*, vol. 7, no. 6, pp. 32–39, 2019.
- [33] S. Sadanand, *Rasa Tarangini with Sanskrit Commentary Prasadini by Shri. Haridatta Shastri and Hundi Rasa Vigyan Commentary*, Motilal Banarsidas, Delhi, India, 11th edition, 202 pages, Motilal Banarsidas, Delhi, India, 1979.
- [34] P. Rai and S. J. Rajput, "Preparation and physicochemical characterization of ingredients of Indian traditional medicine, Mahamrutyunjaya Rasa," *Journal of Ayurveda and Integrative Medicine*, vol. 8, pp. 159–168, 2017.
- [35] Z. Bujnakova, P. Balaz, P. Makreski et al., "Arsenic sulfide nanoparticles prepared by milling: properties, five-volume characterization and anti-cancer effects," *Journal of Material Science*, vol. 50, pp. 1973–1985, 2015.
- [36] J. Z. Wu and P. C. Ho, "Evaluation of the in vitro activity and in vivo bioavailability of realgar nanoparticles prepared by cryogrinding," *European Journal of Pharmaceutical Sciences*, vol. 29, pp. 35–44, 2006.
- [37] Y. HQ, L. Gan, X. L. Yang, and H. B. Xu, "Membrane-associated cytotoxicity induced by realgar in promyelocytic leukemia HL-60 cells," *Journal of Ethnopharmacology*, vol. 103, pp. 366–371, 2006.
- [38] J. Wu, Y. Shao, J. Liu, G. Chen, and P. C. Ho, "The medicinal use of Realgar (As₂S₄) and its recent development as an anticancer agent," *Journal of Ethnopharmacology*, vol. 135, no. 3, pp. 595–602, 2011.
- [39] A. K. Panda and J. Hazra, "Arsenical compounds in Ayurveda medicine: a prospective analysis," *International Journal of Research in Ayurveda and Pharmacy*, vol. 3, no. 6, p. 772, 2012.
- [40] P. Bairwa, A. K. Bhatt, and S. Soni, "Comprehensive review of sankhiya," *World Journal of Pharmaceutical Research*, vol. 9, no. 12, pp. 492–497, 2020.
- [41] G. C. Cruz, Z. Din, C. D. Feri et al., "Analysis of toxic heavy metals (arsenic, lead, and mercury) in selected infant formula milk commercially available in the Philippines by AAS," *E-International Scientific Research Journal*, vol. 1, pp. 40–51, 2009.
- [42] V. Sharma, K. R. C. Reddy, and D. N. S. Gautam, "An ayurvedic review on therapeutic potentials of manahshila: a literature review," *Innovare Journal of Ayurveda Science*, vol. 4, no. 3, pp. 1–6, 2016.
- [43] N. Kodlady, M. S. Doddamani, and B. J. Patgiri, "Pharmaceutical-analytic study of the ayurvedic purification of Manahshila (realgar)," *Asian Journal of Traditional Medicines*, vol. 7, no. 4, pp. 143–150, 2012.
- [44] M. G. Sharma, *Ayurved Prakashp*. 314, 1st edition, Chaukhabha Bharati Academy, Varanasi, Uttar Pradesh, India, 1962.
- [45] B. R. Govindadasa, *Vidyothini Hindi Commentary*. 861, 16th edition, Chaukambha Sanskrit Samsthana, Varanasi, Uttar Pradesh, India, 2002.
- [46] I. Tripathi, *Rasa Ratna Samucchayap*. 77, 3rd edition, Chaukhabha Sanskrit Bhavan, Varanasi, Uttar Pradesh, India, 2006.
- [47] D. S. Mukhyopadhyaya, *Rasajalnidhi*, p. 163, Choukhamba Publishers, Varanasi, Uttar Pradesh, India, 1998.
- [48] V. A. Dole and P. Paranjpe, *A Text Book of Rasashastra*, p. 251, Chaukamba Sanskrit Pratishthan, Delhi, India, 2004.
- [49] A. D. Satpute, *Vagbhata's Rasaratna Samuchchaya*, p. 31, Chetan Prakash, Mysore, India, 2003.
- [50] Raghuvveer, "A comparative antimicrobial study of navasadara satva by taking two different samples of navasadara," Dissertation, Rajiv Gandhi University of Health Sciences, Bangalore, India, 2009.
- [51] Ministry of Health and Family Welfare, *Ayurvrdha Pharmacopoeia, Vol 1, Part 1p*. 72, 2nd edition, Ministry of Health and Family Welfare, Delhi, India, 1976.
- [52] Sarangadhara, *Sarangadhara Samhita with Adhamallas's Dipika & Kasirama's Gudhartha Dipika Commentary of Kasirama*, p. 398, Chaukambha Krishnadas Academy Publications, Varanasi, Uttar Pradesh, India, 2006.
- [53] S. Sharma, *Rasatarangini*, Motilal Banarasidas, Delhi, India, 11th edition, 2004.
- [54] A. Kadam, "Mercury in ayurveda: a poison turned nectar," *Rasamruta, World's Firste-Journal of Ayurveda*, pp. 1–7, 2013.
- [55] K. Pardeshi and V. Kadibagil, "Parada shodhana (purification of mercury) by classical method," *International Journal of Ayurveda and Pharmaceutical Chemistry*, vol. 9, no. 2, pp. 137–147, 2018.
- [56] S. Bandari, P. Bhadra Dev, and P. H. C. Murthy, "A concept of Sodhana (Purification) w.s.r. to parada (mercury)," *International Journal of Ayurvedic Medicine*, vol. 2, no. 3, 2011.
- [57] B. Prakash, *Use of Purified Mercury in Ayurveda and its Safety Evaluation*, pp. 1–12, VCP Cancer Research Foundation, Dehradun, Uttrakhand, India, 2019.
- [58] A. K. Panda and S. Rout, "Zinc in Ayurvedic herbo-mineral products," *Natural Product Radiance*, vol. 5, no. 4, pp. 284–288, 2006.
- [59] S. Sharma, *Rasatarangini*, K. Shastri, Ed., p. 362, 11th edition, Motilal Banarasidas Publications, Delhi, India, 2009.
- [60] D. Joseph, "Elemental detection of zinc in ayurvedic drug (jasad bhasma) by radioisotope induced energy dispersive x-ray fluorescence (EDXRF) technique," *Madridge Journal of Analytical Sciences and Instrumentation*, vol. 3, no. 1, pp. 73–76, 2018.
- [61] K. M. Nadkarni, *The Indian Materia Medica*, Doothpeshwar Prakashan Ltd, Bombay, India, 3rd edition, 2005.
- [62] S. H. Doddamani, M. N. Shubhashree, S. K. Giri, N. Kavya, and G. Venkateshwarlu, "The safety of ayurvedic herbomineral formulations on renal function: an observational study," *International Journal of Research in Ayurveda and Pharmacy*, vol. 6, no. 3, pp. 299–302, 2015.

Research Article

Ulmus parvifolia Jacq. Exhibits Antiobesity Properties and Potentially Induces Browning of White Adipose Tissue

Yuan Yee Lee ¹, Minki Kim ¹, Muhammad Irfan ¹, Heung Joo Yuk ²,
Dong-Seon Kim ², Seung Eun Lee,³ Seung-Hyung Kim ⁴, Suk Kim ⁵, Sung-Dae Kim ⁶,
and Man Hee Rhee ¹

¹Laboratory of Physiology and Cell Signaling, College of Veterinary Medicine, Kyungpook National University, Daegu 41566, Republic of Korea

²Herbal Medicine Research Division, Korea Institute of Oriental Medicine, Daejeon 34054, Republic of Korea

³Department of Herbal Crop Research, National Institute of Horticultural and Herbal Science, Chungbuk 27709, Republic of Korea

⁴Institute of Traditional Medicine and Bioscience, Daejeon University, Daejeon, Republic of Korea

⁵Department of Veterinary Medicine, College of Veterinary Medicine, Gyeongsang National University, Jinju 52828, Republic of Korea

⁶Research Center, Dongnam Institute of Radiological and Medical Sciences, Busan 46033, Republic of Korea

Correspondence should be addressed to Man Hee Rhee; rheemh@knu.ac.kr

Received 2 June 2020; Revised 30 October 2020; Accepted 18 November 2020; Published 23 December 2020

Academic Editor: Uma Maheswari Krishnan

Copyright © 2020 Yuan Yee Lee et al. This is an open access article distributed under the Creative Commons Attribution License, which permits unrestricted use, distribution, and reproduction in any medium, provided the original work is properly cited.

The bark of *Ulmus parvifolia* Jacq. (UP) was traditionally used as a diuretic and to treat intestinal inflammation. With modern evidence of the correlation of diuretics, gut inflammation, and obesity, our study has shown the antiobesity effects of the bark of UP. UP treatment reduced lipid production and adipogenic genes *in vitro*. *In vivo* studies revealed that UP 100 mg/kg and UP 300 mg/kg treatment significantly reduced mouse weight without reducing food intake, indicating increased energy expenditure. UP significantly reduced the weight of epididymal and subcutaneous adipose tissue and decreased liver weight. Histological analysis revealed improvement in the progression of nonalcoholic fatty liver disease and epididymal white adipose tissue hypertrophy induced by a HFD. Real-Time PCR of epididymal adipose tissue revealed significant increases of uncoupling protein-1 (UCP-1) and peroxisome proliferator-activated receptor gamma coactivator 1-alpha (PGC-1 α) expression after UP 300 mg/kg treatments. Phosphorylation of AMP-activated protein α (AMPK α) was increased, while phosphorylation of Acetyl-CoA Carboxylase (ACC) was reduced. Our findings reveal the ability of UP to reduce the occurrence of obesity through increased browning of white adipose tissue via increased AMPK α , PPAR γ , PGC-1 α , and UCP-1 expression.

1. Introduction

The *Ulmus* genus are elm trees found in North America [1], the Himalayas, and East Asia [2]. *Ulmus parvifolia* Jacq. (UP) which is native to Japan, Korea, and China has been reported for its antioxidant and anti-inflammatory activities [3]. The leaves of UP were traditionally used as an external dressing on wounds and ulcerous tissue [4] and as a lithontripic agent [5]. According to the Chinese Supplement to Materia Medica (Bencao Gangmu Shiyi), the bark of UP is nontoxic

and was used to treat strangury, burns, and intestinal inflammation [6]. Its bark was also used for its demulcent and lithontripic properties other than treating cough and fever. It was also used as a diuretic [7]. Insulin resistance was said to be related to hypertension as the release of free fatty acids due to excess adipose tissue lipolysis induces various metabolic abnormalities, as well as vascular dysfunction. There was also evidence suggesting that peptides derived from adipocytes may affect arterial pressure, contributing to hypertension [8,9]. Diuretics have also been commonly used

to treat obesity [10,11]. In obesity, adipocytes secrete proinflammatory cytokines (TNF- α and IL-6), also known as adipokines, into the circulation [12]. The ability of UP to treat burn injury and intestinal inflammation suggests its anti-inflammatory properties that could inhibit the proinflammatory state in adipose tissue. Gut anti-inflammatory agents were also used to regulate obesity-related insulin resistance [13], which suggests that UP may also be used to treat obesity as UP was traditionally used to treat intestinal inflammation. We have also reported that UP exhibits antiplatelet and antithrombotic activity [14]. Existing traditional and modern evidence and reports suggest that UP may exhibit antiobesity properties.

UP was also reported to inhibit nitric oxide production in lipopolysaccharide-treated RAW 264.7 murine macrophages [15], exhibit anticancer and antiviral properties [16], and accelerates skin wound healing [17]. However, there were no reports on the antiobesity effects of the bark extract of UP. Fat tissue is an organ that serves as a survival adaptation in humans by providing a source of energy during starvation and heat insulation in cold weather. Adipose tissue exists in two forms, white adipose tissue (WAT) and brown adipose tissue (BAT) [18]. Triglycerides are stored in WAT as lipids in unilocular white adipocytes. Excessive accumulation of WAT has been shown to lead to cardiovascular diseases [19], type 2 diabetes [20], and cancer [21]. BAT dissipates heat due to the activity of uncoupling protein-1 (UCP-1). Hence, BAT is active metabolically. UCP-1 functions through the dissipation of the proton gradient into the inner mitochondrial membrane [22]. Increasing UCP-1 expression increases the conversion of free fatty acids during heat dissipation, hence reducing the amount of triglycerides in the body. This could potentially be one target for therapeutic methods for reducing the incidence of obesity.

In this study, we investigate the antiobesity effects of ethanol extracts of the bark of UP *in vitro* using 3T3-L1 preadipocytes and *in vivo* in a model of mice fed a high-fat diet (HFD). Our study demonstrates that UP inhibits lipid generation and adipocyte differentiation and also inhibits expression of various adipogenic genes. *In vivo* studies reveal effective inhibition of HFD-induced obesity, as well as decreased serum triglyceride levels, decreased body weight, and reduction of fatty liver. Orlistat, also known as tetrahydrolipstatin, is an inhibitor of gastric and pancreatic lipases. It acts in the gastrointestinal (GI) lumen, and it is also a widely used pharmacological drug to treat obesity [23]. Although orlistat has produced positive results in randomized placebo-controlled trials [24], there have been occurrences of fatty and oily stool and faecal urgency in patients [25]. Hence, our study aims to discover natural health supplement alternatives with the potential to treat obesity.

Our study has also revealed the ability of UP to increase metabolic activity via increased the expression of *UCP-1* and *PGC-1 α* in WAT. UP has increased browning of WAT. Therefore, energy expenditure is increased by increasing thermogenesis. However, more studies should be conducted to confirm the conversion of triglycerides through fatty acid

oxidation and the role of Sirtuin 1 (Sirt1) in mitochondrial biogenesis in conjunction with treatment with UP.

2. Materials and Methods

2.1. Reagents. The bark of UP was kindly provided by the Herbal Crop Research department of the Korean National Institute of Horticultural and Herbal Science (voucher number: NIHHS-0169), which is sourced from Danyang Province, Chungbuk, Republic of Korea. UP was verified by Professor Lee Seung Eun. Dulbecco's modified Eagle Medium (DMEM), fetal bovine serum (FBS), streptomycin, and penicillin were purchased from Welgene (Daegu, Republic of Korea). Insulin, 3-isobutyl-1-methylxanthine (IBMX), indomethacin, Oil Red O, orlistat, and neutral buffered formalin were purchased from Sigma-Aldrich (St. Louis, MI, USA). TRIzol reagent was purchased from Invitrogen (Carlsbad, CA, USA). Primers used in this study displayed in Table 1 were purchased from Bioneer (Daejeon, South Korea). Antibodies for p-AMPK α , AMPK α , p-ACC, and β -actin were purchased from Cell Signaling Technology (Danvers, MA, USA). Standards of (+)-catechin (product no. ES090-A) and catechin-7-O- β -D-apiofuranoside (product no. ES060-A) were purchased from Ensol Biosciences Inc. (Daejeon, Republic of Korea), both having a purity $\geq 95\%$.

2.2. Preparation of *U. parvifolia*. Bark of UP was collected and shredded. The bark was extracted using 70% ethanol at 80°C, filtered through filter paper (Whatman, USA), and condensed using a rotary evaporator before lyophilization to obtain the powder form of the extracts and weighed according to the desired concentrations.

2.3. UPLC-QToFMS Analysis of *U. parvifolia*. A UPLC system (Waters Corp., Milford, MA, USA) equipped with a binary solvent delivery system, an autosampler, and a UV detector was used. Briefly, aliquots of 2.0 μ L of UP were injected into a BEH C₁₈ column (2.1 \times 100 mm \times 1.7 μ m) at a flow rate of 0.4 mL/min and were eluted with a chromatographic gradient consisting of two mobile phases, which are A, water containing 0.1% formic acid; B, acetonitrile containing 0.1% formic acid. A linear gradient was optimized: 0 min, 5%; 0–8 min, 5–15% B; 8–11 min, 15–80% B; 11–12 min, 80–100% B; 12–13.3 min, 100% B; and 13.4–15 min, back to 5% B. Using a negative ion mode with a capillary voltage of 2.3 kV, cone voltage of 50 V, source temperature of 110°C, and a desolvation temperature of 350°C, the quadrupole time-of-flight mass spectrometer (Q-ToF Premier™, Waters Corp., Milford, MA, USA) was operated. A reference solution of leucine-enkephalin ([M – H][–] *m/z* 554.2615) in the form of a spray was used as the lock mass. The full-scan data and the MS/MS spectra were collected with MassLynx software (Thermo Fisher, MA, USA).

2.4. GCMS Analysis of *U. parvifolia*. An Agilent 7890A GC (Agilent Technologies, Santa Clara, CA, USA) with a

TABLE 1: Primer sequences for real-time PCR.

| Gene | Primer | Sequence |
|-----------------|---------|-------------------------------------|
| FAS | Forward | 5'-CTGAGATCCCAGCACTTCTTGA-3' |
| | Reverse | 5'-GCCTCCGAAGCCAAATGAG-3' |
| PPAR γ | FAM | 5'-TCGGAATCAGCTCTGTGGACCTCTCC-3' |
| | Forward | 5'-TGGGAACCTGGAAGCTTGTCTC-3' |
| aP2/FABP4 | Reverse | 5'-GAATCCACGCCAGTTTGA-3' |
| | Forward | 5'-TGGACAAGAACAGCAACGAGTAC-3' |
| C/EBP α | Reverse | 5'-CGGTCATTGTCACCTGGTCAACT-3' |
| | Forward | 5'-CACCATCGACCACGACCTC-3' |
| Adipsin | Reverse | 5'-AGTGTGGCCTTCTCCGACAG-3' |
| | Forward | 5'-CCGTCGATAGTGGCATCCATGAAAC-3' |
| IGF-1 | Reverse | 5'-GGACCAATACCTGCTATAGGG-3' |
| | Forward | 5'-ATTGTGGCTCAAACCTGCAGGT-3' |
| ACC | Reverse | 5'-GCCAATCCACTCGAAGACCA-3' |
| | Forward | 5'-GTCTCAGCTGTGGTCTTCCCCT-3' |
| Adiponectin | Reverse | 5'-CCCTGGCTTTATGCTCTTTGC-3' |
| | Forward | 5'-CCAAAACCCTCATCAAGACC-3' |
| Leptin | Reverse | 5'-GTCCAACCTGTTGAAGAATGTCCC-3' |
| | Forward | 5'-AAGCCGACCCAATGACATCA-3' |
| AMPK α 1 | Reverse | 5'-CTTCCTTCGTACACGCAAAT-3' |
| | Forward | 5'-GATGATGAGGTGGTGA-3' |
| AMPK α 2 | Reverse | 5'-GCCGAGGACAAAGTGC-3' |
| | Forward | 5'-AGCCTGGCCATCTGTGAGAA-3' |
| SREBP1c/ADD1 | Reverse | 5'-CAGACTGGTACGGGCCACAA-3' |
| | Forward | 5'-AAGACAGGTGCCTTCAGTTCACTCTCAG-3' |
| PGC-1 α | Reverse | 5'-AGCAGCACACTCTATGTCACTCCATACAG-3' |
| | Forward | 5'-ACTGCCACACCTCCAGTCATT-3' |
| UCP-1 | Reverse | 5'-CTTTGCCTCACTCAGGATTGG-3' |
| | Forward | 5'-CACTCACGGCAAATTCACGGGCAC-3' |
| GAPDH | Reverse | 5'-GACTCCACGACATACTCAGCAC-3' |

30 m \times 0.25 mm i.d. DB-5MS column and an Agilent 5975C mass selective detector (MSD) were used to separate and quantify the constituents of UP. Samples were injected in split mode with a temperature of 250°C. The transfer line temperature was 280°C, and the ion source temperature was 230°C. The column temperature was held at an initial temperature of 70°C for 1 min and was raised to 300°C at a rate of 5°C/min and held at a final temperature of 300°C for 30 min. Helium was used as a carrier gas at a constant flow rate of 1 mL/min. Mass spectrometry was performed using the electron ionization (EI) and scan modes.

2.5. Cell Culture. 3T3-L1 preadipocytes purchased from ATCC (Manassas, VA, USA) were cultured in Dulbecco's Modified Eagle Medium (DMEM) supplemented with 10% fetal bovine serum, 100 IU/mL penicillin, and streptomycin and maintained at 5% CO₂ and 37°C. Differentiation was induced with media supplemented with insulin, indomethacin, and IBMX. Cells were allowed to differentiate for 3 days and then cultured with normal media supplemented with insulin for postdifferentiation maintenance. Cells were differentiated for a total of 10 days for consecutive experiments.

2.6. Oil Red O Staining. Cells were differentiated using differentiation media and simultaneously treated with 6.25, 12.5, and 25 μ g/mL of UP. After 10 days, the cells were

stained with Oil Red O staining. Oil Red O solution was then added to plates cultured with 3T3-L1 cells for visualization of lipids secreted by the cells under a microscope.

2.7. Cell Viability Assay. Viability of undifferentiated 3T3-L1 cells were assessed by using a 3-(4,5-dimethylthiazol-2-yl)-2,5-diphenyltetrazolium bromide (MTT) assay. The cells were seeded in 24-well plates for 24 h. Incubation of UP in specified concentrations was performed. Proceeding steps were carried out as previously reported [26]. Briefly, MTT was added to wells and left to incubate for 3 h. DMSO was added to each well to dissolve violet crystals of MTT and left on a rocker for 10 min. Plates were then read at 560 nm using a plate reader.

2.8. High-Fat Diet Induced Obesity in Mice. All experiments were approved by the Institutional Animal Care Committee of Kyungpook National University in accordance to NIH guidelines (approval number: 2018-0117). Four-week-old male ICR mice were purchased from Orient Bio (Gyeonggi-do, Republic of Korea), maintained in a 12-h light/dark controlled room with regulated temperature at 22 \pm 2°C and humidity of 50 \pm 10%. The mice were given access to chow and water *ad libitum* and allowed to acclimatize for one week, grouped in numbers of 6 with a total of 5 groups. Six mice were given normal chow, and the remaining mice were fed an HFD (D12492; Research Diets, New Brunswick, NJ,

USA). Mouse weight, food intake, and water intake were measured weekly. After four weeks of a HFD, mice were given an oral administration of orlistat (10 mg/kg) and UP at 100 mg/kg and 300 mg/kg for an additional 8 weeks. Twenty-four hours after the final administration, mice were anaesthetized and blood was collected by cardiac puncture. Organs and adipose tissue were immediately harvested, weighed, frozen, and fixed in neutral buffered formalin. The food efficiency ratio (FER) was calculated as the amount of intake per mouse divided by the weight of the mouse.

2.9. RT-PCR and Real-Time PCR of 3T3-L1 Preadipocytes and Epididymal Adipose Tissue of Mice. RNA was extracted from 3T3-L1 preadipocytes and epididymal adipose tissue from HFD mice using TRIzol solution. Brown adipose tissue was extracted from mice fed with normal chow and used as a positive control for browning genes. Proceeding steps were conducted as reported [27]. Briefly, RNA was separated using chloroform and purified using alcohol. The RNA was resuspended in DEPC-DW, and the concentration was measured using a nanophotometer. Reverse-transcriptase PCR was conducted using a premix (Bioneer, Daejeon, Republic of Korea). Real-Time PCR was then conducted with the resultant cDNA using target primers of adipogenesis-related genes and browning-related genes, as shown in Table 1. For *C/EBP α* and *PPAR γ* , RNA was extracted at day 5 of differentiation, while RNA was extracted at day 8 for other target genes.

2.10. Western Blot Analysis of Epididymal Adipose Tissue and Liver Tissue. Proteins were extracted from 3T3-L1 cells and liver tissues of mice and analyzed using western blot analysis. Cells and liver tissues were homogenized with Pro-Prep protein lysis solution (Invitrogen, Daejeon, Republic of Korea), and protein concentrations were analyzed using the Bradford method. Proceeding procedures were conducted as previously reported [28]. Briefly, proteins were separated using 10% SDS-PAGE and transferred to a PVDF membrane, followed by blocking with 5% skim milk at room temperature for 1 h. The membranes were then incubated with the respective primary antibodies (1 : 3,000) overnight, followed by incubation with a secondary antibody (1 : 1,000) at room temperature for 90 min. The membranes were then washed with 1% Tween-20 TBS before developing the membranes using ECL chemiluminescence in a gel developer (General Electric, Boston, MA, USA). Western blot analysis was repeated in triplicate, and the relative expressions were quantified using ImageJ software (NIH, USA).

2.11. Serum Chemistry. Collected blood was allowed to separate for 2 h and centrifuged at 3,000 rpm for 15 min. Serum was collected and analyzed using a blood analyzer for triglyceride, glucose, total cholesterol, LDL, HDL, ALT, and AST levels.

2.12. Hematoxylin and Eosin (H&E) Staining. Harvested liver tissue and epididymal adipose tissue were directly fixed

in neutral buffered formalin after harvesting and weighing. Images of the slides were acquired using a Nikon Eclipse E6000 microscope (Nikon, Minato-ku, Tokyo, Japan). Dehydrated tissues were fixed in paraffin and sectioned before staining with H&E. Size of adipocytes was determined using AdipoCount [29].

2.13. Statistical Analysis. Statistical significance was analyzed using Graphpad Prism version 7.00 (San Diego, CA, USA) and one-way ANOVA with Dunnett's posttest. $P < 0.05$ was considered significant. Data were presented as mean \pm SD.

3. Results

3.1. UPLC-QToF MS Analysis and GCMS Analysis of *U. parvifolia*. Using UPLC-QToF MS, the compounds identified in ethanol extract of the bark of UP are as shown in Figure 1(a). Peak 1 was identified as +(-) catechin as compared to its standard shown in Figure 1(b), and peak 2 was identified as catechin-7-O- β -D-apiofuranoside as compared to its standard, as shown in Figure 1(c). The concentration of catechin detected is 6.14 mg/g, whereas that of catechin-7-O- β -D-apiofuranoside was 156.3 mg/g, as previously described [14]. GCMS analysis revealed that the main components are hexadecanoic acid and β -sitosterol (Table 2).

3.2. *U. parvifolia* Inhibited Production of Lipid in 3T3-L1 Preadipocytes. Lipid is produced when preadipocytes differentiate into adipocytes. UP reduced lipid production in differentiated 3T3-L1 preadipocytes (Figure 2(a)). The concentrations of UP used were not toxic, as determined by an MTT assay on 3T3-L1 cells (Figure 2(b)). Expression of adipogenic genes *FAS*, *PPAR γ* , *aP2/FABP4*, *C/EBP α* , *adiponectin*, *IGF-1*, *ACC*, *adiponectin*, *leptin*, *AMPK α 1*, and *SREBP1c/ADD1* was decreased with increasing concentrations of UP treatment (Figure 2(c)). However, *AMPK α 2* expression was increased. AMPK is a main regulator of metabolism, and its phosphorylated form was increased with increasing concentrations of UP treatment, while p-ACC protein expression was reduced (Figure 2(d)). No change was observed in ACC expression. The relative expressions of AMPK α and ACC were quantified using ImageJ software (NIH, USA), as shown in Figures 2(e) and 2(f).

3.3. *U. parvifolia* Inhibits Development of Obesity in Mice Fed an HFD. There were no significant differences in food and water intake between the groups (Figures 3(a)–3(c)). However, mice that were administered orlistat daily and UP 100 or UP 300 exhibited notable decreases in weight (Figure 3(e)). Orlistat group mice exhibited a significant reduction as compared to mice consuming only an HFD from week 5, whereas UP 100- and 300-treated groups exhibited a significant reduction from week 6. FER was significantly reduced in both UP-treated groups in a dose-dependent manner (Figure 3(d)). Subcutaneous adipose

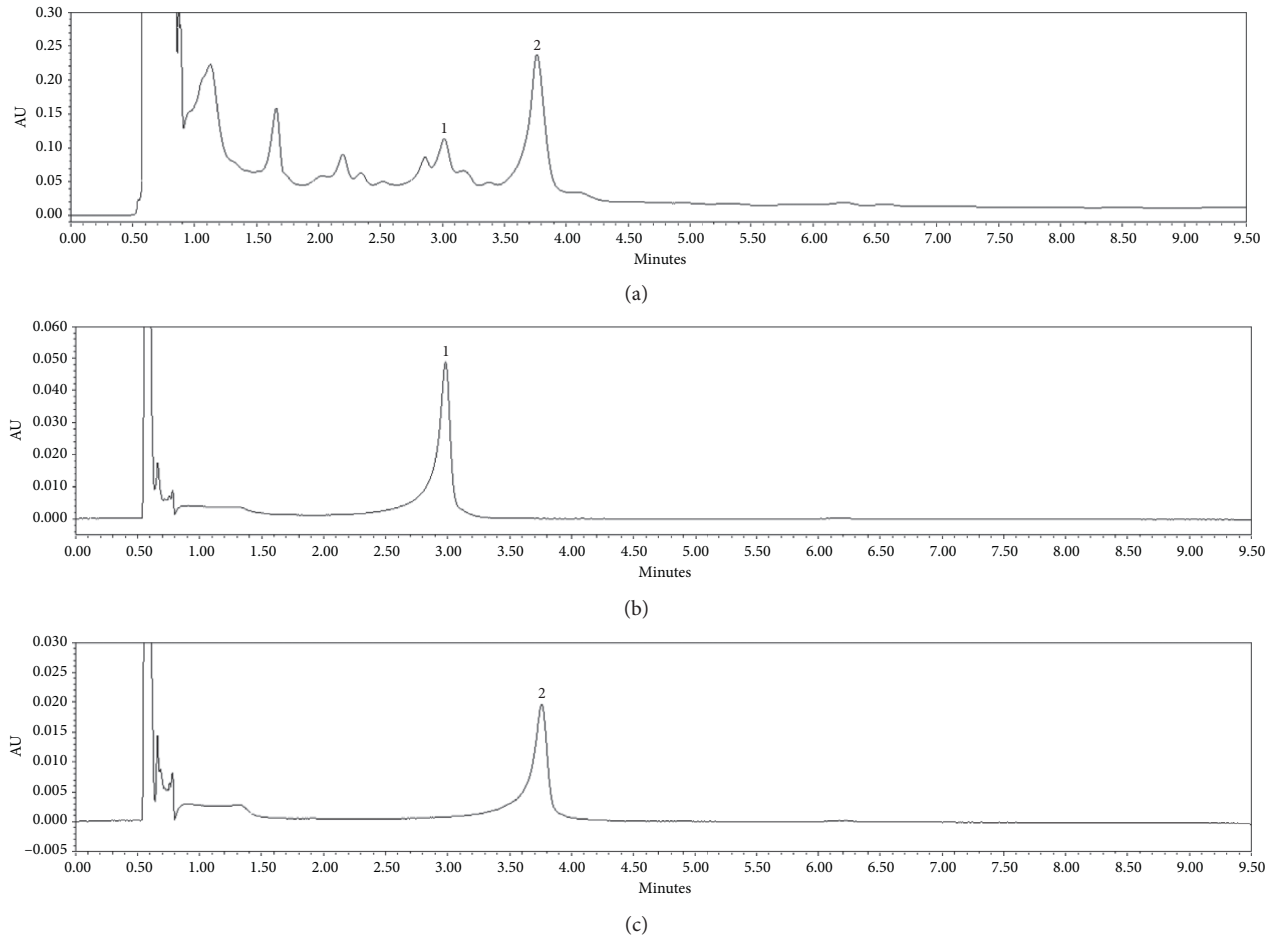


FIGURE 1: UPLC-QToF MS identification of UP. Peaks detected in ethanol extract of the bark of UP (a). Peaks 1 and 2 were quantified by using a UV detector at 280 nm for target catechin glycosides. Peak 1 was identified as (+/-) catechin as compared to its standard shown in (b), and peak 2 was identified as catechin-7-O- β -D-apiofuranoside as compared to its standard as shown in (c).

TABLE 2: Components detected by GCMS analysis of UP.

| Retention time | Area (%) | Compound |
|----------------|----------|-----------------------------|
| 29.993 | 20.37 | Hexadecanoic acid |
| 51.024 | 14.83 | β -Sitosterol |
| 51.861 | 7.1 | 2(1H) Naphthalenone |
| 47.525 | 5.84 | 1-Naphthalene-sulfonic acid |
| 47.138 | 3.78 | 2-Ethylacridine |

tissues were significantly reduced in the orlistat and UP 300-treated groups, whereas epididymal adipose tissue was reduced significantly only in UP 300 (Figure 3(f)). The weight of the liver has decreased in treated groups, whereas there was no significant change in kidney and spleen weight in all groups (Figure 3(g)). From the results, it can be seen that UP treatment significantly reversed weight gain in mice and reduced FER and weight of adipose tissue and the liver.

3.4. *U. parvifolia* Improved Histological Damage Induced by an HFD in Mice. There was a visible change in body size as shown in the representative pictures of mice for each group; mice were significantly increased in size in the HFD-group,

whereas there was a visible reduction in size in mice from the groups treated with orlistat and UP 100 or UP 300 (Figure 4(a)). Liver tissue extracted after the mice were euthanized was compared (Figure 4(b)). There was a visible increase in size and change in coloration to a paler shade, indicating the occurrence of fatty liver after consuming an HFD. This change was improved with orlistat and UP 100 or UP 300 treatment. This observation was further confirmed with histological analysis of liver tissue and epididymal adipose tissue stained with H&E. The hepatocytes in HFD-treated mice were remarkably increased in size, and the pale coloration was visible due to accumulation of lipids. There was also a visible decrease in size of hepatocytes in the orlistat and UP-treated groups. Ballooning of hepatocytes, macrovesicular steatosis (indicated by arrows), and the foamy characteristics of the hepatocytes as depicted in microvesicular steatosis were also identified in the HFD-treated group, indicating the occurrence of nonalcoholic fatty liver disease (NAFLD). Infiltration of inflammatory cells was also observed (indicated by arrowheads) (Figure 4(c)). Therefore, treatment of orlistat and UP has remarkably inhibited the progression of NAFLD. The size of adipocytes in HFD-treated mice was significantly larger, as

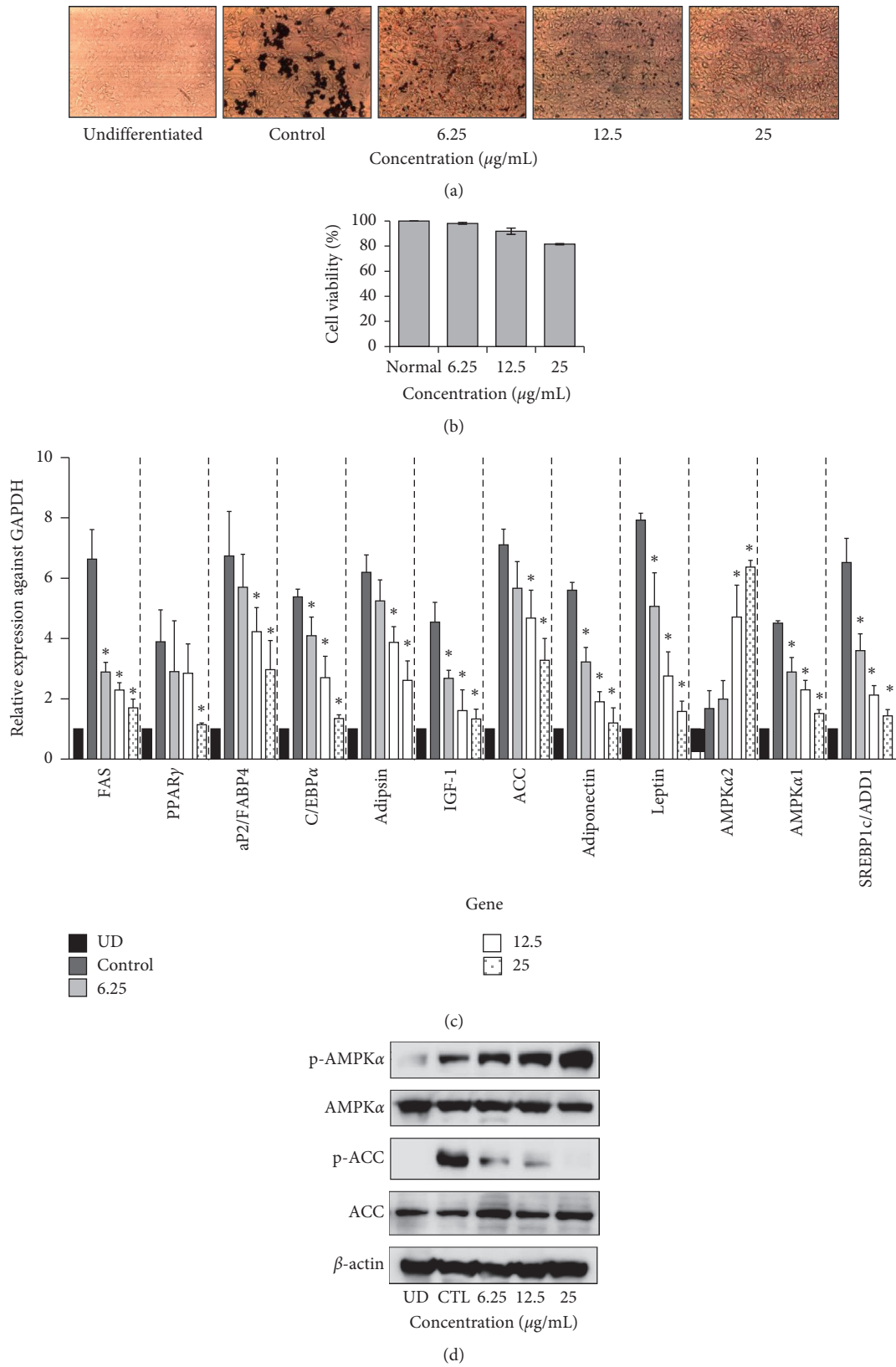


FIGURE 2: Continued.

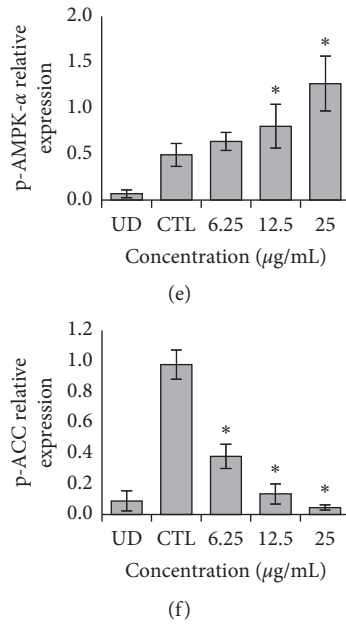


FIGURE 2: UP inhibits secretion of lipid droplets in 3T3-L1 preadipocytes. 3T3-L1 preadipocytes were differentiated or undifferentiated (UD) and treated with or without UP for 10 days before they were stained with oil red O (a). Cell viability was confirmed with an MTT assay after 3T3-L1 cells were treated with different concentrations of UP (b). Real-Time PCR was carried out by extracting RNA of differentiated 3T3-L1 cells with or without treatment of UP (c). Western blot analysis of p-AMPK α and p-ACC against the housekeeping gene β -Actin. 3T3-L1 cells were treated with or without UP after differentiation. After 10 days, protein was extracted from the cells, separated using SDS-PAGE, transferred to a PVDF membrane, incubated overnight with the primary antibody, incubated with secondary antibody, and developed (d). Expressions of genes were compared against the differentiated control group. Western blot was repeated in triplicate, and images were quantified using ImageJ (e and f). Statistical analysis was performed using one-way ANOVA with Dunnett's posttest, and $P < 0.05$ was considered significant.

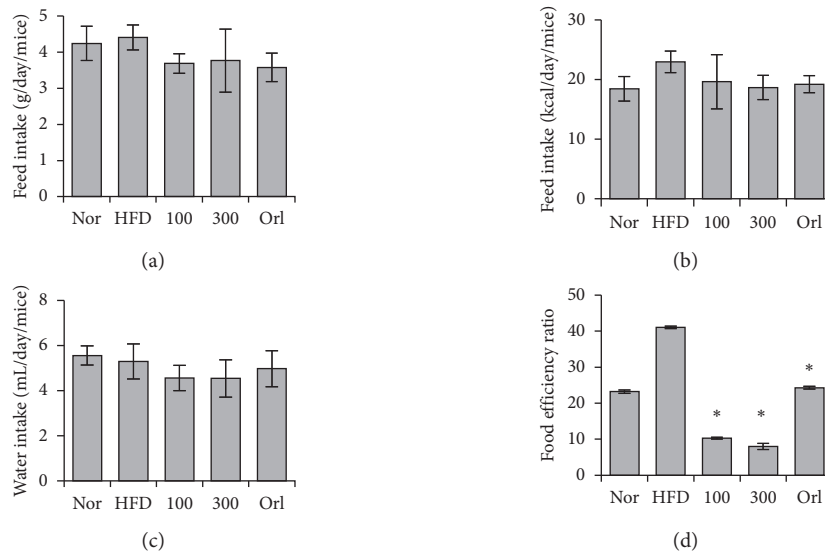


FIGURE 3: Continued.

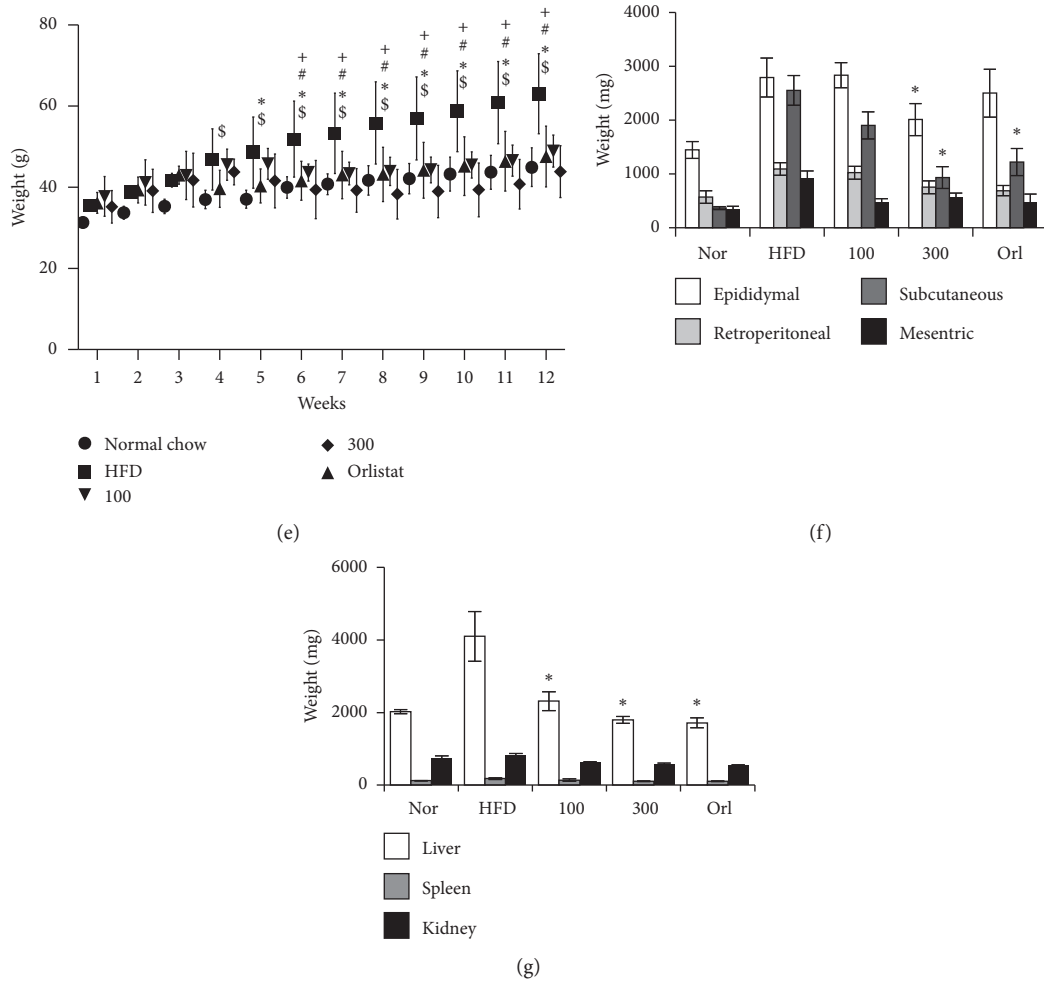


FIGURE 3: UP reduced obesity in mice. Food intake and water intake were monitored weekly and averaged as shown in (a–c). Food efficiency ratio was calculated using the weight gain to intake of food ratio (d). Weight of mice for each group was recorded every week for a period of 12 weeks. Mice in the normal group (nor) were given normal chow, whereas all other groups were given a HFD. After 4 weeks, oral administration of orlistat and UP was given daily for 8 weeks (e). After 12 weeks, mice were euthanized, and the fat tissue, liver, spleen, and kidney were harvested and weighed immediately (f and g). Statistics were analyzed using one-way ANOVA with Dunnett's posttest, and $P < 0.05$ was considered significant. Statistical significance of HFD as compared to the control group in (d) are indicated by \$; *, for the orlistat group against HFD; #, for UP 100 against HFD; and +, for UP 300 against HFD.

compared to mice fed normal chow, indicating hypertrophy of adipocytes. Adipocytes were shown to decrease with treatment of orlistat and UP. UP 300 in particular reduced the size of adipocytes as compared to the adipocytes of mice fed normal chow. Adipocyte count per frame was also significantly recovered in UP 300-treated mice (Figure 4(d)). This has confirmed the efficacy of UP in reversing obesity induced with an HFD and demonstrates the therapeutic potential of this compound for increasing metabolism and reversing obesity.

3.5. *U. parvifolia* Increased Browning-Related Genes in Adipose WAT. Using real-time PCR, the expression of *PGC-1 α* and *UCP-1* were shown to increase in particular with treatment of UP 300 (Figures 5(c) and 5(e)). The products of real-time PCR were run on ethidium bromide-stained

agarose gel for confirmation (Figure 5(a)). The protein expression of p-AMPK α was increased significantly, whereas the expression of p-ACC was decreased only in UP 300 (Figure 5(b)). No change was observed in ACC expression. The gel images were quantified using ImageJ (Figures 5(d) and 5(f)). Our results have shown that UP has induced browning of epididymal adipose tissue in mice fed an HFD.

3.6. Serum Biochemistry of Mice in a High-Fat Model.

Serum triglyceride levels were significantly reduced by orlistat and UP 100 or UP 300 treatment. LDL levels were decreased with UP treatment. However, there were no significant decreases in glucose levels, total cholesterol, and HDL in any treated groups. ALT and AST are both markers of liver damage and did not show significant change in all groups (Figures 6(a)–6(g)).

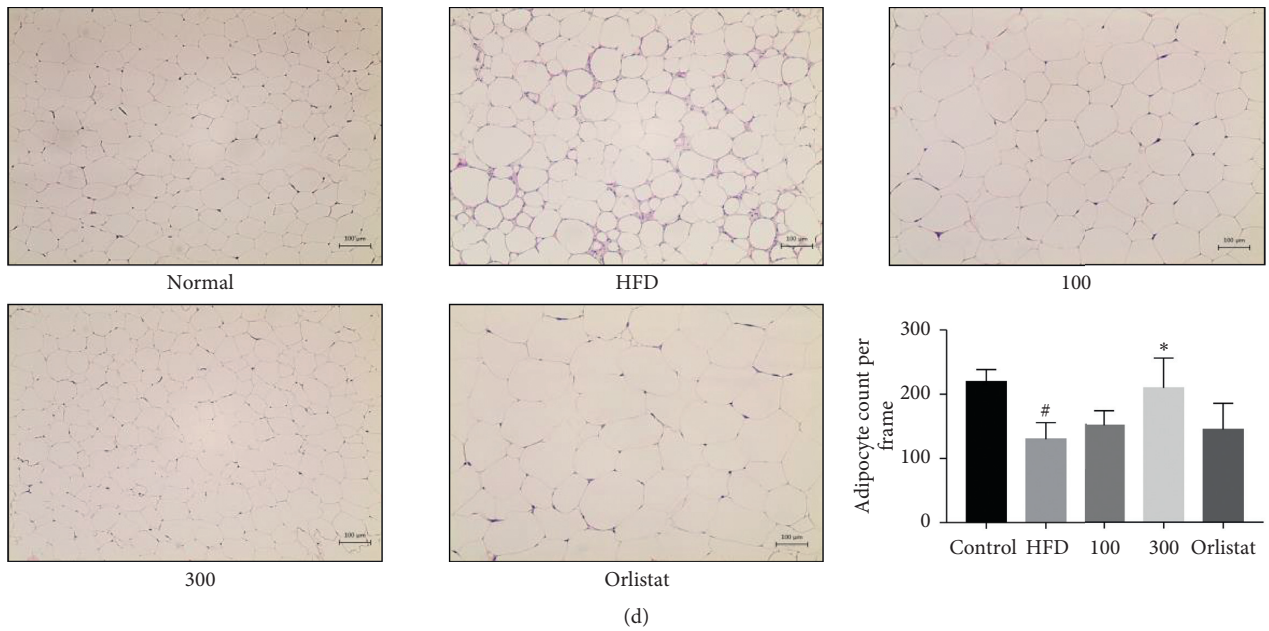


FIGURE 4: UP reduced the size of mice and mouse livers and improved the histology of the liver and adipose tissue induced by an HFD. Mice were fed with an HFD for a total of 12 weeks, and oral administration of orlistat and UP was carried out after 4 weeks of a daily HFD. Representative images of mice and livers for each group (a-b). Liver tissues and epididymal adipose tissue were dehydrated and fixed in paraffin and then sectioned before staining with H&E (c-d). Liver tissues (c) and epididymal adipose tissue (d) were observed at 100x. Arrows indicate balloon cells, and arrowheads indicate the infiltration of inflammatory cells. CV indicates the location of the central vein, whereas PV indicates the portal veins. Magnified image of the CV area of the liver tissue in HFD-treated group was taken at 200x. Statistical analysis for adipocyte count performed using one-way ANOVA with Dunnett’s posttest, and * indicates $P < 0.05$ compared to the HFD group, whereas [#] indicates a $P < 0.05$ as compared to the control group.

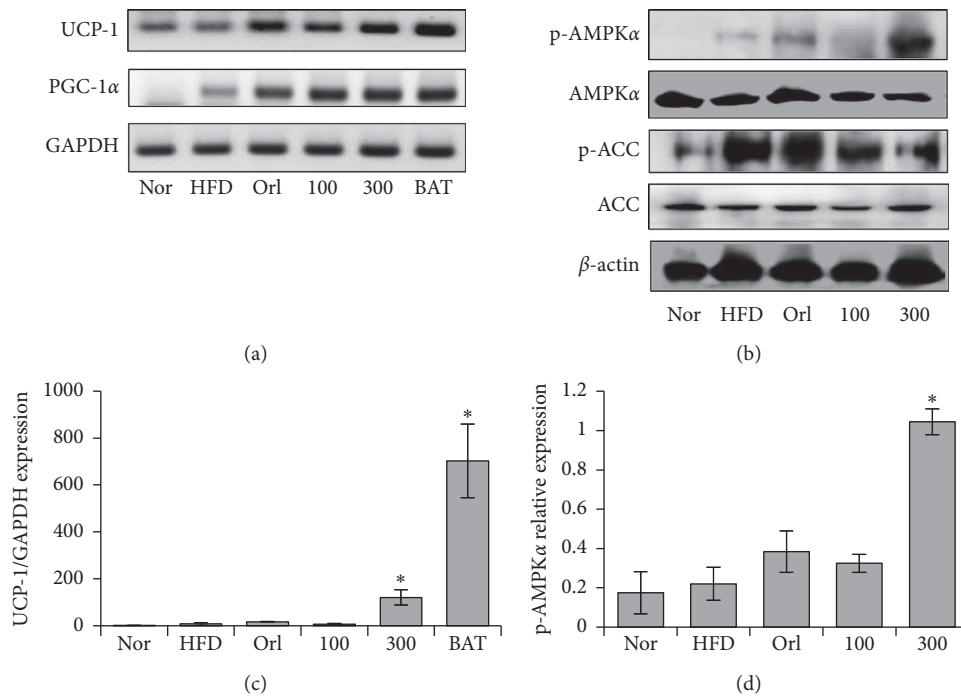


FIGURE 5: Continued.

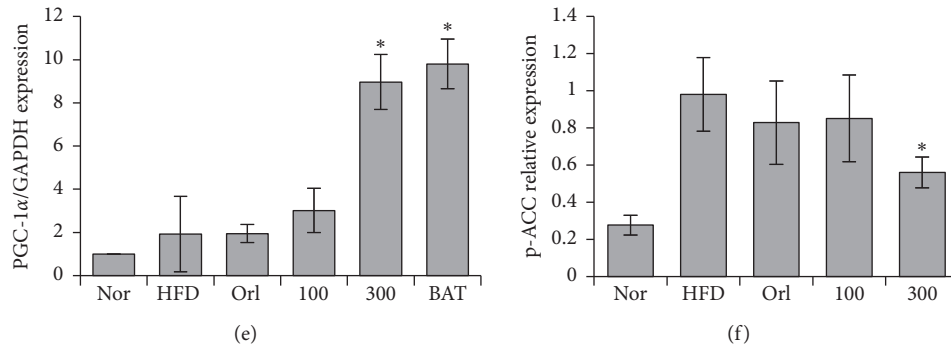


FIGURE 5: UP increased expression of browning markers in mice. Extracted RNA was reverse transcribed, and the browning related genes *UCP-1* and *PGC-1 α* were investigated using Real-Time PCR conducted using the resultant cDNA (a). Quantification of gel images (c and e). Protein expressions of p-AMPK α and p-ACC in liver tissue were investigated using western blot analysis, as shown in (b), and the gel images were quantified using ImageJ (d and f). All experiments were conducted in triplicate. Statistics were analyzed using one-way ANOVA, and $P < 0.05$ was considered significant.

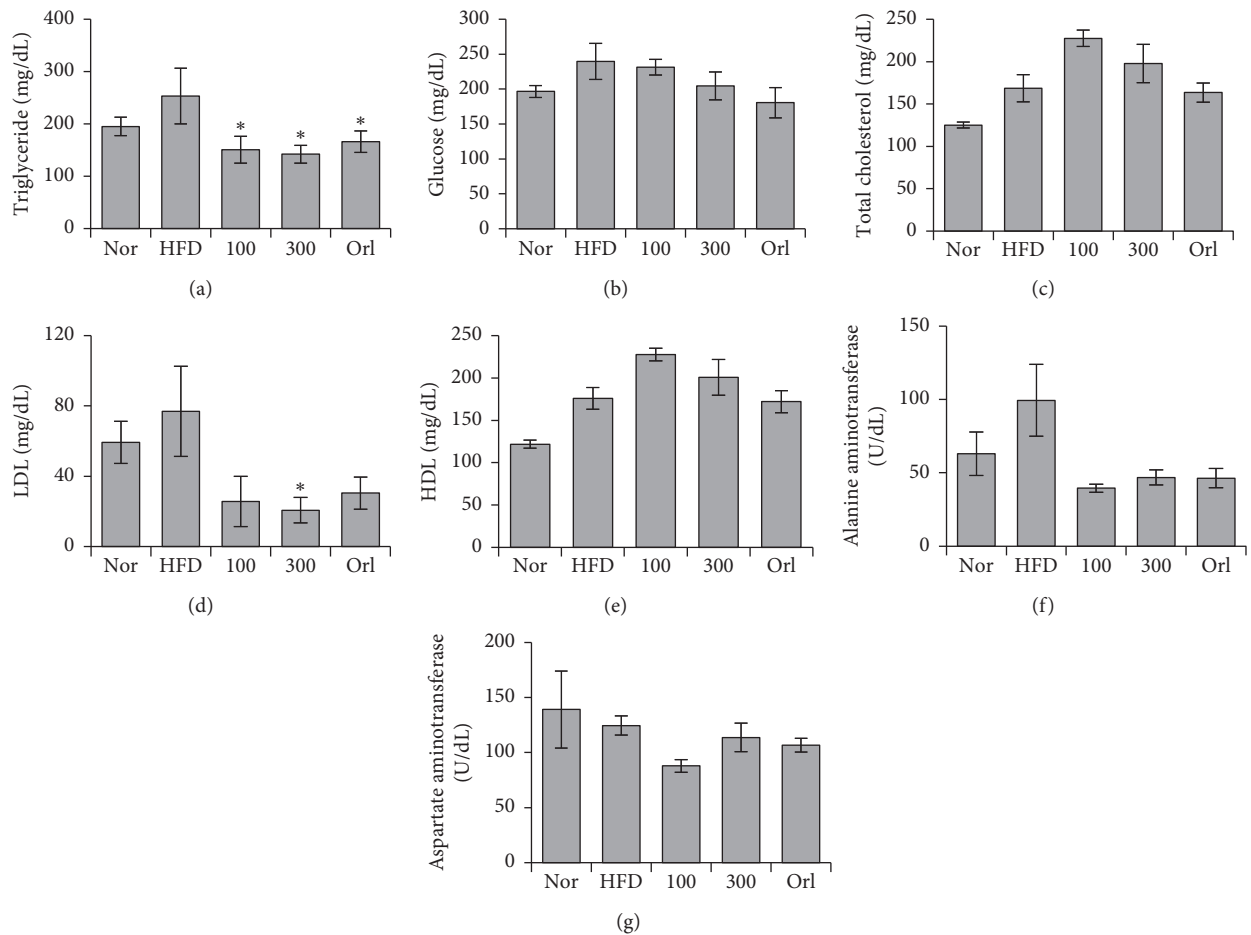


FIGURE 6: UP improved serum biochemical concentrations induced by an HFD in mice. Blood was collected by cardiac puncture, and serum was separated. Levels of (a) triglyceride, (b) glucose, (c) total cholesterol, (d) LDL, (e) HDL, (f) ALT, and (g) AST were investigated using a blood analyzer. Statistical analysis was performed using one-way ANOVA with Dunnett's posttest, and $P < 0.05$ was considered significant.

4. Discussion

Other than storing lipids, white adipose tissue also functions as an endocrine organ, secreting mainly adiponectin and

leptin [30]. Additionally, white adipose tissues secrete TNF- α in an obese rodent model [31]. IL-6 was also detected in white adipose tissues in cases of obesity and insulin resistance [32]. Both TNF- α and IL-6 are also known as

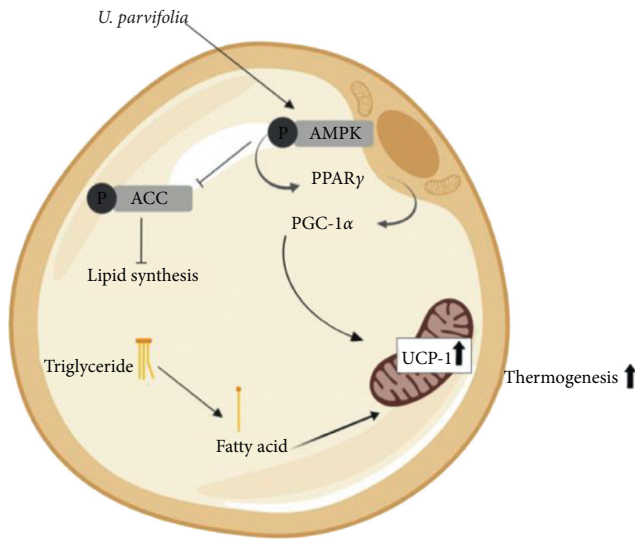


FIGURE 7: Schematic diagram of the proposed mechanism of action of UP. UP increased the browning of WAT by acting through increased AMPK α expression, which, in turn, increases PPAR γ expression followed by the increase of PGC-1 α expression, which induces upregulation of mitochondrial UCP-1 in white adipocytes and increases the usage of stored triglycerides and thermogenesis. Phosphorylation of ACC was also inhibited, subsequently inhibiting lipid synthesis.

adipokines and proinflammatory cytokines. Secretion of adipokines by WAT is a response to hypoxia in areas of fat deposits in obese individuals, as the vasculature is insufficient to maintain normoxia throughout the WAT due to its constant expansion. This causes the adipocytes to be hypoxic, and an inflammatory response increases blood flow and stimulates angiogenesis [33]. Therefore, obesity should be treated not only merely as a metabolic disorder but also as the root cause of many chronic diseases.

3T3-L1 preadipocytes were used to investigate adipogenesis *in vitro*. Peroxisome proliferator-activated receptor γ (PPAR γ) and CCAAT/enhancer binding protein α (C/EBP α) are responsible for preadipocyte growth arrest and their differentiation into adipocytes. As the shift in gene expression indicates cellular differentiation, we studied the related gene expression for confirmation of preadipocyte differentiation. Our results have shown that PPAR γ , C/EBP α , and SREBP1c/ADD1 are downregulated in 3T3-L1 preadipocytes after treatment with UP. Furthermore, *leptin* and *adiponectin* are also adipokines secreted by adipose tissue. *Leptin* in serum is elevated in the case of obesity as it functions to accelerate energy expenditure [34], whereas insulin levels are negatively correlated with adiponectin levels in 3T3-L1 preadipocytes [35]. Treatment with UP also reduced both *leptin* and *adiponectin* mRNA levels in 3T3-L1 preadipocytes in this study. *Adipsin* is upregulated in the presence of insulin in 3T3-L1 preadipocytes [36]. As FAS, ACC, and aP2/FABP4 are regulated by PPAR γ [37,38], these genes were downregulated with UP treatment. *Insulin growth factor 1 (IGF-1)* is essential in the differentiation of 3T3-L1 preadipocytes [39], and its expression has been reduced with treatment of UP. AMPK is the master regulator

of metabolism. Phosphorylation of AMPK inhibits the phosphorylation of ACC which then inhibits lipid synthesis and, at the same time, promotes fatty acid oxidation by increasing CPT1 (carnitine palmitoyltransferase 1) expression. As leptin inhibits the phosphorylation of AMPK α 2 [40], suppression of leptin explains the increase of AMPK α 2 (Figure 2(c)). UP has been shown to reduce lipid production and did not show signs of cytotoxicity in 3T3-L1 preadipocytes for the concentrations of UP used *in vitro* and additionally resulted in the downregulation of mRNA expressions of adipogenesis-related genes and increased expression of AMPK α 2. Western blot analysis has also revealed that UP is capable of upregulating p-AMPK α and suppressing p-ACC (Figures 2(d)–2(f)).

PGC-1 α was previously identified to be expressed only in BAT. Recent studies revealed the browning of WAT, also known as brite or inducible brown adipocytes [41]. Brown adipocytes are dominant in BAT, whereas beige adipocytes are found in WAT in cases of increased energy expenditure or exposure to cold. Therefore, the increase of beige adipocytes is marked by increases of PGC-1 α and UCP-1 and results in increased energy expenditure that can then counter obesity. Brown adipocytes have large numbers of mitochondria and highly express UCP-1, which is located in the inner mitochondrial membrane. Fatty acids from triglycerides will undergo β -oxidation followed by conversion into chemical energy by mitochondrial UCP-1 [42]. Therefore, increasing the expression of PGC-1 α and UCP-1 in white adipose tissue increases energy expenditure, which will reduce the amount of triglycerides stored in WAT. Our results have shown that mice fed with UP have markedly increased PGC-1 α and UCP-1 expression in the epididymal adipose tissue of mice (Figure 5), indicating that UP increases the browning of WAT. The reduced weight of the mice and the respective adipose tissues in mice indicated the conversion of triglycerides in WAT to fatty acids which are then dissipated into heat energy through conversion by UCP-1, with no observed reduction of feed intake in all groups. UP also upregulated p-AMPK α expression and downregulated p-ACC expression in epididymal adipose tissue of mice fed a HFD, confirming the role of UP in countering obesity. These findings are further supported by evaluation of the levels of serum biomarkers, namely triglyceride, glucose, cholesterol, ALT, and AST, accompanied by the improvement in histological analysis of liver tissue and epididymal adipose tissue (Figures 4 and 6). UP increased lipid metabolism as there were lesser fat droplets deposited in the liver as observed in H&E staining, preventing NAFLD as previously reported [43].

UPLC-QToF MS was carried out to identify the polar compounds in UP. Our findings revealed that the most abundant polar compounds in UP are catechin and catechin-7-O- β -D-apiofuranoside (Figure 1). Catechin has been known for antiobesity properties, explaining its possible contribution in the efficacy of UP in curbing obesity [44]. Catechin-7-O- β -D-apiofuranoside prevents hepatic fibrogenesis by inhibiting stellate cell activation [45]. GCMS analysis was carried out to identify the nonpolar constituents of UP. Our findings have shown that the major nonpolar compounds

are hexadecanoic acid and β -sitosterol (Table 2). While hexadecanoic acid has been reported to have anti-inflammatory properties [46], β -sitosterol has been reported to induce apoptosis of cancer cells, have hypocholesterolemic and antidiabetic properties, and increase the activity of NK cells [47]. Moreover, sitosterol has also been reported to reduce choric inflammation induced by obesity [48]. Taken altogether, we believe that β -sitosterol and catechin in UP are the main ingredients that induce WAT browning.

5. Conclusions

Our findings reveal that UP increased browning in WAT in mice, possibly acting through the PGC-1 α /SIRT1/UCP-1 axis. Further studies should be conducted to confirm the role of SIRT1 and PRDM16. In conclusion, we have revealed the mechanism of action of UP on white adipocytes is via increased mitochondrial biogenesis in WAT, inducing an increase in energy expenditure and thermogenesis (Figure 7).

Abbreviations

| | |
|------------------|--|
| WAT: | White adipose tissue |
| BAT: | Brown adipose tissue |
| UCP-1: | Uncoupling protein 1 |
| PGC-1 α : | Peroxisome proliferator-activated receptor gamma coactivator 1-alpha |
| LDL: | Low-density lipoprotein |
| HDL: | High-density lipoprotein |
| ALT: | Alanine aminotransferase |
| AST: | Aspartate aminotransferase. |

Data Availability

The data used to support the findings of this study are included within the article.

Conflicts of Interest

All authors declare no conflicts of interest.

Authors' Contributions

Y.Y.L. designed the research plan, conducted the research, analyzed data, and wrote the paper. M.K. and S-H.K. designed the research plan and conducted the research. I.M. partially conducted the research. D-S.K., H.J.Y., S.E.L., S.K., and S-D.K. analyzed the data. M. H. R. has primary responsibility for the final content. All authors have read and approved the final manuscript.

Acknowledgments

This research was supported by the National Research Foundation of Korea (2018R1D1A1A09083797).

References

- [1] F. S. Santamour Jr. and S. E. Bentz, "Updated checklist of elm (*Ulmus*) cultivars for use in North America," *Journal of Arboriculture*, vol. 21, no. 3, pp. 122–131, 1995.
- [2] E. C. Bate-Smith and R. H. Richens, "Flavonoid chemistry and taxonomy in *Ulmus*," *Biochemical Systematics and Ecology*, vol. 1, no. 3, pp. 141–146, 1973.
- [3] S. A. Mina, "LC/ESI-MS/MS profiling of *Ulmus parvifolia* extracts and evaluation of its anti-inflammatory, cytotoxic, and antioxidant activities," *Zeitschrift für Naturforschung C*, vol. 71, no. 11–12, pp. 415–421, 2016.
- [4] C.-P. Li, *Chinese Herbal Medicine*, US Department of Health, Education, and Welfare, Public Health Service, National Institute of Health, Washington, DC, USA, 1974.
- [5] W. Vent, J. A. Duke, and E. S. Ayensu, *Medicinal Plants of China*, Vol. 2, Reference Publ., Inc., Algonac, MI, USA, 1987.
- [6] Zhao X. and S. Li, Ben Cao Gang Mu Shi Yi, Shang Wu Yin Shu Guan Xianggang Fen Guan, 1971.
- [7] G. Stuart, "A translation of an ancient Chinese herbal," *Chinese Materia Medica Taipei*, Southern Materials Centre, 1984.
- [8] T. A. Kotchen, "Obesity-related hypertension: epidemiology, pathophysiology, and clinical management," *American Journal of Hypertension*, vol. 23, no. 11, pp. 1170–1178, 2010.
- [9] A. N. D. Cat, "Adipocytes, aldosterone and obesity-related hypertension," *Journal of Molecular Endocrinology*, vol. 57, no. 1, pp. F7–F21, 2016.
- [10] C. Manrique, M. Johnson, and J. R. Sowers, "Thiazide diuretics alone or with β -blockers impair glucose metabolism in hypertensive patients with abdominal obesity," *Hypertension*, vol. 55, no. 1, pp. 15–17, 2010.
- [11] J.-M. Yuan, J. Castela, M. Gago-Dominguez, R. Ross, and M. Yu, "Hypertension, obesity and their medications in relation to renal cell carcinoma," *British Journal of Cancer*, vol. 77, no. 9, pp. 1508–1513, 1998.
- [12] N. Ouchi, J. L. Parker, J. J. Lugus, and K. Walsh, "Adipokines in inflammation and metabolic disease," *Nature Reviews Immunology*, vol. 11, no. 2, pp. 85–97, 2011.
- [13] H. Luck, S. Tsai, J. Chung et al., "Regulation of obesity-related insulin resistance with gut anti-inflammatory agents," *Cell Metabolism*, vol. 21, no. 4, pp. 527–542, 2015.
- [14] M. Irfan, "Ulmus parvifolia modulates platelet functions and inhibits thrombus formation by regulating integrin α IIb β 3 and cAMP signaling," *Frontiers in Pharmacology*, vol. 11, p. 698, 2020.
- [15] E.-J. Yang, E.-Y. Yim, G. Song, G.-O. Kim, and C.-G. Hyun, "Inhibition of nitric oxide production in lipopolysaccharide-activated RAW 264.7 macrophages by Jeju plant extracts," *Interdisciplinary Toxicology*, vol. 2, no. 4, pp. 245–249, 2009.
- [16] M. M. Hamed, "Anticancer and antiviral estimation of three *Ulmus parvifolia* extracts and their chemical constituents," *Oriental Journal of Chemistry*, vol. 31, no. 3, pp. 1621–1634, 2015.
- [17] M. C. Kang, "Ulmus parvifolia accelerates skin wound healing by regulating the expression of MMPs and TGF- β ," *Journal of Clinical Medicine*, vol. 9, no. 1, p. 59, 2020.
- [18] K. A. Virtanen, M. E. Lidell, J. Orava et al., "Functional brown adipose tissue in healthy adults," *New England Journal of Medicine*, vol. 360, no. 15, pp. 1518–1525, 2009.
- [19] Y. Matsuzawa, "White adipose tissue and cardiovascular disease," *Best Practice & Research Clinical Endocrinology & Metabolism*, vol. 19, no. 4, pp. 637–647, 2005.
- [20] C. M. Steppan, S. T. Bailey, S. Bhat et al., "The hormone resistin links obesity to diabetes," *Nature*, vol. 409, no. 6818, pp. 307–312, 2001.
- [21] Y. Zhang, A. Daquinag, D. O. Traktuev et al., "White adipose tissue cells are recruited by experimental tumors and promote

- cancer progression in mouse models,” *Cancer Research*, vol. 69, no. 12, pp. 5259–5266, 2009.
- [22] K. D. Garlid, M. Jabůrek, and P. Ježek, “The mechanism of proton transport mediated by mitochondrial uncoupling proteins,” *FEBS Letters*, vol. 438, no. 1–2, pp. 10–14, 1998.
- [23] W. McNeely and P. Benfield, “Orlistat,” *Drugs*, vol. 56, no. 2, pp. 241–249, 1998.
- [24] L. Sjöström, A. Rissanen, T. Andersen et al., “Randomised placebo-controlled trial of orlistat for weight loss and prevention of weight regain in obese patients,” *The Lancet*, vol. 352, no. 9123, pp. 167–172, 1998.
- [25] R. S. Padwal, S. K. Li, and D. C. W. Lau, “Long-term pharmacotherapy for obesity and overweight,” *Cochrane Database of Systematic Reviews*, no. 4, Article ID CD004094, 2003.
- [26] E. Saba, B. R. Jeon, D.-H. Jeong et al., “A novel Korean red ginseng compound gintonin inhibited inflammation by MAPK and NF- κ B pathways and recovered the levels of mir-34a and mir-93 in RAW 264.7 cells,” *Evidence-Based Complementary and Alternative Medicine*, vol. 2015, Article ID 6241132, 11 pages, 2015.
- [27] E. Saba, M. Irfan, D. Jeong et al., “Mediation of anti-inflammatory effects of Rg3-enriched red ginseng extract from Korean red ginseng via retinoid X receptor α -peroxisome-proliferating receptor γ nuclear receptors,” *Journal of Ginseng Research*, vol. 43, no. 3, pp. 442–451, 2019.
- [28] E. Saba, D. Jeong, M. Irfan et al., “Anti-inflammatory activity of Rg3-enriched Korean red ginseng extract in murine model of sepsis,” *Evidence-Based Complementary and Alternative Medicine*, vol. 2018, Article ID 6874692, 11 pages, 2018.
- [29] X. Zhi, J. Wang, P. Lu, J. Jia, H.-B. Shen, and G. Ning, “AdipoCount: a new software for automatic adipocyte counting,” *Frontiers in Physiology*, vol. 9, p. 85, 2018.
- [30] J. H. Stern, J. M. Rutkowski, and P. E. Scherer, “Adiponectin, leptin, and fatty acids in the maintenance of metabolic homeostasis through adipose tissue crosstalk,” *Cell Metabolism*, vol. 23, no. 5, pp. 770–784, 2016.
- [31] G. Hotamisligil, N. Shargill, and B. Spiegelman, “Adipose expression of tumor necrosis factor- α : direct role in obesity-linked insulin resistance,” *Science*, vol. 259, no. 5091, pp. 87–91, 1993.
- [32] V. Mohamed-Ali, “Subcutaneous adipose tissue releases interleukin-6, but not tumor necrosis factor- α , in vivo,” *Journal of Clinical Endocrinology & Metabolism*, vol. 82, no. 12, pp. 4196–4200, 1997.
- [33] P. Trayhurn and I. S. Wood, “Adipokines: inflammation and the pleiotropic role of white adipose tissue,” *British Journal of Nutrition*, vol. 92, no. 3, pp. 347–355, 2004.
- [34] Y. Minokoshi, Y.-B. Kim, O. D. Peroni et al., “Leptin stimulates fatty-acid oxidation by activating AMP-activated protein kinase,” *Nature*, vol. 415, no. 6869, pp. 339–343, 2002.
- [35] M. Fasshauer, J. Klein, S. Neumann, M. Eszlinger, and R. Paschke, “Hormonal regulation of adiponectin gene expression in 3T3-L1 adipocytes,” *Biochemical and Biophysical Research Communications*, vol. 290, no. 3, pp. 1084–1089, 2002.
- [36] K. Kitagawa, B. S. Rosen, B. M. Spiegelman, G. E. Lienhard, and L. I. Tanner, “Insulin stimulates the acute release of adipin from 3T3-L1 adipocytes,” *Biochimica et Biophysica Acta (BBA)—Molecular Cell Research*, vol. 1014, no. 1, pp. 83–89, 1989.
- [37] I. Szatmari, E. Rajnavolgyi, and L. Nagy, “PPAR, a lipid-activated transcription factor as a regulator of dendritic cell function,” *Annals of the New York Academy of Sciences*, vol. 1088, no. 1, pp. 207–218, 2006.
- [38] S. R. Farmer, “Transcriptional control of adipocyte formation,” *Cell Metabolism*, vol. 4, no. 4, pp. 263–273, 2006.
- [39] P. J. Smith, L. S. Wise, R. Berkowitz, C. Wan, and C. S. Rubin, “Insulin-like growth factor-I is an essential regulator of the differentiation of 3T3-L1 adipocytes,” *The Journal of Biological Chemistry*, vol. 263, no. 19, pp. 9402–9408, 1988.
- [40] Y. Dagon, E. Hur, B. Zheng, K. Wellenstein, L. C. Cantley, and B. B. Kahn, “p70S6 kinase phosphorylates AMPK on serine 491 to mediate leptin’s effect on food intake,” *Cell Metabolism*, vol. 16, no. 1, pp. 104–112, 2012.
- [41] A. Bartelt and J. Heeren, “Adipose tissue browning and metabolic health,” *Nature Reviews Endocrinology*, vol. 10, no. 1, pp. 24–36, 2014.
- [42] B. Cannon and J. Nedergaard, “Brown adipose tissue: function and physiological significance,” *Physiological Reviews*, vol. 84, no. 1, pp. 277–359, 2004.
- [43] Z. Li, H. J. Kim, M. S. Park, and G. E. Ji, “Effects of fermented ginseng root and ginseng berry on obesity and lipid metabolism in mice fed a high-fat diet,” *Journal of Ginseng Research*, vol. 42, no. 3, pp. 312–319, 2018.
- [44] G. Zheng, “Anti-obesity effects of three major components of green tea, catechins, caffeine and theanine, in mice,” *In Vivo*, vol. 18, no. 1, pp. 55–62, 2004.
- [45] Y. J. Park, “(-)-catechin-7-O- β -D-apiofuranoside inhibits hepatic stellate cell activation by suppressing the STAT3 signaling pathway,” *Cells*, vol. 9, no. 1, p. 30, 2020.
- [46] V. Aparna, K. V. Dileep, P. K. Mandal, P. Karthe, C. Sadasivan, and M. Haridas, “Anti-inflammatory property of *n*-hexadecanoic acid: structural evidence and kinetic assessment,” *Chemical Biology & Drug Design*, vol. 80, no. 3, pp. 434–439, 2012.
- [47] S. Saeidnia, “The story of beta-sitosterol—a review,” *European Journal of Medicinal Plants*, vol. 4, no. 5, pp. 590–609, 2014.
- [48] M. Kurano, K. Hasegawa, M. Kunimi et al., “Sitosterol prevents obesity-related chronic inflammation,” *Biochimica et Biophysica Acta (BBA)—Molecular and Cell Biology of Lipids*, vol. 1863, no. 2, pp. 191–198, 2018.

Research Article

Mode of Action of Shan-Zhu-Yu (*Cornus officinalis* Sieb. et Zucc.) in the Treatment of Depression Based on Network Pharmacology

Ping Liu ^{1,2}, Ping Yang ^{1,2} and Lan Zhang ¹

¹Department of Pharmacy, Xuanwu Hospital of Capital Medical University, National Clinical Research Center for Geriatric Diseases, Beijing Engineering Research Center for Nervous System Drugs, Beijing Institute for Brain Disorders, Key Laboratory for Neurodegenerative Diseases of Ministry of Education, Beijing 100053, China

²Department of Clinical Pharmacy, Key Laboratory of Basic Pharmacology of Guizhou Province and School of Pharmacy, Zunyi Medical University, Zunyi, Guizhou 563000, China

Correspondence should be addressed to Lan Zhang; xwzhanglan@126.com

Received 14 September 2020; Revised 21 October 2020; Accepted 24 October 2020; Published 23 November 2020

Academic Editor: Jie Liu

Copyright © 2020 Ping Liu et al. This is an open access article distributed under the Creative Commons Attribution License, which permits unrestricted use, distribution, and reproduction in any medium, provided the original work is properly cited.

Background. Although the traditional Chinese medicine Shan-Zhu-Yu may be efficacious against depression, its mechanism of action is unknown. In this study, we aimed to explore the possible mechanisms of action of Shan-Zhu-Yu in the treatment of depression using network pharmacology. **Methods.** The active ingredients and targets of Shan-Zhu-Yu were obtained from the Traditional Chinese Medicine System Pharmacology Database (TCMSP) database and converted into gene names using UniProt. Then, the target genes of depression were collected using GeneCards and OMIM. Drug disease intersection genes were obtained using a Venn tool, and a protein-protein interaction network was constructed using STRING. Cytoscape was used to construct an active ingredients-targets-drug-disease network. GO and KEGG pathway enrichment analyses were performed using DAVID. Furthermore, Autodock was used to evaluate drug and target binding and explore possible molecular mechanisms. **Results.** We identified 9721 disease genes, 13 active ingredients, 50 target genes, and 48 drug disease intersecting genes. The results of the GO enrichment analysis suggested that Shan-Zhu-Yu affects the activity of G protein-coupled amine, neurotransmitter, steroid hormone, nuclear, and G protein-coupled neurotransmitter receptors in the treatment of depression by acting on hormone and nuclear receptor binding. The main signaling pathways were associated with neuroactive ligand-receptor interaction, calcium, cGMP-PKG, apoptosis, estrogen, p53, and AGE-RAGE. Molecular docking confirmed that the active components of Shan-Zhu-Yu (e.g., telocinobufagin and β -sitosterol) docked suitably with *NR3C1*, *Bax*, *Bcl-2*, and *caspase-3*. Shan-Zhu-Yu may exert its therapeutic effects on depression via multiple targets and pathways. **Conclusions.** The present study elucidates that Shan-Zhu-Yu suppresses the expression of *Bax* and *caspase-3* and promotes that of *NR3C1* and *Bcl-2* through neuroactive ligand-receptor interaction and apoptosis signaling pathways. Therefore, Shan-Zhu-Yu is a potential treatment option for depression, and the results of this study will provide new reference points for future experimental research and a scientific basis for its widespread clinical application.

1. Introduction

Depression, a mood or affective mental disorder characterized by anxiety or depressive behaviors, can be caused by various factors. The main symptoms of depression include permanent low spirit, mental retardation, physical

discomfort, decreased volitional activity, and cognitive impairment, and the main clinical manifestations are low mood, lack of pleasure, decreased self-worth, and even suicidal thoughts [1]. In addition, depression is a risk factor for diabetes [2] and cardiovascular disease [3]. Murray and Lopez [4] in a 4.5 year Global Burden of Disease study

showed that unipolar major depression accounted for 3.7% of disability-adjusted life years (DALYs) in 1990, ranking the fourth, and predicted this to be up to 5.7% in 2020. In China, the prevalence of depression and DALY rates increased in all provinces [5]; however, the etiology and pathogenesis of depression remain unclear.

Depression, which is caused by a combination of genetic, environmental, and spiritual factors, involves neurotransmitters, inflammation, and hypothalamic pituitary adrenal (HPA) axis changes, among other processes [6]. Currently, negative treatment outcomes are common. The main clinical treatment of depression involves Western medicine, and the most widely used classic antidepressants are based on the “monoamine hypothesis” [7], which states that blocking the reuptake of catecholamine neurotransmitters at the pre-synaptic membrane effectively increases the concentration of catecholamine neurotransmitters in the synaptic cleft, thereby improving depressive symptoms. The antidepressants developed based on this theory include selective serotonin reuptake inhibitors and serotonin and norepinephrine reuptake inhibitors. Although these drugs are tolerated and cause only mild side effects, they have a single-target and slow onset [8]. Therefore, new effective drugs need to be developed; however, owing to the existence of various complex pathways and negative feedback regulation mechanisms in the nervous system [9], the development of more effective single-target drugs and monotherapies is difficult. In the future, multitarget and combination drugs will be essential in the treatment of depression [10].

Traditional Chinese medicine has unique advantages and potential in the treatment of depression. It has “theories” to understand the pathogenic mechanism and classify the syndrome [11]. Furthermore, traditional Chinese medicine, alone and in combination with Western medicine, has been shown to have a rapid onset, increase the cure rate, and reduce the incidence of side effects compared with Western medicine treatment alone; however, research on the mechanisms of action is warranted [12].

Shan-Zhu-Yu, the dried and mature pulp of *Cornus officinalis* Sieb. et Zucc., also known as fructus corni and jujube, is included in the Chinese Pharmacopoeia (2020), in sections related to the liver, kidney homeostasis, liver and kidney tonics, and astringent effects. This herb has a wide range of pharmacological activities, such as hepatic and renal protection, antidiabetic, cardioprotective, antioxidant, neuroprotective, antitumor, anti-inflammatory, analgesic, antiaging, anti-amnesic, anti-osteoporotic, antidepressive, and immunoregulatory effects [13]. For example, fructus corni-containing Liuwei Dihuang pills have been shown to improve depressive symptoms, reduce the incidence of adverse reactions, and improve the quality of life in patients with depression compared with Western medicine treatment alone [14] and exert antidepressant effects in rats under chronic mild stress [15]. Nonetheless, there is still a lack of systematic studies on the use of Shan-Zhu-Yu for the treatment of depression-like symptoms and its mechanism of action.

Although the multitarget and multichannel approach of traditional Chinese medicine can provide new ideas for the treatment of clinically complex diseases, it also increases the difficulty in research. Network pharmacology, a new approach for drug design based on the rapid development of systems biology and multidirectional pharmacology, goes beyond the *single target*. In network pharmacology, a *multitarget* research strategy, which has scalability, effectiveness, and reliability [16], is implemented for drug discovery. It is widely used to determine disease targets, the clinical efficacy of compounds, the mechanism of action, and toxicity, as well as the material basis and mechanism of action of traditional Chinese medicine [17, 18]. In this study, network pharmacology was used to screen biomarkers of depression and predict the therapeutic targets of Shan-Zhu-Yu, in the hope of providing ideas for basic research and treatment of depression.

2. Materials and Methods

2.1. Screening of Active Compounds and Prediction of Putative Targets of Shan-Zhu-Yu. We searched the Traditional Chinese Medicine System Pharmacology Database (TCMSP, <http://tcmssp.com/tcmssp.php>) using “Shan-Zhu-Yu” as the key word, selected the active ingredients with an oral bioavailability (OB) $\geq 30\%$ and drug-likeness (DL) ≥ 0.18 , and obtained their corresponding targets using “Related Targets [19]”. Next, the target names were input into the Universal Protein Database (UniProt, <https://www.uniprot.org/>), and *Homo sapiens* was selected to normalize the gene information.

2.2. Identification of Depression-Related Targets. Online Mendelian Inheritance in Man (OMIM, <https://omim.org/>) and GeneCards (<https://www.genecards.org/>) were used to obtain the related depression targets, and the results were summarized to remove duplicates.

2.3. Filtering Intersecting Targets. We imported the depression targets and putative targets of Shan-Zhu-Yu into a Venn tool (<http://bioinformatics.psb.ugent.be/webtools/Venn/>) to obtain intersecting targets.

2.4. Protein-Protein Interaction (PPI) Construction. The intersecting targets of Shan-Zhu-Yu and depression were input into STRING (<https://string-db.org/>) to generate a protein-protein interaction network. The minimum interaction score was set to 0.70, and the nodes that were not connected with the main network were hidden. The TSV file format was downloaded to construct an active ingredients-targets-drug-disease network with Cytoscape 3.2.1 software; the network in STRING is the PPI.

2.5. Gene Ontology (GO) and Kyoto Encyclopedia of Genes and Genomes (KEGG) Pathway Enrichment Analyses. We imported intersecting targets into the functional annotation tool of the Database for Annotation, Visualization and

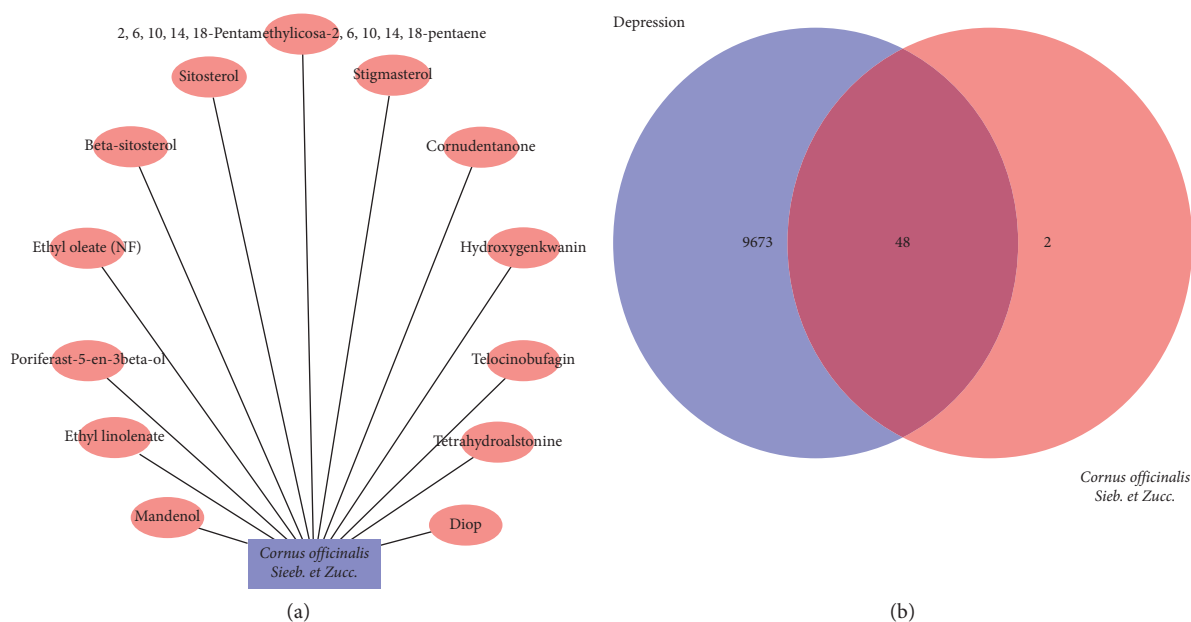


FIGURE 1: Shan-Zhu-Yu active ingredients and potential targets of treating depression. Shan-Zhu-Yu and its active ingredients (a). Intersecting genes Venn diagram of Shan-Zhu-Yu and treating depression (b).

TABLE 1: Intersecting genes of Shan-Zhu-Yu in treating depression.

| | SZY target genes |
|-------------------------------|---|
| Potential genes of depression | PTGS1, PTGS2, NCOA2, PGR, SCN5A, ADRB2, CHRM3, CHRM1, CHRM4, CASP3, NOS2, ADRA1A, CHRM2, ADRA1B, CHRNA2, SLC6A4, OPRM1, GABRA1, BCL2, BAX, CASP9, JUN, CASP8, PRKCA, PON1, MAP2, NR3C2, ADH1C, RXRA, NCOA1, ADRA2A, SLC6A2, SLC6A3, AKR1B1, PLAU, LTA4H, MAOB, MAOA, NR3C1, AR, PPARG, CHRM5, ADRA2C, OPRD1, ACHE, ADRA1D, ADRB1, KCNH2 |

Integrated Discovery (DAVID, <https://david.ncifcrf.gov/>) and used R 3.6.1 to produce simple and clear results [20].

2.6. Molecular Docking Simulation

2.6.1. Ligand Preparation. We used the PubChem database (<https://www.ncbi.nlm.nih.gov/pubmed>) to collect and download the 2D structure of small molecule compounds. These were saved in Mol2 format after energy minimization in Chem3D and PDBQT formats after setting as spin by AutoDockTools (ADT).

2.6.2. Target Protein Preparation. The crystal structures of nuclear receptor subfamily 3 group C member 1 (*NR3C1*) (PDBID: 1NHZ) and *caspase-3* genes (PDBID: 1NMS) were downloaded from the Protein Data Bank (<http://www.rcsb.org/>). As B-cell lymphoma 2 (*Bcl-2*) and Bcl-2-like protein 4 (*Bax*) have no crystal structure in the database, homology modeling was performed, UniProt was used to query the amino acid sequence, and the SWISS-MODEL server was used to model and evaluate quality. The downloaded complexes were embellished using PyMol1.7 to remove the original ligand and water molecules and saved in PDBQT format. Moreover, AutoDockTools-1.5.6 software was used to prepare receptors, including the addition of hydrogen and charge.

2.6.3. Molecular Docking. The prepared files were imported into Discovery Studio 3.5 Client software to search for active pockets. Telocinobufagin was set to dock with *NR3C1* and β -sitosterol with *Bax*, *Bcl-2*, and *caspase-3*. The lowest energy conformation was selected as the optimal for analysis. PyMol was used for dock site analysis, and Discovery Studio was used to analyze the interaction force between small molecule ligands and amino acid residues.

3. Results

3.1. Shan-Zhu-Yu Target Predictions. OB, which is a measure of the pharmacokinetic process and druggability *in vivo*, and DL, which represents the similarity between unknown components and the known chemical structure of drugs, are important parameters to analyze the effectiveness of traditional Chinese medicine [21]. The study combined $OB \geq 30\%$ and $DL \geq 0.18$ and identified 13 active ingredients (Figure 1(a)). In total, 50 genes were obtained after transforming with UniProt.

3.2. Potential Targets of Shan-Zhu-Yu in the Treatment of Depression. In the present study, 9721 genes were documented as potential targets of depression and 48 intersecting

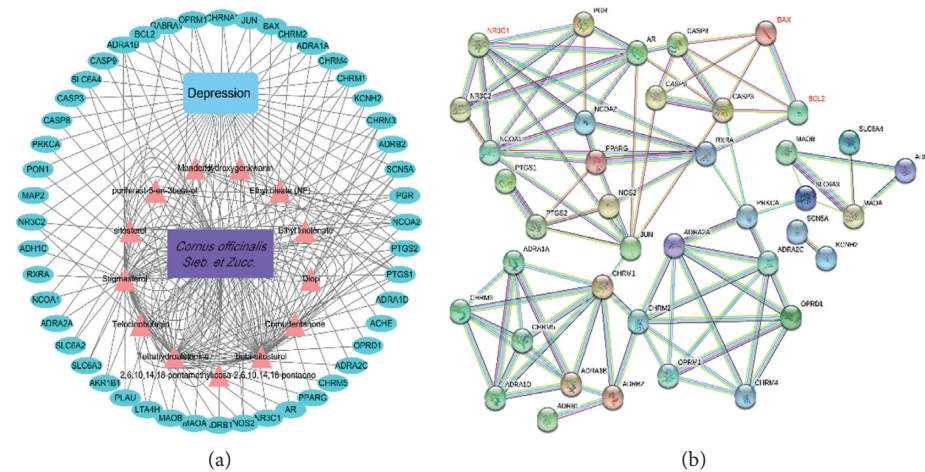


FIGURE 2: Active ingredients-targets-drug-disease network and PPI network. Purple rectangle node represents drug, orange triangle nodes represent active ingredients, blue rectangle node represents disease, and blue-green oval nodes represent target genes. (a) PPI network. Nodes represent genes, connections represent interactions, and different colored connections represent different types of interactions (b).

TABLE 2: Enriched genes in the biological processes.

| Description | <i>P</i> value | Enriched genes |
|--|------------------------|--|
| G protein-coupled amine receptor activity | 3.94×10^{-15} | ADRB2, CHRM3, ADRA1A, CHRM2, ADRA2A, ADRB1, ADRA2C, ADRA1D |
| Neurotransmitter receptor activity | 3.58×10^{-9} | CHRM3, CHRM1, CHRM2, CHRNA2, OPRM1, GABRA1, ADRB1 |
| Steroid hormone receptor activity | 7.58×10^{-9} | PGR, NR3C2, RXRA, NR3C1, AR, PPARG |
| Nuclear receptor activity | 1.65×10^{-7} | PGR, RXRA, NR3C1, AR, PPARG |
| Transcription factor activity, direct ligand regulated sequence-specific DNA binding | 1.65×10^{-7} | PGR, RXRA, NR3C1, AR, PPARG |
| G protein-coupled neurotransmitter receptor activity | 3.64×10^{-7} | CHRM3, CHRM2, OPRM1, ADRB1 |
| Protein heterodimerization activity | 8.30×10^{-7} | ADRA1A, ADRA1B, BCL2, BAX, JUN, RXRA, ADRA2A, ADRB1, PPARG, ADRA2C |
| Hormone binding | 2.87×10^{-6} | CHRM3, CHRNA2, NR3C1, AR, ACHE |
| Anion: cation symporter activity | 4.31×10^{-6} | SLC6A4, SLC6A2, SLC6A3 |
| Acetylcholine receptor activity | 4.31×10^{-6} | CHRM3, CHRM2, CHRNA2 |
| Catecholamine binding | 4.31×10^{-6} | ADRB2, ADRA2A, ADRA2C |
| Ammonium ion binding | 9.19×10^{-6} | CHRM3, CHRNA2, SLC6A4, ACHE |
| Adrenergic receptor binding | 1.32×10^{-5} | ADRA2A, ADRB1, ADRA2C |
| Nuclear receptor binding | 1.58×10^{-5} | NCOA2, RXRA, NCOA1 |
| Phosphatidylinositol phospholipase C activity | 1.87×10^{-5} | CHRM3, CHRM1, CHRM5 |
| Neurotransmitter: sodium symporter activity | 2.20×10^{-5} | SLC6A4, SLC6A2, SLC6A3 |
| Phospholipase C activity | 3.87×10^{-5} | CHRM3, CHRM1, CHRM5 |
| Chloride transmembrane transporter activity | 5.44×10^{-5} | SLC6A4, GABRA1, SLC6A2, SLC6A3 |
| Channel activity | 6.57×10^{-5} | SCN5A, KCNH2, CHRNA2, OPRM1, GABRA1, BCL2, BAX |
| Passive transmembrane transporter activity | 6.68×10^{-5} | SCN5A, KCNH2, CHRNA2, OPRM1, GABRA1, BCL2, BAX |

genes between Shan-Zhu-Yu and depression were obtained using the Venn online database (Table 1 and Figure 1(b)).

3.3. PPI Network Construction and Visualization. The 48 intersecting genes were input into the STRING network. The core genes were screened thoroughly, and 40 genes were identified. Using the Cytoscape software, the results were clearly obtained in the TSV file format (Figure 2(a)), and the PPI network was downloaded (Figure 2(b)). The PPI network revealed that the main active ingredients of Shan-Zhu-Yu in the treatment of depression are sitosterol,

beta-sitosterol, telocinobufagin, stigmasterol, DTOP, coronudentanone, 2,6,10,14,18-pentamethylcosa-2,6,10,14,18-pentaene, ethyl linolenate, hydroxygenkwanin, ethylolate, mandenol, and periferast-5-en-3-beta-ol.

3.4. GO and KEGG Pathway Enrichment Analyses. To further elucidate the mechanism of drug treatment systematically, enrichment analysis of the 48 intersecting genes was performed using DAVID. The top 20 GO items and KEGG pathways were selected based on *P* values, which represent the degree of enrichment. GO enrichment analysis

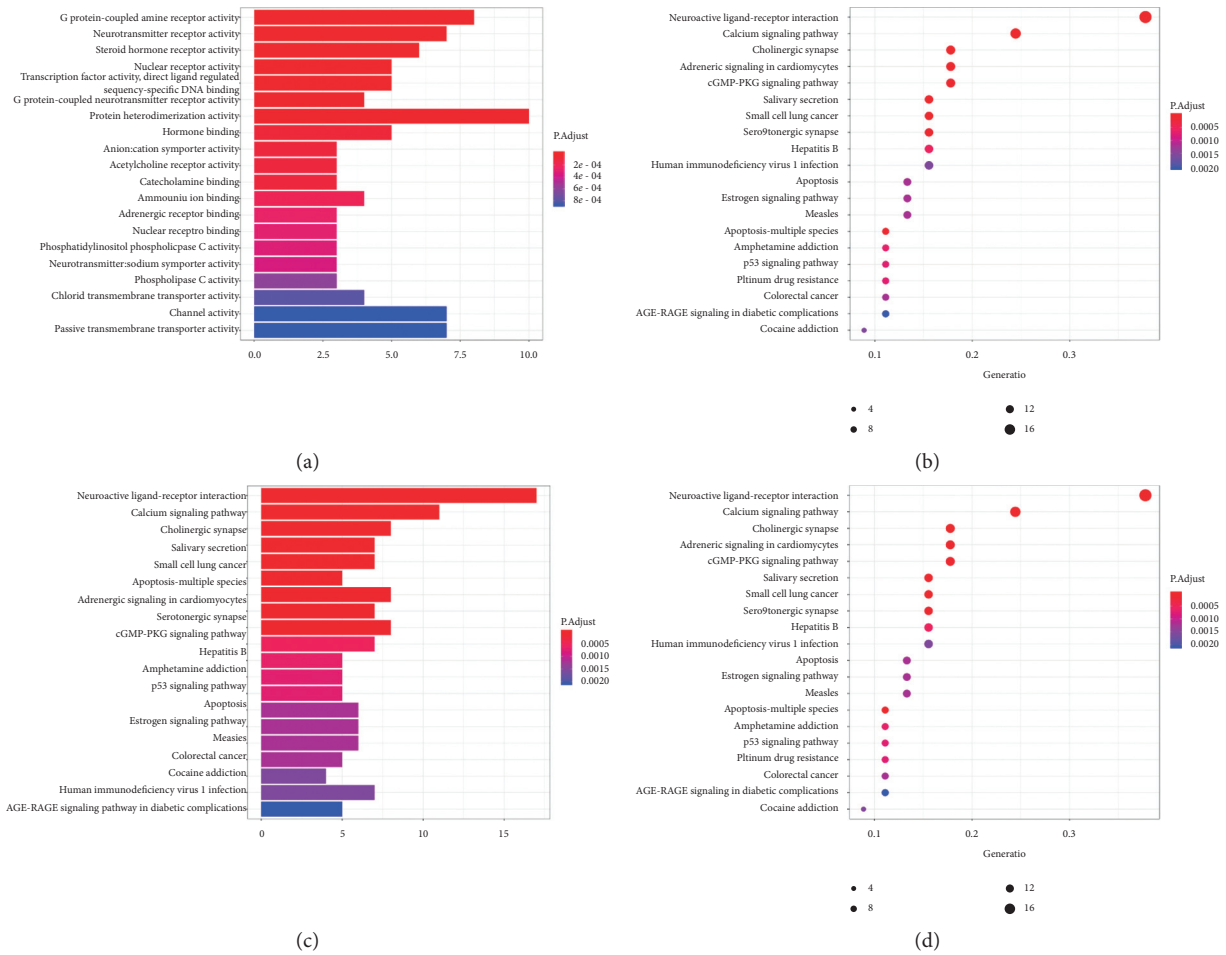


FIGURE 3: Enrichment analysis of intersecting genes (the top 20 terms of each part are shown). GO enrichment analysis (a). KEGG pathway analysis (b). The higher the column and the redder the color, the more the intersecting genes of enrichment; the sizes of the bubbles are illustrated from big to small in descending order of the number of the intersecting genes involved in the pathways.

describes the biological mechanisms of the drug in the treatment of diseases from three aspects: biological processes, molecular functions, and cellular components. Regarding biological processes, Shan-Zhu-Yu might affect the activity of G protein-coupled amine receptors, neurotransmitter receptors, steroid hormone receptors, nuclear receptors, G protein-coupled neurotransmitter receptors, protein heterodimerization, an acetylcholine receptor, and phosphatidylinositol phospholipase C in the treatment of depression by acting on hormone, catecholamine, and adrenergic receptors as well as nuclear receptor binding (Table 2 and Figure 3(a)). In the pathway analysis, 59 signal pathways were identified, which were mainly enriched in neuroactive ligand-receptor interaction, calcium, cGMP-protein kinase G, apoptosis, estrogen, p53, and advanced glycation end products-receptor for advanced glycation end products (Figure 3(b)).

3.5. Molecular Docking Analysis. The most important signaling pathway of Shan-Zhu-Yu in the treatment of depression was determined to be apoptosis. The genes enriched in the apoptosis pathway (Figure 4, granted permission already) include *Bax*, *Bcl-2*, and *caspase-3*; the major effective ingredient may be beta-sitosterol. Among the core genes, *NR3C1* (glucocorticoid receptor (GR); Figure 5, granted permission already) may regulate the apoptosis pathway; the ingredient that regulates *NR3C1* is telocinobufagin.

Molecular docking (Figure 6) was performed to study the interactions between active ingredients and target genes. The lower the energy of the molecule, the more stable the conformation.

We searched the UniProt Database and obtained the NRLBD domain of *NR3C1* protein, in which the gray part of the structure interacts with CRY1. The optimal conformation

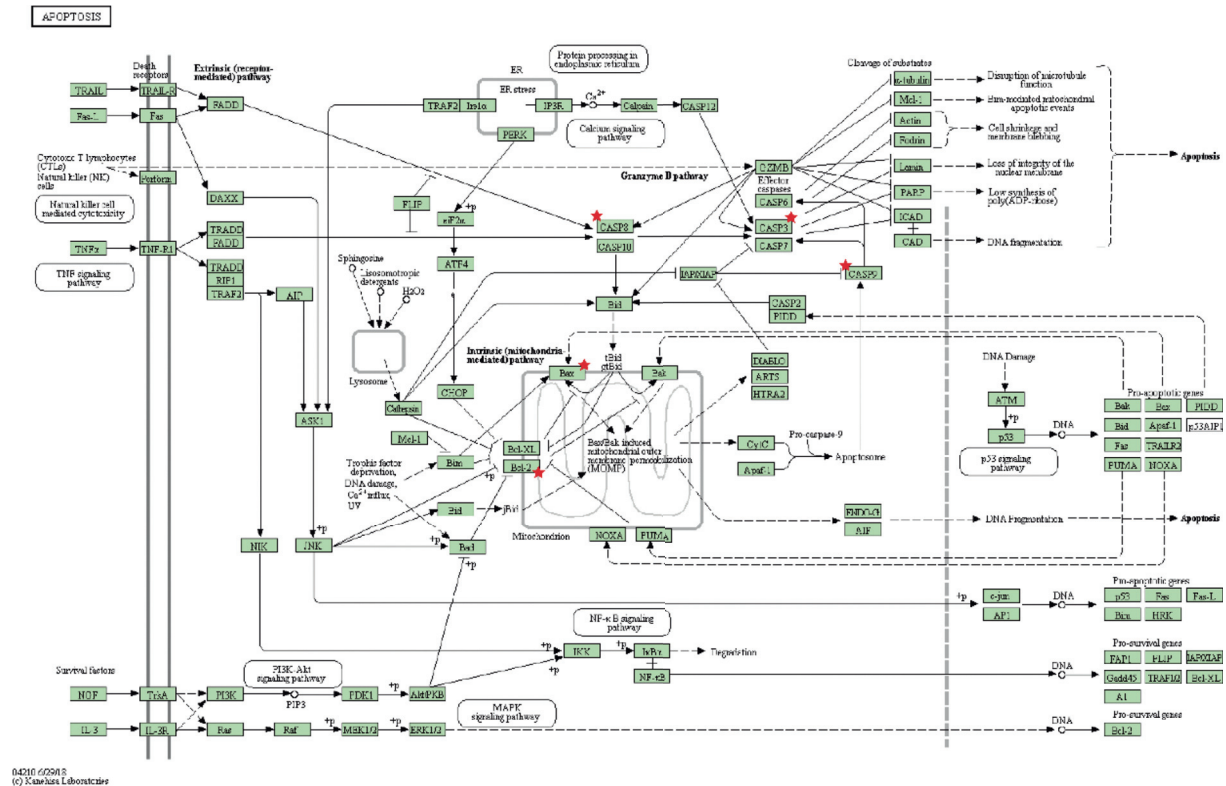


FIGURE 4: Apoptosis signaling pathway. The genes with a five-pointed star are potential target for Shan-Zhu-Yu in treating depression predicted by network pharmacology.

of telocinobufagin binds to the active pocket of the nuclear receptor ligand-binding domain of *NR3C1*; the lowest binding free energy is -9.43 kcal/mol, and the main forces involved are van der Waals forces, hydrophobic forces, and carbon-hydrogen bonds.

The optimal conformation of beta-sitosterol binds with *Bax*; the secondary structure of the green region is a randomly coiled domain, and small molecule is bound in the pocket near the random coil domain of the *Bax* protein; the lowest binding free energy is -7.9 kcal/mol, and the main forces are van der Waals forces, hydrophobic forces, and carbon hydrogen bonds.

The docking results show that the optimal conformation of the beta-sitosterol is bound between the random coil and BH4 of the *Bcl-2* protein, the lowest binding free energy is -8.21 kcal/mol, and there are alkyl hydrophobic forces between Pro88, Pro59, and Leu86 and beta-sitosterol. Hydroxyl hydrogen atoms form a conventional hydrogen bond with Gly8 and carbon-hydrogen bond with Tyr9. Thr74, Ser87, Asp10, and Val89 form van der Waals forces with each other.

The crystal structure of *caspase-3* was downloaded from UniPort. The optimal conformation of beta-sitosterol was bound between p12 and p17 subunits, and the lowest binding free energy was -7.16 kcal/mol (Table 3).

4. Discussion

In the present study, network pharmacology methods were used to explore possible targets and mechanisms of Shan-Zhu-Yu in the treatment of depression. Using TCMSP, 13 active ingredients of Shan-Zhu-Yu with $OB \geq 30\%$ and $DL \geq 0.18$ were identified, and using GeneCards and OMIM, 9721 disease-related genes were identified. Using a Venn tool, 48 drug-disease intersecting genes were identified, which are the potential targets for Shan-Zhu-Yu in the treatment of depression. A PPI network was constructed with 40 genes, and active ingredients that may affect depression were determined. GO enrichment analysis identified 97 genes, and KEGG enrichment analysis identified 59 pathways involved although only the top 20 are shown owing to space limitations. Genes involved in the neuroactive ligand-receptor interaction signaling pathway and apoptosis signaling pathway are likely related to the pathological mechanism of depression; therefore, genes in these pathways are key targets for the treatment of depression. Additionally, the connection between these pathways in depression may be a focus in the study of depression [22].

Depression is caused by multiple factors [23], and studying the relationship between factors is essential to clarify the pathogenesis of depression. High levels of

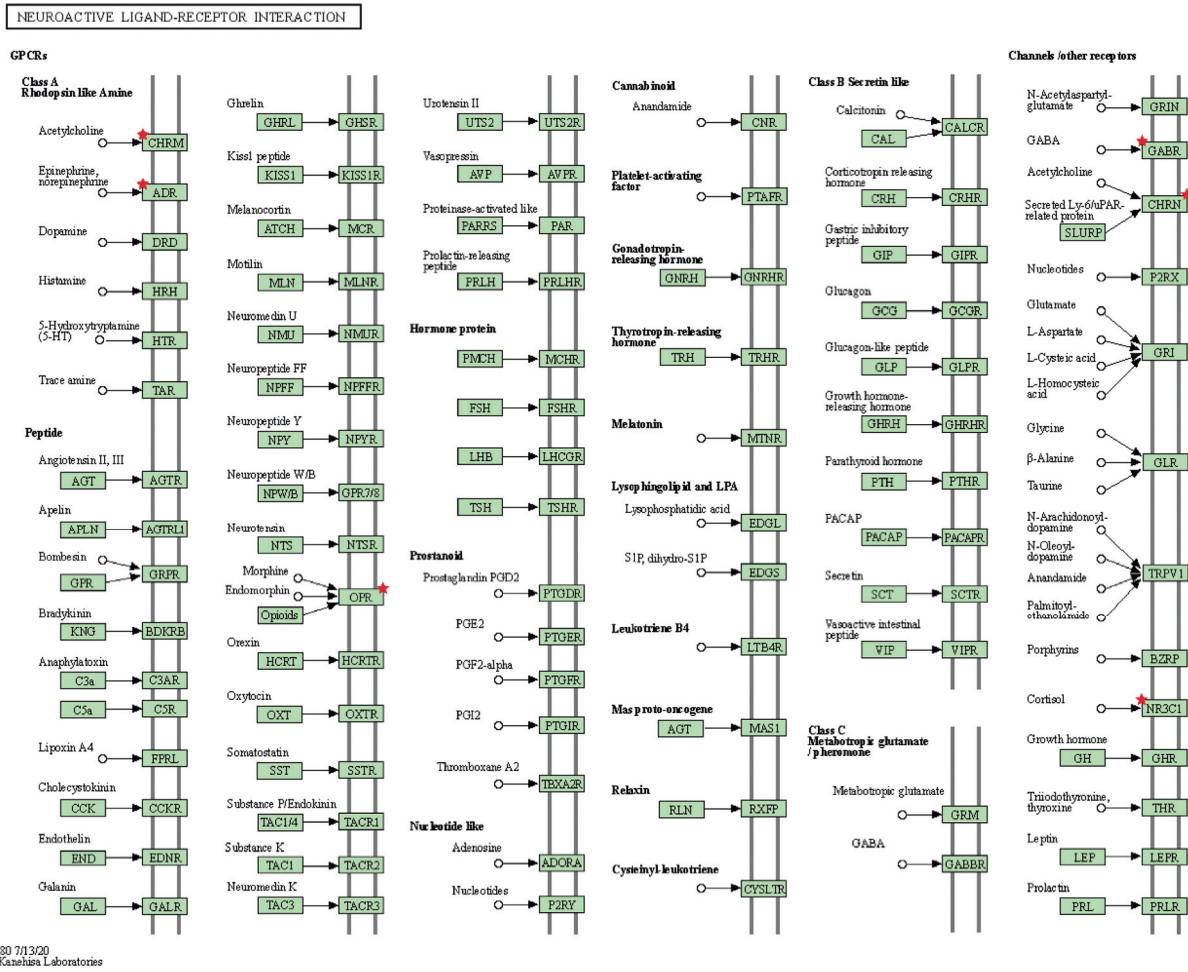


FIGURE 5: Neuroactive ligand-receptor interaction signaling pathway. The genes with a five-pointed star are potential targets for Shan-Zhu-Yu in treating depression predicted by network pharmacology.

glucocorticoids can induce neuronal death, weaken hippocampal neurogenesis, damage the normal function of the HPA axis, and cause depression-like behavior [24], and GR is a major mediator of glucocorticoids. In patients with depression, the expression of GR and GR mRNA in multiple brain regions (especially in the hippocampus) is reduced [25] and NR3C1 is abnormally methylated [26]. Furthermore, NR3C1, which encodes GR, is related to affective disorders, and any abnormalities in NR3C1 affect the function and activity of GR, thereby leading to disorders of the neuroendocrine system [27]. Moreover, NR3C1 down-regulation promotes the expression of micro-RNA-22, which results in the increased expression of downstream genes, namely, Bcl-2-associated agonist of cell death, Bax, and caspase-3, and decreased expression of Bcl-2 and Bcl-xL, thereby promoting cell apoptosis [22].

In addition, Shan-Zhu-Yu extract can increase the ratio of Bcl-2/Bax and reduce the expression of caspase-3 in the

damaged cortex; increase the levels of nerve growth factor and brain-derived neurotrophic factor in the chronic phase; enhance the expression of synaptophysin I, synaptophysin, and postsynaptic density protein 95; inhibit brain trauma apoptosis regulation in the chronic phase [28]; and regulate the level of corticosterone [29], all could play a neuro-protective effect. Molecular docking showed that telocinobufagin and beta-sitosterol, the active ingredients of Shan-Zhu-Yu, can act on NR3C1, Bax, and Bcl-2 to treat depression.

Cinnabar (HgS) is a mineral in traditional Chinese medicine for sedation and antianxiety [30, 31]. Shan-Zhu-Yu has various pharmacological effects, including antidepressant effects, when used alone and as a component in antidepressant recipes, such as Liuwei Dihuang pills [13, 15]. Shan-Zhu-Yu could also work with other traditional medicines, such as cinnabar (HgS) to exert better beneficial effects on the brain.

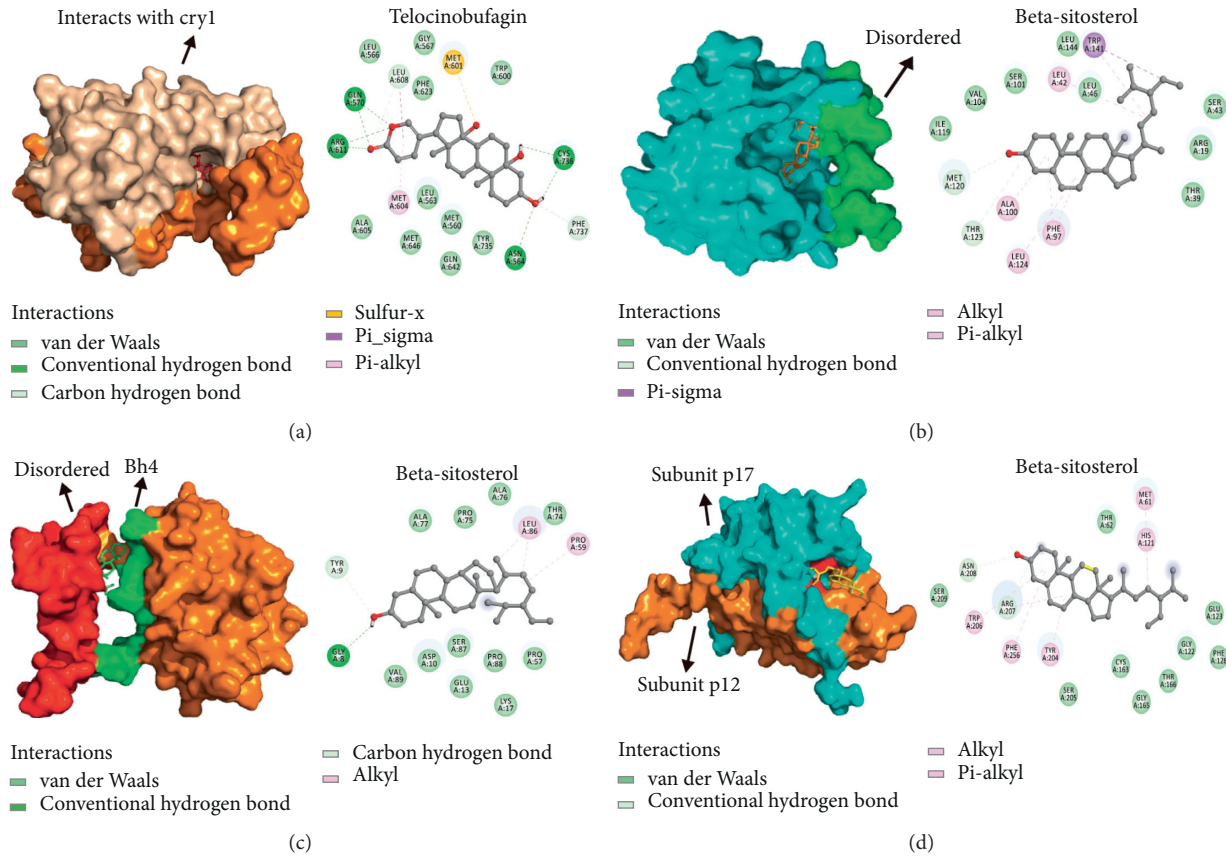


FIGURE 6: Docking conformation of active ingredients and potential targets. Telocinobufagin and NR3C1 (a); beta-sitosterol and Bax (b). The secondary structure of the green region is random coils, near which small molecules are bound; Bcl-2 (c); beta-sitosterol and caspase-3 (d). The cyan and brown parts are subunit p17 and subunit p12 domains, respectively. The red part is the two key amino acid residues, His121 and 163Cys, in the active center of caspase-3.

TABLE 3: Molecular docking results.

| Compound | Compound 2D structure | Target and PDB ID | Structure with initial ligand | Grid box size | Affinity (kcal/mol) |
|---------------------------------|---|---------------------------|-------------------------------|---------------|---------------------|
| Telocinobufagin (CAS: 472-26-4) | <chem>O=C1OC(=O)C=C1C23CC4C(=O)CC(O)C4(C)CC23</chem> | NR3C1 (1NHZ) | | 80*80*80 | -9.43 |
| Beta-sitosterol (CAS: 83-46-5) | <chem>CC(C)CC(C)C[C@H]1CC[C@@H]2[C@@]1(CC[C@H]3[C@H]2CC=C4[C@@]3(CC[C@@H](C4)O)C)C</chem> | Bax (homology modeling) | | 90*90*90 | -7.9 |
| | | Bcl-2 (homology modeling) | | 70*70*70 | -8.21 |
| | | Caspase-3 (1NMS) | | 90*90*90 | -7.16 |

Currently, there are few *in vivo* and *in vitro* studies of Shan-Zhu-Yu in the treatment of depression. Therefore, related research should be developed, which can provide insights into the application of Shan-Zhu-Yu for depression treatment. The results of this study can lay the foundation for research of Shan-Zhu-Yu in treating depression and its mechanism. *Nevertheless, there is also a limitation to this study. Network pharmacology is a research based on database and literature; thus, some action pathways are not selected or some irrelevant pathways are selected and unguided conclusions are obtained owing to the imperfection of selection methods, parameter settings, and calculation models. Overcoming this limitation will render this method more practical, help in better drug mechanism research, and even aid in the development of new drugs and disease treatments.*

5. Conclusion

In summary, network pharmacological analysis showed that there are as many as 48 possible targets for Shan-Zhu-Yu in the treatment of depression. The active ingredients, telocinobufagin and beta-sitosterol, may play an important role in the antidepressant effect of Shan-Zhu-Yu via the GR and apoptosis pathway. A signaling pathway comprising *NR3C1* and its downstream genes *Bax*, *Bcl-2*, and *caspase-3* could be one of the possible mechanisms. Therefore, the results of this study provide evidence for follow-up research and a basis for the clinical application of Shan-Zhu-Yu and its prescriptions in the treatment of depression.

Data Availability

The data used to support the findings of this study are included within the article.

Conflicts of Interest

The authors declare that they have no conflicts of interest.

Acknowledgments

The authors wish to thank Kanehisa Laboratories for granting permission to publish the KEGG pathway map. The authors wish to thank the timely help of Editage Insights Ltd. with language touchups. This study was supported by the Beijing Hospitals Authority Ascent Plan (DFL20190803) and Capital Science and Technology Leading Talent Training Project (Z191100006119017).

References

- [1] P. Willner, J. Scheel-Kruger, and C. Belzung, "The neurobiology of depression and antidepressant action," *Neuroscience & Biobehavioral Reviews*, vol. 37, no. 10, pp. 2331–2371, 2013.
- [2] K. Semenkovich, M. E. Brown, D. M. Svrakic, and P. J. Lustman, "Depression in type 2 diabetes mellitus: prevalence, impact, and treatment," *Drugs*, vol. 75, no. 6, pp. 577–587, 2015.
- [3] D. N. Silverman and S. J. Shah, "Treatment of heart failure with preserved ejection fraction (HFpEF): the phenotype-guided approach," *Current Treatment Options in Cardiovascular Medicine*, vol. 21, no. 4, p. 20, 2019.
- [4] C. J. L. Murray and A. D. Lopez, "Evidence-based health policy--lessons from the global burden of disease study," *Science*, vol. 274, no. 5288, pp. 740–743, 1996.
- [5] X. Ren, S. Yu, W. Dong, P. Yin, X. Xu, and M. Zhou, "Burden of depression in China, 1990-2017: findings from the global burden of disease study 2017," *Journal of Affective Disorders*, vol. 268, pp. 95–101, 2020.
- [6] G.-J. Peng, J.-S. Tian, X.-X. Gao, Y.-Z. Zhou, and X.-M. Qin, "Research on the pathological mechanism and drug treatment mechanism of depression," *Current Neuropharmacology*, vol. 13, no. 4, pp. 514–523, 2015.
- [7] S. Boku, S. Nakagawa, H. Toda, and A. Hishimoto, "Neural basis of major depressive disorder: beyond monoamine hypothesis," *Psychiatry and Clinical Neurosciences*, vol. 72, no. 1, pp. 3–12, 2018.
- [8] X.-M. Liao, Y.-A. Su, Y. Wang, X. Yu, and T.-M. Si, "Antidepressant treatment strategy with an early onset of action improves the clinical outcome in patients with major depressive disorder and high anxiety," *Chinese Medical Journal*, vol. 133, no. 6, pp. 726–728, 2020.
- [9] R. N. Gunn and E. A. Rabiner, "Imaging in central nervous system drug discovery," *Seminars in Nuclear Medicine*, vol. 47, no. 1, pp. 89–98, 2017.
- [10] G. R. Villas Boas, R. Boerngen de Lacerda, M. M. Paes et al., "Molecular aspects of depression: a review from neurobiology to treatment," *European Journal of Pharmacology*, vol. 851, pp. 99–121, 2019.
- [11] L.-Y. Liu, B. Feng, J. Chen et al., "Herbal medicine for hospitalized patients with severe depressive episode: a retrospective controlled study," *Journal of Affective Disorders*, vol. 170, pp. 71–77, 2015.
- [12] W. Xue, X. Zhou, N. Yi et al., "Yueju pill rapidly induces antidepressant-like effects and acutely enhances BDNF expression in mouse brain," *Evidence-Based Complementary and Alternative Medicine*, vol. 2013, Article ID 184367, 2013.
- [13] J. Huang, Y. Zhang, L. Dong et al., "Ethnopharmacology, phytochemistry, and pharmacology of *Cornus officinalis* Sieb. et Zucc.," *Journal of Ethnopharmacology*, vol. 213, pp. 280–301, 2018.
- [14] J. Wang and S. Lu, "Observation on therapeutic effect of Liuwei Dihuang Pills on neurosis and menopausal depression," *Huaihai Medicine*, vol. 17, no. 1, p. 47, 1999.
- [15] M. Kang, D. Shin, J.-W. Oh et al., "The anti-depressant effect of Nelumbinis semen on rats under chronic mild stress induced depression-like symptoms," *The American Journal of Chinese Medicine*, vol. 33, no. 2, pp. 205–213, 2005.
- [16] A. L. Hopkins, "Network pharmacology: the next paradigm in drug discovery," *Nature Chemical Biology*, vol. 4, no. 11, pp. 682–690, 2008.
- [17] S. Li and B. Zhang, "Traditional Chinese medicine network pharmacology: theory, methodology and application," *Chinese Journal of Natural Medicines*, vol. 11, no. 2, pp. 110–120, 2013.
- [18] W. Guo, J. Huang, N. Wang et al., "Integrating network pharmacology and pharmacological evaluation for deciphering the action mechanism of herbal formula zuojin pill in suppressing hepatocellular carcinoma," *Frontiers in Pharmacology*, vol. 10, p. 1185, 2019.
- [19] J. Ru, P. Li, J. Wang et al., "TCMSP: a database of systems pharmacology for drug discovery from herbal medicines," *J Cheminform*, vol. 6, p. 13, 2014.

- [20] A. Masoudi-Nejad, S. Goto, T. R. Endo, and M. Kanehisa, "KEGG bioinformatics resource for plant genomics research," *Plant Bioinformatics*, vol. 406, pp. 437–458, 2007.
- [21] X. Xu, W. Zhang, C. Huang et al., "A novel chemometric method for the prediction of human oral bioavailability," *International Journal of Molecular Sciences*, vol. 13, no. 6, pp. 6964–6982, 2012.
- [22] Q. Fu, C.-J. Liu, X. Zhang et al., "Glucocorticoid receptor regulates expression of microRNA-22 and downstream signaling pathway in apoptosis of pancreatic acinar cells," *World Journal of Gastroenterology*, vol. 24, no. 45, pp. 5120–5130, 2018.
- [23] G. S. Malhi and J. J. Mann, "Depression," *The Lancet*, vol. 392, no. 10161, pp. 2299–2312, 2018.
- [24] A. L. Lee, W. O. Ogle, and R. M. Sapolsky, "Stress and depression: possible links to neuron death in the hippocampus," *Bipolar Disorders*, vol. 4, no. 2, pp. 117–128, 2002.
- [25] Y.-T. Lin, T.-Y. Liu, C.-Y. Yang et al., "Chronic activation of NPFRR2 stimulates the stress-related depressive behaviors through HPA axis modulation," *Psychoneuroendocrinology*, vol. 71, pp. 73–85, 2016.
- [26] P. O. McGowan, A. Sasaki, A. C. D'Alessio et al., "Epigenetic regulation of the glucocorticoid receptor in human brain associates with childhood abuse," *Nature Neuroscience*, vol. 12, no. 3, pp. 342–348, 2009.
- [27] S. Ceulemans, S. De Zutter, L. Heyrman et al., "Evidence for the involvement of the glucocorticoid receptor gene in bipolar disorder in an isolated northern Swedish population," *Bipolar Disorder*, vol. 13, no. 7-8, pp. 614–623, 2011.
- [28] D. Ma, N. Wang, X. Fan et al., "Protective effects of cornel iridoid glycoside in rats after traumatic brain injury," *Neurochemical Research*, vol. 43, no. 4, pp. 959–971, 2018.
- [29] W. Tian, J. Zhao, J.-H. Lee et al., "Neuroprotective effects of *Cornus officinalis* on stress-induced hippocampal deficits in rats and H₂O₂-induced neurotoxicity in SH-SY5Y neuroblastoma cells," *Antioxidants (Basel)*, vol. 9, no. 1, 2019.
- [30] Q. Wang, X. Yang, B. Zhang, X. Yang, and K. Wang, "Cinnabar is different from mercuric chloride in mercury absorption and influence on the brain serotonin level," *Basic & Clinical Pharmacology & Toxicology*, vol. 112, no. 6, pp. 412–417, 2013.
- [31] Q. Wang, X. Yang, B. Zhang, X. Yang, and K. Wang, "The anxiolytic effect of cinnabar involves changes of serotonin levels," *European Journal of Pharmacology*, vol. 565, no. 1-3, pp. 132–137, 2007.

Research Article

Potential Molecular Target Prediction and Docking Verification of Hua-Feng-Dan in Stroke Based on Network Pharmacology

Ping Yang ^{1,2}, Haifeng He,² Shangfu Xu,¹ Ping Liu ^{1,2} and Xinyu Bai ¹

¹Key Laboratory of Basic Pharmacology of Ministry of Education and Joint International Research Laboratory of Ethnomedicine of Ministry of Education, Zunyi Medical University, Zunyi 563000, China

²Department of Clinical Pharmacy, Key Laboratory of Basic Pharmacology of Guizhou Province and School of Pharmacy, Zunyi Medical University, Zunyi, Guizhou 563000, China

Correspondence should be addressed to Ping Liu; lpuiung@163.com and Xinyu Bai; bxyspu@163.com

Received 5 September 2020; Revised 12 October 2020; Accepted 15 October 2020; Published 28 October 2020

Academic Editor: Lixin Wei

Copyright © 2020 Ping Yang et al. This is an open access article distributed under the Creative Commons Attribution License, which permits unrestricted use, distribution, and reproduction in any medium, provided the original work is properly cited.

Objective. Hua-Feng-Dan (HFD) is a Chinese medicine for stroke. This study is to predict and verify potential molecular targets and pathways of HFD against stroke using network pharmacology. **Methods.** The TCMSP database and TCMID were used to search for the active ingredients of HFD, and GeneCards and DrugBank databases were used to search for stroke-related target genes to construct the “component-target-disease” by Cytoscape 3.7.1, which was further filtered by MCODE to build a core network. The STRING database was used to obtain interrelationships by topology and to construct a protein-protein interaction network. GO and KEGG were carried out through DAVID Bioinformatics. Autodock 4.2 was used for molecular docking. BaseSpace was used to correlate target genes with the GEO database. **Results.** Based on $OB \geq 30\%$ and $DL \geq 0.18$, 42 active ingredients were extracted from HFD, and 107 associated targets were obtained. PPI network and Cytoscape analysis identified 22 key targets. GO analysis suggested 51 cellular biological processes, and KEGG suggested that 60 pathways were related to the antistroke mechanism of HFD, with p53, PI3K-Akt, and apoptosis signaling pathways being most important for HFD effects. Molecular docking verified interactions between the core target (CASP8, CASP9, MDM2, CYCS, RELA, and CCND1) and the active ingredients (beta-sitosterol, luteolin, baicalein, and wogonin). The identified gene targets were highly correlated with the GEO biosets, and the stroke-protection effects of Xuesaitong in the database were verified by identified targets. **Conclusion.** HFD could regulate the symptoms of stroke through signaling pathways with core targets. This work provided a bioinformatic method to clarify the antistroke mechanism of HFD, and the identified core targets could be valuable to evaluate the antistroke effects of traditional Chinese medicines.

1. Introduction

Hua-Feng-Dan (HFD) is a classical Chinese medicine preparation for the treatment of neurological disorders since the Ming dynasty. After more than 370 years of historical inheritance, it is listed as the National Protection Heritage in 1950 and is still in clinical use today. HFD consists of *Aconitum coreanum* (Bai Fu Zi), *Arum ternatum* Thunb. (Ban Xia), *Arisaema erubescens* (Tian Nan Xing), *Aconiti Radix* (Chuan Wu), *Curcumae Radix* (Yu Jin), *Gastrodia elata* (Tian Ma), *Nepeta cataria* (Jing Jie), *Atractylodes japonica* (Cang Shu), *Perilla frutescens* (Zi Su), *Crotonis fructus* (Ba Dou), *Moschus moschiferus* (She

Xiang), *Borneolum syntheticum* (Bing Pian), and *Santalum album* L. (Tan Xiang). HFD also contains cinnabar, realgar, and other minerals. As a famous traditional Chinese medicine, it has excellent therapeutic effects on stroke, hemiplegia, epilepsy, mouth-eye crookedness, and other head wind and encephalopathy. It is recorded in “Yi Fang Ju Lei,” “Ying Tong Bai Wen,” etc.

Modern pharmacological studies have shown that HFD has a protective effect on a variety of central nervous system injury and neuroinflammation models. HFD protects mice from bacterial lipopolysaccharide (LPS) plus neurotoxin MPTP toxicity [1] and ameliorates LPS plus pesticide rotenone-induced neuroinflammation and

dopaminergic neuron loss in rats [2]. HFD also has modulatory effects on gut microbiota (submitted), which are in line with the clinical experience and theory of traditional Chinese medicines.

Chinese herbal medicine preparations are composed of many different compounds with various structures and functions, and all components act together on multiple targets instead of a specific target to achieve therapeutic effects and to reduce toxicity. Some of the components act as the main medicine (JUN), some as secondary medicine (Zou), some as complementary medicine (Chen), and some as guide-drug (Shi) [3]. HFD is such an example, and the traditional recipe of HFD is more effective than the modified (removing cinnabar and/or realgar) recipe in protecting against LPS-induced neuroinflammation in neuron/microglia cultures [4] and in animals [2]. Thus, to illustrate the antistroke mechanism of HFD more systematically and comprehensively, this research intends to analyze and expound the potential molecular mechanisms of HFD based on system pharmacology. As an emerging discipline, systems pharmacology includes many disciplines such as systems biology, systems pharmacology/toxicology, computational biology, and network analysis, which break the traditional framework (drug-target-disease) to a multilevel network (disease-phenotype-gene-drug) and explore the correlation between drugs and diseases from the perspective of wholeness and systematic view, corresponding to the theory of holistic view and dialectical treatment of traditional Chinese medicine [5, 6].

In this work, the active molecules in HFD were identified that transcend the physiological barriers and interact with the network targets. We aim to use a comprehensive network pharmacology-based approach to investigate the mechanisms of how HFD exerts therapeutic effects on stroke, and the built network was further verified by correlating with the GEO database of antistroke Chinese medicine.

2. Materials and Methods

2.1. Establishment of a Database of HFD Target Genes and Stroke-Related Genes. Through the Traditional Chinese Medicine Systems Pharmacology (TCMSP) database (<https://tcmssp.com/tcmssp.php>) [7] and the Traditional Chinese Medicines Integrated Database (TCMID) (<http://119.341.228:8000/tcmid/>) [8], the components and target genes of 13 Chinese herbal medicines of HFD were retrieved from two databases satisfying the criteria of oral bioavailability (OB) greater than or equal to 30% and drug-likeness (DL) greater than or equal to 0.18% [9, 10]. Stroke-related genes were collected through the GeneCards database (<https://www.genecards.org/MyGenes/>) and the DrugBank database (<https://www.drugbank.ca/>) using the keyword “Stroke.”

2.2. Establishment of Ingredients and Chinese Herbal Medicines Network. Candidate potential ingredients and herbals of HFD were retrieved and screened from TCMSP retrieved and TCMID database. All the ingredients and their quantitative targets were visualized analysis using Cytoscape 3.7.1 software [11].

2.3. Intersection Target Constructions of HFD and Stroke. HFD targets and stroke targets were transferred to uniform generic names through the UniProt database (<https://www.uniprot.org/>). The “Draw Venn Diagram” online tool (<http://bioinformatics.psb.ugent.be/webtools/Venn/>) was used to input the previously collected HFD genes and stroke genes to achieve common genes [12].

2.4. Construction of the Ingredient-Target-Disease Interaction Network of HFD and Stroke. The previously collected active ingredients were combined, and the frequent targets of HFD and stroke were visually analyzed using Cytoscape 3.7.1 software.

2.5. Constructions of the Protein-Protein Interaction (PPI) Network Map. The previously collected common targets were entered into the STRING online database (<https://string-db.org/>), the species were selected as “Homo sapiens,” and the obtained “tsv” file was imported into Cytoscape 3.7.1 software for further analysis of the core network.

2.6. Core Network Constructions. In the previously obtained “tsv” file, the top twenty-two targets were selected in the number of nodes, and the “R” 4.0.2 software was run to draw a histogram. Then, the obtained “tsv” file was imported into Cytoscape 3.7.1 software. The MCODE plug-in was run to analyze the core network, and the network ranked first was selected for the next analysis [13].

2.7. GO and KEGG Pathway Enrichment Analysis. DAVID online database (<https://david.ncicrf.gov/>) was used to perform gene ontology (GO) and Kyoto Encyclopedia of Genes and Genomes (KEGG) pathway enrichment analysis to reflect the biological process, molecular function, cellular component, and pathway of HFD in the treatment of stroke. The results are displayed in a bar chart or bubble chart. The smaller the p value is, the higher the degree of enrichment is; the larger the count is, the more genes are enriched on it [14].

2.8. Molecular Docking. First, the top 6 core target genes were selected, and the compounds that might regulate these targets were reviewed. The two-dimensional (2D) structure diagrams of these compounds were downloaded through the PubChem database and imported into the Chem3D software to draw three-dimensional structure diagrams and optimize energy and save them in mol2 format. Then, the files were imported into AutoDockTools-1.5.6 software to add the charge and display rotatable keys and then saved in pdbqt format. Next, the protein crystal structures corresponding to the core target genes were downloaded from the PDB database, imported into PyMOL software to remove water molecules and heteromolecules, imported into AutoDockTools-1.5.6 software to add hydrogen atoms, saved in pdbqt format, and imported into Discovery Studio 3.5 Client software to search for active pockets. Finally, the compound

is used as a ligand, and the protein corresponding to the core target gene is used as a receptor for molecular docking. PyMOL software and Discovery Studio 3.5 Client were used to analyze and interpret the results.

2.9. Correlation with the GEO Database. BaseSpace Correlation Engine (BSCE) (<https://www.illumina.com/products/by-type/informatics-products/basespace-correlationengine.html>; formerly NextBio) is an RNA sequencing and microarray database curated over 23,000 scientific studies to get data-driven answers for genes, experiments, drugs, and phenotypes for the research. The 26 key targets analyzed by the MCODE plug-in were individually input into BSCE for curated studies, followed by filtering with the keyword “stroke” and then combined as the “template.” Using “Chinese medicine” and “stroke” for curated studies, there is one study using Xuesaitong against MOCA-induced stroke in mice with two biosets and a summary p value by the Running Fisher test. The $-\log(p$ value) was calculated and VLOOKUP with the “template” to make a correlation. This method provides a correlation of the overlapping genes between DEGs and biosets curated in BSCE [15]. Biosets that were positively correlated with the DEGs were predicted to produce similar effects, either directly or indirectly; the larger the $-\log(p$ value), the higher the degree of similarity. Biosets that were negatively correlated with DEG were predicted to produce opposite effects. The Treeview 1.6 (https://download.cnet.com/TreeView/3000-2352_4-75666005.html) was used to visualize differences [16,17].

The multistep strategy flow chart in Figure 1 was constructed to explain the method of the manuscript.

3. Results and Analysis

3.1. HFD Active Ingredients and Chinese Herbal Medicine Network. The 13 Chinese herbal medicines of HFD were searched through the TCMSP and TCMID databases, and there were 42 active ingredients that met the screening conditions ($OB \geq 30\%$, $DL \geq 0.18$), including 3 in *Typhonii rhizoma*, 10 in *Arum ternatum* Thunb, 5 in *Aconiti Radix*, 3 in *Curcumae Radix*, 3 in *Crotonis fructus*, 1 in *Borneolum syntheticum*, 5 in *Atractylodes lancea* (Thunb.) Dc, 9 in *Schizonepetae herba*, 1 in *Moschus moschiferus*, 3 in *Santalum album* L., 4 in *Gastrodia elata*, 5 in *Arisaematis rhizoma*, and 11 in *Perilla frutescens* as shown in Figure 2.

3.2. Intersection Targets of HFD and Stroke. According to the 42 active ingredients of HFD, 121 targets were retrieved in the TCMSP database. 7408 and 49 targets were achieved by searching for “Stroke” in GeneCards and DrugBank databases, respectively. The targets obtained above were entered into the Venn database to obtain a common target, as shown in Figure 3. 106 targets were intersected by HFD and GeneCards and 15 targets were intersected by HFD and DrugBank. A total of 107 targets were analyzed for the next step.

3.3. Ingredient-Target-Disease Interaction Network of HFD and Stroke. The 42 active ingredients of HFD collected before and 107 intersection genes of HFD and stroke were imported into Cytoscape 3.7.1 software for visual analysis. As shown in Figure 4, green is the active ingredient and purple is the target, showing the active ingredient direct relationship network with target diseases and HFD.

3.4. Core Network. The previously collected 107 common targets were entered into the STRING online database, the species were selected as “Homo sapiens,” and the obtained “tsv” file was imported into Cytoscape 3.7.1 software, as shown in Figure 5(a) (one target has not connected with others, which cannot be displayed). The 22 targets in pink are the first-ranked core networks analyzed by the MCODE plug-in. The 22 targets are entered into the Cytoscape 3.7.1 software to show the network relationship, as shown in Figure 5(b). The “tsv” file was used to run the “R” 4.0.2 software to draw a histogram, and the first 20 targets of the number of nodes were selected to display as shown in Figure 5(c).

3.5. Constructions of the Protein-Protein Interaction (PPI) Network Map. The 22 core targets selected by the MCODE plug-in were entered into the STRING database for PPI network analysis (Figure 5(d)). There were 22 nodes and 194 edges in the PPI network, and the average node degree is 17.6, the number of the expected edges is 56, the average local clustering coefficient is 0.887, and the PPI enrichment p value is $<1.0e-16$. Besides, in all the nodes in Figure 5, the darker the color is, the more important it was.

3.6. GO Analysis and KEGG Pathway Enrichment Analysis. R language was used for GO analysis and KEGG analysis. Based on the DAVID database, it was used to analyze the core intersection genes of HFD and stroke. Go analysis includes a biological process (BP), cell composition (CC), and molecular function (MF). Fifty-one significant changes in biological processes were screened, and the top 20 were displayed as bar graphs (Figure 6(a)). KEGG pathway enrichment analysis screened 60 signal pathways with significant enrichment of core genes, of which the top 20 were selected and represented by a bubble chart (see Figure 6(b)).

3.7. Verification of the Interaction between Active Ingredients and Target Genes. Through in-depth analysis, the three most important signaling pathways, apoptosis, phosphatidylinositol-3 kinase (PI3K)/AKT, and P53 signaling pathway, were selected. The genes enriched in the abovementioned pathways include 14 genes in the core genes, in which the six genes were in two or more of the pathways (Figure 7(a)). The top 6 core target genes trace ingredients back to 9 (Figure 7(b)), and 9 kinds of herbs contain these ingredients (Figure 7(c)).

Molecular docking was used for verification of the interaction between active ingredients and target genes. The results obtained by the molecular docking software are shown in

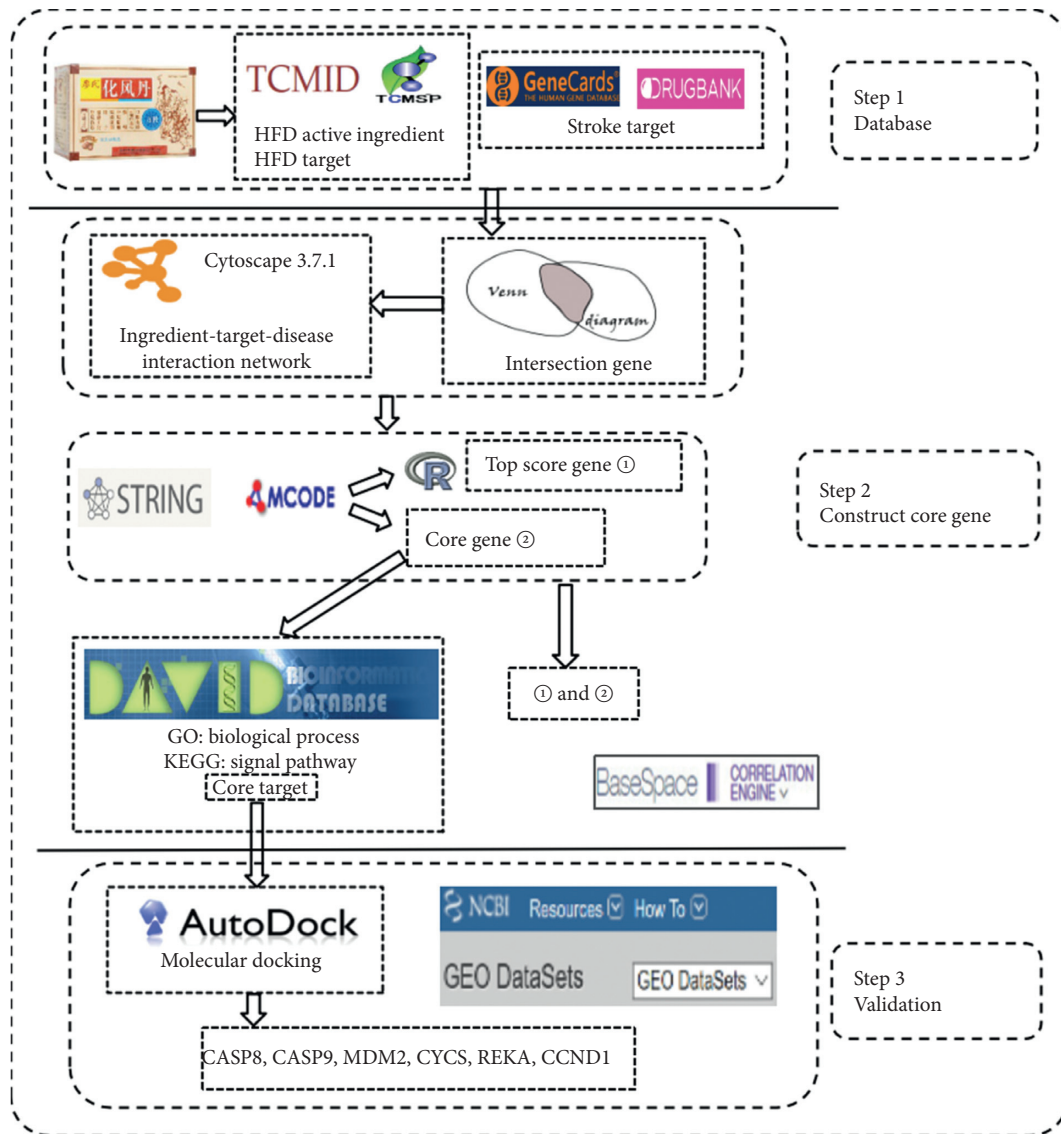


FIGURE 1: Technological road-map of HFD.

Supplementary Table 1. From the results, the lowest binding free energy of beta-sitosterol and caspase-8 was -8.64 kcal/mol. There are Alkyl/Pi-Alkyl hydrophobic interactions between Ile257, His317, Cys360, and beta-sitosterol. Among them, His317 and Cys360 belong to the active site of the caspase-8 protein. In addition, there were three hydrogen bonds: Lys253, Tyr324, Asp319, and beta-sitosterol; there was van der Waals force between Asp363, Gln358, Arg260, Arg413, Tyr412, and beta-sitosterol. On the other hand, the lowest binding free energy of beta-sitosterol and caspase-9 was -9.0 kcal/mol, and there are hydrophobic interactions between His237, Cys287, Arg178, Arg180, Phe351, Pro357, and beta-sitosterol. His237 and Cys287 are the key amino acid residues in the active site of the caspase-9 protein. There are van der Waals interactions between Thr179, Thr181, Lys358, Ser183, Ser361, Asp186, Gln285, Gly182, and beta-sitosterol (Figure 8(a)). The lowest binding free energy of luteolin and MDM2 was -6.97 kcal/mol, there were 9 hydrogen bond forces between Tyr100, His96,

Ile19, Gln18, Gln24, and luteolin, and there was a carbon-hydrogen bond between Ile99 and luteolin. In addition, there was a Pi-Cation hydrophobic force between His96 and luteolin, and there is a Pi-Sigma hydrophobic force between Leu54 and luteolin (Figure 8(b)). The lowest binding free energy of baicalein and CyCS was -7.35 kcal/mol, and there were Pi-Sigma and Pi-Alkyl hydrophobic interactions between Ile81, Lys72, Pro71, and baicalein. At the same time, 6 hydrogen bonds are established between baicalein and Lys72, Phe82, and Val83. There are also carbon-hydrogen bonds between Ile81, Asn70, and Pro71 and baicalein. The lowest binding free energy of baicalein and Rela was -7.01 kcal/mol, and there were 8 hydrogen bonds between Ser97, Ile95, Arg93, His96, Cys90, and baicalein. In addition, there were Pi-Pi/Pi-Alkyl hydrophobic interactions between Tyr85, Lys78, and baicalein. Gln99, Asn100, Phe98, Leu89, and baicalein had van der Waals forces (Figure 8(c)). The lowest binding free energy of luteolin and CCND1 was -7.35 kcal/mol. Leu65, Ala187, His158, and Pro79

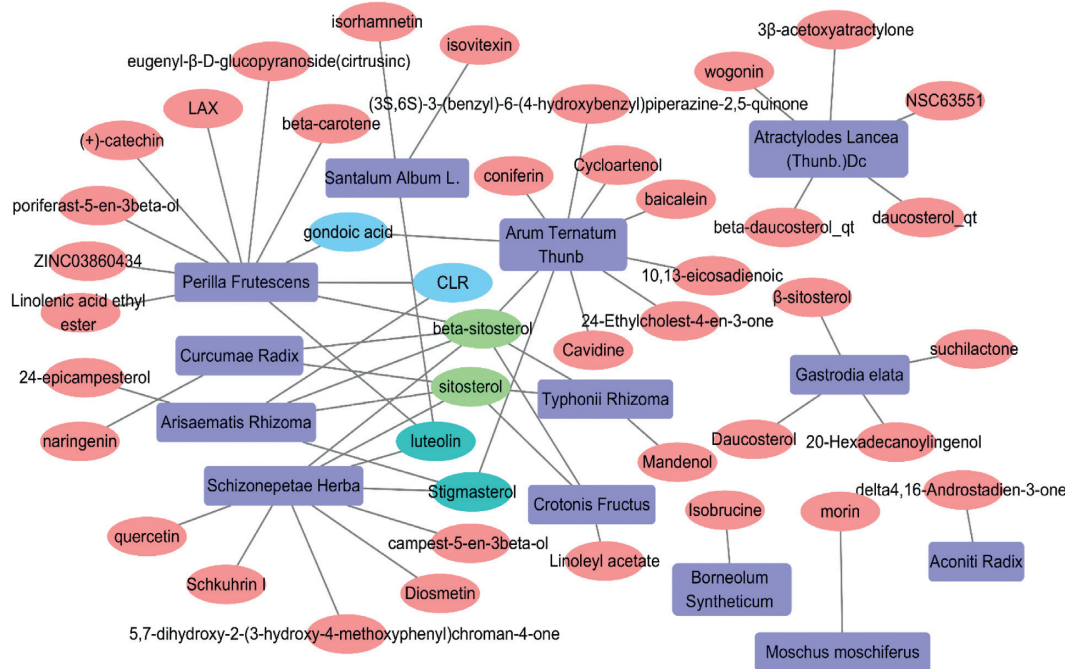


FIGURE 2: HFD active ingredients and Chinese herbal medicine network.

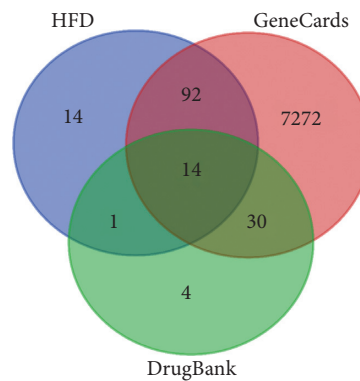


FIGURE 3: Intersection targets' Venn diagram of HFD and stroke.

had hydrophobic interactions with luteolin. There were 6 hydrogen bonding forces between Cys68, Cys73, Val77, Glu74, Phe78, Glu75 and luteolin. Glu69, Lys72, Thr184, and luteolin also have van der Waals forces (Figure 8(d)).

3.8. Correlation with GEO Database. Figure 9 shows 26 core gene targets from Figures 5(b) and 5(c) in correlation with the GEO curated database (keyword: stroke) based on the MOCA stroke model [17] (GSE61616). The selected 26 targets were highly correlated with brain stroke database across curated studies (Figure 9). Xuesaitong treatment reversed all of these changes, indicating that these molecules were valid biomarkers for the therapeutic effects of Chinese medicine against stroke. The correlation of $-\log(p\text{-values}) > 4$ or < -4 with the 26 gene targets in 153 gene biosets (17 GSE studies) except for Igf2 (2.92) was provided as Supplementary Table 2D.

4. Discussion

In this study, the active ingredients and potential targets of HFD in the treatment of stroke were studied through network pharmacology. 42 active substances were identified by TCMSP and TCMID ($OB \geq 30\%$, $DL \geq 0.18$); 107 targets were identified with GeneCards and DrugBank. MCODE screened out 22 target genes. STRING constructed 194 Edges in PPI, GO analyzed 51 biological processes, and KEGG enriched 60 significantly related pathways. Molecular docking of 6 targets with 4 active ingredients provided an in-depth analysis of network pharmacology. In addition, the 26 targets from Figures 5(b) and 5(c) were highly correlated with the GEO database, and the antistroke effects of Xuesaitong in the database were verified with these targets. It suggests that the key genes screened in this study may become a potential biomarker for evaluating stroke severity and stroke treatment efficacy of Chinese medicines.

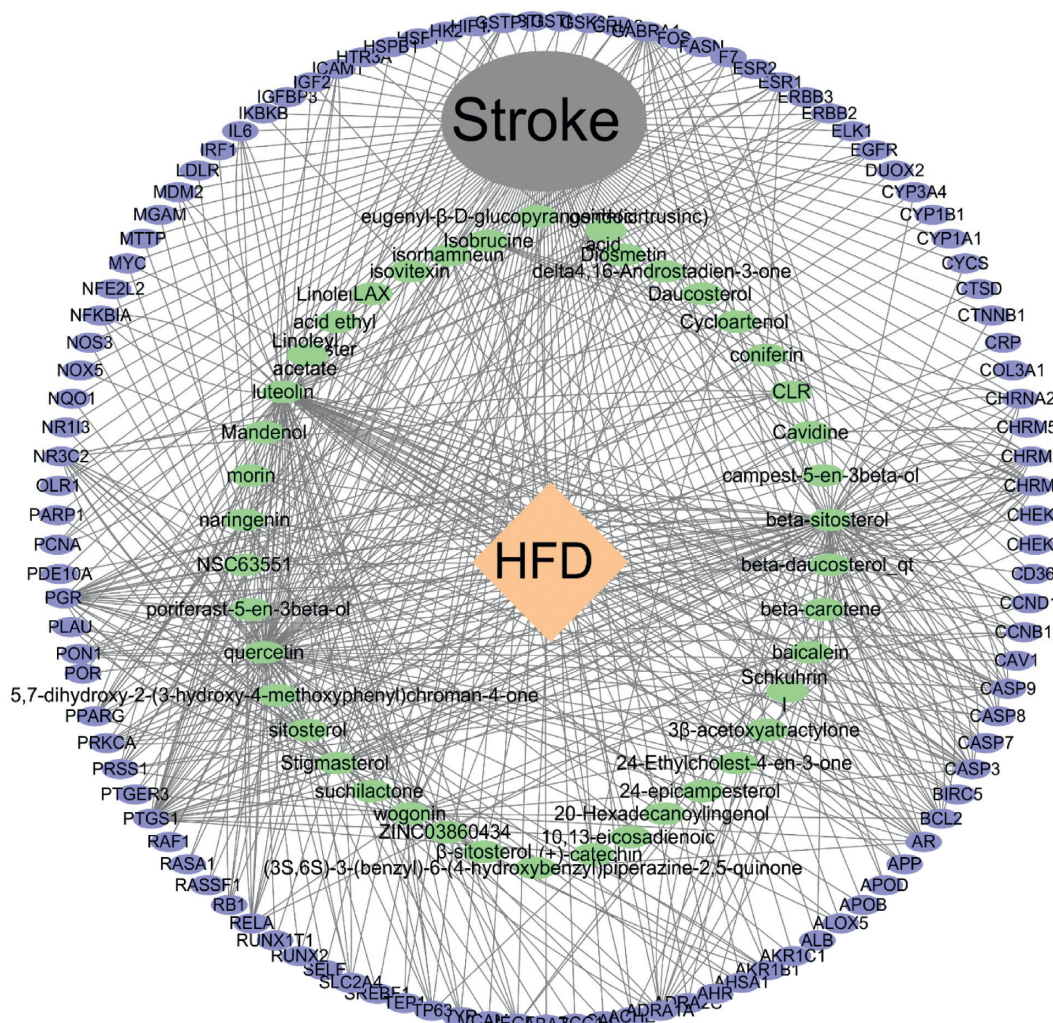


FIGURE 4: Ingredient-target-disease interaction network of HFD and stroke.

Since its creation in the Ming Dynasty, HFD has played an important role in the improvement of stroke and post-stroke symptoms. The formulation of HFD has been continuously improved; for example, through the fermentation, the macromolecules could be degraded into small molecular substances by microorganisms to improve the bioavailability, and the processing by the “Shui-Fei method” is important to reduce the toxicity of heavy metals such as cinnabar and realgar. In recent years, studies have demonstrated that the safety of HFD is different from environmental mercury and arsenic compounds [18–21]. However, the mechanism of HFD has not been fully elucidated.

Due to the complexity of the components of traditional Chinese medicine, it is difficult to fully discuss the mechanism of HFD in the treatment of brain diseases through the point-to-point research model of “the animal model-signal pathway,” which requires a lot of tedious work and away from the theory of traditional medicine. Network pharmacology studies may provide a novel approach by constructing a drug-target-disease network from the perspective of the intersection of drugs and disease regulation, through

the analysis of the action network, the representative active ingredients are screened, and the target genes are verified by molecular docking, to reveal the active ingredients and mechanism of HFD action in stroke prevention and treatment.

In this study, the HFD recipe was first screened by TCMSP and TCMID database, and 13 herbs and 42 ingredients were obtained. Subsequently, 107 interactions with GenCard and DrugBank were found. The core network was obtained through Cytoscape analysis, which contained 22 genes. Typically, the core gene is considered a key role, so we have shown up core gene (Figure 5(b)), STRING constructed 194 Edges in PPI, we selected the intersection of the largest gene interactions which are 26 genes (Figures 5(b) and 5(c)), and the genes screened by the two methods are highly similar, suggesting that the analysis results are more accurate.

GO analyzed 51 biological processes, and KEGG enriched 60 significantly related pathways. In the KEGG analysis, the 3 most important signal pathways were selected through in-depth analysis: apoptosis, phosphatidylinositol-3 kinase (PI3K)/AKT, and P53 signaling pathway. Multiple

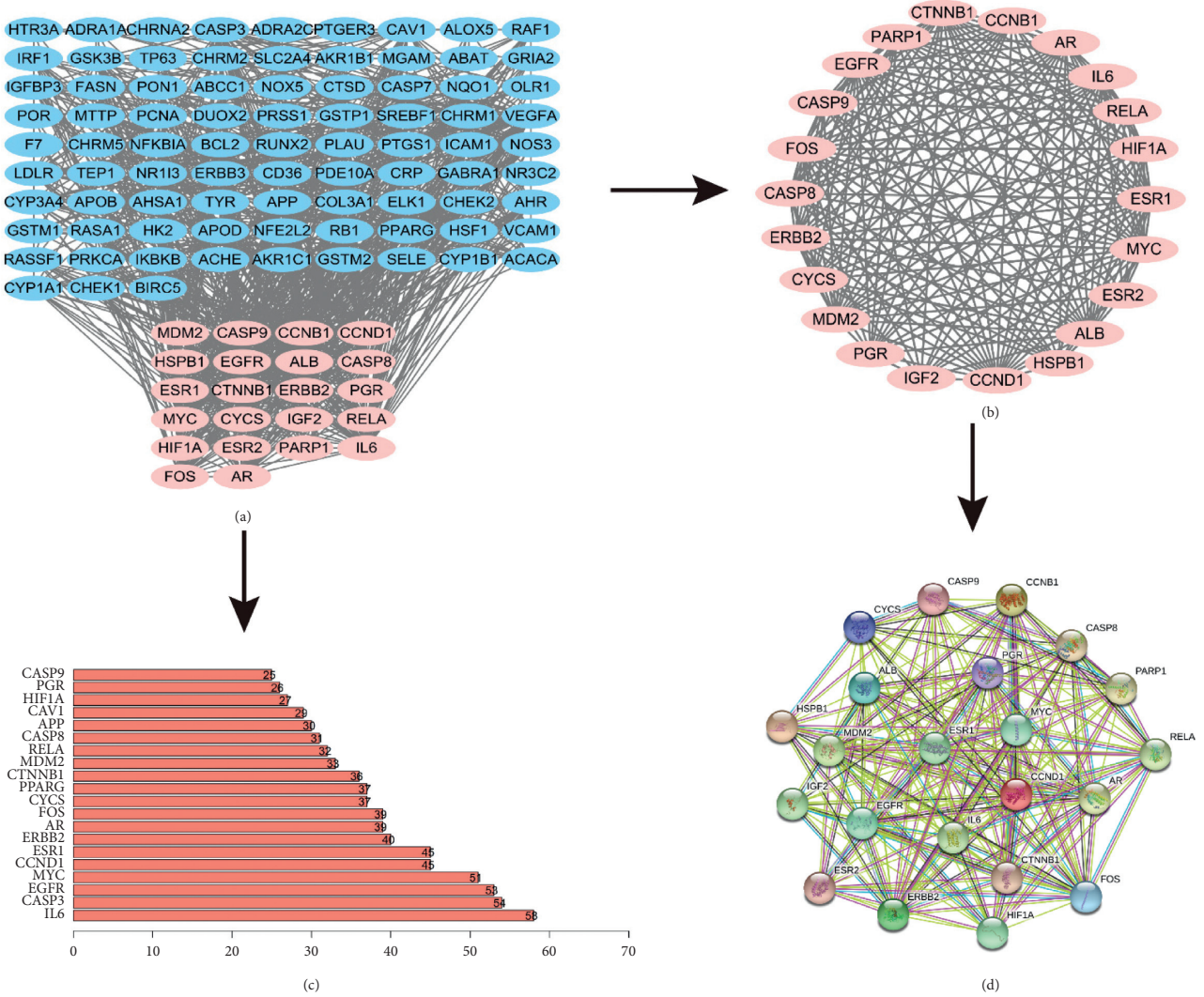


FIGURE 5: Analysis of core genes at the intersection of HFD regulatory genes and stroke target genes. HFD regulatory gene and stroke target gene intersection (a). Core genes of HFD and stroke (b). Barplot statistical results of the interaction between HFD and stroke regulatory genes (c). PPI network of core gene corresponding protein (d).

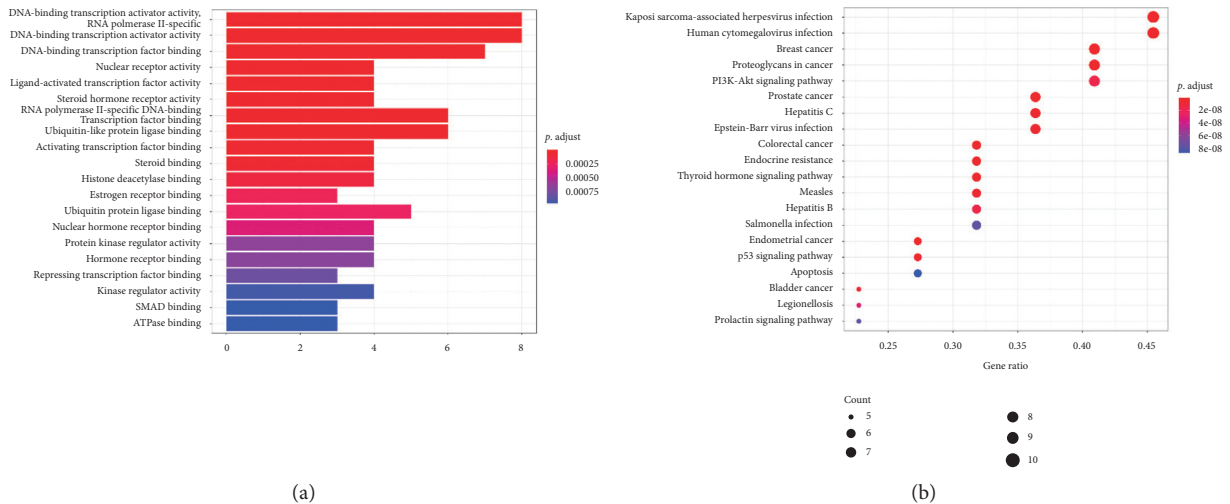


FIGURE 6: Enrichment analysis. GO analysis of HFD and stroke target genes (a). KEGG analysis of HFD and stroke target genes (b).

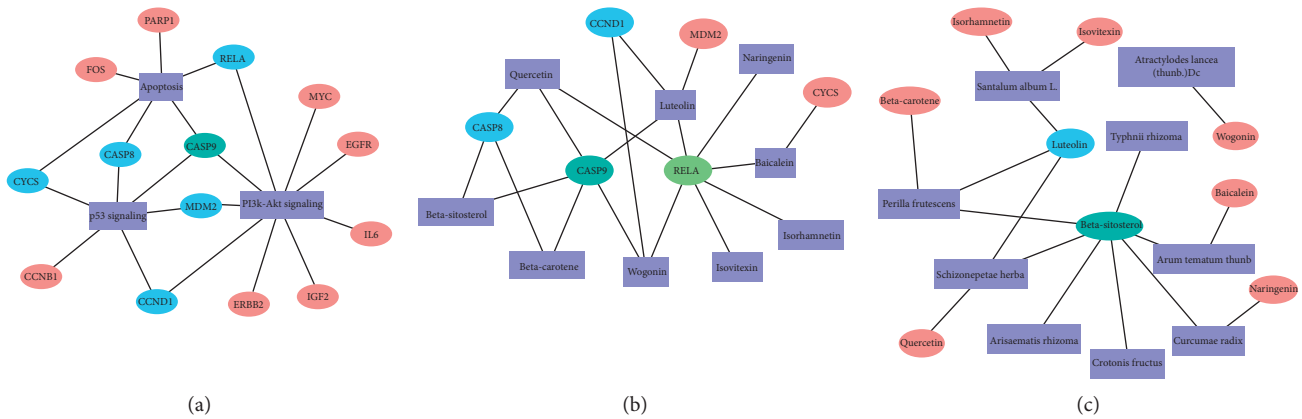


FIGURE 7: Key signaling pathways and target genes of HFD and stroke intersection genes (a). Key target genes and ingredients of HFD and stroke intersection genes (b). Key ingredients and Herbal medicine of HFD and stroke intersection genes (c).

studies have confirmed that apoptosis is initiated in stroke. Caspase-3, caspase-8, and caspase-9 are important members of the caspase family; upon receipt of specific stress, cytochrome c released by mitochondria will combine with procaspase-9/Apaf-1 to activate and cleave caspase-9 [22]. The cleaved caspase-9 further processes other caspase members, initiates the caspase cascade, and then initiates apoptosis [23]. Activated caspase-8 synergistically cleaves and activates the caspase of downstream effector molecules, such as caspase-1, caspase-3, caspase-6, and caspase-7, and amplifies the apoptosis signal [24]. PI3K/Akt signaling pathway participates in various cellular processes, and the activation of the pathway has been revealed to be implicated in the occurrence and development of angiogenesis, which negatively modulates genes that promote thrombogenicity, vascular permeability, and inflammation, and thereby protects vascular function [25]. RelA, one of the nuclear transcription factor κ B (NF- κ B)/Rel families, plays an important role in inflammation and immune response, which may be a PI3K-AKT regulatory signal, which in turn regulates the apoptosis pathway [26]. On the other hand, multiple studies have confirmed that drugs can improve stroke symptoms by regulating the PI3K/Akt pathway [27]. Studies have also reported that PI3K/Akt regulates cell apoptosis, and activation of the PI3K/Akt pathway after stroke plays a protective role in neuronal apoptosis [25]. Under pathological conditions of stroke, p53 plays an important role in the regulation of apoptosis and cell cycle [28]. The increased level of Cyclin chaperone D (cyclin D) levels affects the process of cells entering the S phase under the regulation of P53 [9]. The degradation of P53 hinders its role in the regulation of apoptosis [29]. MDM2 is the ubiquitin ligase of p53 and plays a central role in regulating the stability of p53. Akt mediates the phosphorylation of MDM2 at Ser166 and Ser186, increasing its interaction with p300, so that MDM2 mediates the ubiquitination and degradation of

p53 [30]. Phosphorylation of MDM2 also blocks its binding to p19ARF and increases the degradation of p53 [31].

It can be seen that multiple pathways play an important role in stroke through their interactions. In order to further verify the interaction between the 6 core genes and the active ingredients, the HFD effective ingredients were docked with the target to molecular events against stroke. Normally, the binding free energy is lower than -5.0 kcal/mol, indicating good binding activity between the docking molecule and the target, and the values are lower than -7.0 kcal/mol indicating strong binding activity, which indicates a significant interaction. As shown by the results, except for luteolin and MDM2 (6.97 kcal/mol), the lowest binding free energy between other small molecules and their targets is all lower than -7.0 kcal/mol.

In order to study this core network in evaluating the general applicability of traditional Chinese medicine in the treatment of stroke, the 26 genes from Figures 5(b) and 5(c) with stroke were curated in the GEO database and then compared with the GSE biosets related to curated studies using Chinese medicine against stroke. The $-\log(p$ value) was used to study the correlation of selected genes. The cutoff of $-\log(p$ value) is set at ± 4 [15]. Under this criterion, 153 gene biosets from 17 studies in the GEO database were significantly correlated with MOCA-induced stroke [17]. In Figure 9, the GSE database for brain stroke included mice GSE30655 [32], GSE35338 [33], GSE13353 [34], GSE 51566 [35], rat GSE 61616 [17], GSE21136 [36], GSE41453 [37], and GSE 17929 [38] and was used to evaluate the correlation of the built core gene targets with stroke. All 26 core targets were highly correlated with the MOCA stroke model [17], and more interestingly, when treated with antistroke Chinese medicine Xuesaitong, the increased $-\log(p$ values) were returned to the normal, or to the opposite direction, confirming the therapeutic effects of this Chinese medicine. It should be mentioned that when there is one type of “Chinese medicine” and “stroke,” only this study was curated in the database; and when there is one type of

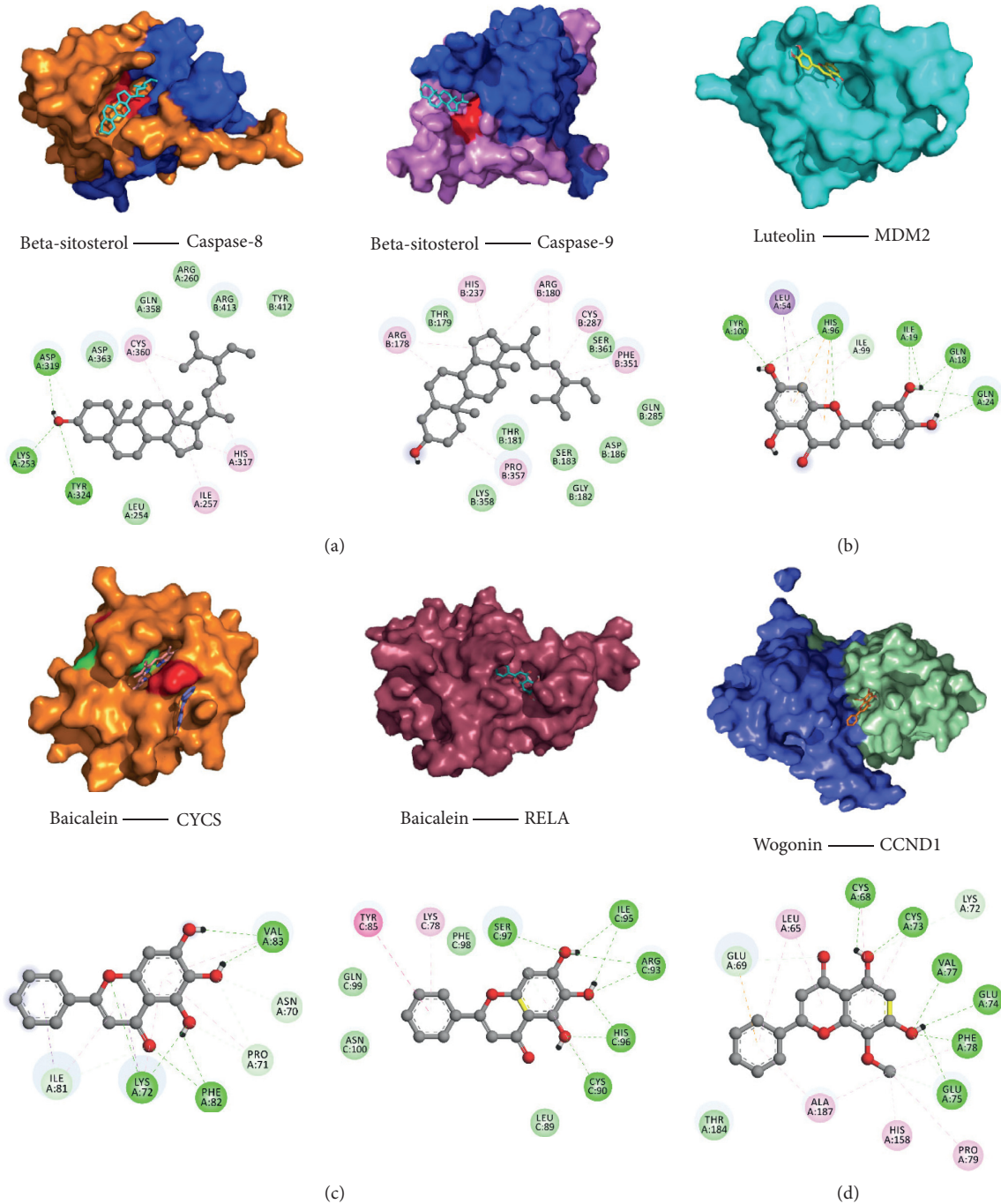


FIGURE 8: Molecular docking of key target genes and ingredients. Docking concept and binding site analysis of beta-sitosterol (a). Docking concept and binding site analysis of luteolin (b). Docking concept and binding site analysis of baicalein (c). Docking concept and binding site analysis of wogonin (d).

“cinnabar” and “stroke,” the same study appeared. Cinnabar is an active ingredient in Chinese medicines including HFD and An-Gong-Niu-Huang Wan for brain diseases [18], and the effects of cinnabar-containing Chinese medicines against stroke are worth of further verification.

In summary, this study predicted the active ingredients, targets, and signal pathways of HFD treatment stroke

through network pharmacology and verified the core ingredients and targets, laying a foundation for elucidating the mechanism of action. It also provides a systematic evaluation of the degree of stroke and the effect of drug treatment. The selected 26 core targets could be valuable biomarkers to evaluate the efficacy of HFD and Chinese medicines against stroke.



FIGURE 9: BaseSpace Correlation Engine analysis of 26 target genes with the GSE biosets based on $-\log(p \text{ value})$ with the MOCA biosets (GSE61616). Red indicates the upregulation, and blue indicates the downregulation in the style of Target gene_ GSE_biosets. MOCA bioset (first column) was highly correlated with identified 26 target genes. In MOCA + Xuesaitong treatment (2nd column), all MOCA-induced target changes were returned to the normal or to the opposite direction (negative correlations).

5. Conclusion

The mechanism of action of HFD in stroke involves multiple compounds, targets, and pathways. HFD could regulate the symptoms of stroke through signaling pathways with core targets. This work provided a bioinformatic method to clarify the antistroke mechanism of HFD, and the identified core targets could serve as a biomarker to study antistroke traditional Chinese medicines including mineral-containing remedies.

Data Availability

The data used to support the findings of this study are included within the article.

Conflicts of Interest

The authors declare that they have no conflicts of interest.

Acknowledgments

This study was supported by the National Natural Science Foundation of China (81560592) and the Shijingshan's Tuor Studio of Pharmacology [GZS-2016(07)].

Supplementary Materials

Supplementary Table 1: the results obtained by the molecular docking software. Supplementary Table 2: correlation

analysis of 26 core targets with the GEO database. (*Supplementary Materials*)

References

- [1] A.-L. Hu, S. Song, Y. Li et al., "Mercury sulfide-containing Hua-Feng-Dan and 70W (Rannasangpei) protect against LPS plus MPTP-induced neurotoxicity and disturbance of gut microbiota in mice," *Journal of Ethnopharmacology*, vol. 254, Article ID 112674, 2020.
- [2] C. Chen, B.-B. Zhang, A.-L. Hu, H. Li, J. Liu, and F. Zhang, "Protective role of cinnabar and realgar in Hua-Feng-Dan against LPS plus rotenone-induced neurotoxicity and disturbance of gut microbiota in rats," *Journal of Ethnopharmacology*, vol. 247, p. 112299, 2020.
- [3] R. Zhang, X. Zhu, H. Bai, and K. Ning, "Network pharmacology databases for traditional Chinese medicine: review and assessment," *Frontiers in Pharmacology*, vol. 10, p. 123, 2019.
- [4] F. Zhang, Y. Lu, Q. Wu, J. Yan, J. Shi, and J. Liu, "Role of cinnabar and realgar of WSHFD in protecting against LPS-induced neurotoxicity," *Journal of Ethnopharmacology*, vol. 139, no. 3, pp. 822–828, 2012.
- [5] Y. Qu, Z. Zhang, Y. Lu, Zheng, and Y. Wei, "Network pharmacology reveals the molecular mechanism of cuyuxunxi prescription in promoting wound healing in patients with anal fistula," *Evidence-Based Complementary and Alternative Medicine*, vol. 2019, Article ID 3865121, 9 pages, 2019.
- [6] G. Yu, W. Wang, X. Wang et al., "Network pharmacology-based strategy to investigate pharmacological mechanisms of Zuojinwan for treatment of gastritis," *BMC Complementary Medicine and Therapies*, vol. 18, p. 292, 2018.

- [7] J. Ru, P. Li, J. Wang et al., "TCMSP: a database of systems pharmacology for drug discovery from herbal medicines," *Journal of Cheminformatics*, vol. 6, p. 13, 2014.
- [8] R. Xue, Z. Fang, M. Zhang, Z. Yi, C. Wen, and T. Shi, "TCMID: traditional Chinese Medicine integrative database for herb molecular mechanism analysis," *Nucleic Acids Research*, vol. 41, pp. D1089–D1095, 2013.
- [9] L. Guo, J. S. Kang, N. J. Kang, and Y. W. Choi, "S-petasin induces apoptosis and inhibits cell migration through activation of p53 pathway signaling in melanoma B16F10 cells and A375 cells," *Archives of Biochemistry and Biophysics*, vol. 692, p. 108519, 2020.
- [10] M. Shi, B. Li, Q. Yuan et al., "Network pharmacology-based approach to investigate the mechanisms of mahai capsules in the treatment of cardiovascular diseases," *Evidence-Based Complementary and Alternative Medicine*, vol. 2020, Article ID 9180982, 15 pages, 2020.
- [11] L. N. Yang, Z. L. Wu, Z. J. Yang, S. G. Li, and C. S. Ouyang, "Exploring mechanism of key Chinese herbal medicine on breast cancer by data mining and network pharmacology methods," *Chinese Journal of Integrative Medicine*, 2020.
- [12] J. Huang, H. Tang, S. Cao et al., "Molecular targets and associated potential pathways of danlu capsules in hyperplasia of mammary glands based on systems pharmacology," *Evidence-Based Complementary and Alternative Medicine*, vol. 2017, Article ID 1930598, 2017.
- [13] S. Gu, Y. Xue, Y. Zhang et al., "An investigation of the mechanism of rapid relief of ulcerative colitis induced by five-flavor *Sophora flavescens* enteric-coated capsules based on network pharmacology," *Combinatorial Chemistry & High Throughput Screening*, vol. 23, no. 3, pp. 239–252, 2020.
- [14] X. Lu, X. Wu, L. Jing et al., "Network pharmacology analysis and experiments validation of the inhibitory effect of JianPi Fu recipe on colorectal cancer LoVo cells metastasis and growth," *Evidence-Based Complementary and Alternative Medicine*, vol. 2020, Article ID 4517483, 15 pages, 2020.
- [15] J. C. Corton, N. C. Kleinstreuer, and R. S. Judson, "Identification of potential endocrine disrupting chemicals using gene expression biomarkers," *Toxicology and Applied Pharmacology*, vol. 380, p. 114683, 2019.
- [16] Q. Cui, Y.-l. Zhang, Y.-h. Ma et al., "A network pharmacology approach to investigate the mechanism of Shuxuening injection in the treatment of ischemic stroke," *Journal of Ethnopharmacology*, vol. 257, p. 112891, 2020.
- [17] L. Wang, Y. Yu, J. Yang, X. Zhao, and Z. Li, "Dissecting Xuesaitong's mechanisms on preventing stroke based on the microarray and connectivity map," *Molecular BioSystems*, vol. 11, no. 11, pp. 3033–3039, 2015.
- [18] J. Liu, L.-X. Wei, Q. Wang et al., "A review of cinnabar (HgS) and/or realgar (As₄S₄)-containing traditional medicines," *Journal of Ethnopharmacology*, vol. 210, pp. 340–350, 2018.
- [19] F. Peng, H. Yang, Q. Wu, J. Liu, and J. Shi, "Studies on subacute toxicity of Wansheng huafeng dan in rats," *Zhongguo Zhong Yao Za Zhi*, vol. 37, pp. 1017–1022, 2012.
- [20] J. W. Yan, J. W. Miao, H. Y. He et al., "Comparative study of hepatotoxicity and nephrotoxicity produced by Wan-Sheng-Hua-Feng Dan, relagar and cinnabar," *Chinese Journal of Pharmacology and Toxicology*, vol. 25, pp. 380–385, 2011.
- [21] Q. N. Zhu, Y. F. Lu, J. Z. Shi et al., "Distinct effect of Wansheng Huafeng Dan containing *ardisia crenata* on renal transporters, mercury accumulation and Kim-1 expression from mercuric chloride," *Zhongguo Zhong Yao Za Zhi*, vol. 39, pp. 1892–1896, 2014.
- [22] J. Ying, J. Wu, Y. Zhang et al., "Ligustrazine suppresses renal NMDAR1 and caspase-3 expressions in a mouse model of sepsis-associated acute kidney injury," *Molecular and Cellular Biochemistry*, vol. 464, no. 1-2, pp. 73–81, 2020.
- [23] J. Li, Z. Liu, L. Wang, H. Xu, and Y. Wang, "Thousand and one kinase 1 protects MCAO-induced cerebral ischemic stroke in rats by decreasing apoptosis and pro-inflammatory factors," *Bioscience Reports*, vol. 39, 2019.
- [24] J. M. Buschhaus, B. Humphries, K. E. Luker, and G. D. Luker, "A caspase-3 reporter for fluorescence lifetime imaging of single-cell apoptosis," *Cells*, vol. 7, 2018.
- [25] A. V. Lugovaya, V. S. Emanuel, N. M. Kalinina, A. M. Ivanov, and A. V. Artemova, "Apoptosis and autophagy in the pathogenesis of acute ischemic stroke (review of literature)," *Russian Clinical Laboratory Diagnostics*, vol. 65, no. 7, pp. 428–434, 2020.
- [26] X. Gao, H. Li, Z. Dong et al., "Relationship between Erk1/2 signal pathway and nerve cell apoptosis rats with ischemic stroke," *Cellular and Molecular Biology*, vol. 65, no. 7, pp. 127–131, 2019.
- [27] H. An, Y. Duan, D. Wu et al., "Phenothiazines enhance mild hypothermia-induced neuroprotection via PI3K/Akt regulation in experimental stroke," *Scientific Reports*, vol. 7, p. 7469, 2017.
- [28] A. Saito, T. Hayashi, S. Okuno, T. Nishi, and P. H. Chan, "Modulation of p53 degradation via MDM2-mediated ubiquitylation and the ubiquitin-proteasome system during reperfusion after stroke: role of oxidative stress," *Journal of Cerebral Blood Flow & Metabolism*, vol. 25, no. 2, pp. 267–280, 2005.
- [29] X. Gao, Q. Li, G. Chen, H. He, and Y. Ma, "MAGEA3 promotes proliferation and suppresses apoptosis in cervical cancer cells by inhibiting the KAP1/p53 signaling pathway," *American Journal of Translational Research*, vol. 12, no. 7, pp. 3596–3612, 2020.
- [30] K. Liu, B. Xue, G. Bai, and W. Zhang, "F-box protein FBXO31 modulates apoptosis and epithelial-mesenchymal transition of cervical cancer via inactivation of the PI3K/AKT-mediated MDM2/p53 axis," *Life Sciences*, vol. 259, p. 118277, 2020.
- [31] Y. Wang, J. Zhao, C. Zhang, P. Wang, C. Huang, and H. Peng, "MDM2 promotes the proliferation and inhibits the apoptosis of pituitary adenomas cells by directly interacting with p53," *Endokrynologia Polska*, 2020.
- [32] R. E. White, C. Palm, L. Xu et al., "Mice lacking the beta2 adrenergic receptor have a unique genetic profile before and after focal brain ischaemia," *ASN Neuro*, vol. 4, no. 5, Article ID e00096, 2012.
- [33] J. L. Zamanian, L. Xu, L. C. Foo et al., "Genomic analysis of reactive astrogliosis," *Journal of Neuroscience*, vol. 32, no. 18, pp. 6391–6410, 2012.
- [34] M. I. Kurki, S.-K. Häkkinen, J. Frösen et al., "Upregulated signaling pathways in ruptured human saccular intracranial aneurysm wall: an emerging regulative role of toll-like receptor signaling and nuclear factor- κ B, hypoxia-inducible factor-1A, and ETS transcription factors," *Neurosurgery*, vol. 68, no. 6, pp. 1667–1676, 2011.
- [35] A. Arac, M. A. Grimaldeston, A. R. B. Nepomuceno et al., "Evidence that meningeal mast cells can worsen stroke pathology in mice," *The American Journal of Pathology*, vol. 184, no. 9, pp. 2493–2504, 2014.
- [36] G. C. Jickling, X. Zhan, B. P. Ander et al., "Genome response to tissue plasminogen activator in experimental ischemic stroke," *BMC Genomics*, vol. 11, no. 1, p. 254, 2010.

- [37] Y. Watanabe, M. Yoshida, K. Yamanishi et al., "Genetic analysis of genes causing hypertension and stroke in spontaneously hypertensive rats: gene expression profiles in the kidneys," *International Journal of Molecular Medicine*, vol. 36, no. 3, pp. 712–724, 2015.
- [38] A. Armugam, C.D. Cher, K. Lim et al., "A secretory phospholipase A2-mediated neuroprotection and anti-apoptosis," *BMC Neuroscience*, vol. 10, p. 120, 2009.

Review Article

Advances in the Study of the Potential Hepatotoxic Components and Mechanism of *Polygonum multiflorum*

He-Shui Yu,^{1,2} Lin-Lin Wang,³ Ying He,³ Li-Feng Han ,² Hui Ding,¹ Xin-Bo Song,^{1,4} Xiu-Mei Gao ,² Nai-Ru Yun ,³ and Zheng Li ^{1,2}

¹College of Pharmaceutical Engineering of Traditional Chinese Medicine, Tianjin University of Traditional Chinese Medicine, Tianjin 301617, China

²Tianjin State Key Laboratory of Modern Chinese Medicine, Tianjin University of Traditional Chinese Medicine, Tianjin 301617, China

³Second Affiliated Hospital of Tianjin University of Traditional Chinese Medicine, Tianjin 300250, China

⁴Tianjin Modern Innovative TCM Technology Co., Ltd., Tianjin 300000, China

Correspondence should be addressed to Nai-Ru Yun; yunnairu987@126.com and Zheng Li; lizheng@tjutcm.edu.cn

Received 2 June 2020; Revised 26 August 2020; Accepted 14 September 2020; Published 30 September 2020

Academic Editor: Jie Liu

Copyright © 2020 He-Shui Yu et al. This is an open access article distributed under the Creative Commons Attribution License, which permits unrestricted use, distribution, and reproduction in any medium, provided the original work is properly cited.

The roots of *Polygonum multiflorum* (PM) (He Shou Wu in Chinese) are one of the most commonly used tonic traditional Chinese medicines (TCMs) in China. PM is traditionally valued for its antiaging, liver- and kidney-tonifying, and hair-blackening effects. However, an increasing number of hepatotoxicity cases induced by PM attract the attention of scholars worldwide. Thus far, the potential liver injury compounds and the mechanism are still uncertain. The aim of this review is to provide comprehensive information on the potential hepatotoxic components and mechanism of PM based on the scientific literature. Moreover, perspectives for future investigations of hepatotoxic components are discussed. This study will build a new foundation for further study on the hepatotoxic components and mechanism of PM.

1. Introduction

The occurrence of adverse reactions caused by TCMs and their agents has increased, as they are widely used as disease treatments, in healthcare, etc. The liver, as an important drug-metabolizing organ, is particularly vulnerable to damage. PM, as a traditional tonic medicine, has antiaging, liver- and kidney-tonifying, hair-blackening, etc. effects [1–3].

However, PM-induced hepatotoxicity cases have been frequently reported in China and other countries. Hepatotoxicity cases caused by PM were reported by the Medicines and Healthcare Products Regulatory Agency (MHRA) [4–6]. Then, the China National Medical Products Administration (NMPA) also issued a notice on strengthening the supervision of health foods containing PM. Additionally, “Focus on Risk of Liver Damage Caused by Oral PM and Its Preparation” was published in “Adverse Drug Reaction Information Bulletin” by National Center for ADR

Monitoring, China. As PM and its preparations are widely used in the treatment and prevention of diseases, the hepatotoxic effects of PM-based products limit its long-term usage, and the safety of PM requires attention.

The clinical hepatotoxic feature of PM was summarized according to the literature. The ingestion of PM formulations or preparations leads to liver injury, including PM soaked in wine after steaming, PM dried and ground into powder after steaming, oral liquid containing PM, capsules containing PM, Shou Wu tea, etc. PM and its preparations have been reported to lead to liver injury after injection for several days to several months and at a large range of doses. The ingestion of PM leads to liver injury in many populations, including the general population and people with hair loss, white hair, vitiligo, itchy skin, high blood pressure, coronary heart disease, cerebrovascular stenosis, high cholesterol, dermatitis, eczema, acne, and cerebral infarction. The clinical features of liver injury that result from the ingestion of PM or its preparations include nausea,

vomiting, diarrhea, abdominal pain, nervous, restlessness, difficulty breathing, tic, upper gastrointestinal bleeding, hybrid hepatitis, cholestasis hepatitis, etc. The ingestion of PM leads to liver injury in people aged 5 ~ 78 years, and the occurrences in men and women are almost equal. In conclusion, the clinical features of liver injury that result from the ingestion of PM are not definitively related to processing, duration, dosage, age, gender, complications, etc. [4–10] (Table 1).

However, although PM extracts are generally considered to be relatively safe, PM extracts may still show hepatotoxicity. Most ancient books recorded that PM is not poisonous, but a small number of ancient books, such as “*Ben Cao Hui Yan*,” recorded that raw PM is qi cold and cold having property of contraction, and raw PM is poisonous. PPM is qi warm and not poisonous. These prove that PM contains compounds that could induce adverse reactions. Unfortunately, although extensive experiments have been performed both in vivo and in vitro in recent years, the potential toxic components and possible mechanisms that cause liver injury remain unclear.

The aim of this review is to provide comprehensive information on the potential hepatotoxic components and mechanism of PM based on the scientific literature. Moreover, perspectives for future investigations of hepatotoxic components are discussed. This study will build a new foundation for further study on the hepatotoxic components and mechanism of PM.

2. Study of Potential Hepatotoxic Compounds in PM

Modern research on PM begins with the study of its composition. Stilbenes, anthraquinones, procyanidins, flavonoids, phospholipids, catechins, and other compounds were isolated and identified from PM [15–17]. All these compounds play indispensable roles in the pharmacological effects of PM. However, scholars have begun to study potential hepatotoxic compounds, as frequent reports of liver injury involve PM. Anthraquinones (AQs), stilbenes, and catechins or their derivatives are the main controversial potentially toxic ingredients.

2.1. AQs or Their Derivatives and Liver Injury. AQs are one of the major potential hepatotoxic compounds in PM. The effects of raw PM and processed PM (PPM) with 70% ethanol extract on the liver were studied. These results showed that the 95% ethanol elution of the ethanol extract could inhibit the growth of L02 cells [18–20]. The 95% ethanol elution of raw PM and PPM ethanol extract are considered to be potential hepatotoxic parts of PM. In addition, researchers found that the order of toxicity was raw PM ethanol extract > raw PM water extract > PPM ethanol extract > PPM water extract [21–25]. It is worth noting that the content of AQs, such as emodin, and its derivatives were higher or main compounds in PM ethanol extract and 95% ethanol elution of PM ethanol extract [15], which reveals that AQs may be toxic ingredients. Therefore, the effect of

main anthraquinone compounds, such as emodin, rhein, physcion, chrysophanol, etc., on the liver was studied in vivo and in vitro [26–38].

Studies have shown that emodin and rhein can deplete GSH, promote the production of intracellular ROS and the depolarization of the mitochondrial membrane, and upregulate the levels of cleaved Caspase-8, Caspase-9, Caspase-3, etc., inducing the apoptosis in L02 and HepG2 cells [39–43]. AQs and anthranone from PM, such as emodin and chrysophanol, significantly inhibited the activity of the bile salt export pump (Bsep), multidrug resistance-associated protein 2 (Mrp2), and basolateral efflux transporters; downregulated the activity of Na⁺/taurocholate cotransporting polypeptide (Ntcp) [44]; altered bile acid (BA) disposition; and resulted in liver injury. While anthraquinone and dianthrone exhibited the strongest inhibitory effect on UGT1A1 activity [34, 45, 46], UGT1A1 is an important UGT isoform involved in the metabolic clearance of bilirubin, which is a toxic waste product of heme degradation [47]. The inhibition of UGT1A1 may lead to bilirubin accumulation, which could induce jaundice, liver injury, etc. [48–50]. In addition, research has shown that the oral administration of emodin to rats can directly induce liver damage, and emodin can induce intracellular oxidative stress and ER stress through the AhR-CYP1A1 pathway and then induce the apoptosis pathways in hepatocytes [32, 33, 51].

The above results suggest that emodin, rhein, physcion, chrysophanol, emodin-8-O-glc, emodin-O-(acetyl)-hex, emodin-O-hex-sulfate, emodin-O-glc, emodin-O-(malonyl)-hex, and other anthraquinone components or their derivatives might be potential hepatotoxic compounds in PM.

However, some studies have noted that the speculation that AQs are the hepatotoxic components in PM lacks scientific evidence. Emodin, as well as other components, has a low bioavailability and might lead to liver damage only at high concentrations. According to the literature, to have liver damage, healthy adults need at least 339 g of PM in a single oral dose. However, the clinical dose of PM is 3 ~ 6 g of raw Shou Wu and 6 ~ 12 g of PPM [52, 53]. Thus, the hepatotoxic dose of AQs in PM is far from the actual dose, and the speculation that AQs are the hepatotoxic component of PM needs to be further explored.

2.2. Tannin and Liver Injury. Tannins can cause liver damage in grazing animals and were the main cause of cryptogenic liver damage in the past. The content of tannins in PM is high, up to 15%, and its content decreases as processing time increases [54]. Scholars have studied the role of tannins in liver damage caused by PM and found that tannins could significantly increase serum ALT, AST, AKP, TP, AIB, and TBA enzyme activity and induce significant damage in hepatocytes [55]. The administration of long-term high-doses and short-term medium doses is harmful to the liver in mice, and small doses induce no obvious liver damage. However, liver damage can be restored after stopping drug administration [56]. Research has also shown that gallic acid

TABLE 1: Retrospective analysis on cases of liver injury of *Polygonum multiflorum*.

| Case | Age | Duration of intake, day | Preparations | Presenting PM | Extrahepatic manifestation | Type of liver injury | Reference |
|------|---------|-------------------------|---|----------------|---|------------------------------------|-----------|
| 264 | 5 ~ 63 | 7 ~ 365 | Shou Wu tablet, Yangxue Shengfa capsule, Yanshou tablet, Jingwu capsule, Yishen Wufa oral liquid, Qibao Meiran pill, Tianma Shouwu tablet, Huo Li Su oral liquid, Geng Nian An tablet, Kunbao pill, Xinyuan capsule, Zhi Shou Wu granule, Renshen Shouwu capsule, Fu Fang Shou Wu oral liquid, Shou Wu pill, Anshen Bunao liquid, Jiang Zhi Ling tablet, Bantu pill, Bushen Yishou capsule, Huichun Ruyi capsule, Shenbao tablet, Jiangzhi Huazhuo capsule, Heishou Shengfa granule, Baishi pill, Shou Wu tea, etc. | PPM | Fever, fatigue, loss of appetite, jaundice, erythra, myalgia, nausea and vomiting, etc. | Mixed, hepatocellular, cholestasis | [10, 11] |
| 214 | 19 ~ 78 | 3 ~ 120 | He Shou Wu powder, He Shou Wu tea, He Shou Wu wine, etc. | Raw PM | Fever, fatigue, loss of appetite, jaundice, erythra, myalgia, nausea and vomiting, ascites, liver-palms, gray stool, etc. | Mixed, hepatocellular, cholestasis | [9, 12] |
| 5 | 36 ~ 60 | 30 ~ 90 | Runzao Zhiyang capsule | raw PM and PPM | Fever, fatigue, loss of appetite, jaundice, erythra, myalgia, nausea and vomiting, ascites, liver-palms, gray stool, etc. | Mixed, hepatocellular, cholestasis | [10, 13] |
| 326 | 19 ~ 70 | 5 ~ 180 | Huangjing Zanyu capsule, Huichun Ruyi capsule, Shenjiao capsule, He Shou Wu powder, He Shou Wu tea, He Shou Wu wine, decoction containing PM, herbal paste, healthcare product, etc. | PM | Fever, fatigue, loss of appetite, jaundice, erythra, myalgia, nausea and vomiting, ascites, liver-palms, gray stool, abdominal distension, etc. | Mixed, hepatocellular, cholestasis | [7, 14] |

Note. PM means *Polygonum multiflorum*; the literature does not clearly indicate whether it is raw PM or PPM.

impaired the folding and processing of functional proteins, causing endoplasmic reticulum stress and generating liver cell apoptosis by repressing the biological control of the transcription and expression of peptidyl-prolyl *cis-trans*-isomerase A (PPIA) in a dose-dependent manner [57].

In addition, tannins induce the CYP2E1 enzyme [58], and previous studies concluded that the induction of CYP2E1 by tannin may affect the conversion and metabolism of AQs in vivo, which may lead to liver damage.

2.3. TSG (2,3,4',5-Tetrahydroxystilbene-2-O- β -D-glucoside) and Liver Injury. Stilbenes, especially TSG, are considered to be the main liver-protective components in PM. However, research has found that TSG might be associated with the hepatotoxicity of PM.

Generally, the adverse effect of PM will diminish or vanish, and it has tonifying effect after processing; in other words, the hepatotoxicity of raw PM is higher than that of PPM [21–25]. Coincidentally, studies have found that the content of *trans*-TSG in PPM was reduced by 55.8% and the

content of emodin in PPM was increased by 34% compared with that in PM; that is, the content of *trans*-TSG was reduced and the content of emodin was increased during the processing. Therefore, some reports speculated that the toxicity of PM might not be correlated with the content of emodin or its derivatives but depended on the contents of *trans*-TSG, conventionally thought to be a liver-protective compound, or the relative content of *trans*-TSG and emodin [59, 60]. Reports have also shown that *trans*-TSG might inhibit the activation of the nuclear factor κ B (NF- κ B) signaling pathway, which is necessary for the HGF-mediated proliferation of WBF-344 cells. *Trans*-TSG may have some influence on the proliferation of liver cells [61–64].

Trans-TSG was unstable in irradiation and alkaline conditions and could convert to *cis*-TSG. Unfortunately, the latest research shows that *cis*-TSG has a higher cytotoxicity than *trans*-TSG in normal L02 cells, and *cis*-TSG could induce hepatotoxicity in LPS-treated rats. In addition, the contents of *cis*-TSG were higher in PM preparations or serum from patients with liver intoxication associated with PM than those in control samples, which may be because

trans-TSG converted to *cis*-TSG in the course of preparation of PM and thus led to liver toxicity. All these results suggested that *cis*-TSG is closely associated with the hepatotoxicity of PM [65–67].

3. Hepatotoxic Mechanism of PM

In summary, the existing literature shows that the mechanism of PM-induced liver damage is mainly categorized into four viewpoints: (1) active substances in PM cause cholestasis, which leads to liver injury caused by lipid peroxidation or directly causes liver cell damage; (2) active substances in PM affect the CYP450 enzyme system, affecting drug transport or metabolism and leading to liver damage; (3) active substances in PM cause mitochondrial dysfunction, which leads to liver injury through the oxidative stress response; and (4) active substances in PM cause drug-induced liver injury (DILI).

3.1. Cholestasis and Liver Injury. Cholestasis and bile duct injury are the main clinical manifestations of cholestasis caused by chemical drugs. Serum biochemical parameters, including alkaline phosphatase (ALP), total bilirubin (TBIL), and bile acid (TBA), are preferred in clinical practice. Studies have shown that the ALP, TBIL, and TBA were significantly different in the serum of rats after administration with PM compared with the serum of control rats [11, 22, 45], of which TBA increased in serum and increased in liver. Intrahepatic deposition of bile acids is considered to be the primary cause of cholestatic liver injury [68]. While cholic acid (CA), glycodeoxycholic acid (GDCA), chenodeoxycholic acid (CDCA), deoxycholic acid (DCA), and ursodeoxycholic acid were all significantly decreased, TCA was significantly increased, and GCA and GCDCA showed no significant changes [69]. These results indicated that the distribution of bile was also affected. The ethanol extract of PPM could affect the synthesis of bile acids and alter the composition of intestinal bile acids by activating Fxr-Fgf15 signaling in the intestine, and it can inhibit the expression of CYP7A1 in the liver [70]. In addition, AQs and dianthrone from PM, such as emodin and chrysophanol, significantly affected the activity of Bsep, Mrp2, and CYP8B1 and exhibited the strongest inhibitory effect on UGT1A1 activity, leading to bilirubin accumulation and resulting in cholestasis [34, 44–50, 71–73]. Meanwhile, hydrodeoxycholic acid (HDCA) in serum and tauro- β -muricholic acid (T β MCA) in urine were identified in rats with PM-induced liver injury [74–76]. Clinical analysis of drug-induced liver injury caused by PM or its preparations also indicated that there are many symptoms related to jaundice in patients with liver injury, including an increase in related indicators such as TBIL [7–10]. Therefore, liver injury caused by PM might be associated with cholestasis.

In the process of the generation, formation, transportation, and discharge of bile acid, failure at any step could cause cholestasis. When bile acid accumulation in liver cells or antioxidants decreases, the body will produce an oxidative stress reaction. This phenomenon could reduce the

activity of superoxide dismutase (SOD), catalase (CAT), and glutathione peroxidase (GPx). First, ROS production increases; then, intestinal barrier dysfunction develops due to the lack of bile salts in the intestine. Next, excessive intestinal endotoxin (LPS) enters the systemic circulation, inducing the production of the inflammatory cytokines IL-1, IL-7, TNF- α , etc. and generating additional ROS, which further aggravate oxidative damage in the body [76–78].

Excessive ROS in the body cause peroxidative damage in liver cells by directly damaging biomacromolecules such as proteins and DNA [79, 80]. ROS act as direct functional signaling molecules, activate intracellular stress-sensitive signaling pathways, and mediate hepatocyte apoptosis. ROS induce hepatocyte apoptosis by interfering with mitochondrial function and indirectly by activating apoptotic signaling pathways. In addition, ROS can mediate inflammatory reactions and then cause liver damage [81, 82], which explains the mechanisms of hepatitis symptoms in patients with PM-induced liver injury [83, 84].

3.2. CYP450s and Liver Injury. The CYP450 enzymes, which are highly concentrated and exhibit activities in the human liver, are responsible for the oxidation or reduction of medicines [85, 86]. To date, more than 57 isoforms have been discovered in the CYP450 family; however, the CYP1A1, CYP1A2, CYP2B6, CYP2C8, CYP2C9, CYP2C19, CYP2D6, CYP2E1, CYP3A4, and CYP3A5 isoforms can metabolize nearly 90% of the drugs in the market [85]. It is well known that the activities of these CYP isoforms may be inhibited or induced by several compounds, and the modulation of their drug-metabolizing activities may have effects on pharmacodynamics and toxicology, such as DDI [86–88]. CYP450 and its isoenzymes are widely used in research fields such as drug metabolism, clinical rational drug use, toxicology, tumor biochemistry, and new drug research and development. In recent years, marked progress has been made in drug metabolism enzyme research.

Enzyme activity can be induced or inhibited by certain drugs to promote drug metabolism or to inhibit drug metabolism. If the metabolism of the drug inhibits the activity of a drug-metabolizing liver enzyme, the drug or its metabolites will accumulate in the liver and cause adverse reactions. The composition of traditional Chinese medicines is complex, but most TCM components are metabolized by the CYP450 enzyme and may further affect the metabolism or interaction of other drugs, such as the “eighteen incompatible medicaments,” in which the combined application of *Salvia*, *Sophora*, *Ginseng*, and gourd inhibits the activity of CYP3A and CYP2E1 [89]. The combined administration of aconite, melon, *Bletilla*, *Pinellia*, *Fritillaria*, and *Radix Ampelopsis* inhibited the activity of CYP3A and CYP1A2 [90]. The activity of these metabolic enzymes is altered to impair the metabolism of the drug in the body, producing toxic effects.

3.2.1. CYP450 Inhibition. Research found that raw PM and PPM could significantly inhibit the expression of CYP2E1 mRNA [91]. The alcoholic extract of PM inhibited the activity of CYP2C19 and CYP2C9, and the aqueous extract of PM inhibited the activity of CYP2C19, CYP2C9, CYP2B6,

CYP2D6, and CYP1A2 [92, 93]. TSG has inhibitory effects on mouse liver CYP1A2, CYP2E1, and CYP3A11 protein expression through the suppression of AhR, PXR, and PPAR α activation [94]. CYP1A2, 2C19, and 2E1 have been reported as the main CYP450s which participated in phase I metabolism of AQs such as emodin [92, 95]. Therefore, it is speculated that the mechanism by which PM induces liver injury may be that some components in PM inhibit the activity of CYP2E1, which causes the accumulation of AQs or other toxic substances metabolized by CYP2E1, causing liver damage.

3.2.2. CYP450 Allelic Defect. The proportion of people with genetic defects in CYP450 enzymes is large [96]. However, due to the poor specificity of each CYP450 enzyme subtype substrate, each gene defect affects the metabolism of multiple drugs. Moreover, the incidence of different mutations that slow metabolism is different in different populations.

According to reports, whether CYP1A2 allele polymorphisms are associated with the acute liver injury induced by PM was tested by researchers using 43 cases of PM-induced liver injury. The results show that the frequency of the CYP1A21C allele was 46.5% in PM-induced DILI patients, which was significantly different from the frequency of 27.9% observed in healthy subjects. The frequency of the CYP1A21F allele was 63.9% in PM-induced DILI patients, compared to 57.0% in healthy controls; this difference was not significant. The allelic frequencies of CYP1A22, CYP1A27, CYP1A29, and CYP1A211 were not detected [97]. These results indicate that the CYP1A2 allelic mutation is most likely related to the metabolism of compounds in PM, followed by acute liver injury. Coincidentally, tannins, contained in rhubarb, are inducers of CYP2E1, which accelerate the conversion of CCl₄ to CCl₃, aggravating the liver injury caused by CCl₄ [98]. Additionally, the activity of CYP450 may be related to the liver damage induced by PM.

3.3. Mitochondrial Damage and Liver Injury. Mitochondria are important organelles that generate energy, oxidize materials in cells, and play a fundamental role in energy metabolism, free radical production, aging, and apoptotic regulation. Possible factors leading to mitochondrial dysfunction include respiratory chain defects, metabolic enzyme inactivation, structural changes, and mutations. All of these factors affect the normal function of cells, resulting in the occurrence of diseases. Mitochondria are important targets of drug toxicity, and mitochondria are also the organelles most vulnerable to drug toxicity. The liver is also a major target of drug damage because it is an important organ in drug metabolism. Drugs induce liver injury primarily by changing the activity of enzymes, modulating the structure of mitochondria and/or decreasing the synthesis of mtDNA, further undermining β -oxidation and other oxidative processes in liver cells [99–101].

Research shows that rhein could be changed into a reactive metabolite by CYP2C19, and the structure of reactive metabolite was inferred to be an epoxide compound. The reactive metabolite covalently binds to intracellular

mitochondria, leading to ROS overproduction and respiratory chain dysfunction. In addition, the reactive metabolite overproduction depletes GSH, which could result in hepatotoxicity [102–104]. Research also found that emodin could conjugate with GSH, forming emodin-GSH and depleting GSH in PM-induced liver injury rats [40–42]. An increasing number of studies have shown that mitochondrial damage may be a factor and pathway that predisposes individuals to PM-induced liver injury.

3.4. Drug-Induced Liver Injury

3.4.1. Misuse of Counterfeit Goods. He Shou Wu, the roots of *Polygonum multiflorum*, was originally published in “Kai Bao Materia Medica” in the Northern Song Dynasty. This medicine has two kinds, red and white; the red type is commonly used in clinic. Common species used to as counterfeits of this medicine are *Musa basjoo* S. & Z., *Pteroxygonum giraldii* Dammer & Diels, *Polygonum cilii-nerve* (Nakai) Ohwi, *Stephania cepharantha* Hayata, *Cynanchum auriculatum* Royle ex Wight, etc. In addition, PM has many origins, including Henan, Jiangxi, Guangdong, and Guangxi. The chemical content and efficacy of PM samples from different origins are also different [105–107]. Additionally, there is a large difference in quality. At present, due to insufficient market supervision, the confusion of origin and variety is also an important consideration in the safety of PM.

3.4.2. Improper Processing. Records on the processing of PM include the “Huatuo’s Zhongzang Classic” in the eastern Han Dynasty, the “Chinese Pharmacopeia,” national processing norms, and local processing norm. PM was primary processed in the pre-Tang Dynasty, steamed or cooked with black bean juice in the Tang Dynasty, and repeatedly steamed and sun-dried nine times in the Song and Qing Dynasty. The processing of PM has evolved from simple to complex, which indicates that people’s understanding of the nourishing effect of PM continues to improve. The attenuating effects and efficiency of PM processing are constantly improving and have received increasing attention [108, 109]. The continuous improvement of PM processing also indicates that there is a connection between the adverse reactions of PM and its processing. Modern research also proves that the toxicity of PM is significantly reduced after processing [29, 110–112]. Therefore, processing is an important factor that impacts the effect of PM.

However, the processing of PM has changed from complicated to simple in modern times; for example, PM processing was simplified from nine cycles of steaming and sun-drying to steaming once without sun-drying. Additionally, the methods of PM processing vary among regions. There are many kinds of processing methods, including ancient processing and modern processing, such as boiling, steaming, exposure, frying, and roasting, which were without accessories; black beans, wine, vinegar, rice swill, and so on; nine cycles of steaming and sun-drying; high pressure processing, microwave processing, fermentation

processing, extrusion technology, etc. [109, 113]. Due to the diversity of processing norms, the types and contents of the chemical components in different processed products are different, which results in safety hazards in the clinical use of PM. The processing of PM could be combined with modern science and technology, such as the use of modern machinery and equipment (drum type frying machine, vacuum drying box) to achieve the homogeneity and stability of processing conditions. Furthermore, modern detection methods (HPLC, UV, GC, etc.) are used to achieve real-time quality monitoring.

In addition, researches have also speculated that the liver injury induced by PM might be related to an imbalance in intestinal flora [114], immune-specific effects, or idiosyncratic hepatotoxicity [115, 116].

3.4.3. Metals and Elements Were Associated with Liver Injury. During the process of planting medicinal materials, planting conditions such as sunlight, moisture, climate, and soil should be fully guaranteed. However, with the development of agriculture, organophosphorus pesticides and heavy metal residues have become a major environmental factor affecting the quality of Chinese herbal medicine. The heavy metals that cause environmental and soil pollution mainly include mercury, cadmium, lead, chromium, and arsenic.

Recent studies have also demonstrated that heavy metal and element concentrations are associated with PM-induced liver injury [117, 118]. Reports have also shown that heavy metal contamination may lead to adverse reaction [119]. PM has many kinds of habitats, and different habitats have different environmental conditions such as temperature and humidity. Thus, the components and inorganic elements, and even heavy metal residues of PM, are correlated to geographical, climatic, and soil factors [120, 121]. Therefore, it is necessary to strengthen pharmacognosy traceability and quality control in order to prevent and reduce adverse reactions.

4. Discussion

According to the literature, the potential chemical composition and mechanism of liver injury caused by PM are summarized. The hepatotoxic compounds in PM (Figure 1) and the mechanism of the liver injury caused by PM need further study due to the integrity, complexity, and multi-targeted and synergistic effects of this natural product.

First, as cholestasis in the body stimulates oxidative stress, the level of reactive oxygen species in the body increases, causing a series of reactions that lead to liver cell damage. Modern pharmacological studies have shown that many of the active ingredients in Chinese herbal medicines have antioxidation activity, and that they directly or indirectly reduce or eliminate the liver injury caused by cholestasis. For example, curcumin, a natural antioxidant in turmeric, plays an important role in the liver damage model caused by cholestasis by reducing the level of the inflammatory factor TNF- α in the liver [122, 123]. Additionally, the active ingredients in herbs associated with liver injury have

been reported to directly or indirectly cause oxidative damage to the body, resulting in hepatotoxicity, such as *Melia toosendan*, *Dioscorea bulbifera* L., and *Radix Bupleuri* [124, 125], and causing liver damage by inducing oxidative stress in the body. What is the mechanism of the liver injury caused by PM? The potential hepatotoxic components of PM can cause oxidative stress by destroying mitochondrial function, leading to cholestasis and then resulting in liver injury, or the potential hepatotoxic components of PM can affect the synthesis, transport, secretion, etc. of bile acid, causing cholestasis, which in turn disturbs oxidative balance in the body, leading to liver injury. These mechanisms need to be further studied.

Second, the clinical manifestation of liver injury caused by PM is the accumulation of bile acid in the liver. The accumulation of bile acid in the liver is considered to be the leading cause of cholestasis-induced liver injury. Any failure in the synthesis, transport, secretion, etc. of bile acids may cause cholestasis. There are two ways to synthesize bile acids in liver cells: the classic pathway, catalyzed by cholesterol 7 α -hydroxylase (CYP7A1), and the alternative pathway, catalyzed by sterol 27 α -hydroxylase. However, the alternative route is usually activated when the classic pathway is blocked. CYP3A is a key CYP450 enzyme that breaks down bile acids [126]. After bile acid is synthesized, it is secreted by active transport; approximately 95% of bile acids rely on a variety of transporters and energy to enter the liver and intestinal circulation. A variety of protein molecules with transport functions present on hepatocytes, bile duct cell membranes, and small intestinal cell membranes, such as Ntcp, Bsep Mrp2, Asbt, etc., directly affect the transport and secretion of bile acids [127]. Certain chemical constituents of PM function by inhibiting the expression of these transporters or by mutating these transporters, thus causing cholestasis [128]. In addition, as described above, cholestasis in vivo can induce an inflammatory response and the production of inflammatory factors. Studies have shown that intracellular LPS and some inflammatory factors can rapidly reduce the expression of Ntcp on hepatocytes, of which IL-1 is the most effective [129, 130]. Notably, emodin and hydroxyemodin can inhibit the activity of Mrp2 according to reports. Is this the cause of liver damage in PM? Do the other medicinal substances in PM affect the activity of certain bile acid synthases or transport proteins; cause cholestasis in the synthesis, transport, and secretion of bile acids; and then promote liver injury?

Moreover, the degree of cholestasis-induced liver injury caused by PM processed with black bean was significantly decreased compared to that caused by PM without auxiliary materials (steamed PM). Additionally, steamed PM has a strong inhibitory effect on the activity of CYP2E1 [90, 131]. Black beans are common auxiliary materials in PM processing, and they are rich in protein, unsaturated fatty acids, vitamins, and phenolic acids, which have antioxidant and immunomodulatory effects [132, 133]. PM processed with black bean has been used since ancient times and is included in the Pharmacopeia. However, whether changes in the chemical composition and content of PM occur after processing with black beans is uncertain. The mechanism of the positive effect of PM processed with black beans is unknown.

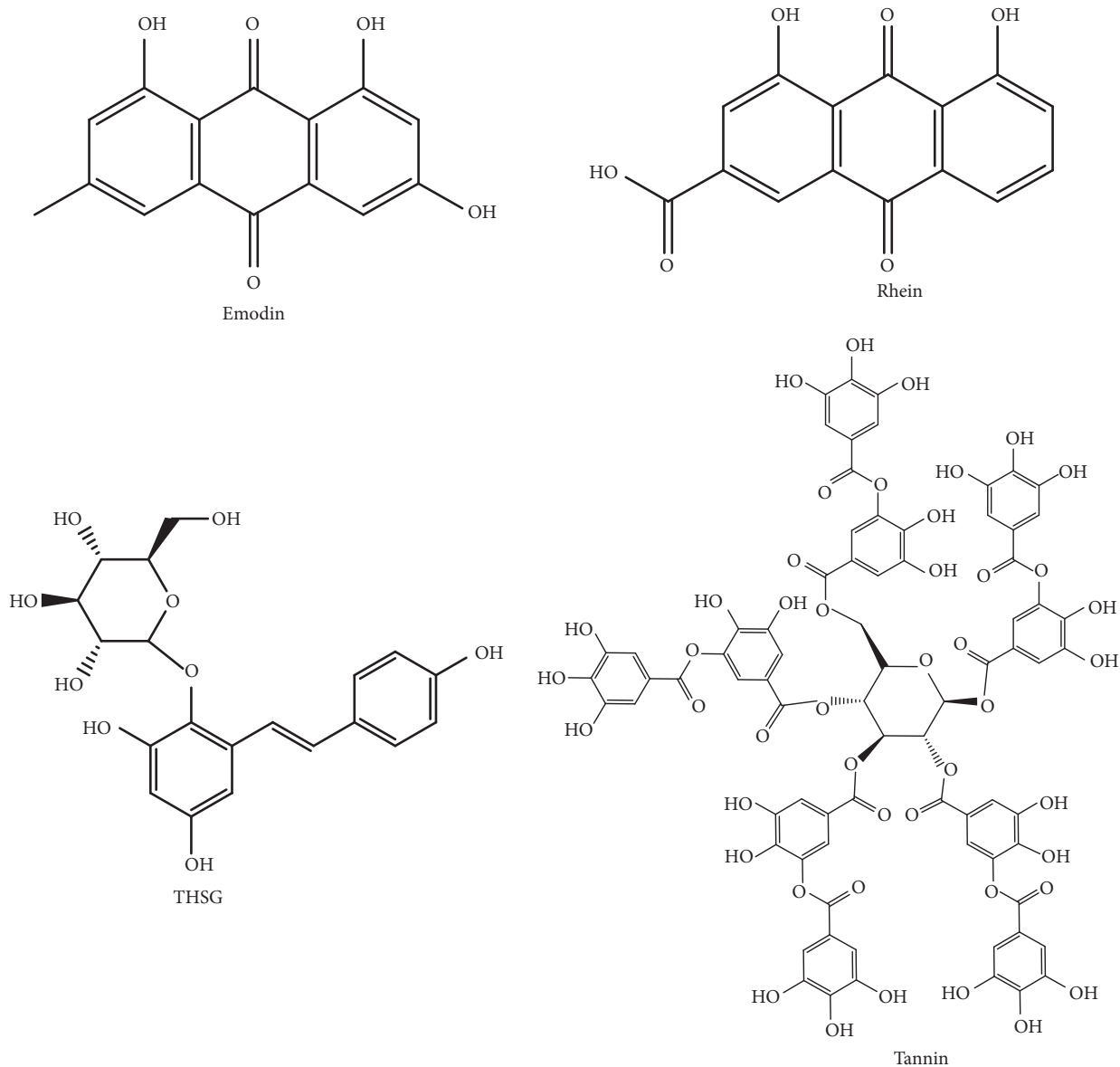


FIGURE 1: The structures of potential hepatotoxic compounds in PM.

Moreover, can black beans enhance the antioxidant activity of PM when PM is processed with black beans? Do the ingredients in black beans participate in the synthesis, transport, and secretion of bile acids? Is the attenuation of liver injury caused by PM exerted through these pathways? Is the mechanism of the positive effects of PM processed with black bean related to these factors? These questions require further study.

For example, as described in Section 1, researchers have speculated that the hepatotoxic compound in PM may be the emodin. However, emodin has strong antibacterial and anti-inflammatory [124] activities [134] and inhibits the expression of inflammatory factors in the liver [135, 136]. Additionally, emodin also has a certain antioxidant effect, which can reduce the level of oxidative stress in the liver and play a role in liver protection [137]. Researchers found that prepared rhubarb has a significant therapeutic effect on liver

injury in animals, but it has certain hepatotoxic effects on normal animals. Thus, researchers have proposed the symptom-based prescription theory [138]. Based on the theory, the hepatotoxicity of PM was studied, and a high dosage of PM had a toxic effect on normal rats and a therapeutic effect on rats with chronic liver injury [139]. Thus, if emodin is the hepatotoxic component in PM, perhaps it is possible to study the hepatotoxic component in PM based on the symptom-based prescription theory.

5. Conclusion

PM has been widely used because of its tonifying function. There are 380 Chinese patent medicines containing PM. With the increasing number of clinical cases of adverse drug reactions caused by PM and its preparations, its safety issues have aroused great attention of domestic and foreign

researchers and drug regulatory authorities. Thus, the liver injury of PM has become a practical problem that seriously affects the safety of its clinical medication and needs to be solved urgently. However, so far, there are still controversies about the liver damage components and mechanisms of PM. Research will be necessary for further understanding of the hepatotoxicity induced by PM so as to take reasonable and effective measures to prevent it. In addition, the clinical features of liver injury that result from PM include cholestasis hepatitis. Besides, the AQs in PM could interfere with bile acid metabolism according to the references. PM should be avoided in combination with drugs that can cause cholestatic liver injury such as chlorpromazine and rifampicin.

Data Availability

The data used to support the findings of this study are available from the corresponding author upon request.

Conflicts of Interest

The authors declare that they have no conflicts of interest regarding the publication of this paper.

Authors' Contributions

He-Shui Yu and Lin-Lin Wang contributed equally to this work.

Acknowledgments

This research was funded by the National Science and Technology Major Project of China (Grant no. 2018ZX09201011) and Science and Technology Program of Tianjin Municipal Commission of Education (Grant no. 2019KJ079).

References

- [1] Chinese Pharmacopoeia Commission, *Pharmacopoeia of the People's Republic of China*, Beijing: Chemical Industry Press, vol. 1, 2020.
- [2] T.-T. Ho, H. N. Murthy, D. Dalawai, M. A. Bhat, K.-Y. Paek, and S.-Y. Park, "Attributes of Polygonum multiflorum to transfigure red biotechnology," *Applied Microbiology and Biotechnology*, vol. 103, no. 8, pp. 3317–3326, 2019.
- [3] L. Lin, B. Ni, H. Lin et al., "Traditional usages, botany, phytochemistry, pharmacology and toxicology of Polygonum multiflorum Thunb.: a review," *Journal of Ethnopharmacology*, vol. 159, pp. 158–183, 2015.
- [4] H. Dong, D. Slain, J. Cheng, W. Ma, and W. Liang, "Eighteen cases of liver injury following ingestion of Polygonum multiflorum," *Complementary Therapies in Medicine*, vol. 22, no. 1, pp. 70–74, 2014.
- [5] K. A. Jung, H. J. Min, S. S. Yoo et al., "Drug-induced liver injury: twenty five cases of acute hepatitis following ingestion of Polygonum multiflorum thunb.," *Gut and Liver*, vol. 5, no. 4, pp. 493–499, 2011.
- [6] J.-B. Yang, W.-F. Li, Y. Liu et al., "Acute toxicity screening of different extractions, components and constituents of Polygonum multiflorum Thunb. on zebrafish (*Danio rerio*) embryos in vivo," *Biomedicine & Pharmacotherapy*, vol. 99, pp. 205–213, 2018.
- [7] H.-Z. Wang and X.-H. Li, "Clinical analysis of 33 cases of drug induced liver injury caused by Polygonum multiflorum Thunb and its preparations," *Chinese Journal of Integrated Traditional and Western Medicine on Liver Diseases*, vol. 28, no. 1, pp. 25–27, 2018.
- [8] Y. Zhu, Y.-G. Li, Y. Wang et al., "Analysis of clinical characteristics in 595 patients with Herb-induced liver injury," *Chinese Journal of Integrated Traditional and Western Medicine*, vol. 36, pp. 44–48, 2016.
- [9] L. Xiang, T.-T. Ke, and A.-R. Hu, "Clinical analysis of 52 patients with liver injury induced by Polygonum multiflorum and its preparation," *Chinese Archives of Traditional Chinese Medicine*, vol. 31, pp. 1133–1134, 2013.
- [10] Y. Zhu, S.-H. Liu, J.-B. Wang et al., "Clinical analysis of drug-induced liver injury caused by Polygonum multiflorum and its preparations," *Chinese Journal of Integrated Traditional and Western Medicine*, vol. 35, no. 12, pp. 1442–1447, 2015.
- [11] Y. Zhang, S. Chen, and L. Lu, "Clinical analysis of 36 cases of drug-induced liver injury by Polygonum multiflorum Thunb.," *Hainan Medical Journal*, vol. 24, no. 2, pp. 235–237, 2013.
- [12] Q.-B. Fu, T.-C. Liu, Y.-Z. Yu, F.-X. Xiao, and Z. Zhou, "Epidemiological and clinical characteristics of 140 cases of drug-induced liver injury caused by Polygonum multiflorum and its preparations," *Chinese Journal of Integrated Traditional and Western Medicine on Liver Diseases*, vol. 30, no. 1, pp. 6–9, 2020.
- [13] X.-J. Xie, K.-F. Ma, and Y. Liu, "Case analysis of liver injury induced by Polygonum multiflorum radix case analysis of liver injury induced by Polygonum multiflorum radix," *Drug Evaluation*, vol. 9, no. 32, pp. 36–38, 2012.
- [14] Y. Chang, Q.-Y. Liu, C.-J. Lv, Y.-P. Ding, W. Zhang, and H. Li, "Clinical features of 39 patients with acute liver injury induced by Polygonum multiflorum," *Chinese Hepatology*, vol. 23, no. 8, pp. 670–672, 2018.
- [15] L. Wang, M. Sang, E. Liu et al., "Rapid profiling and pharmacokinetic studies of major compounds in crude extract from Polygonum multiflorum by UHPLC-Q-TOF-MS and UPLC-MS/MS," *Journal of Pharmaceutical and Biomedical Analysis*, vol. 140, pp. 45–61, 2017.
- [16] J.-B. Yang, Y. Liu, Q. Wang et al., "Characterization and identification of the chemical constituents of Polygonum multiflorum Thunb. by high-performance liquid chromatography coupled with ultraviolet detection and linear ion trap FT-ICR hybrid mass spectrometry," *Journal of Pharmaceutical and Biomedical Analysis*, vol. 172, pp. 149–166, 2019.
- [17] Y. Liu, Q. Wang, J.-B. Yang et al., "Polygonum multiflorum thunb: a review on chemical analysis, processing mechanism, quality evaluation, and hepatotoxicity," *Frontiers in Pharmacology*, vol. 9, p. 364, 2018.
- [18] R. Zhang, B. Liu, Z.-X. Sun, and D.-Y. Xu, "Effects of extract of Polygonum multiflorum on cell cycle arrest and apoptosis of human liver cell line L02," *Journal of Chinese Integrative Medicine*, vol. 8, no. 6, pp. 554–561, 2010.
- [19] Z.-Z. Ge, C. Zhang, G.-Y. Feng, H.-L. Yang, L.-Y. Shi, and Z.-X. Sun, "Study on acute hepatotoxicity of Polygonum multiflorum extract in normal and hepatocarcinoma-bearing mice," *China Pharmacy*, vol. 25, pp. 1358–1360, 2014.
- [20] T. Wang, J.-Y. Wang, Z.-X. Zhou, Y.-Y. Li, L. Zhang, and L.-P. Zhang, "Study on hepatotoxicity of aqueous extracts of Polygonum multiflorum in rats after 28-day oral

- administration: cholelithiasis-related mechanism," *China Journal of Chinese Materia Medica*, vol. 40, pp. 2163–2167, 2015.
- [21] C. Tu, B.-Q. Jiang, Y.-L. Zhao et al., "Comparison of processed and crude *Polygoni multiflori* radix induced rat liver injury and screening for sensitive indicators," *China Journal of Chinese Materia Medica*, vol. 40, pp. 654–660, 2015.
- [22] Q. Li, K.-J. Zhao, Y.-L. Zhao et al., "High dosage administration of *Polygonum multiflorum* alcohol extract caused the multi-organ injury," *Global Traditional Chinese Medicine*, vol. 6, pp. 1–7, 2013.
- [23] W. Huang, Y.-N. Zhang, and R. Sun, "Experimental study on the "Dose-Time-Toxicity" relationship of acute hepatotoxicity induced by different components from *Polygonum multiflorum* in Mice," *Chinese Journal of Pharmacovigilance*, vol. 18, pp. 193–197, 2011.
- [24] T. Noda, T. Yamada, T. Ohkubo et al., "Hot-water-extracts of *Polygonum multiflorum* do not induce any toxicity but elicit limited beneficial effects on the liver in mice," *Journal of Health Science*, vol. 55, no. 5, pp. 720–725, 2009.
- [25] T. Wang, J.-Y. Wang, Z.-Z. Jiang et al., "Study on hepatotoxicity of aqueous extracts of *Polygonum multiflorum* in rats after 28-day oral administration-analysis on correlation of cholestasis," *China Journal of Chinese Materia Medica*, vol. 37, pp. 1445–1450, 2012.
- [26] X.-B. Sun, Y.-W. Sun, H. Li, and W. Sun, "Influence of main component of *Heshouwu* such as emodin, rhein and toluylene glycoside on hepatic cells and hepatoma carcinoma cell," *Modern Journal of Integrated Traditional Chinese and Western Medicine*, vol. 19, pp. 1315–1319, 2010.
- [27] M. Zhang, L.-F. Lin, H.-M. Lin, C.-H. Qu, L. Yan, and J. Ni, "Interpretation the hepatotoxicity based on pharmacokinetics investigated through oral administrated different extraction parts of *Polygonum multiflorum* on rats," *Frontiers in Pharmacology*, vol. 9, p. 505, 2018.
- [28] L. Lin, H. Lin, M. Zhang et al., "A novel method to analyze hepatotoxic components in *Polygonum multiflorum* using ultra-performance liquid chromatography-quadrupole time-of-flight mass spectrometry florum using ultra-performance liquid chromatography-quadrupole time-of-flight mass spectrometry," *Journal of Hazardous Materials*, vol. 299, pp. 249–259, 2015.
- [29] G. P. Lv, L. Z. Meng, D. Q. Han, H. Y. Li, J. Zhao, and S. P. Li, "Effect of sample preparation on components and liver toxicity of *Polygonum*," *Journal of Pharmaceutical and Biomedical Analysis*, vol. 109, pp. 105–111, 2015.
- [30] W. Rui, W. Xia, W. Zhao et al., "Differential constituents in roots, stems and leaves of *Polygonum multiflorum* thubn. screened by UPLC/ESI-Q-TOF-MS and multivariate statistical analysis," *Journal of Chromatographic Science*, vol. 58, no. 2, pp. 136–143, 2020.
- [31] J. Yu, J. Xie, X.-J. Mao et al., "Hepatotoxicity of major constituents and extractions of radix *polygoni multiflori* and radix *polygoni multiflori praeparata*," *Journal of Ethnopharmacology*, vol. 137, no. 3, pp. 1291–1299, 2011.
- [32] B. Zhang, S.-H. Din, X.-M. Qian, and W.-S. Zhu, "Q Lu, "Liver function of drug-induced liver injury induced by emodin in rats," *Military Medical Journal of South China*, vol. 29, pp. 735–738, 2015.
- [33] M.-X. Wang, Y.-G. Wang, H.-H. Xu et al., "Effects of emodin in *Polygonum multiflorum* on liver cytotoxicity and CYP450 isoenzymes expression in L02 cells," *Chinese Pharmacological Bulletin*, vol. 32, pp. 1543–1548, 2016.
- [34] Q. Wang, Z. Dai, Y.-J. Zhang, and S.-C. Ma, "Study on the hepatotoxicity of dianthrone in *Polygoni multiflori* radix," *Chinese Journal of Pharmaceutical Analysis*, vol. 38, pp. 268–274, 2018.
- [35] J. Ma, L. Zheng, Y.-S. He, and H.-J. Li, "Hepatotoxic assessment of *Polygoni multiflori* Radix extract and toxicokinetic study of stilbene glucoside and anthraquinones in rats," *Journal of Ethnopharmacology*, vol. 162, no. 13, pp. 61–68, 2015.
- [36] L. F. Han, P. Wang, Y. L. Wang et al., "Rapid discovery of the potential toxic compounds in *Polygonum multiflorum* by UHPLC/Q-Orbitrap-MS-Based metabolomics and correlation analysis," *Frontiers in Pharmacology*, vol. 10, p. 329, 2019.
- [37] D.-Q. Luo, P. Jia, S. S. Zhao et al., "Identification and differentiation of *Polygonum multiflorum* Radix and *Polygoni multiflori* Radix preaparata through the quantitative analysis of multicomponents by the single-marker method," *Journal of Analytical Methods in Chemistry*, vol. 2019, Article ID 7430717, 2019.
- [38] T.-T. A. Nguyen, M. T. Ha, S.-E. Park, J. S. Choi, B. S. Min, and J. A. Kim, "Stilbenes with potent protein tyrosine phosphatase-1B inhibitory activity from the roots of *Polygonum multiflorum*," *Journal of Natural Products*, vol. 83, no. 2, pp. 323–332, 2020.
- [39] L. Zhang, D. He, K. Li et al., "Emodin targets mitochondrial cyclophilin D to induce apoptosis in HepG2 cells," *Biomedicine & Pharmacotherapy*, vol. 90, pp. 222–228, 2017.
- [40] L.-L. Jiang, D.-S. Zhao, Y.-X. Fan, Q. Yu, P. Li, and H.-J. Li, "Detection of emodin derived glutathione adduct in normal rats administered with large dosage of *Polygoni multiflori* Radix," *Frontiers in Pharmacology*, vol. 8, p. 446, 2017.
- [41] D.-M. Liu, C.-Y. Zhou, J.-S. Wu, P. Wang, and X.-L. Meng, "Emodin induces apoptosis in HepG2 cells via mitochondrial pathway," *Chinese Journal of Experimental Traditional Medical Formulae*, vol. 24, no. 3, pp. 104–108, 2018.
- [42] D.-M. Liu, C.-Y. Zhou, J.-S. Wu, P. Wang, and X.-L. Meng, "Emodin induces apoptosis of L02 via caspase-8-mediated activation of the mitochondrial death pathway," *Pharmacology and Clinics of Chinese Materia Medica*, vol. 33, no. 5, pp. 23–26, 2017.
- [43] L. Lin, Y. Liu, S. Fu, C. Qu, H. Li, and J. Ni, "Inhibition of mitochondrial complex function-the hepatotoxicity mechanism of emodin based on quantitative proteomic analyses," *Cells*, vol. 8, no. 3, p. 263, 2019.
- [44] L. Kang, L. Si, J. Rao et al., "*Polygoni Multiflori* Radix derived anthraquinones alter bile acid disposition in sandwich-cultured rat hepatocytes," *Toxicology in Vitro*, vol. 40, pp. 313–323, 2017.
- [45] Q. Wang, Y.-D. Wang, Y. Li et al., "Identification and characterization of the structure-activity relationships involved in UGT1A1 inhibition by anthraquinone and dianthrone constituents of *Polygonum multiflorum*," *Scientific Reports*, vol. 7, no. 1, Article ID 17952, 2017.
- [46] M.-J. Wei, J. Huang, J.-Q. Bai, X.-C. Cai, and X.-H. Qiu, "Effects of emodin on serum liver function, liver transporter and metabolic enzyme UGT1A1 expression in rats," *Lishizhen Medicine and Materia Medica Research*, vol. 29, no. 7, pp. 1551–1555, 2018.
- [47] J. Seppen, P. J. Bosma, B. G. Goldhoorn et al., "Discrimination between Crigler-Najjar type I and II by expression of mutant bilirubin uridine diphosphate-glucuronosyltransferase," *Journal of Clinical Investigation*, vol. 94, no. 6, pp. 2385–2391, 1994.

- [48] M. G. Mustafa, M. L. Cowger, and T. E. King, "Effects of bilirubin on mitochondrial reactions," *The Journal of Biological Chemistry*, vol. 244, no. 23, pp. 6403–6414, 1969.
- [49] M. L. Cowger, "Mechanism of bilirubin toxicity on tissue culture cells: factors that affect toxicity, reversibility by albumin, and comparison with other respiratory poisons and surfactants," *Biochemical Medicine*, vol. 5, no. 1, pp. 1–16, 1971.
- [50] E. Sticova and M. Jirsa, "New insights in bilirubin metabolism and their clinical implications," *World Journal of Gastroenterology*, vol. 19, no. 38, pp. 6398–6307, 2013.
- [51] M.-X. Wang, *Study on the Mechanisms of Emodin Increasing Liver Injury in Polygonum Multiflorum Thunb through Activating CYP1A1*, Guangdong Pharmaceutical University, Guangzhou, China, 2018.
- [52] W. Liu, *Metabolism of Emodin in Liver and Intestine and its Gender-dependent Differences*, Southern Medical University, Guangzhou, China, 2010.
- [53] M. Yang, T. Liu, W.-H. Feng et al., "Exploration research on hepatotoxic constituents from Polygonum multiflorum root," *China Journal of Chinese Materia Medica*, vol. 41, no. 10, pp. 1289–1296, 2016.
- [54] Z.-L. Liu, Z.-Q. Song, L. Zhang, and S.-L. Li, "Influence of process methods on contents of chemical component radix Polygoni multiflori," *China Journal of Chinese Materia Medica*, vol. 30, no. 5, pp. 336–340, 2005.
- [55] X. Zhou, W.-J. Luo, L.-P. Wang, and P.-F. Wei, "Study on the toxic mechanism of different components of Polygonum multiflorum Thunb," *Journal of Liaoning University of Traditional Chinese Medicine*, vol. 21, no. 1, pp. 51–53, 2019.
- [56] X.-Q. Hu, Y.-L. Li, and L. Wang, "Effect of tannin in Polygonum multiflorum on liver biochemical indexes of rats," *Drug Evaluation Research*, vol. 33, no. 1, pp. 63–65, 2010.
- [57] Y. Wu, *Screening of in Vitro Model in Drug-Induced Liver Injury and Preliminary in Vestigation of Polygonum Multiflorum Induced Liver Injury*, Chinese Academy of Medical Sciences & China Union Medical College, Beijing, China, 2016.
- [58] R.-B. Huang, L.-Q. Zang, G. Liang, X. Lin, and N.-P. Wang, "Effect of EGCG on hepatic microsomal drug-metabolizing enzyme and CCL4-induced liver injury," *Journal of Guangxi University of Chinese Medicine*, vol. 16, no. 3, pp. 129–131, 1999.
- [59] X. Wu, X. Chen, Q. Huang, D. Fang, G. Li, and G. Zhang, "Toxicity of raw and processed roots of Polygonum multiflorum," *Fitoterapia*, vol. 83, no. 3, pp. 469–475, 2012.
- [60] Y.-Q. Bao, F. Shen, Y.-L. Li, D.-M. Chen, and H. Lu, "Toxicity and mechanism of Polygoni multiflori radix alcohol extract on L02 cells," *Chinese Journal of Experimental Traditional Medical Formulae*, vol. 26, no. 10, pp. 23–28, 2020.
- [61] X.-Q. Hu, M. Lin, H.-L. Yang et al., "Effects of different ratios of Tannins and Stilbene glucoside from Polygonum multiflorum on liver biochemical indexes in rats," *Shanghai Journal of Traditional Chinese Medicine*, vol. 45, no. 4, pp. 56–59, 2011.
- [62] P. Yao and D.-R. Hu, "Role of NF- κ B in HGF-mediated proliferation of WBF-344 cell," *Medical Journal of Chinese People's Liberation Army*, vol. 34, no. 3, pp. 271–273, 2009.
- [63] S.-Y. Long, C.-P. Zhang, X.-Q. Gao et al., "Effects of 2,3,5,4'-tetrahydroxystilbene-2-O- β -D-glucoside on the expression of NF- κ B/I κ B and apoptosis of HUVECs induced by H₂O₂," *Chinese Pharmacological Bulletin*, vol. 27, no. 10, pp. 1353–1357, 2011.
- [64] R.-C. Zhang, C. Zhang, Z.-X. Sun, and Q.-H. Deng, "Damage effect of Polygonum multiflorum fractions on human normal liver cells L02 and liver cancer cells HepG2," *China Journal of Chinese Materia Medica*, vol. 37, no. 12, pp. 1830–1835, 2012.
- [65] C. Li, M. Niu, Z. Bai et al., "Screening for main components associated with the idiosyncratic hepatotoxicity of a tonic herb, Polygonum multiflorum," *Frontiers of Medicine*, vol. 11, no. 2, pp. 253–265, 2017.
- [66] X.-L. Xu, J. Ren, W.-Z. Zhai et al., "Evaluation of hepatotoxicity of different parts of Polygonum multiflorum and Polygonum multiflorum by HPLC fingerprint," *Chinese Traditional Patent Medicine*, vol. 42, no. 3, pp. 792–795, 2020.
- [67] Y.-K. Meng, C.-Y. Li, R.-Y. Li et al., "Cis-stilbene glucoside in Polygonum multiflorum induces immunological idiosyncratic hepatotoxicity in LPS-treated rats by suppressing PPAR- γ ," *Acta Pharmacologica Sinica*, vol. 38, no. 10, pp. 1340–1352, 2017.
- [68] B. Copple, H. Jaeschke, and C. Klaassen, "Oxidative stress and the pathogenesis of cholestasis," *Seminars in Liver Disease*, vol. 30, no. 02, pp. 195–204, 2010.
- [69] Z.-J. Ma, *The Initial Study of Objectivity, Clinical Metabolic Biomarker and Injury Mechanism of Hepatotoxicity of Polygoni Multiflori Radix*, Chengdu University of TCM, Chengdu, China, 2013.
- [70] J. Wei, J. Chen, L. Fu et al., "Polygonum multiflorum Thunb suppress bile acid synthesis by activating Fxr-Fgf15 signaling in the intestine," *Journal of Ethnopharmacology*, vol. 235, pp. 472–480, 2019.
- [71] Z.-F. Tang, G. Ma, and Q.-X. Mei, "Effect of bilirubin on hepatocyte uptake and bile excretion before and after processing of Polygonum multiflorum," *Lishizhen Medicine and Materia Medica Research*, vol. 29, no. 3, pp. 595–598, 2018.
- [72] X. Wang, L. Han, Y. Bi et al., "Paradoxical effects of emodin on ANIT-induced intrahepatic cholestasis and herb-induced hepatotoxicity in mice," *Toxicological Sciences*, vol. 168, no. 1, pp. 264–278, 2019.
- [73] L. Wu, W. Han, Y. Chen et al., "Gender differences in the hepatotoxicity and toxicokinetics of emodin: the potential mechanisms mediated by UGT2B7 and MRP2," *Molecular Pharmaceutics*, vol. 15, no. 9, pp. 3931–3945, 2018.
- [74] X. Jing, C.-Q. Wu, G. Han et al., "Study on cholestasis and related protein express in rats with liver injury induced by Polygonum multiflorum," *Drug Evaluation Research*, vol. 40, no. 5, pp. 612–619, 2017.
- [75] D.-S. Zhao, L.-L. Jiang, Y.-X. Fan et al., "Identification of urine tauro- β -muricholic acid as a promising biomarker in Polygoni multiflori radix-induced hepatotoxicity by targeted metabolomics of bile acids," *Food and Chemical Toxicology*, vol. 108, pp. 532–542, 2017.
- [76] N. Singh and L. Li, "Reduced oxidative tissue damage during endotoxemia in IRAK-1 deficient mice," *Molecular Immunology*, vol. 50, no. 4, pp. 244–252, 2012.
- [77] D. Weber-Mzell, P. Zaupa, T. Petnehazy et al., "The role of nuclear factor-kappa B in bacterial translocation in cholestatic rats," *Pediatric Surgery International*, vol. 22, no. 1, pp. 43–49, 2006.
- [78] H. Jaeschke, "Reactive oxygen and mechanisms of inflammatory liver injury: present concepts," *Journal of Gastroenterology and Hepatology*, vol. 26, pp. 173–179, 2011.
- [79] K. Allen, H. Jaeschke, and B. L. Copple, "Bile acids induce inflammatory genes in hepatocytes," *The American Journal of Pathology*, vol. 178, no. 1, pp. 175–186, 2011.

- [80] M. J. Vallejo, L. Salazar, and M. Grijalva, "Oxidative stress modulation and ROS-mediated toxicity in cancer: a review on in vitro models for plant-derived compounds," *Oxidative Medicine and Cellular Longevity*, vol. 2017, Article ID 4586068, 2017.
- [81] C.-X. Shang, Y.-B. Chen, L. Heng et al., "Damage to mtDNA in liver injury of patients with extrahepatic cholestasis: the protective effects of mitochondrial transcription Factor A," *Free Radical Biology and Medicine*, vol. 52, no. 9, pp. 1543–1551, 2012.
- [82] E. Oqlodek, B. Augustyńska, A. Araszkievicz, and D. Moś, "The bile acids as an example of pathogens destructive hepatocytes in alcoholic liver injury," *Polski Merkuriusz Lekarski*, vol. 27, no. 160, pp. 346–348, 2009.
- [83] S.-L. Yang, "Clinical analysis of 30 cases of drug-induced hepatitis caused by fallopia multiflora," *Chinese Community Doctors*, vol. 34, no. 28, pp. 118–120, 2018.
- [84] G. Mazzanti, L. Battinelli, C. Daniele et al., "New case of acute hepatitis following the consumption of Shou Wu Pian, a Chinese herbal product derived from Polygonum multiflorum," *Annals of Internal Medicine*, vol. 140, no. 7, Article ID IDW30, 2004.
- [85] P. R. Ortiz de Montellano and J. J. De Voss, "Oxidizing species in the mechanism of cytochrome P450," *Natural Product Reports*, vol. 19, no. 4, pp. 477–493, 2002.
- [86] U. M. Zanger and M. Schwab, "Cytochrome P450 enzymes in drug metabolism: regulation of gene expression, enzyme activities, and impact of genetic variation," *Pharmacology & Therapeutics*, vol. 138, no. 1, pp. 103–141, 2013.
- [87] C. Inglese, M. Grazia Perrone, F. Berardi, R. Perrone, and N. Antonio Colabufo, "Modulation and absorption of xenobiotics: the synergistic role of CYP450 and P-gp activities in cancer and neurodegenerative disorders," *Current Drug Metabolism*, vol. 12, no. 8, pp. 702–712, 2011.
- [88] Y. Masubuchi and T. Horie, "Toxicological significance of mechanism-based inactivation of cytochrome p450 enzymes by drugs," *Critical Reviews in Toxicology*, vol. 37, no. 5, pp. 389–412, 2007.
- [89] H.-Y. Dong, J.-W. Shao, J.-F. Chen, T. Wang, F.-P. Lin, and Y.-H. Guo, "Transcriptional regulation of cytochrome P450 3A4 by four kinds of traditional Chinese medicines," *China Journal of Chinese Materia Medica*, vol. 33, no. 9, pp. 1014–1017, 2008.
- [90] K.-T. Jin, Y.-G. Wang, S.-Y. Shi, J.-X. Sheng, and Y. Gao, "Interaction between radix aconiti and rhizoma bletillae based on cytochrome P450 in rat livers," *China Journal of Traditional Chinese Medicine and Pharmacy*, vol. 22, pp. 598–602, 2007.
- [91] P.-F. Wei, M. Zhang, C.-L. Jiao, and Y.-Y. Wu, "Effect of different radix Polygoni multiflori preparata on CYP2E1 mRNA expression in rat liver," *Chinese Journal of Hospital Pharmacy*, vol. 30, no. 17, pp. 1445–1448, 2010.
- [92] Y. Zhang, T. Ding, T. Diao, M. Deng, and S. Chen, "Effects of Polygonum multiflorum on the activity of cytochrome P450 isoforms in rats," *Die Pharmazie*, vol. 70, no. 1, pp. 47–54, 2015.
- [93] H. Li, H.-L. Yang, D.-K. Li et al., "Study on inhibitory effect of water extract of Polygonum multiflorum on CYP1A2 and CYP2E1 enzymatic activities and mRNA expressions in rat liver," *China Journal of Chinese Materia Medica*, vol. 40, no. 7, pp. 1370–1375, 2015.
- [94] Y.-Y. Wang, J. Yang, H. Liu, F.-Q. Lin, J.-S. Shi, and F. Zhang, "Effects of tetrahydroxystilbene glucoside on mouse liver cytochrome P450 enzyme expressions," *Xenobiotica*, vol. 45, no. 4, pp. 279–285, 2015.
- [95] L.-L. Ouyang, W. Xu, J.-Q. Bai, L. Guo, and X.-H. Qiu, "In vitro metabolism of emodin in human liver microsomes," *Guiding Journal of Traditional Chinese Medicine and Pharmacology*, vol. 21, pp. 14–18, 2015.
- [96] A. K. Daly, "Genetic polymorphisms affecting drug metabolism," *Current Concepts in Drug Metabolism and Toxicology*, vol. 63, pp. 137–167, 2012.
- [97] K. F. Ma, X. G. Zhang, and H. Y. Jia, "CYP1A2 polymorphism in Chinese patients with acute liver injury induced by Polygonum multiflorum," *Genetics and Molecular Research*, vol. 13, no. 3, pp. 5637–5643, 2014.
- [98] J.-B. Wang, Y.-G. Ma, P. Zhang et al., "Effect of processing on the chemical contents and hepatic and renal toxicity of rhubarb studied by canonical correlation analysis," *Acta Pharmaceutica Sinica*, vol. 44, no. 8, pp. 885–890, 2009.
- [99] T.-T. Yang, Z.-Z. Jiang, and L.-Y. Zhang, "Research progress in drug-induced liver injury via mitochondrial damage," *Progress in Pharmaceutical Sciences*, vol. 38, no. 11, pp. 809–818, 2014.
- [100] M. P. C. Ribeiro, A. E. Santos, and J. B. A. Custódio, "Mitochondria: the gateway for tamoxifen-induced liver injury," *Toxicology*, vol. 323, pp. 10–18, 2014.
- [101] I. Shokolenko, N. Venediktova, A. Bochkareva, G. L. Wilson, and M. F. Alexeyev, "Oxidative stress induces degradation of mitochondrial DNA," *Nucleic Acids Research*, vol. 37, no. 8, pp. 2539–2548, 2009.
- [102] L.-N. He, A.-H. Yang, T.-Y. Cui et al., "Reactive metabolite activation by CYP2C19-mediated rhein hepatotoxicity," *Xenobiotica*, vol. 45, no. 4, pp. 361–372, 2015.
- [103] D. Bironaite and K. Öllinger, "The hepatotoxicity of rhein involves impairment of mitochondrial functions," *Chemico-biological Interactions*, vol. 103, no. 1, pp. 35–50, 1997.
- [104] Q. Du, X.-L. Bian, X.-L. Xu, B. Zhu, B. Yu, and Q. Zhai, "Role of mitochondrial permeability transition in human hepatocellular carcinoma Hep-G2 cell death induced by rhein," *Fitoterapia*, vol. 91, no. 6, pp. 68–73, 2013.
- [105] C. Ma, H.-J. Yan, C.-P. Tang, and Z.-J. Fang, "Study on antioxidant effects of intragastric administration with water decoction of Polygonum multiflorum thumb from different provenances on aging mice," *Journal of Guangdong College of Pharmacy*, vol. 24, no. 6, pp. 581–583, 2008.
- [106] Y.-Y. Luo, J.-X. Liu, X.-H. Liu et al., "Difference of chemical compositions in Polygoni multiflori radix from different habitats by UPLC-Triple TOF MS/MS," *Journal of Chinese Mass Spectrometry Society*, vol. 38, no. 6, pp. 679–689, 2017.
- [107] Y. Chen, *The Study of Quality Evaluation and Regional Division of Polygonum Multiflorum Thunb*, Guangzhou University of Chinese Medicine, Guangdong, China, 2013.
- [108] H. Gu and Y. Zhang, "A study on ancient and modern preparation of Heshouwu," *Clinical Journal of Chinese Medicine*, vol. 7, no. 34, pp. 24–26, 2015.
- [109] H.-R. Cui, Z.-F. Bai, H.-B. Song, T.-Z. Jia, J.-B. Wang, and X.-H. Xiao, "Investigation of potential toxic factors for fleece-flower root: from perspective of processing methods evolution," *China Journal of Chinese Materia Medica*, vol. 41, no. 2, pp. 333–339, 2016.
- [110] Y.-M. Zhou, M.-J. Zhao, X.-H. Gong et al., "The influence of different processing time on composition and content of Polygoni multiflori," *Natural Product Research and Development*, vol. 29, no. 10, pp. 1759–1765, 2017.
- [111] X.-M. Zhao, X.-Y. Li, R. Sun et al., "Study on acute toxicity of different processed ethanol extract of Polygoni multiflori in

- mice," *Chinese Journal of Pharmacovigilance*, vol. 14, no. 10, pp. 603–610, 2017.
- [112] D. Gao, X.-F. Li, P. Yin et al., "Preliminary study on hepatotoxic components in Polygoni multiflori radix based on processing and toxicity-decreasing," *Chinese Traditional and Herbal Drugs*, vol. 48, no. 10, pp. 2044–2050, 2017.
- [113] R. Zou, J.-J. Xiao, Y.-Y. Wang, and Y.-X. Wu, "Brief description of processing technology of Polygoni multiflori Radix; a study on ancient and modern preparation of heshouwu," *Guangzhou Chemical Industry*, vol. 48, no. 7, pp. 21–23, 2020.
- [114] H. Zheng, *Study on Gut Microbiota Changes in Polygonum Multiflorum Thunb. Induced Liver Injury Rats by High-Throughput Sequencing and Real-Time Quantitative PCR*, Guangdong Pharmaceutical University, Guangdong, China, 2017.
- [115] L.-Z. He, P. Yin, Y.-K. Meng et al., "Study on the mechanism of PPAR- γ dependent immunological idiosyncrasy liver injury induced by Polygonum multiflorum," *Acta Pharmaceutica Sinica*, vol. 52, no. 7, pp. 1027–1032, 2017.
- [116] C.-P. Li, T. Rao, X.-P. Chen et al., "HLA-B*35:01 allele is a potential biomarker for predicting polygonummultiflorum-induced liver injury in humans," *Hepatology*, vol. 70, no. 1, pp. 346–357, 2019.
- [117] E. J. Werder, J. I. Beier, D. P. Sandler et al., "Blood BTEXS and heavy metal levels are associated with liver injury and systemic inflammation in Gulf states residents," *Food and Chemical Toxicology*, vol. 139, Article ID 111242, 2020.
- [118] M. Şahin, F. Karayakar, K. E. Erdogan, F. Bas, and T. Colak, "Liver tissue trace element levels in HepB patients and the relationship of these elements with histological injury in the liver and with clinical parameters," *Journal of Trace Elements in Medicine and Biology: Organ of the Society for Minerals and Trace Elements (GMS)*, vol. 45, pp. 70–77, 2018.
- [119] J. Wang, Z. Ma, M. Niu et al., "Evidence chain-based causality identification in herb-induced liver injury: exemplification of a well-known liver-restorative herb Polygonum multiflorum," *Frontiers of Medicine*, vol. 9, no. 4, pp. 457–467, 2015.
- [120] L. Xin, L. Meng, S.-L. Wei, X.-J. Qi, and B.-Y. Zhuo, "Analysis on functional components of Polygonum multiflorum from different habitats," *Modern Chinese Medicine*, vol. 22, no. 3, pp. 384–390, 2020.
- [121] J. Yang, L. Zhou, L. Hu et al., "Quantitative analysis of 40 inorganic elements in Polygoni multiflori radix from different origins by ICP-MS," *World Chinese Medicine*, vol. 14, no. 11, pp. 2819–2828, 2019.
- [122] Y.-Y. Yang, K.-C. Lee, Y.-T. Huang et al., "Effects of N-acetylcysteine administration in hepatic microcirculation of rats with biliary cirrhosis," *Journal of Hepatology*, vol. 49, no. 1, pp. 25–33, 2008.
- [123] T. Y. Lee, F.-Y. Chen, H.-H. Chang, and H.-C. Lin, "The effect of capillarisin on glycochenodeoxycholic acid-induced apoptosis and heme oxygenase-1 in rat primary hepatocytes," *Molecular and Cellular Biochemistry*, vol. 325, no. 1–2, pp. 53–59, 2009.
- [124] S.-Y. Qi, R.-M. Jin, H.-J. Liu, and Y.-W. Huang, "Mechanism studies on hepatotoxicity of rats induced by fructus toosendan," *China Journal of Chinese Materia Medica*, vol. 33, no. 16, pp. 2045–2047, 2008.
- [125] T. Li, Z.-Z. Jiang, T. Wang et al., "Hepatotoxicity and its mechanism of saikosaponin on the human liver L02 cells in vitro," *Chinese Journal of Clinical Pharmacology and Therapeutics*, vol. 12, no. 4, pp. 396–400, 2007.
- [126] D.-N. Qiu, *Gene Regulations of Bile Acids Classic Synthesis Pathway*, Fudan University, Shanghai, China, 2008.
- [127] A.-H. Wang, L. Liu, and K. Zhou, "The progress in the study of the relation between cholestasis and bile acid transporters," *Medical Recapitulate*, vol. 19, no. 1, pp. 16–18, 2013.
- [128] Z. H. Wang and Y. B. Qian, "Expression and significance of bsep and mrp2 after hepatic ischemia-reperfusion: experiment with rats," *Journal of Hepatobiliary Surgery*, vol. 19, no. 2, pp. 136–140, 2011.
- [129] M. Trauner, M. Arrese, H. Lee, J. L. Boyer, and S. J. Karpen, "Endotoxin downregulates rat hepatic Ntcp gene expression via decreased activity of critical transcription factors," *Journal of Clinical Investigation*, vol. 101, no. 10, pp. 2092–2100, 1998.
- [130] R. Green, D. Beier, and J. Gollan, "Regulation of hepatocyte bile salt transporters by endotoxin and inflammatory cytokines in rodents," *Gastroenterology*, vol. 111, no. 1, pp. 193–198, 1996.
- [131] Y. Lv, X.-H. Sun, Q.-T. Chen et al., "Effect on rat liver about the compatibility of Polygonum multiflorum and black bean," *Lishizhen Medicine and Materia Medica Research*, vol. 24, no. 3, pp. 538–540, 2013.
- [132] C. Zhang, Z.-Y. Liu, H.-J. Yu, and D.-L. Liu, "Phenolic acids from seed coats of Glycinemax," *Chinese Traditional and Herbal Drugs*, vol. 44, no. 24, pp. 3440–3443, 2013.
- [133] Y.-L. Wang, H.-W. Ren, Z.-Z. Li, Y.-G. Wang, J.-L. Jiang, and X.-L. Dong, "Study on antioxidative activity evaluation medicinal black soybean pigments by scavenging DPPH," *Science and Technology of Food Industry*, vol. 30, no. 8, pp. 102–105, 2009.
- [134] A.-J. Shen and W.-R. Cai, "The research progress on anti-inflammatory effects and the therapy to acute lung injury of emodin," *Journal of Zhejiang Chinese Medical University*, vol. 37, no. 10, pp. 1261–1264, 2013.
- [135] F.-X. Zhou, *Intervention Effects of Emodin on Rats with Nonalcoholic Fatty Liver Disease Induced by Fat-Rich Diet and its Mechanisms*, Central South University, Hunan, China, 2011.
- [136] T.-X. Yao, *The Effect of Emodin on Non-alcoholic Fatty Liver Rat Liver Injury Induced by Endotoxemia*, Central South University, Hunan, China, 2011.
- [137] L. L. Zhang, X. J. Li, and J. T. Jia, "Effect of emodin on the oxidative stress in the liver of hepatic fibrosis rats," *Journal of Changzhi Medical College*, vol. 28, no. 2, pp. 81–84, 2014.
- [138] Y. H. Wang, H. P. Zhao, J. B. Wang, Y. L. Zhao, and X. H. Xiao, "Study on dosage-toxicity/efficacy relationship of prepared rhubarb on basis of symptom-based prescription theory," *China Journal of Chinese Materia Medica*, vol. 39, no. 15, pp. 2918–2923, 2014.
- [139] J. Y. Pang, Z. F. Bai, M. Niu et al., "The toxic and protective effects of Polygonum multiflorum on normal and liver injured rats based on the symptom-based prescription theory," *Acta Pharmaceutica Sinica*, vol. 50, no. 8, pp. 973–979, 2015.